



National Library  
of Canada

Acquisitions and  
Bibliographic Services Branch

395 Wellington Street  
Ottawa, Ontario  
K1A 0N4

Bibliothèque nationale  
du Canada

Direction des acquisitions et  
des services bibliographiques

395, rue Wellington  
Ottawa (Ontario)  
K1A 0N4

*Your file* *Votre référence*

*Our file* *Notre référence*

## NOTICE

## AVIS

The quality of this microform is heavily dependent upon the quality of the original thesis submitted for microfilming. Every effort has been made to ensure the highest quality of reproduction possible.

If pages are missing, contact the university which granted the degree.

Some pages may have indistinct print especially if the original pages were typed with a poor typewriter ribbon or if the university sent us an inferior photocopy.

Reproduction in full or in part of this microform is governed by the Canadian Copyright Act, R.S.C. 1970, c. C-30, and subsequent amendments.

La qualité de cette microforme dépend grandement de la qualité de la thèse soumise au microfilmage. Nous avons tout fait pour assurer une qualité supérieure de reproduction.

S'il manque des pages, veuillez communiquer avec l'université qui a conféré le grade.

La qualité d'impression de certaines pages peut laisser à désirer, surtout si les pages originales ont été dactylographiées à l'aide d'un ruban usé ou si l'université nous a fait parvenir une photocopie de qualité inférieure.

La reproduction, même partielle, de cette microforme est soumise à la Loi canadienne sur le droit d'auteur, SRC 1970, c. C-30, et ses amendements subséquents.

Canada

**University of Alberta**

Strategies for high-temperature oxygen isotope thermometry

by

James Farquhar ©

A thesis submitted to the Faculty of Graduate Studies and Research in partial fulfillment  
of the requirements for the degree of Doctor of Philosophy

Department of Earth and Atmospheric Sciences

Edmonton, Alberta  
Fall 1995



National Library  
of Canada

Acquisitions and  
Bibliographic Services Branch

395 Wellington Street  
Ottawa, Ontario  
K1A 0N4

Bibliothèque nationale  
du Canada

Direction des acquisitions et  
des services bibliographiques

395, rue Wellington  
Ottawa (Ontario)  
K1A 0N4

*Your file* *Voire référence*

*Our file* *Notre référence*

THE AUTHOR HAS GRANTED AN IRREVOCABLE NON-EXCLUSIVE LICENCE ALLOWING THE NATIONAL LIBRARY OF CANADA TO REPRODUCE, LOAN, DISTRIBUTE OR SELL COPIES OF HIS/HER THESIS BY ANY MEANS AND IN ANY FORM OR FORMAT, MAKING THIS THESIS AVAILABLE TO INTERESTED PERSONS.

L'AUTEUR A ACCORDE UNE LICENCE IRREVOCABLE ET NON EXCLUSIVE PERMETTANT A LA BIBLIOTHEQUE NATIONALE DU CANADA DE REPRODUIRE, PRETER, DISTRIBUER OU VENDRE DES COPIES DE SA THESE DE QUELQUE MANIERE ET SOUS QUELQUE FORME QUE CE SOIT POUR METTRE DES EXEMPLAIRES DE CETTE THESE A LA DISPOSITION DES PERSONNE INTERESSEES.

THE AUTHOR RETAINS OWNERSHIP OF THE COPYRIGHT IN HIS/HER THESIS. NEITHER THE THESIS NOR SUBSTANTIAL EXTRACTS FROM IT MAY BE PRINTED OR OTHERWISE REPRODUCED WITHOUT HIS/HER PERMISSION.

L'AUTEUR CONSERVE LA PROPRIETE DU DROIT D'AUTEUR QUI PROTEGE SA THESE. NI LA THESE NI DES EXTRAITS SUBSTANTIELS DE CELLE-CI NE DOIVENT ETRE IMPRIMES OU AUTREMENT REPRODUITS SANS SON AUTORISATION.


ISBN 0-612-06209-0

Canada

### MANUSCRIPT RELEASE

Permission is hereby granted to James Farquhar to reproduce parts of the manuscript *Exsolution-enhanced oxygen exchange: Implications for oxygen isotope closure temperatures in minerals*, published in *Geology* (1994), volume 22, pages 751-754, in his thesis *Strategies for high-temperature oxygen isotope thermometry*. This permission is subject to the conditions of the general University of Alberta Release Form for the entire thesis.

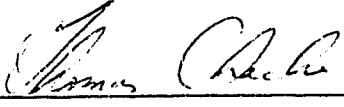
Co-authors:


Thomas Chacko  Date Aug. 15, 1995  
Department of Earth and Atmospheric Sciences, University of Alberta, Edmonton, Alberta,  
T6G2E3, Canada

MANUSCRIPT RELEASE

Permission is hereby granted to James Farquhar to reproduce parts of the manuscript *Strategies for high-temperature oxygen isotope thermometry: a worked example from the Laramie Anorthosite Complex, Wyoming USA*, published in *Earth and Planetary Science Letters* (1993), volume 117, pages 407-422 (1993), in his thesis *Strategies for high-temperature oxygen isotope thermometry*. This permission is subject to the conditions of the general University of Alberta Release Form for the entire thesis.

Co-authors:

Thomas Chacko  Date 7/25/95  
Department of Earth and Atmospheric Sciences, University of Alberta, Edmonton, Alberta,  
T6G2E3, Canada

B. Ronald Frost  Date 7/13/95  
Department of Geology and Geophysics, University of Wyoming, Laramie, Wyoming,  
82071, USA

UNIVERSITY OF ALBERTA

RELEASE FORM

NAME OF AUTHOR: James Farquhar

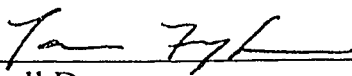
TITLE OF THESIS: Strategies for high-temperature oxygen isotope thermometry

DEGREE: Doctor of Philosophy

YEAR THIS DEGREE GRANTED: 1995

Permission is hereby granted to the University of Alberta Library to reproduce single copies of this thesis and to lend or sell such copies for private scholarly or scientific research purposes only.

The author retains all other publication and other rights in association with the copyright in the thesis and except as hereinbefore provided neither the thesis nor any substantial portion thereof may be printed or otherwise reproduced in any material form whatever without the authors prior written permission.

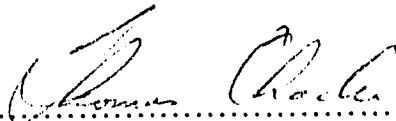
  
\_\_\_\_\_  
507 Powell Dr.  
Annapolis Maryland  
USA 21401

Date: *Aug 18, 1995*

UNIVERSITY OF ALBERTA

FACULTY OF GRADUATE STUDIES AND RESEARCH

The undersigned certify that they have read, and recommended to the Faculty of Graduate Studies and Research for acceptance, a thesis entitled *Strategies for high-temperature oxygen isotope thermometry* submitted by James Farquhar in partial fulfillment of the requirements for the degree of Doctor of Philosophy.

  
.....

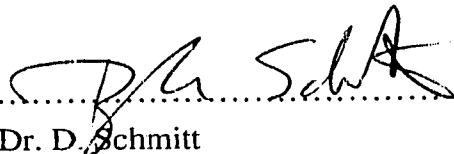
Dr. T. Chacko (Supervisor)

  
.....

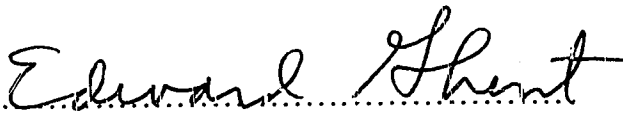
Dr. B.E. Nesbitt

  
.....

Dr. K. Muchlenbachs

  
.....

Dr. D. Schmitt

  
.....

Dr. E.D. Ghent

Date August 15, 1995.....

## **Acknowledgements**

There is never enough space for acknowledgments. Below are listed debts to my friends and colleagues. Tom Chacko suggested, advised, and encouraged this study. Karlis Muehlenbachs encouraged it, too, was appreciated for his dedication, laboratory support, and his critical approach to thinking. Bruce Nesbitt provided tactical support, advice, and a regional geological perspective. Rob Creaser, Bob Luth, and the rest of the faculty at the University of Alberta maintained a challenging and collegial working environment. Paul Wagner helped with the electron microprobe. Diane Caird made my XRD analyses. Alex Stelmac discussed safety. George Braybrook provided SEM analyses. Don Resultay made many thin sections and influenced the departmental mood, positively. Ron Frost supported and guided my work in Laramie. Ed Ghent provided samples and helped with my work in BC. Dave Ellis provided samples of the Napier Complex. Page Chamberlain read this manuscript and provided enjoyable questions for its defense. The Killam Foundation, DIAND, and the CCI funded this and other work that I undertook at Alberta. Fellow Graduate students Paul Blanchon, Alan Brandon, Bjarni Gautason, Barb Henderson, Chris Holmden, Agnes Koffyberg, Andrew Locock, Jacqueline Staveley, James Steer, Rob Stevens, and Gerard Zaluski were stimulating, supportive colleagues, and, most importantly, good friends. My parents, sisters and grandparents gave important familial and technical support. Finally, Lisa Tuit, who during the course of my studies remained my friend and became my wife, taught me to write, to think, and to formulate coherent arguments about geology and chemistry. I also thank Lisa for bringing me to Paris for my final year. It is a wonderful place to write a thesis. I am deeply grateful to each and every one for much more. This said, I claim full responsibility for the prejudices and errors that remain in this thesis.



## Abstract

An understanding of the factors that affect the magnitude and direction of isotopic exchange is fundamental to application of oxygen isotope geothermometers. This is particularly true in high-temperature rocks where isotopic exchange between minerals can be significant. The isotopic compositions of minerals in samples that behave as a closed system change in a predictable way during cooling. These changes are controlled by modal abundances of minerals and equilibrium fractionation factors. In traditional isotopic thermometry, temperatures are calculated by comparing isotopic compositions of two minerals. Because these calculations ignore mass balance and retrograde resetting, traditional methods can give spurious temperatures. Herein, I present an approach to isotopic thermometry that combines mass balance and equilibrium constraints and, therefore, directly accounts for the retrograde exchange process. By combining these methods with a directed sampling strategy one can obtain temperature data that can be directly correlated with a sample's thermal history. These temperature data provide more consistent and meaningful results than traditional mineral-pair thermometry and can be used to obtain insight into the cooling history of the sample.

Application of these methods to three metamorphic and plutonic igneous environments gives excellent results. Using these methods, I retrieved magmatic temperatures from plutonic igneous rocks of the Laramie Anorthosite Complex, Wyoming, and temperatures of  $\sim 1000^{\circ}\text{C}$  for garnet from the Napier Complex, Antarctica and Taltson Magmatic Zone, Canada. These isotopic temperatures are the highest yet reported from slowly cooled rocks. I was also able to use these methods to gain insight into the mechanics

of the isotopic exchange process and the length-scales over which oxygen isotope exchange occurred. At Mica Creek, Canada, although conventional quartz-garnet temperature data are in excellent agreement with metamorphic temperature estimates, careful application of these methods suggests that these rocks have experienced high-temperature interactions with externally-derived fluids. This last result renders the quartz-garnet temperatures invalid and highlights an important extension for this approach - evaluating the temperatures of open system interactions.

## Table of Contents

Chapter	Page
Chapter 1 Background	1
Theoretical basis for isotopic fractionations	10
Crystalline Solids	17
Temperature dependence	19
Robustness of $1/T^2$ dependence and accuracy and precision of theoretical predictions	21
Summary	24
Chapter 2: Isotopic thermometry : Principles and methods	26
Apparent temperatures: Mineral-pair thermometry	28
Uncertainties for mineral-pair thermometry	29
Optimization of mineral-pair thermometry	32
Single sample model temperatures	33
Calculation of mineral closure temperatures	34
Uncertainties for mineral closure temperatures	38
Optimization of mineral closure temperature data	39
System closure temperatures	40
Uncertainties for multiple sample method	42
Optimization of multiple sample thermometry	43
Summary	44
Chapter 3: Assumptions and checks for model temperature equations	54
The equilibration volume	56
Open system interactions	63
Retrograde isotopic zoning and isotopic thermometry	67
Summary and conclusions	69
Chapter 4 Case study 1: The Sybille Fe-Ti Oxide Pit	83

Analytical procedures and results	85
Conventional isotopic thermometry	88
Application of the single sample model	90
Application of the multiple sample model	92
Testing closed system	94
Testing equilibration volume	95
Mechanics of isotopic exchange	96
Conclusions	102
Chapter 5 Case study 2: high-temperature granulites, Northwestern Canada and Enderby land Antarctica	123
Methods	125
Isotopic systematics	126
Isotopic thermometry	127
Preservation of high-temperature isotopic compositions	129
Retrograde information	131
Summary and conclusions	132
Chapter 6 Case study 3: Mica Creek Barrovian sequence and adjacent Monashee Complex, British Columbia	139
Regional geology	139
Methods	141
Results	144
Isotopic temperature data	144
Sample 1-9	146
MC118A	149
Additional evidence for open system	150
Discussion	151
Chapter 7 Concluding remarks	163
References	165

## List of Figures

Figure	Page
Figure 2.1 Plots of quartz-hornblende and quartz-clinopyroxene apparent temperature surfaces in modal space. (After Giletti, 1986 and Chacko, 1990).	47
Figure 2.2 Plots of quartz-hornblende, quartz-feldspar, and feldspar hornblende apparent temperature surfaces. (After Eiler et al., 1992)	48
Figure 2.3 Plots of hornblende and clinopyroxene closure surfaces and uncertainty surfaces in modal space. Calculated by using data of Giletti (1986), Chacko (1990) and Eiler et al. (1992).	49
Figure 2.4 Schematic evolution diagram for a four mineral rock. (After Farquhar et al., 1993)	50
Figure 2.5 Schematic diagram of real isotopic exchange trajectory, calculated trajectory and model temperature.	51
Figure 2.6 Schematic diagram of establishment of a system closure temperature. Large scale equilibrium breaks down and local equilibrium continues.	52
Figure 3.1 Sketch of a hypothetical outcrop to illustrate the concept of an equilibration volume problem.	72
Figure 3.2 Diagram illustrating position of external and internal high closing phases on isotopic evolution diagrams.	73
Figure 3.3 Schematic diagrams illustrating the feasible spaces and pivot points for internal high closing phases. Equilibration volume problems.	74
Figure 3.4 Schematic diagram illustrating the feasible spaces and pivot points for external high closing phases. Equilibration volume problems.	75
Figure 3.5 Calculated model to represent the effect of the incorrect assumptions about the equilibration volume on a model rock.	76
Figure 3.6 Cartoon of open system processes operating in a crustal rock.	77
Figure 3.7 Schematic diagram illustrating the effect of open system interactions on the isotope exchange trajectories.	78

Figure 3.8 Schematic diagram illustrating tests for the equilibration volume and open system assumptions. Tests involve comparing isotopic exchange trajectories between more than one sample.	79
Figure 3.9 Plot of the closure profiles in spinel grains for a cooling rate of 10 °C/My. Plot of core-rim reintegrated bulk closure temperatures as a function of position in grain. Calculated using Dodson (1986) and Gautason and Muehlenbachs (1993).	80
Figure 4.1 Map showing location of Laramie Anorthosite Complex and Sybille Pit (After Grant and Frost (1990) and Newhouse and Hagner (1957)).	104
Figure 4.2 Map of the north wall of the Sybille quarry (After Bolsover, 1986).	105
Figure 4.3 Grain maps with isotopic composition data for feldspar, magnetite and ilmenite for two samples from Sybille. SP-2 and SP-7.	106
Figure 4.4 SEM photomicrographs of ilmenite exsolution lamellae in magnetite from the ore (A) and troctolite (B) for the Sybille Pit.	107
Figure 4.5 Plot of isotope exchange trajectories and closure temperatures for sample SP-1. Recalculated from Farquhar et al. (1993).	108
Figure 4.6 Plot of plagioclase trajectories for Sybille samples to illustrate the determination of a system closure temperature. Recalculated from Farquhar et al. (1993).	109
Figure 4.7 Plot of olivine trajectories and closure temperatures for Sybille samples. Illustration of equilibration volume and open system checks for assumptions.	110
Figure 4.8 Schematic diagram of equilibration volume problem influencing ilmenite model temperature data. Presented to argue for a possible equilibration volume problem during ilmenite closure.	111
Figure 4.9 Plot of $\Delta \log f_{O_2}$ (deviation from QFM) versus temperature to illustrate evolution of oxides during cooling and different exsolution histories for ores and troctolites. (After Farquhar and Chacko, 1994)	112
Figure 4.10 Calculate contours of reaction progress (%spinel exsolved for ores) as a function of $\Delta \log f_{O_2}$ and temperature.	113

Figure 4.11 Plot of cumulative exsolution and exsolution rate as a function of temperature for the spinel phase in the ores and troctolites. (After Farquhar and Chacko, 1994).	114
Figure 5.1 A. Sketch Map showing location and general geology of Taltson Magmatic zone (After Bostock et al., 1987). B. Sketch map showing location and metamorphic isograds of the Napier Complex, Antarctica (After Harley and Henson, 1990).	133
Figure 6.1 General map of the southern Omineca Belt (After Parrish et al., 1988) showing general area of study.	153
Figure 6.2 Metamorphic map of study area (After Ghent et al. 1982 and 1990) showing sample localities in Mica Creek Area and also in Monashee Complex area.	154
Figure 6.3 Map showing quartz-garnet and quartz-aluminosilicate isotopic temperature results for Mica Creek and Monashee Complex areas.	155
Figure 6.4 Plot of calculated cation compositions for samples from outcrop 1-9 and MC118. Calculated from modal and composition data collected by this study and by Nyman et al. (in press).	156
Figure 6.5 Plot of intercept temperatures versus leucosome/(leucosome+mesosome) to illustrate the effect of an equilibration volume problem for sample 1-9.	157
Figure 6.6 Plot of intercept temperatures versus open system shift to illustrate the effect of an open system shift for sample 1-9	158

## List of Tables

<b>Table</b>	<b>Page</b>
Table 2.1 Data for sample calculation of closure temperatures	53
Table 3.1 Model data used to calculate equilibration volume problem trajectories in figure 3.5	81
Table 3.2 Model data used to calculate open system shifts and trajectories for figure 3.8.	82
Table 4.1 Stable isotope geochemistry and modal abundance data for Sybille samples	115
Table 4.2 Isotopic analyses of apatite from size fractions for sample SP-3.	116
Table 4.3a Composition data for Sybille ilmenites.	117
Table 4.3b Composition data for Sybille magnetites.	118
Table 4.4 Mineral-pair apparent temperatures for Sybille samples.	119
Table 4.5 Mineral closure temperatures for Sybille samples.	120
Table 4.6 Calculated values of system closure temperatures for Sybille samples.	121
Table 4.7 Observed and predicted closure temperatures for minerals from the Sybille quarry.	122
Table 5.1 Calculation parameters used for calculation of model temperature data.	134
Table 5.2 Isotopic and modal data for Napier and Taltson samples.	135
Table 5.3 Mineral-pair isotopic temperature data for Napier and Taltson samples.	136
Table 5.4 Observed closure temperatures for Napier complex samples.	137
Table 5.5 Dodson closure temperatures and observed closure temperatures for Napier Complex samples. Wet and Dry diffusion data.	138
Table 6.1 Isotopic composition data for quartz, garnet and aluminosilicate minerals from the Mica Creek and Monashee Complex areas, British Columbia.	159



Table 6.2 Mineral-pair isotopic temperature data for Mica Creek and Monashee Complex samples.	160
Table 6.3 Isotopic composition and modal data for Mica Creek sample MC118A and Monashee Complex sample 1-9.	161
Table 6.4 Intercept temperature data for samples MC118A and 1-9.	162

## Definition of terms and symbols

---

$$\delta^{18}\text{O} = 1000 \frac{[(^{18}\text{O}/^{16}\text{O})_{\text{std}} - (^{18}\text{O}/^{16}\text{O})_{\text{sample}}]}{(^{18}\text{O}/^{16}\text{O})_{\text{std}}}$$

$$\alpha_{ij} = (1000 + \delta^{18}\text{O}_i) / (1000 + \delta^{18}\text{O}_j)$$

$$\Delta_{ij} = 1000 \ln(\alpha_{ij})$$

$h$  = Planck's Constant

$k$  = Boltzmann's Constant

$c$  = speed of light

$R$  = natural gas constant

$\nu_i$  = vibrational frequency of  $i$ th mode

$\omega_i$  = wave number ( $\nu_i/c$ )

$N$  = number of Atoms in substance

$N_A$  = Avogadro's Number

$n$  = quantum number (0,1,2,3, ...)

$n_a$  = number of atoms exchanged

$s$  = number of atoms in unit cell

$r$  = number of exchangeable atoms

$Q_A$  = partition function of molecule A

$Q^*$  = partition function for heavy isotope molecule

$\frac{Q^*}{Q}$  = partition function ratio

$\frac{Q^*'}{Q'}$  = reduced partition function ratio

$X_i$  = fraction of oxygen held by mineral  $i$  relative to the total oxygen in the rock

$A_{ij}$  = Temperature coefficient of equilibrium fractionation factor

$a_p$  = activity of phase component  $p$

$\mu_p$  = chemical potential of  $p$

$K$  = equilibrium constant

$E_i$  = internal energy

$I_A$  = moment of inertia in direction A

$\sigma_A$  = symmetry number of molecule A

$\sigma$  = statistical measure of certainty

$m$  = mass of light isotope

$m^*$  = mass of heavy isotope

$M_A$  = mass of molecule A

## **Chapter 1: Background**

This dissertation focuses on the subfield of stable isotope studies that deals with isotopic thermometry, a subfield that uses measured isotopic fractionation data to calculate geologic paleotemperatures. The concept of isotopic thermometry has been around for more than forty years. It has a complicated history that includes several cycles of discovery and rediscovery. Early workers with an excellent grasp of the fundamental assumptions outlined its advantages and pitfalls. Later, other workers who had used isotopic thermometry as a tool rediscovered these same fundamental insights, enumerated them in more detail, and applied them to the study of the crust. In this dissertation, I outline the fundamental assumptions, uncertainties and pitfalls of isotopic thermometry. I have tried to contribute to this field by extending the methods rather than to repeat past work. In the first chapter I review the history of isotopic thermometry. This is done to highlight the cycle of discovery and rediscovery and to emphasize the importance that a well grounded understanding of assumptions holds for one's level of insight and foresight. The second and third chapters focus on the basic science of isotopic thermometry - strategies, uncertainties and assumptions. The final three chapters apply these methods to three different environments. The goal is to understand the assumptions, uncertainties and strategies for isotopic thermometry. The fundamental emphasis is on combining mass balance and stable isotope constraints in isotopic thermometry.

In 1947, Urey published "The thermodynamic properties of isotopic substances" and set the groundwork for a new field in the earth sciences. His paper suggested uses for light-stable isotope analyses that ranged from determining "the amount of carbon dioxide in the air during past epochs" and investigating biochemical fractionation processes to calibrating experimentally "the true temperature coefficient(s)" and making temperature determinations from natural isotopic fractionations. He also acknowledged the possibility that late exchange and "diffusion processes" might change the isotopic compositions of minerals and complicate the interpretations of isotopic data. In 1947 Urey both formed the foundation of

the fields of high- and low-temperature isotopic thermometry and touched on the fundamental concern with the establishment and preservation of equilibria.

Urey (1947) did not, however, mention the very important use of isotopes as geochemical tracers. This omission was probably not due to ignorance - isotopic differences had already been measured between samples of different materials (e.g., Nier and Gulbransen, 1939) - but because the use of stable isotopes as tracers was, ultimately, a study of isotopic disequilibrium. Subsequent studies undertaken by Urey and his coworkers focused on the use of isotopes as tracers for waters (Friedman, 1953; Epstein and Mayeda, 1953; Epstein, 1956; Craig and Boata, 1956; Craig et al., 1956) and rocks (e.g., Silverman, 1951; Baertschi and Silverman, 1951; Craig, 1953; McCrea, 1950).

The specific use of stable isotopes for high-temperature isotopic thermometry is absent from Urey's (1947) study. He states:

It would be interesting indeed to know not only the temperature but also the variations of temperature on an ancient beach or in the forests where coal was deposited and whether a prehistoric animal had warm blood or not. However, too much optimism is not justified, for all the thermometers may be destroyed.

When Urey wrote, the Nier mass spectrometer had just been developed (Nier, 1947), and the analytical uncertainties were approximately  $\pm 0.003$  ( $\pm 3$  ‰ ( $\sigma$ ) recalculated by using data of Nier (1947) and discarding one  $3\sigma$  outlier). Improvements in precision were expected, but the ultimate limits remained uncertain. Urey's omission of high-temperature isotopic thermometry may have reflected a belief that the  $1/T^2$  dependence of isotopic fractionations, when combined with the analytical uncertainty would make it an impossible task. His own questions about retrograde exchange also may have raised doubts about the efficacy of this use for stable isotopes. Slightly more than ten years passed before the first advocates of high-temperature isotopic thermometry surfaced.

Clayton and Epstein (1958) seized on instrumental and analytical developments of the intervening decade to argue for the use of isotopes in high-temperature thermometry. These developments included the Nier mass spectrometer (Nier, 1947) and its subsequent

refinement by McKinney et al. (1950). The Nier mass spectrometer was a 60°, double-collecting machine that used a null method (Nier et al., 1946, 1947) of simultaneously comparing counts for ion beams at two masses. The McKinney et al. (1950) modifications included redesigning the electronic components for higher stability, replacing the amplifier system for measuring the smaller ion beam with a more stable vibrating reed electrometer and adding a dual gas feed system that allowed rapid comparison of sample and reference gases. These modifications yielded an order of magnitude improvement in sensitivity and precision. McKinney et al. (1950) reported precision better than  $\pm 0.2\%$ , and subsequent studies that used the same machine reported precision approaching  $\pm 0.05\%$  (McCrea, 1950; Craig, 1953). Present instrumental precision is comparable to the values reported by McCrea (1950) and Craig (1953). Analytical developments that made thermometry possible included the establishment of the  $\text{H}_3\text{PO}_4$  acid digestion technique for carbonates (McCrea, 1950) and the establishment of accurate and precise methods for extracting oxygen from silicates and metal-oxides. Baertschi and Silverman (1951) describe two oxygen extraction techniques for silicate rocks. They noted that the oxygen yields and isotopic compositions of oxygen gas produced by reaction of the samples with  $\text{HF} + \text{F}_{2(\text{gas})}$  in nickel reaction vessels at  $420^\circ\text{C}$  were better and more constant ( $\pm 0.5\%$ ) than for oxygen gas produced by reaction with  $\text{HF} + \text{ClF}_3$  at similar temperature conditions ( $\pm 1.5\%$ ). To test the accuracy of the fluorination techniques, Clayton and Epstein (1958) developed an independent technique for extraction of oxygen from silicate minerals. Their carbon reduction technique relies on reactions such as:



to extract oxygen from silicates and oxides. Reactions like (1.1), are driven by using an induction furnace to heat silicate (or oxide) minerals in a graphite crucible at vacuum to temperatures of approximately 2000 K. Clayton and Epstein (1958) reported 90-100 % oxygen yields for quartz, magnetite and zircon with a precision of  $\pm 0.15$  to  $0.20\%$ . They noted that this technique is not suitable for isotopic determinations on compounds containing

alkali metals, alkaline earths, aluminum, and zinc (most minerals except quartz, magnetite and zircon). Their isotopic determinations for quartz are in excellent agreement with those of Silverman (1951) and reflect the accuracy of both techniques. Present oxygen extraction techniques are variations and refinements of the fluorination techniques described by Baertschi and Silverman (1951). The principal differences are the use of higher reaction temperatures, the conversion of oxygen to CO<sub>2</sub> for analysis (Taylor and Epstein, 1962a), the use of BrF<sub>5</sub> as a fluorinating agent (Clayton and Mayeda, 1963) and the resurrection of ClF<sub>3</sub> as a reagent (Venneman and Smith, 1990). Laser heating (Sharp, 1990) and laser ablation techniques (Wiechert and Hoefs, 1994) in an atmosphere of F<sub>2</sub> or BrF<sub>5</sub> are more recent. Present estimates on the precision of these techniques range from ± 0.05 to 0.2 ‰ (Clayton and Mayeda, 1963; Hoefs, 1983; O'Neil, 1986; Valley et al., 1994). These analytical uncertainties propagate to temperature uncertainties in the 10's of degrees for metamorphic and igneous rocks and make isotopic thermometry a viable tool for studying high-temperature environments.

By documenting isotopic fractionations between minerals from high-temperature environments, Clayton and Epstein (1958) and Engel et al. (1958) marked the beginning of the field of high-temperature stable isotope thermometry. In these studies, they documented a correlation between lower  $\delta^{18}\text{O}_{\text{calcite}}$ ,  $\delta^{18}\text{O}_{\text{quartz}}$ , and  $\delta^{18}\text{O}_{\text{dolomite}}$ , smaller fractionations between quartz and calcite, and proximity to "sites of intense hydrothermal dolomitization and sulfide mineralization" in the Leadville Formation of Colorado. The lower  $\delta^{18}\text{O}$  of the country rocks is explained by interaction of the rocks with hydrothermal fluids near the sites of mineralization. The smaller fractionations are interpreted to reflect correspondingly higher country rock temperatures. In a study that followed, "The use of oxygen isotopes in high-temperature geological thermometry," Clayton and Epstein (1961) reevaluated their (1958) data. There, they combined the high temperature experimental calibration of the calcite-water system (Clayton, 1961) with elegant reasoning to empirically calibrate isotopic thermometers involving quartz, calcite and hematite. They wrote equations for isotopic equilibria between quartz, calcite, hematite and water in the form,  $\ln K_{ij} = A_{ij}/T^2 - B_{ij}$ , and noted that there were three independent equations with six independent terms that could be

used to describe equilibrium between the four phases. They used the calcite-water calibration to get two of the terms and a correlation between  $\Delta_{\text{quartz-calcite}}$  and  $\delta_{\text{calcite}}$  from Clayton and Epstein (1958) and an assumption that  $\delta_{\text{water}}$  was constant to calculate a third. The fourth and fifth terms were derived from natural isotopic data that formed a linear correlation between  $\Delta_{\text{quartz-hematite}}$  and  $\Delta_{\text{calcite-hematite}}$  for rocks that contain quartz, calcite and hematite, and the sixth term was derived on the basis of their conviction that intermineral fractionations obey a  $1/T^2$  temperature dependence and approach zero at high temperature. They used these calibrations to undertake isotopic thermometry for rocks that contained quartz, calcite, and hematite. Many of the studies that followed Clayton and Epstein's (1958, 1961) groundbreaking work used isotopic thermometry to study a wide variety of igneous and metamorphic rocks (e.g., James and Clayton, 1962; Garlick and Epstein, 1967; Anderson, 1966, 1967, 1968; Taylor, 1968; Taylor and Coleman, 1968; Shieh and Taylor, 1969; Vogel and Garlick, 1970; Wilson et al., 1970; Javoy et al., 1970; Anderson et al. 1971).

Some of these studies noted the possibility that isotopic thermometers may be disturbed after their setting. James and Clayton (1962) reported oxygen isotopic data for minerals from a greenschist to upper amphibolite facies sequence (possibly higher) for metamorphosed iron formations of the Lake Superior region. They stated:

Mineral pairs such as quartz-hematite and calcite-hematite have isotopic differences that bear consistent relation to inferred thermal gradients in the lower metamorphic zones. By relating the observed isotopic fractionation to the experimentally derived fractionation curve for  $\text{CaCO}_3\text{-H}_2\text{O}$ , it is possible to estimate that apparent temperatures of last crystallization reached about 200° C in the chlorite zone, 275° C in the biotite zone, and 350° C in the garnet zone. The indicated temperatures for rocks formed at temperatures above that of the garnet zone do not show a similar consistent pattern; we attribute this largely to retrograde equilibration during the cooling period.

Their observation that the systematic decrease in size of mineral-pair fractionations disappeared in the staurolite and sillimanite zones is the first documented case of systematic retrograde resetting of isotopic thermometers. It is also one of the earliest applications of

isotopic thermometry to rocks. James and Clayton's (1962) statement demonstrates that early studies were not driven by blind faith in a new technique. Early stable isotope geochemists were well aware of their assumptions and tried to avoid the pitfalls that accompany carefree interpretation. They recognized that their data commonly reflected equilibrium, but that resetting and disequilibrium were not uncommon. Subsequent studies also focused on the attainment of equilibrium and the viability of high temperature isotopic thermometry. Two camps surfaced. One camp followed the assumption that isotopic equilibrium was more common than not (e.g., Taylor et al., 1963; Taylor and Coleman, 1968; Taylor, 1968; Shieh and Taylor, 1969; Vogel and Garlick, 1970; Javoy et al., 1970). The other camp argued that isotopic resetting was a more significant concern that should be considered (e.g., Anderson, 1966, 1967, 1968; Garlick and Epstein, 1967; Wilson et al., 1970; Anderson et al., 1971). Anderson (1966) described isotopic data for the Labrieville Anorthosite in terms of resetting when he states:

The oxygen isotopic fractionation between coexisting (hemo-)ilmenite and plagioclase is larger (about 4.5 per mil) than that observed between the same minerals from the Skaergaard intrusion (about 3.3 per mil, Taylor and Epstein, 1963) and suggests relatively lower temperatures of recrystallization. However, there is a convincing correlation between the oxygen isotopic composition of the (hemo-) ilmenites and the modal abundance of iron-titanium oxide minerals in the rocks...

He continues:

The correlation is a natural consequence of closed system retrograde recrystallization: as temperature decreases the fractionation of oxygen isotopes between oxides and silicates increases, and material balance within a locally closed system requires that the resultant oxygen isotopic composition of all minerals participating in retrograde recrystallization reflects the modal composition of the rock. Accordingly all minerals in a rock initially rich in iron-titanium oxide minerals will acquire an  $O^{18}$ -rich composition as a result of retrograde recrystallization relative to those in a rock initially rich in feldspar. The (hemo-) ilmenite in an ilmenite rock will retain the primary oxygen isotopic composition of the ilmenite and the feldspar in a feldspar rock will retain its primary isotopic ratio; therefore, the primary plagioclase-ilmenite oxygen isotopic fractionation may be deduced.



These passages are an eloquent deductive argument for retrograde exchange; they formulate the basis for a methodology that can be used to "see through" retrograde exchange to the primary, high-temperature isotopic fractionations. The mathematical and physical formalization of Anderson's statements is only just now being realized (e.g., Farquhar et al., 1993). The premise of this dissertation can be traced to many of Anderson's basic ideas.

In a study entitled "The dimensions of oxygen isotopic equilibrium attainment during prograde metamorphism," Anderson (1967) outlines questions for all studies of isotopic thermometry. Was isotopic equilibrium attained between the minerals under study? Was it preserved during the cooling history of the samples? To what dimension (volume) do assumptions about equilibrium attainment and preservation apply? Similar questions were also posed by Garlick and Epstein (1967) in their paper, "Oxygen isotope ratios in coexisting minerals of regionally metamorphosed rocks." Garlick and Epstein (1967) argued that although fractionations between quartz-muscovite and biotite are consistent with equilibrium, they do not "adequately reflect metamorphic grade." They concluded that "muscovite and biotite usually undergo isotopic re-equilibration during retrogradation whereas quartz, garnet, ilmenite and magnetite (do not)." In a third study, Shieh and Taylor (1969) attempted to determine the scale of the equilibration volume and examined the role of pore fluids. Yet Shieh and Taylor (1969) were convinced that isotopic equilibrium between minerals was the rule rather than the exception for their rocks. Ultimately, it was critical examination of isotopic data like those from these studies that shifted the emphasis from isotopic thermometers as a tool to isotopic exchange and equilibration as a process to be studied in its own right. Nevertheless, interest in isotopic thermometry continued through the mid-1970's (e.g., Bottinga and Javoy, 1973, 1975; Hoernes and Friedrechs, 1974, 1978; O'Neil and Ghent, 1975; Becker and Clayton, 1976).

Deines (1977) may have dealt the most critical blow to isotopic thermometry. His elegant study used  $\Delta-\Delta$  diagrams and isotopic equilibria among mineral triplets to compare datasets of mineral-pair isotopic fractionations. These plots were initially used by Clayton and Epstein (1961) to calibrate empirically unknown equilibria by bootstrapping them to

known equilibria. Subsequently, many studies used these plots both to calibrate unknown equilibria and to assess equilibrium assumptions (e.g., Garlick and Epstein, 1967; Taylor and Coleman, 1968; Bottinga and Javoy, 1975). The axes of the plot are defined by  $\Delta$  values ( $\Delta = 1000 \ln \alpha$  and  $\Delta_{12}$  represents the fractionation between mineral 1 and mineral 2) for two different mineral pairs. Three distinct permutations of the  $\Delta$ - $\Delta$  plot can be made for a three-mineral system ( $\Delta_{12}$  vs.  $\Delta_{23}$ ,  $\Delta_{12}$  vs.  $\Delta_{13}$ , and  $\Delta_{13}$  vs.  $\Delta_{23}$ ). Arguing on the basis that all three of these permutations be strongly correlated in equilibrium systems, Dienes (1977) reported that  $\Delta$ - $\Delta$  plots for 87% of the mineral triplets that he examined are sufficiently irregular to preclude their use for empirical calibrations of isotopic thermometers. Of the 13% of the mineral triplets that remain, he stated that they are "compatible with the existence of isotopic equilibrium," but that they cannot be unambiguously ascribed to equilibrium because partial retrograde exchange that occurs in a systematic way can lead to "well-defined relationships in  $\Delta^{18}\text{O}$  diagrams which can be linear and may deviate significantly from those established on the basis of isotope equilibrium." Of the 13% of the mineral triplets that are compatible with equilibrium, only one out of seven exhibits a linear correlation that converges on the origin of the  $\Delta$ - $\Delta$  diagrams. Only this one mineral triplet (plagioclase-pyroxene-olivine) is consistent with isotopic equilibria that have  $1/T^2$  temperature dependence and converge to zero at  $T \rightarrow \infty$ . The remaining six mineral triplets, however, are consistent with "partial retrograde exchange that occurs in a systematic way."

By the mid-1980's, many workers were realizing the limits of isotopic thermometry. In 1986 Bowman and Ghent (1986) expressed this position:

Retrograde oxygen isotope exchange may be a general characteristic of high-grade metamorphic rocks and oxygen isotope thermometry may not usually record peak metamorphic temperatures if they significantly exceed 600°C.

At the same time, in a study entitled "Diffusion effects on oxygen isotope temperatures of slowly cooled igneous and metamorphic rocks", Gilotti (1986) argued that measured isotopic fractionations between different minerals in slowly cooled metamorphic and igneous rocks would neither correspond to their closure temperatures, nor to any other physically real

temperature in the cooling history of the rocks. He argued that different minerals "closed" to isotopic exchange at different temperatures and that the fractionations between them would reflect the entire exchange and closure history of the minerals in the rock. It is interesting to compare Giletti's (1986) conclusions with Taylor et al.'s (1963) personal communication from R.N. Clayton:

Also, as has been pointed out by R.N. Clayton (personal communication), the existence of a ubiquitous oxygen-bearing pore fluid may provide a further complication in interpreting the oxygen-isotopic data. The possibility exists that during the period of declining temperatures subsequent to the main metamorphic recrystallization, some minerals may continue to exchange oxygen with the pore fluid. If the  $O^{18}/O^{16}$  ratios of these minerals are each "frozen in" at a different, but constant, characteristic temperature, then similar  $\Delta$ -values might be obtained in each rock. Even though this still would represent equilibrium exchange of a sort, such a process would imply that the measured  $\Delta$ -values would not be equal to the equilibrium  $\Delta$ -values at any one single temperature for all the mineral pairs.

In one sense the field had come full circle. In another, the twenty-three years that separated the two studies may have been necessary to provide enough time, thought, and data collection, to fell the preferred hypothesis - isotopic thermometry can work.

Several important developments in the late 1980's renewed interest in the field of stable isotope thermometry. Experimental techniques that used carbonate-mineral pairs, provided a very high quality calibrations of isotopic equilibria (Clayton et al. 1989, Chiba et al. 1989). Convergence of experimental, theoretical and semi-empirical calibrations (e.g., Clayton et al., 1989; Chiba et al., 1989; Kieffer, 1982; Smyth and Clayton, 1988) increased confidence in the results obtained from their application to natural systems. Finally, calibrations of minerals, through which oxygen diffuses slowly, provided field evidence for the preservation of high temperatures by isotopic thermometers (e.g., Chiba et al., 1989). Chacko (1990) used the observations of Giletti to suggest sampling strategies that could be used to reduce the size of the retrograde effects on isotopic thermometers. Despite these developments, new microanalytical techniques, such as the use of laser fluorination and the

ion probe. have provided ammunition for proponents of retrograde resetting and against isotopic thermometry. In an ion microprobe study of magnetites from the Adirondacks, Valley and Graham (1993) stated:

The implications of the results in this study for oxygen isotope thermometry or for cooling rate speedometry are profound. Even an unusually detailed study of different sized grains by bulk mineral analysis gives only a hint of the shocking heterogeneity seen in 90LP9a [their sample]. The complexity of the  $\delta^{18}\text{O}$  pattern precludes the use of oxygen isotope compositions of 90LP9a magnetites for either thermometry or cooling-rate speedometry.

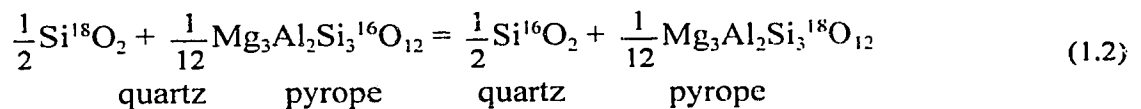
These statements, and others made by Eiler et al. (1992) clearly show that there are problems with some applications of isotopic thermometry. However, the work for this dissertation shows that a clear understanding of the difficulties allow us to avoid them. In 1993, the first parts of this dissertation were published (Farquhar et al., 1993). By using data handling techniques that quantitatively account for retrograde exchange, we outlined a methodology that could be used to improve significantly the usefulness and range of temperature of isotopic thermometry. This dissertation, expands the application of these techniques and investigates the applicability of this methodology in a variety of metamorphic and igneous environments. In so doing, I hope to illustrate that high-temperature isotopic thermometry is a viable and important tool for the study of crustal processes.

### **Theoretical Basis for Isotopic Fractionations**

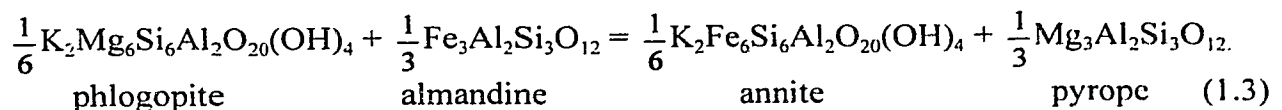
The most important feature of stable isotope geochemistry is, arguably, the temperature dependence of interphase fractionations. Although the statistical mechanical calculations of isotopic fractionations among many gaseous molecules were described before 1947 (e.g., Urey and Grief, 1935), introduction of this concept to the earth sciences has been attributed to Urey (1947) and Bigeleisen and Mayer (1947). These two studies outlined the statistical-mechanics theory for describing these fractionations and discussed their temperature dependence in relation to geological problems. A number of subsequent

papers in the earth sciences have further examined the theoretical underpinnings isotopic exchange (e.g., Bigeleisen, 1958; Stern et al, 1968; Bottinga, 1969; Bottinga and Javoy, 1973; Richet et al., 1977; Kawabe, 1978; Kieffer, 1982; O'Neil, 1986; Criss, 1991). Isotopic fractionations arise because small differences in internal energy accompany isotopic substitutions. Calculations of isotopic fractionations made by Urey and Grief (1935), Urey (1947) and Bigeleisen and Mayer (1947) were for molecular gases. Application of their equations to crystalline solids is more complex because calculations are done on a per atom basis and the quantity over which the terms in the equations are summed equals the number of independent vibrational frequencies ( $3N-6$ , where  $N$  is the number of atoms in the solid). However, the extension of these calculations to crystalline solids was greatly simplified by lattice dynamics approximations (i.e., making the calculations on a per unit cell basis). These approximations are possible because the regularity of the crystalline structure imposes a regularity in the distribution of vibrational modes within the solid (Born and Huang, 1954). Below, I summarize the statistical mechanical basis for isotopic fractionations between molecular gases and the simplifying assumptions made in applying them to crystalline solids.

Isotopic exchange reactions are analogous to cation exchange reactions in the respect that no growth or resorption of phases occurs as a result of reaction progress. The oxygen isotope exchange reaction between quartz and pyrope can be written as



and the  $\text{Fe}^{2+}$  -  $\text{Mg}^{2+}$  cation exchange reaction between garnet and biotite can be written as



Equilibrium constants provide a way of describing the partitioning of isotopes, in the case

of the isotopic exchange reaction, and the partitioning of cations, in the case of the cation exchange reaction. For the isotope exchange reaction (1.2), the equilibrium constant takes the form

$$K = \left( \frac{Q_{(Mg_3Al_2Si_3^{18}O_{12})}}{Q_{(Mg_3Al_2Si_3^{16}O_{12})}} \right)^{\frac{1}{12}} \bigg/ \left( \frac{Q_{(Si^{18}O_2)}}{Q_{(Si^{16}O_2)}} \right)^{\frac{1}{2}} \quad (1.4)$$

where Q refers to the partition function for the molecule. The equilibrium constant for the cation exchange reaction (1.3) takes a similar form

$$K = \left( \frac{a_{(K_2Fe_6Si_6Al_2O_{20}(OH)_4)}}{a_{(K_2Mg_6Si_6Al_2O_{20}(OH)_4)}} \right)^{\frac{1}{6}} \bigg/ \left( \frac{a_{(Fe_3Al_2Si_3O_{12})}}{a_{(Mg_3Al_2Si_3O_{12})}} \right)^{\frac{1}{3}} \quad (1.5)$$

but is written in terms of activities ( $a_p$ ) of phase components ( $p$ ) instead of partition functions (Q) of the molecules. This difference arises because isotopic exchange is described according to statistical mechanical conventions (partition functions and atoms) and cation exchange is described according to thermodynamic conventions (activities and moles). Here, we have written both equilibria in terms of the exchange of one atom between the different phases. One  $^{18}O$  is exchanged for one  $^{16}O$  in the isotopic exchange equation and one Fe is exchanged for one Mg in the cation exchange equation. Isotopic equilibrium constants are most often written on a one atom basis by using  $\alpha$  instead of K to represent the equilibrium constant.  $\alpha$  is related to K by

$$\alpha = K^{1/n_a} \quad (1.6)$$

where  $n_a$  is the number of atoms exchanged in the equilibrium. Because the reaction (1.2) is written on the basis of one atom exchanged, we can write,

$$\alpha = K = \left( \frac{Q^*}{Q} \right)_{\text{pyrope}}^{\frac{1}{12}} \left/ \left( \frac{Q^*}{Q} \right)_{\text{quartz}}^{\frac{1}{2}} \right. \quad (1.7)$$

Here, I use the abbreviated notation for the partition function by using Q to represent the partition function for the light isotope molecule and Q\* to represent the partition function for the heavy isotope molecule. This notation is the convention in isotope literature. One final simplification can be made with respect to  $\alpha$ . Because isotopic substitutions are ideal, we can simplify  $\alpha$  by noting that

$$\alpha = \left( \frac{Q^*}{Q} \right)_{\text{almandine}}^{\frac{1}{12}} \left/ \left( \frac{Q^*}{Q} \right)_{\text{quartz}}^{\frac{1}{2}} \right. = \left( \frac{{}^{18}\text{O}}{{}^{16}\text{O}} \right)_{\text{almandine}} \left/ \left( \frac{{}^{18}\text{O}}{{}^{16}\text{O}} \right)_{\text{quartz}} \right. \quad (1.8)$$

Cation substitutions are not usually ideal, so the simplification to an equation of the form

$$K = \left( \frac{Fe}{Mg} \right)_{\text{biotite}} \left/ \left( \frac{Fe}{Mg} \right)_{\text{garnet}} \right. \quad (1.9)$$

is generally not justifiable, and additional terms such as activity coefficients are introduced to account for the non-ideality of cation substitutions.

There are other similarities between cation exchange reactions and isotopic exchange reactions. The activity of each phase component ( $a_p$ ) in the cation exchange reactions is related to the thermodynamic, chemical-potential energy ( $\mu_p$ ) by

$$\mu_p = RT \ln(a_p) \quad (1.10)$$

which can be solved in terms of activity ( $a_p$ ) to get

$$a_p = e^{-\frac{\mu_p}{RT}} \quad (1.11)$$

The analogous statistical mechanical equation that relates the partition function  $Q$  to internal energy  $E_i$  is

$$Q = \sum_i^{3N-6} g_i e^{-E_i/kT} \quad (1.12)$$

Again, the difference between the thermodynamic equation and this statistical mechanical equation is that the latter is done on a per atom basis ( $N$ ) and uses the corresponding atomic quantity  $k$  (Boltzmann's constant =  $1.381 \times 10^{-16}$  erg/K) instead of the molar quantity  $R$  (the natural gas constant =  $8.31415$  Joules/K). The natural gas constant is related to Boltzmann's constant by Avogadro's number  $N_A$  ( $R = N_A \cdot k$ ). The partition function is calculated by taking a summation over the degrees of freedom ( $3N-6$  of independent states) that are accessible to a given molecule. Because of this, the partition function is also called *sum over states* or *zustandsumme* (e.g., Kieffer and Navrotsky, 1985). The important consequence of Equation (1.12) is that it allows us to calculate values for the partition function from a knowledge of the energy and temperature, only.

To understand why isotopic substitutions change the vibrational energy of the chemical bond, one must first examine the energetics of the chemical bond. Chemical bonds can be described in terms of a potential energy well that is lowest at the ideal bond length, increases as the bond length is decreased because of internuclear repulsive forces and increases as the bond length is increased because of interatomic attractive forces. Molecular vibrations can be thought of as oscillations within the potential well. It is assumed that isotopic substitutions do not change the shape of the potential well because the nuclear charge and electronic configurations are essentially identical for different isotopes of the same element. Equations that model the shape of this well are critical for determining the energy changes that accompany isotopic substitutions. The simplest equations model the potential well as a harmonic oscillator and take the form

$$E_i = \left( n + \frac{1}{2} \right) h\nu_i \quad (1.13)$$



where  $n$  is the quantum state of the bond. The vibrational energy of the bond is determined by the difference between the energy at state ( $n$ ) and the energy defined by the bottom of the potential well. The difference between the bottom of the potential well and the energy at state  $n=0$ , the ground state, is known as the zero point energy. The harmonic oscillator approximation constrains the potential well to a symmetric shape and the zero point energy is given by  $E_0 = h\nu/2$ . Because potential wells for chemical bonds are not symmetric the harmonic oscillator approximation for the chemical bond underestimates the zero point energy. More complex equations that better account for the shape of the potential well and the zero point energy have also been advanced (e.g., the Morse, 1929, Dunham, 1932). Different energy shifts are realized by these equations, and it is important, therefore, to determine whether, these energy differences affect calculated values for isotopic fractionations. It turns out that the most significant contribution of anharmonic models for the potential well is for the zero point energy. Using this as a starting point, Urey (1947) and Richet et al. (1977) use more detailed models to correct the zero point terms and less detailed models (sometimes the harmonic model) to model the higher order vibrational energies. This method is considerably simpler than correcting all terms, and reduces the uncertainty of calculations to that dictated by the (input) spectroscopic data.

In statistical mechanics, the internal energy ( $E_i$ ) is represented by the sum of all forms of energy in the material being studied.

$$E_i = E_{\text{translational}} + E_{\text{zpc}} + E_{\text{rotational}} + E_{\text{vibrational}} + E_{\text{anharmonic}} + E_{\text{rot-vib}} + E_{\text{rot-str}} + E_{\text{electronic}} + \dots \quad (1.14)$$

The first term on the right side of the equation is the energy associated with translations of the molecular center of mass. The next six terms are energy terms associated with atomic bonds within the molecule itself. They are the zero point energy, the energy associated with rotations and vibrations and then three terms associates with the anharmonicity of the rotations and vibrations. Anharmonic vibrations and complex interactions between rotational and vibrational modes are a direct consequence of the asymmetry of the potential wells. These interactions do not occur for perfectly harmonic oscillators. The final term is

the energy associated with the electrons in the system. The contribution of this term is minor at geologically reasonable temperatures because all electrons will be in their ground states (Richet et al., 1977). When these energy terms are put in the exponent of equation (1.12) above to solve for  $Q_{total}$  we get

$$Q_{total} = (Q_{translational})(Q_{zpe})(Q_{rotational})(Q_{vibrational})(Q_{anharmonic})(Q_{rot-vib})(Q_{rot-str})(Q_{electronic}) \dots (1.15)$$

Many calculations of  $Q_{total}$  use only the first four terms in this equation. Some have added the anharmonic terms as well. The last term ( $Q_{electronic}$ ) is generally ignored on the basis that it is difficult to solve (many electrons in the system), the electrons are overwhelmingly in their ground state for all molecules, and the electronic energies are not significantly different for isotopically substituted and unsubstituted molecules in the same energy state. Below, I present a brief outline of the derivation of the isotopic partition function ratio ( $Q^*/Q$ ) for molecular gases that obey the harmonic assumption. I also describe the lattice dynamics methods for applying these equations to crystalline solids.

Solutions for the various terms in the partition function involve substituting the appropriate degeneracy ( $g_i$ ) and energy ( $E_i$ ) terms in to equation (1.12) and taking the sum over all quantum states ( $i$ ) that are accessible to the system. When the quantum states are closely spaced, equation (1.12) can be integrated (e.g., O'Neil, 1976). The energy and degeneracy terms are determined by solving the appropriate Schrödinger equation ( $H\psi = E\psi$ ), where  $H$  is the Hamiltonian operator and  $\psi$  is the wave function. The Hamiltonian operator is a quantum mechanical expression that describes the kinetic and potential energy of all particles in the system (Kieffer and Navrotsky, 1985). By using this technique, various workers have derived the various energy and partition function terms (e.g., Urey, 1947; Bigeleisen and Mayer, 1947; Richet et al., 1977; Kieffer, 1982; O'Neil, 1986). I refer the reader to the listed papers for the appropriate derivations.

By combining all of the harmonic partition function terms for polyatomic molecules to obtain  $Q_{total}^* / Q_{total}$ , we get

$$\frac{Q_{total}^{\cdot}}{Q_{total}} = \underbrace{\left(\frac{M^{\cdot}}{M}\right)^{\frac{3}{2}}}_{translational} \underbrace{\frac{\sigma_A^{\cdot}}{\sigma_A} \left(\frac{I_A^{\cdot} I_B^{\cdot} I_C^{\cdot}}{I_A I_B I_C}\right)^{\frac{1}{2}}}_{rotational} \prod_i^{3N-6} \frac{e^{-h\nu_i^{\cdot}/2kT}}{e^{-h\nu_i/2kT}} \cdot \frac{1 - e^{-h\nu_i/kT}}{1 - e^{-h\nu_i^{\cdot}/kT}} \quad (1.16)$$

This equation is often simplified by using the Teller-Redlich product rule, a theorem that defines the relationship between the moments of inertia and the normal mode frequencies (Urey, 1947; Richet et al., 1977). The Teller-Redlich product rule is

$$\left(\frac{I_A^{\cdot} I_B^{\cdot} I_C^{\cdot}}{I_A I_B I_C}\right)^{\frac{1}{2}} \left(\frac{M^{\cdot}}{M}\right)^{\frac{3}{2}} \left(\frac{m}{m^{\cdot}}\right)^{\frac{3r}{2}} \cdot \prod_i^{3N-6} \frac{\nu_i}{\nu_i^{\cdot}} = 1 \quad (1.17)$$

where  $m$  refers to the mass of the isotopes and  $r$  is the number of exchangeable atoms.  $Q_{total}^{\cdot} / Q_{total}$  then becomes

$$\frac{Q_{total}^{\cdot}}{Q_{total}} = \frac{\sigma_A^{\cdot}}{\sigma_A} \left(\frac{m^{\cdot}}{m}\right)^{\frac{3r}{2}} \prod_i^{3N-6} \frac{\nu_i^{\cdot}}{\nu_i} \cdot \frac{e^{-h\nu_i^{\cdot}/2kT}}{e^{-h\nu_i/2kT}} \cdot \frac{1 - e^{-h\nu_i/kT}}{1 - e^{-h\nu_i^{\cdot}/kT}} \quad (1.18)$$

If an anharmonic approximation for the potential energy curve is used, equations (1.16) and (1.18) will be more complicated because additional terms are introduced and existing terms are adjusted to account for the different energy curves. I refer the reader to the study of Richet et al. (1977) for a discussion of calculations that assume anharmonic potentials. The findings of Richet et al. (1977) suggest that contributions made by anharmonicity of the vibrations are important for making exact calculations, but that they do not change the general trends indicated by equation (1.18).

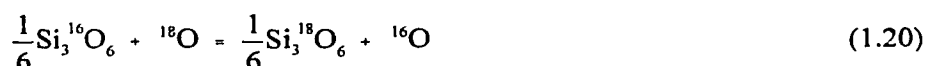
## Crystalline Solids

Strictly speaking, extension of these equations to crystalline solids should be done by assuming that the solids represent one large molecule. This means taking all summations

over  $3N-6$  degrees of freedom, where  $N$  is the number of atoms in the solid under study. In lattice dynamics the calculations are simplified by recognizing that crystalline lattices consist of regularly repeating units (the Bravais or unit cell). The regularity of these cells imposes a vibrational regularity to the crystal (Born and Huang, 1954) and allows us to define a reduced partition function for the unit cell (e.g., Bottinga, 1969; Kawabe, 1978; Kieffer, 1979,1982)

$$f = \frac{Q^{*'}}{Q'} = \frac{Q^*}{Q} \left( \frac{m}{m^*} \right)^{3r/2} \quad (1.19)$$

where  $Q^{*'}$  and  $Q'$  are the partition functions for the unit cell. The reduced partition function thus defined, is analogous to the reduced partition function defined for molecular gases by Urey (1947). The reduced partition functions are also the equilibrium constants between the unit cells of the compounds and the separated atoms of the isotopic element (Urey, 1947; O'Neil, 1986), and can be written like



Note that the chemical formula in the above equation is the chemical formula for the unit cell of quartz ( $\text{Si}_3\text{O}_6$ ). The reduced partition function takes the form

$$\frac{Q_{total}^{*'}}{Q_{total}'} = \frac{\sigma_A^*}{\sigma_A} \prod_i^{3s} \frac{\nu_i^*}{\nu_i} \cdot \frac{e^{-h\nu_i^*/2kT}}{e^{-h\nu_i/2kT}} \cdot \frac{1 - e^{-h\nu_i/kT}}{1 - e^{-h\nu_i^*/kT}} \quad (1.21)$$

The lattice dynamics approximation for the reduced partition function greatly simplifies calculations because the summation is taken over  $3s$  where  $s$  is the number of atoms in the unit cell. The six degrees of freedom from the term  $3N-6$  are not accounted for in the lattice dynamics approximation because they are distributed over the  $N/s$  unit cells that make up the entire crystal. Instead, the  $3s$  degrees of freedom are subdivided into three acoustic modes and  $3s-3$  optic modes.

Calculations of reduced partition function ratios are made from spectroscopic data

by fitting the appropriate vibrational energy equation to spectroscopic data. The parameters determined by this fitting are the unknowns in the equations for the harmonic (or anharmonic) oscillators. Generally, spectroscopic data only exist for compound of the abundant isotope, so spectra for the rare isotopes are calculated with the same equations by using the new isotopic masses and the previously determined constants (see Clayton, 1981 for an example of this calculation). Kieffer (1982) used another strategy that involved identifying the different vibrational modes in mineral spectra (e.g., symmetric Si-O stretching modes, antisymmetric Si-O stretching modes, Si-O bending modes, and etc...), and then adjusting each by a predetermined fixed amount for the isotopically substituted material. Her method of calculation is internally consistent and turns out to be surprisingly accurate (c.f. Clayton et al., 1989; Chiba et al., 1989). Calculations made by using more detailed lattice dynamics models, though more rigorous in principle, have been less successful predictors of isotopic partition functions.

### Temperature Dependence

The temperature dependence of isotopic fractionations has been most thoroughly described by Criss (1991). The derivation that I describe here is identical in most respects to the one made by Criss (1991). The significant difference is that I use the lattice dynamics approximation. The first operation is to take the natural log of equation (1.21),

$$\ln\left(\frac{Q'}{Q}\right) = \ln\left(\frac{\sigma'_A}{\sigma_A}\right) + \ln\prod_i^{3s} \frac{v'_i}{v_i} + \sum_i^{3s} \frac{h(v_i - v'_i)}{2kT} + \ln\prod_i^{3s} \frac{1 - e^{-hv_i/kT}}{1 - e^{-hv'_i/kT}} \quad (1.22)$$

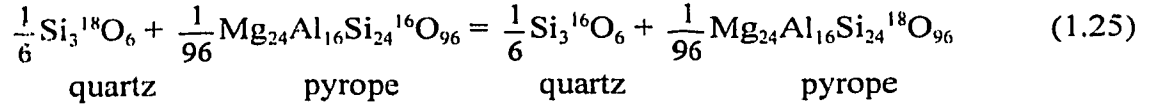
and expand it into a series to get

$$\ln\left(\frac{Q'}{Q}\right) = \ln\left(\frac{\sigma'_A}{\sigma_A}\right) + \ln\prod_i^{3s} \frac{v'_i}{v_i} + \sum_i^{3s} \frac{h(v_i - v'_i)}{2kT} + \left[ \ln\prod_i^{3s} \frac{v'_i}{v_i} + \sum_i^{3s} \left( -\frac{h(v_i - v'_i)}{2kT} + \frac{(hv_i)^2 - (hv'_i)^2}{24(kT)^2} + \frac{(hv_i)^4 - (hv'_i)^4}{2880(kT)^4} + \frac{(hv_i)^6 - (hv'_i)^6}{181440(kT)^6} + \dots \right) \right] \quad (1.23)$$

which simplifies to

$$\ln\left(\frac{Q'}{Q}\right) = \ln\left(\frac{\sigma_A'}{\sigma_A}\right) + \sum_i^{3N} \left( \frac{h^2(v_i'^2 - v_i^2)}{24(kT)^2} + \frac{h^4(v_i'^4 - v_i^4)}{2880(kT)^4} + \frac{h^6(v_i'^6 - v_i^6)}{181440(kT)^6} + \dots \right) \quad (1.24)$$

Rewriting isotope exchange equation (1.2) in terms of lattice dynamics approximation of the unit cells we get



which can be thought of as the exchange reaction between the unit cell of quartz and the unit cell of garnet. The unit cell of quartz contains three SiO<sub>2</sub> formula units and the unit cell of garnet contains 8 Mg<sub>3</sub>Al<sub>2</sub>Si<sub>3</sub>O<sub>12</sub> formula units. This gives us 27 atoms in the unit cell of quartz and 160 atoms in the unit cell of garnet. By writing the exchange reaction in terms of one <sup>18</sup>O exchanged for one <sup>16</sup>O, we get the stoichiometric coefficient 1/6 for the quartz unit cell and 1/96 for the garnet unit cell. The equilibrium constant (α) for this reaction is

$$\alpha = \left( \frac{Q'}{Q} \right)_{\text{pyrope}}^{\frac{1}{96}} \left/ \left( \frac{Q'}{Q} \right)_{\text{quartz}}^{\frac{1}{6}} \right. = \left( \frac{^{18}\text{O}}{^{16}\text{O}} \right)_{\text{pyrope}} \left/ \left( \frac{^{18}\text{O}}{^{16}\text{O}} \right)_{\text{quartz}} \right. \quad (1.26)$$

which can be related to the isotopic equilibrium isotopic fractionation between quartz and garnet by

$$\Delta_{\text{quartz-almandine}} \equiv 1000 \ln \left[ \left( \frac{Q'}{Q} \right)_{\text{almandine}}^{\frac{1}{96}} \left/ \left( \frac{Q'}{Q} \right)_{\text{quartz}}^{\frac{1}{6}} \right. \right] \quad (1.27)$$

By expanding the equation for the isotopic fractionation Δ between the unit cells of quartz and garnet in terms of the series given by equation (1.24) and substituting ω<sub>i,c</sub> for v<sub>i</sub> we get

$$\Delta_{qt-gr} = 1000 \cdot \left( \frac{1}{96} \ln \left( \frac{\sigma_A^*}{\sigma_A} \right)_{gr} + \sum_i^{160} \frac{1}{96} \left( \frac{(hc)^2 (\omega_i^2 - \omega_i'^2)_{gr}}{24(kT)^2} + \frac{(hc)^4 (\omega_i^4 - \omega_i'^4)_{gr}}{2880(kT)^4} + \frac{(hc)^6 (\omega_i^6 - \omega_i'^6)_{gr}}{181440(kT)^6} + \dots \right) \right) \\ - 1000 \cdot \left( \frac{1}{6} \ln \left( \frac{\sigma_A^*}{\sigma_A} \right)_{qt} + \sum_i^{27} \frac{1}{6} \left( \frac{(hc)^2 (\omega_i^2 - \omega_i'^2)_{qt}}{24(kT)^2} + \frac{(hc)^4 (\omega_i^4 - \omega_i'^4)_{qt}}{2880(kT)^4} + \frac{(hc)^6 (\omega_i^6 - \omega_i'^6)_{qt}}{181440(kT)^6} + \dots \right) \right) \quad (1.28)$$

I have introduced the wave numbers ( $\omega$ ) here because spectroscopic data are generally reported in terms of wave number rather than frequency. Bigeleisen (1958) notes that the rotational correction (the  $\ln(\sigma_A^*/\sigma_A)$  term) is negligible except at low temperatures, or for hydrogen fractionations. At high temperatures, this equation simplifies to

$$\Delta_{qt-gr} = 1000 \cdot \left( \frac{1}{96} \sum_i^{160} \left( \frac{(hc)^2 (\omega_i^2 - \omega_i'^2)_{gr}}{24(kT)^2} + \frac{(hc)^4 (\omega_i^4 - \omega_i'^4)_{gr}}{2880(kT)^4} + \frac{(hc)^6 (\omega_i^6 - \omega_i'^6)_{gr}}{181440(kT)^6} + \dots \right) \right) \\ - 1000 \cdot \left( \frac{1}{6} \sum_i^{27} \left( \frac{(hc)^2 (\omega_i^2 - \omega_i'^2)_{qt}}{24(kT)^2} + \frac{(hc)^4 (\omega_i^4 - \omega_i'^4)_{qt}}{2880(kT)^4} + \frac{(hc)^6 (\omega_i^6 - \omega_i'^6)_{qt}}{181440(kT)^6} + \dots \right) \right) \quad (1.29)$$

As temperature increases, the first term in each series becomes the most significant term and the  $1/T^2$  dependence is realized (e.g., Urey, 1947; Bigeleisen and Mayer, 1947; Bigeleisen, 1958; Clayton and Epstein, 1961; Bottinga and Javoy, 1973; Criss, 1991). The temperature corresponding to the onset of the  $1/T^2$  dependence is ultimately decided by our ability to measure isotopic compositions. The total contribution of all terms except the  $(hc)^2 (\omega^2 - \omega'^2)/24(kT)^2$  terms to the equilibrium quartz-garnet fractionation is less than 0.16 ‰ for temperatures above 1100 K (823 °C). This temperature is considerably higher than the traditionally accepted values of approximately 500 °C (Bottinga and Javoy, 1973), or room temperature (Clayton, 1961; O'Neil, 1986).

### **Robustness of $1/T^2$ Dependence and Accuracy and Precision of Theoretical Predictions**

Calculations by Stern et al. (1968) that show dramatic shifts in temperature

dependence for fractionations among polyatomic gases have been used to question the  $1/T^2$  dependence and rarity of crossovers for fractionations involving anhydrous silicates (e.g., O'Neil, 1986; Kyser et al., 1981, 1986; Dunn and Valley, 1991). Kieffer (1982) has argued against this possibility on the basis that the vibrational modes of rock forming silicates vary regularly with polymerization. For anhydrous silicates, none of her calculations deviate significantly from a high-temperature ( $>800$  °C)  $1/T^2$  dependence that converges on an intercept of zero. She does predict minor crossovers for some pairs of structurally dissimilar minerals that fractionate oxygen to a similar degree (e.g., enstatite-anorthite at 325 K), however.

A comment should be made on the accuracy and precision of the different theoretical calculations. Kieffer's calculations have turned out to be surprisingly accurate, which may not be all that surprising when we consider how the uncertainties propagate through the various theoretical calibrations of partition function ratios. Kieffer made several simplifying assumptions in her model that facilitated calculation and also have improved their accuracy and precision. The more rigorous lattice dynamics models turn out to be less precise because they are limited by our understanding of interatomic forces and, possibly, anharmonicity (Kieffer, 1979a). In Kieffer's calculations, the wave numbers of each mode are treated separately and the uncertainties are not compounded as readily. This, however, also makes rigorous determination of uncertainties for her calculations more difficult. She places an estimate on the uncertainty of her calculated partition functions at 298 K of 2 ‰ for structurally dissimilar phases and 1 ‰ for structurally similar phases. This compares with uncertainties in calculated partition function ratios at 298 K of 2.6 ‰ for Richet et al. (1977) and 7-10‰ for Kawabe (1978). For our purposes, we are not interested in uncertainties at 298 K, but at 1000 K.

It is relatively easy to see that the uncertainties exhibit a temperature dependence by integrating equation (1.24). If we write a simplified version of this equation in terms of the Kieffer model we get



$$\ln\left(\frac{Q''}{Q'}\right) = \ln\left(\frac{\sigma_A}{\sigma_A}\right) + \sum_i^{3S} \left( \frac{(hc)^2(1-y_i^2)\omega_i^2}{24(kT)^2} + \frac{(hc)^4(1-y_i^4)\omega_i^4}{2880(kT)^4} + \frac{(hc)^6(1-y_i^6)\omega_i^6}{181440(kT)^6} + \dots \right) \quad (1.30)$$

where  $(\omega_i = y_i \cdot \omega)$  and  $y_i$  refers to Kieffer's semi-empirical shift factor for the wave number. Taking the derivative of this equation with respect to the uncertainties in the wave numbers, but keeping all other terms constant, we get

$$d\ln\left(\frac{Q''}{Q'}\right) = \sum_i^{3S} \left( \frac{2 \cdot (hc)^2(1-y_i^2)\omega_i}{24(kT)^2} + \frac{4 \cdot (hc)^4(1-y_i^4)\omega_i^3}{2880(kT)^4} + \frac{6 \cdot (hc)^6(1-y_i^6)\omega_i^5}{181440(kT)^6} + \dots \right) d\omega_i \quad (1.31)$$

When we take its derivative with respect to the term  $y_i$ , but keeping all other terms constant, we get

$$d\ln\left(\frac{Q''}{Q'}\right) = \sum_i^{3S} \left( \frac{2 \cdot (hc)^2(1-y_i)\omega_i^2}{24(kT)^2} + \frac{4 \cdot (hc)^4(1-y_i^3)\omega_i^4}{2880(kT)^4} + \frac{6 \cdot (hc)^6(1-y_i^5)\omega_i^6}{181440(kT)^6} + \dots \right) dy_i \quad (1.32)$$

For error propagation we substitute both of these equations into an equation of the form

$$\sigma_{\ln(Q''/Q')}^2 = \sigma_{\omega_i}^2 \cdot \left( \frac{d(\ln(Q''/Q'))}{d(\omega_i)} \right)_{y_i}^2 + \sigma_{y_i}^2 \cdot \left( \frac{d(\ln(Q''/Q'))}{d(y_i)} \right)_{\omega_i}^2 \quad (1.33)$$

which gives us an equation of the form

$$\sigma_{\ln(Q''/Q')}^2 = \sum_i^{3S} \sum_{n=2}^{\infty} \left[ \frac{B_n^2 (hc/kT)^{2n}}{n!^2} \left( y_i^{n-1} \cdot \omega_i^n \cdot \sigma_{y_i} \right)^2 + \frac{B_n^2 (hc/kT)^{2n}}{n!^2} \left( (1-y_i)^n \cdot \omega_i^{n-1} \cdot \sigma_{\omega_i} \right)^2 \right] \quad (1.34)$$

(Term A) (Term B)

where  $B_n$  refers to Bernoulli number. I have used the notation with Bernoulli numbers (Bigeleisen, 1958; Criss, 1991) because it allows me to write this equation on one line through a simpler representation of the series. From equation (1.34) we see that the uncertainties for calculated values of  $\ln(Q''/Q')$  decrease as a function of  $1/T^2$  at high temperatures. Note that the functional dependence of  $\ln(Q''/Q')$  on temperature is different

from the functional dependence of  $\sigma_{\ln(Q^*/Q)}$  on temperature so the temperatures that are high enough to give a  $1/T^2$  dependence for  $\ln Q^*/Q$  may not be high enough to give a  $1/T^2$  dependence for  $\sigma_{\ln Q^*/Q}$ . Because I do not have values for the uncertainties ( $\sigma_{y_i}$ ,  $\sigma_{\omega_i}$ ), I have evaluated *Term A* and *Term B* separately, and without their respective uncertainties ( $\sigma_{y_i}$ ,  $\sigma_{\omega_i}$ ). I used the input data for quartz from Kieffer (1982). The first six non-zero terms in the series  $n=2-\infty$  of *Term A* (without  $\sigma_{y_i}^2$ ), converge to within 10% of a stable value at 298 K. This value decreases by approximately an order of magnitude as temperature increases to 1000 K. The first six non-zero terms of *Term B* (without  $\sigma_{\omega_i}^2$ ), do not converge to within 10% of a stable value for temperatures less than approximately 400 K. *Term B* decreases approximately a factor of five between 400 and 1000 K. Kieffer's estimates for the uncertainties are of 1-2 ‰ at 298 K. Uncertainties on Kieffer's partition functions are, therefore, significantly smaller at 1000 K. This may in part explain the excellent agreement between her theoretical calibrations and the experimental calibrations of (Clayton et al., 1989, Chiba et al., 1989 and Rosenbaum et al., 1994). Calculations of uncertainties for more rigorous lattice dynamics models are more complex because they must consider fitting parameters for the force constants (see equation 16 of Kawabe, 1978). Nevertheless, the same decrease in the size of the uncertainties is observed for calculations made at higher temperatures (e.g., Richet et al., 1977; Kawabe, 1978).

## Summary

I have gone into more detail in describing the basis for isotopic fractionations than may have seemed necessary. The point that I hope to have made is that the theory of isotopic fractionations is well understood and conclusions about the temperature dependence of isotopic fractionations are well grounded in this theory. It is, therefore, extremely unlikely that high-temperature isotopic fractionations between anhydrous silicate minerals will deviate significantly from a  $1/T^2$  dependence that converges to zero as  $1/T^2 \rightarrow 0$ . This conclusion may also be applicable to high temperature isotopic fractionations involving hydrous silicates but will depend strongly on the weighting factor for the O-H interactions

which do not obey a  $1/T^2$  dependence until temperatures exceed approximately 3000 to 4000 K. Recent experimental and theoretical studies suggest that hydrous minerals also obey this  $1/T^2$  relationship (Chacko et al., in press)

The rest of this dissertation will focus on applying isotopic thermometers to metamorphic and igneous rocks. The goal will be to integrate constraints imposed by the temperature dependence of isotopic fractionations with those imposed by mass balance to account quantitatively for retrograde exchange. In so doing, I approach the problem of retrograde exchange from the opposite direction from those that use microsampling and diffusion constraints (e.g., Gilotti, 1986; Eiler et al, 1992). The methods developed in this dissertation are more closely akin to data handling techniques than they are to forward modelling techniques. As such, I avoid a priori assumptions about the exchange mechanisms and rates, but I do make assumptions about equilibrium and mass balance. I assume that equilibrium applies to the minerals in my rocks, and I assume that the mass balance determined from point counting is representative of the mass balance that operated throughout the thermal histories of the rocks (closed system and no net transfer reactions). When my models fail, I reassess my initial assumptions and gain insight into the possible causes for isotopic disequilibrium in my samples. When the model succeeds, it can be coupled with other textural and chemical data to obtain significant insights about "physically real" aspects of the mechanics of isotopic exchange in the samples under study. The data handling techniques described herein, are an extremely sensitive and powerful tool for the isotope geochemist and can be used to assess a wide variety of open and closed system processes. The ultimate goal in developing them, however, is to provide insight into the thermal history of the crust by using isotopic thermometry. This goal has been achieved and its methodology and results are outlined in the succeeding chapters.

## **Chapter 2:**

### **Isotopic Thermometry: Principles and Methods**

#### **Introduction**

Successful isotope thermometry requires a knowledge of the magnitude of isotopic fractionations between coexisting phases and a means of obtaining precise isotope composition data. Analytical techniques for obtaining precise isotopic composition data are well established (e.g., McCrea, 1950; Silverman, 1952; Taylor and Epstein, 1962; Clayton and Mayeda, 1963). Although both equilibrium and kinetic processes can fractionate isotopes, we assume that isotopic fractionation in high-temperature igneous and metamorphic environments obey an equilibrium fractionation law. By starting with accurate calibrations of isotopic equilibria and precise isotopic composition data, we should, in principle, be able to obtain important insights into the thermal conditions of crustal processes.

Natural observations, theoretical considerations, and experiments, all compose the basis for calibrations of equilibrium isotopic fractionation laws. The use of field observations to model equilibria is often complicated by non-equilibrium processes which can introduce regular and systematic isotopic variations that can mimic equilibrium (Deines, 1977; Gilotti, 1986). Consequently, empirical methods may integrate systematic secondary processes into the calibration. I outlined the theoretical framework for the existence, temperature dependence and calibration of isotopic fractionations in the last chapter. Theoretical considerations provide our best constraints on the temperature dependence of isotopic fractionations because this dependence arises primarily from the well-understood physics of molecular vibrations (Urey, 1947; Bigeleisen and Mayer, 1947; Bigeleisen, 1958; Criss, 1991). Theoretical calibrations, however, are poor indicators of the absolute values of these fractionations because they are very sensitive to the input spectroscopic data (e.g., Richet et al., 1977; Kawabe, 1978; O'Neill, 1986; Clayton et al., 1989; Chiba et al., 1989; Clayton and Kieffer, 1991). Experimental calibrations have the opposite problem. They provide our best constraints on the values of isotopic fractionations, but do not easily

extrapolate beyond the experimental conditions (e.g., Clayton et al., 1989; Chiba et al., 1989; Clayton and Kieffer, 1991). By using experiments to anchor theoretical curves, we obtain a calibration that is accurate for the temperature interval of the experiments and accurately extrapolated beyond it. Most experimental calibrations of isotopic equilibria are grounded in theory (e.g., Clayton et al., 1989; Chiba et al., 1989), so some extrapolation is possible, but very few, use experiments to anchor spectroscopically constrained theoretical curves (c.f., Clayton and Kieffer, 1991). This latter method provides our best calibrations for isotopic thermometers. In this study, I have chosen experimental, theoretical and semi-empirical calibrations of the University of Chicago Group (e.g., Smyth and Clayton, 1988; Clayton et al., 1989; Chiba et al., 1989; Clayton and Kieffer, 1991; Chacko et al., in press) and Kieffer (1982) because these presently are highest quality published calibrations.

The use of calibrated equilibria to interpret field observations is simple in principle but turns out to be complicated in practice. Many strategies exist for handling isotopic data to obtain temperature information. In this chapter, I focus on the three techniques that warrant the most attention. The first technique involves using the fractionations between two minerals as a direct measure of temperature. It is the conventional way to obtain mineral temperatures, and has been used since the studies of Clayton and Epstein (1958, 1961). The second method is more holistic (e.g., Farquhar et al., 1993, 1994) in that it involves combining mass balance constraints with equilibrium constraints to account quantitatively for the effects of retrograde exchange. With this technique one can calculate the temperatures at which minerals in a rock obtained their present day isotopic compositions. These are the mineral closure temperatures. The third technique is an extension of the second. It also combines mass balance and equilibrium constraints, but extends the calculations to multiple samples. The third strategy allows retrieval of geologically meaningful temperature data for temperature conditions that are higher than the closure temperature of the highest closing phases. At the time that I began this research, I was only aware of a few studies that used similar data handling techniques (e.g., Anderson 1966, 1968; Taylor, 1968). All of the methods described by these studies rely on analysis of graphical trends in isotopic data. The present techniques differ from these in the respect that they quantify compositional and mass

balance constraints. At the time of writing this dissertation, a fourth study (Krylov, 1986 (written in Russian); Krylov and Mineev, 1994) came to my attention. Krylov's methods also incorporate composition and mass balance constraints; however, there remain significant differences and refinements that are present only in the techniques that I describe herein.

### **Apparent Temperatures: Mineral-Pair isotopic thermometry**

Giletti (1986) defines apparent isotopic temperatures as the temperatures given by mineral-pair isotopic fractionations. The temperatures are apparent because the isotopic composition of each mineral used in the temperature determination, is more than just a record of simple two-mineral equilibrium. In perfect equilibrium, only one permutation of compositions can occur. Giletti realized that many natural systems did not preserve equilibrium fractionations because of systematic retrograde resetting processes. This occurs because different minerals exchange oxygen at different rates. Therefore, at certain temperature conditions some minerals cannot effectively exchange oxygen with the rest of the rock while others can. It is this property called 'closure' that makes isotopic thermometry possible. If isotopic exchange did not 'close', then isotopic thermometry would not work. On the other hand, because minerals 'close' at different temperatures, the isotopic fractionation between two minerals reflects not one, but two uniquely different equilibrium and exchange histories. Giletti was the first to enumerate the consequences of closure temperatures for isotopic thermometry. For quartz + hornblende + feldspar rocks, Giletti (1986) showed that apparent temperatures given by quartz-hornblende and feldspar-hornblende shift systematically because of quartz-feldspar exchange that occurs after hornblende closes. The situation becomes more complex as more minerals are added to the rock. In slowly cooled rocks, the temperatures indicated by mineral-pair isotopic fractionations in multi-mineral rocks, therefore, do not correspond to geologically real temperatures. Nonetheless, apparent isotopic temperatures can provide important insight into crustal temperature conditions. This important insight stemmed from Giletti's perspective that was rooted in diffusion and exchange and extended to mass balance and equilibrium.

To calculate apparent mineral-pair isotopic temperatures, we solve an equation that describes isotopic equilibrium as a function of temperature. For example

$$\Delta_{ij} = \frac{10^6 A_{ij}}{T^2} \quad (2.1)$$

describes the equilibrium fractionation ( $\Delta_{ij}$ ) between two phases,  $i$  and  $j$ , as a function of temperature (Clayton and Epstein, 1961).  $A_{ij}$  is the temperature coefficient of the fractionation factor. The solution of equation (2.1) in terms of temperature ( $^{\circ}\text{C}$ ) is

$$T(^{\circ}\text{C}) = \left( \frac{10^6 A_{ij}}{\Delta_{ij}} \right)^{1/2} - 273 \quad (2.2)$$

### Uncertainties for mineral-pair thermometry

We calculate the temperature uncertainty by taking the derivatives of all terms in equation (2.2) with respect to temperature. These include

$$\left( \frac{\partial(T(^{\circ}\text{C}))}{\partial(A_{ij})} \right)_{\Delta_{ij}} = \left( \frac{10^6}{4 \cdot \Delta_{ij} A_{ij}} \right)^{1/2} \quad (2.3)$$

$$\left( \frac{\partial(T(^{\circ}\text{C}))}{\partial(\Delta_{ij})} \right)_{A_{ij}} = \left( \frac{-10^6 A_{ij}}{4 \cdot \Delta_{ij}^3} \right)^{1/2} \quad (2.4)$$

Equation 2.4 can be expanded by noting

$$\left( \frac{\partial(\Delta_{ij})}{\partial(\delta_i)} \right)_{\delta_j} = \frac{1000}{1000 + \delta_i} \quad (2.5)$$

$$\left( \frac{\partial(\Delta_{ij})}{\partial(\delta_j)} \right)_{\delta_i} = -\frac{1000}{1000 + \delta_j} \quad (2.6)$$

to give us

$$\left( \frac{\partial(T(^{\circ}C))}{\partial(\delta_j)} \right)_{A_{ij}, \delta_i} = \left( \frac{-A_{ij}}{4 \cdot 1000 \left( \ln \frac{1000 + \delta_i}{1000 + \delta_j} \right)^3} \right)^{1/2} \left( -\frac{1000}{1000 + \delta_j} \right) \quad (2.7)$$

$$\left( \frac{\partial(T(^{\circ}C))}{\partial(\delta_i)} \right)_{A_{ij}, \delta_j} = \left( \frac{-A_{ij}}{4 \cdot 1000 \left( \ln \frac{1000 + \delta_i}{1000 + \delta_j} \right)^3} \right)^{1/2} \left( \frac{1000}{1000 + \delta_i} \right) \quad (2.8)$$

These partial derivatives can then be substituted into the standard error propagation equation (e.g., Bevington, 1969),

$$\sigma_T^2 = \sigma_{\delta_j}^2 \cdot \left( \frac{\partial(T(^{\circ}C))}{\partial(\delta_j)} \right)_{A_{ij}, \delta_i}^2 + \sigma_{\delta_i}^2 \cdot \left( \frac{\partial(T(^{\circ}C))}{\partial(\delta_i)} \right)_{A_{ij}, \delta_j}^2 + \sigma_{A_{ij}}^2 \cdot \left( \frac{\partial(T(^{\circ}C))}{\partial(A_{ij})} \right)_{\delta_i, \delta_j}^2 \quad (2.9)$$

to get

$$\sigma_T^2 = \left[ \frac{1000 A_{ij}}{4 \cdot \left( \ln \frac{1000 + \delta_i}{1000 + \delta_j} \right)^3} \right] \cdot \left[ \frac{\sigma_{\delta_j}^2}{(1000 + \delta_j)^2} + \frac{\sigma_{\delta_i}^2}{(1000 + \delta_i)^2} + \frac{\sigma_{A_{ij}}^2 \left( \ln \frac{1000 + \delta_i}{1000 + \delta_j} \right)^2}{A_{ij}^2} \right] \quad (2.10)$$

This equation is very useful because it provides an estimate of the temperature uncertainties for mineral-pair isotopic thermometry. By using this equation we assume that temperature uncertainties follow a normal distribution about the mean. Because of the  $T^{-2}$  dependence



of the equilibrium constant, the distribution of temperature uncertainties is asymmetric (skewed). I have undertaken over thirty Monte Carlo simulations to investigate the conditions for which equation 2.10 is valid. The variables that control the asymmetry are  $\sigma_{\Delta_{ij}}/\Delta_{ij}$  and  $\sigma_{A_{ij}}/A_{ij}$ .  $\sigma_{\Delta_{ij}}/\Delta_{ij}$  contributes to the asymmetry by positively skewing the distribution of temperature uncertainties, and  $\sigma_{A_{ij}}/A_{ij}$  contributes negative skewness to the distribution of temperature uncertainties. This behavior arises because T depends on  $1/\sqrt{\Delta_{ij}}$  and  $\sqrt{A_{ij}}$ , respectively. The net effect of equation 2.10 overestimates the size of uncertainties on the low-temperature side and underestimates the size of the uncertainties on the high-temperature side when  $\Delta_{ij}$  is small and to do the opposite when  $A_{ij}$  is small. Because the reciprocal dependence of temperature on the  $\sqrt{\Delta_{ij}}$  term defines an asymptotic relationship between temperature and  $\Delta_{ij}$ , the  $\sigma_{\Delta_{ij}}/\Delta_{ij}$  term contributes more to the asymmetry of the temperature uncertainties than does the  $\sigma_{A_{ij}}/A_{ij}$  term. For most geological problems, the contribution of both terms to asymmetry is minor and skewness is positive. Asymmetry generally contributes less than 5% of the underestimation (or overestimation) of one-sigma uncertainties that are lower than  $\pm 50^\circ\text{C}$  (less than 10% for  $\pm 100^\circ\text{C}$ ). In this thesis I use equation (2.10) to estimate temperature uncertainties for mineral pair thermometers like (2.2). For other temperature equations (e.g., Clayton and Kieffer, 1992), uncertainty estimates are determined by Monte Carlo techniques.

Equation (2.10) provides an important constraint for mineral-pair isotopic thermometry. One sign of a good thermometer is a low associated temperature-uncertainty. Equation (2.10) shows that mineral pairs with large  $A_{ij}$  will make isotopic thermometers with the lowest temperature uncertainties. Another obvious consequence of equation (2.10) is that temperature uncertainties will be lowest for the most precise measurements of isotopic compositions ( $\delta_i$  or  $\delta_j$ ). The standard error of the mean ( $\sigma_{\bar{x}_n} = \sigma_i/\sqrt{n}$ ), where  $n$  is the number of analyses, rewards us if we are diligent analysts. In order to determine the real standard error, we must have a large enough population to determine the real uncertainties. Because it is impractical to analyze statistically significant populations for each mineral, in this study we determine the standard error on the basis of an assumed analytical uncertainty. The mean of four repeat analyses of a single sample yields a value with a standard error one half that

of each analysis that it comprises. Repeat analyses are essential for high precision isotopic thermometry.

### **Optimization of mineral-pair thermometry**

The logical extension of Gilletti's work is to invert his model for describing isotopic equilibration, so that the best samples for mineral-pair isotopic thermometry can be selected. Chacko (1990) suggested that the 'best' samples for isotopic thermometry are those that are bi-mineralic and contain at least one high-closing phase. Figure 2.1 provides the basis for his arguments. Gilletti (1986) was the first to contour the surface of apparent-temperatures in modal space and to illustrate its functional dependence on mineral modes, closure temperatures and equilibrium fractionation behavior. Chacko (1990) seized on the important implications that the shape of the surface of apparent temperatures held for isotopic thermometry. He noted that the best samples for quartz-mineral isotopic thermometry were those that contain a high modal abundance of quartz because during retrograde reequilibration, mass balance forces the quartz "to retain or nearly retain its high-temperature isotopic composition." He also noted that the closure temperature of the highest closing phase would ultimately establish the upper temperature limits intersected by the surface of apparent temperatures in modal space (compare figure 2.1a with 2.1b). Chacko (1990) suggests that the best mineral pairs for isotopic thermometry will include quartz-pyroxene, quartz-garnet, and quartz-rutile.

Eiler et al. (1992) refined the parameters that describe intragranular exchange and thereby extended Gilletti's model. By including grain boundaries in the equation for mineral closure, Eiler et al. (1992) showed that retrograde exchange between the grain boundaries of slow diffusers and the rest of the rock should reduce both the apparent isotopic temperatures and the closure temperatures of minerals in the rock. Lower closure temperatures result when the proportion of slow diffuser present as grain boundary material is high and the proportion of fast diffusers in the rock are low. For these rocks, mass balance dictates that the isotopic composition of low abundance fast diffusers shift to accommodate

equilibrium. Note that the isotopic composition of the slow diffuser does not measurably change, but that the fractionation between the slow diffuser and the fast diffusers does. By describing this process, Eiler et al. (1992) redefined the surface that describes apparent isotopic temperatures (fig 2.2), and imposed an important qualification to the Chacko (1990) sampling strategies. Sampling should focus not only on samples with a high proportion of the fast diffuser, quartz, but with a low proportion of the slow diffuser.

### **Single Sample Model Temperatures: Mineral-Closure Temperatures**

Giletti (1986) and Eiler et al. (1992) showed that it was possible to define surfaces of mineral-pair apparent temperatures from modal data, mineral closure data and equilibrium constraints. It is also possible to define surfaces of closure temperatures for all of these minerals in modal space. The closure surface arises because apparent temperatures, modal abundances and mineral closure temperatures are all functionally interrelated. Neither Giletti (1986) nor Eiler et al. (1992) represented their results in terms of mineral closure surfaces. We define closure temperatures as the temperature corresponding to the fractionation between the mineral of interest and the exchanging phases in the rock. This definition is independent of the processes by which closure occurs. In contrast, Dodson-closure temperatures and Eiler et al.-closure temperatures describe a physical/mathematical model of the process that controls closure, but not the closure temperature itself. Minerals can remain open to exchange well below their diffusional (Dodson, 1973 or Eiler et al., 1992) closure temperature by processes such as dynamic and chemical recrystallization (e.g., Hoffbauer et al., 1994; Farquhar et al., 1994; Farquhar and Chacko, 1994). In these cases, when granular recrystallization ceases, the minerals cease to exchange with the rest of the rock. They 'close' to exchange by processes other than those described by the models of Dodson and Eiler. Despite the particular process, the functional dependence between the closure temperatures, the modes, and the apparent mineral temperatures will exist. I have calculated the closure surfaces corresponding to the surfaces of apparent temperatures given by Giletti (1986), Chacko (1990) and Eiler et al. (1992) in figure 2.3a, b, and c. None of the

input data have changed, just the type of information retrieved from the data has changed. The methods used for these calculations are described shortly. The important questions then become: How can we calculate these temperatures from isotopic and modal data? What are the uncertainties on these calculations? What are the implications for isotopic thermometry? Below, I outline the answers to each of these questions in detail.

### **Calculation of mineral-closure temperatures**

One approach to calculating mineral-closure temperatures is through detailed accounting of isotope exchange trajectories. Isotope exchange trajectories (IETs) are the trajectories in isotopic composition space defined by equilibrium, temperature and mass balance constraints. Isotope exchange trajectories are, in every respect, like the 'feasible reaction spaces' defined by J.B. Thompson (1982). The methods that I use to calculate isotope exchange trajectories are analogous to those described by Gregory and coworkers in their evaluation of open vs. closed system behavior (Gregory and Criss, 1986; Criss et al., 1987). Though the equations are similar to those used by Gregory and coworkers, I have refined the assumptions about mineral equilibrium and exchange to allow for mineral-closure temperatures. These refinements allow us to evaluate mineral closure temperatures in closed systems. We calculate mineral-closure temperatures by solving the isotope exchange trajectory for the measured isotopic composition of the mineral.

Below I outline the derivation of isotope exchange trajectories for isotopic equilibria that can be described by equation (2.1),

$$\Delta_y = 1000 \ln \frac{1000 + \delta_i}{1000 + \delta_j} = \frac{10^6 A_y}{T^2} \quad (2.1a)$$

At this point, I want to stress that other equations for isotopic equilibrium, can be used to derive isotopic exchange trajectories, but that the derivations are increasingly complex and that the calculated IETs are not significantly different. By adding the mass balance constraint,

$$\delta_{system} = \sum_i^{phases} X_i \delta_i \quad (2.11)$$

where  $\delta_{system}$  is the isotopic composition of the system at equilibrium,  $\delta_i$  and  $X_i$  refer to the isotopic composition and the fraction of oxygen (mole%) contained by phase  $i$  in the system over which equilibrium applies. Combining equations (2.1a) and (2.11) and imposing the constraint that the equilibrium system consists only of exchanging phases (*e.p.*), we get

$$\delta_j = \frac{\sum_i^{e.p.} X_i \delta_i - 1000 \cdot \sum_i^{e.p.} X_i \cdot (e^{1000A_{ij}/T^2} - 1)}{\sum_i^{e.p.} X_i e^{1000A_{ij}/T^2}} \quad (2.12)$$

which describes the isotopic composition of phase  $j$  as a function of the system isotopic composition and temperature. Summations are taken over exchanging phases  $i=e.p.$ , and include  $i=j$ . The variation of  $\delta_j$  with temperature defines the isotopic exchange trajectory of phase  $j$ . The isotopic exchange trajectory of phase  $j$  is defined both by changes in temperature and changes in the modal abundances of exchanging phases ( $X_i$ ). The ability of each phase to maintain equilibrium with the rest of the system, decides whether it composed part of the mode of exchanging phases ( $X_i$ ). The isotopic exchange trajectory of mineral  $j$  changes, therefore, as a function of temperature and as a function of the exchanging-system mass balance. The isotopic composition of phase  $j$  becomes fixed when it closes with respect to the exchanging system.

Calculation of isotope exchange trajectories requires isotopic composition and modal data for each phase in the rock, the fractionation factors between all phases, and, in some cases, insight into the closure order for phases in the rock. Commonly, the calculations will yield a single permutation of model temperatures that satisfies the data. When this is not so, we need information about the closure order to choose the correct set of model temperatures.

The 'alternate' permutations that satisfy the data, however, often give results that are geologically unreasonable (e.g., model temperatures  $>1000\text{ }^{\circ}\text{C}$  or  $<100\text{ }^{\circ}\text{C}$  for one or more phases). When the closed system assumption and the closure order are correct, the model temperatures *correspond* to the mineral closure temperatures. In this study, I have assumed that these are correct (i.e., that I have calculated valid closure temperatures), but I have been careful to describe in detail, my reasons for choosing one permutation of closure temperatures over another.

A sample calculation of closure temperatures for a closed system consisting of plagioclase, olivine, ilmenite and magnetite is presented schematically in figure 2.4 and table 2.1. At infinite temperature, the isotopic composition of all minerals is the same and equal to the isotopic composition of the whole rock ( $\delta^{18}\text{O}_{\text{syn}} = 7.2\text{‰}$ ). We start the calculation at some high temperature with the assumption that all phases in the rock are open to exchange. We calculate the model temperature for the highest closing phase (e.g. phase 1) by solving for the intersection of the calculated IET with the measured isotopic composition of that phase. In this case, phase 1 is ilmenite and its closure temperature is  $1023\text{ }^{\circ}\text{C}$ . For model calculations involving phases that close at lower temperatures, we recalculate mass balance to compensate for the closed phase (new  $\delta^{18}\text{O}_{\text{syn}} = 7.31\text{‰}$ ), and obtain the closure temperature for the next closing phase (e.g., phase 2, olivine) by solving for the next IET- $\delta^{18}\text{O}$  intersection ( $810\text{ }^{\circ}\text{C}$ ). We repeat this procedure to calculate the closure temperatures for all remaining phases (phases 3 and 4). The closure temperatures for the final two phases are identical because the closure temperature is, itself, a measure of the exchange *between* these phases. When the exchange couple closes, both phases in it close as well. In this case, the closure temperatures for plagioclase and magnetite (phases 3 and 4) are both  $718\text{ }^{\circ}\text{C}$ .

The representation and calculation of isotope exchange trajectories in figure 2.4 and Table 2.1 makes two implicit approximations. First, by representing isotopic equilibrium with equation 2.1a, we constrain the IETs to straight lines in  $\delta^{18}\text{O}-1/T^2$  space. Both the modal abundances and the fractionation factors, control the slope of these straight-line IETS. If isotopic equilibrium were represented by more rigorous calibrations in these calculations, the IETs would be slightly curved. On this plot, the degree of curvature would be

imperceptible above the olivine closure temperature and only slightly perceptible between the olivine closure temperature and the closure of the plagioclase-magnetite couple.

We make a second approximation by representing mineral closure on these diagrams as an instantaneous phenomenon. In reality, there is never a single temperature at which a whole mineral ceases to exchange oxygen with the rest of the system. Mineral closure occurs because of processes such as diffusion that progressively limit exchange over a range of temperatures. Calculations made on the basis of Dodson (1986) suggest that the temperature interval over which minerals close to exchange, spans many 10's of degrees. The diffusion model of Eiler et al. (1992) and calculations of Jenkin et al. (1994) show that more complex models predict similar closure intervals. No models formulated to date, describe closure intervals for systems where processes other than volume-diffusion moderate exchange. There is no reason to believe that mineral closure should be instantaneous in systems where mineral closure occurs by other mechanisms (e.g., dynamic recrystallization). By consequence of a closure interval rather than a discrete closure temperature, real IETs and the calculated IETs do not track along the same curves. The real IETs will track along curves that cut the corners that define the calculated IETs at closure temperatures (figure 2.5). The IETs cut corners because the closure process is not instantaneous; the grain cores close before the grain rims, and the bulk isotopic composition tracks a trajectory that reflects the integrated closure history of the grain. This does not change the conclusion that the model temperatures for closed systems are the mineral closure temperatures. It illustrates, however, that the closure temperature represents the mass weighted average of the temperatures that define the closure intervals. It also highlights the independence of the present methods from the possibly unjustifiable assumption that volume diffusion is the only process for mineral closure.

We can simplify the procedure for obtaining model temperatures by using the definition of the closure temperatures. Because the closure temperature is the equilibrium temperature given by the fractionation between the phase of interest  $j$  and the rest of the rock, we can insert the terms

$$\delta_{e,p} = \sum_{i=j}^{e,p} X_i \delta_i \quad (2.13)$$

$$A_{e,p.-j} = \sum_{i=j}^{e,p} X_i A_{ij} \quad (2.14)$$

into equation 2.1 to get

$$T [^{\circ}C] = \left[ \frac{10^6 \sum_{i=j}^{e,p} X_i A_{ij}}{1000 \ln \frac{1000 + \sum_{i=j}^{e,p} X_i \delta_i}{1000 + \delta_j}} \right]^{1/2} - 273 \quad (2.15)$$

Equivalent expressions can be derived by solving for temperature in equation (2.12), but the derivation is more involved.

### Uncertainties for mineral closure temperatures

Uncertainties for single sample model temperatures come from several sources. The principal sources include uncertainties in  $X_i$  and  $\delta_i$ . They are most easily visualized by considering the angle produced by the intersection between the IETs and the isotopic composition of the phase of interest. The magnitude of the fractionation factor between the exchanging phases and the phase of interest (equation 2.14), controls this angle of intersection. When  $A_{e,p.-j}$  is small, temperature uncertainties are very large because of low-angle intersections on  $\delta^{18}O$  vs.  $1/T^2$  plots, whereas a large  $A_{e,p.-j}$  leads to a high-angle intersection and correspondingly smaller uncertainties. An explicit equation for closure temperature uncertainties, derived in the same way as equation 2.10, is



$$\begin{aligned}
\sigma_T^2 = & \left[ \frac{1000 A_{e.p.-j}}{4 \cdot \left( \ln \frac{1000 + \delta_{e.p.}}{1000 + \delta_j} \right)^3} \right] \cdot \left[ \frac{\sigma_{\delta_j}^2}{(1000 + \delta_j)^2} + \frac{\sum_{i \neq j}^{e.p.} X_i^2 \sigma_{\delta_i}^2}{(1000 + \delta_{e.p.})^2} + \frac{\sum_{i \neq j}^{e.p.} X_i^2 \sigma_{A_i}^2 \left( \ln \frac{1000 + \delta_{e.p.}}{1000 + \delta_j} \right)^2}{A_{ij}^2} \right] \\
& + \sum_{i \neq j}^{e.p.} \left[ \frac{\delta_i \sigma_{X_i}}{1000 + \delta_{e.p.}} - \frac{1000 A_{ij} \sigma_{X_i}}{1000 A_{e.p.-j}} \ln \frac{1000 + \delta_{e.p.}}{1000 + \delta_j} \right]^2 \\
& + \sum_{k \neq l, j}^{e.p.} \left[ \sum_{i \neq j}^{e.p.} \frac{\delta_i \rho_{kl} \sigma_{X_i}}{1000 + \delta_{e.p.}} - \frac{1000 \rho_{kl} A_{ij} \sigma_{X_i}}{1000 A_{e.p.-j}} \ln \frac{1000 + \delta_{e.p.}}{1000 + \delta_j} \right] \left[ \frac{\delta_k \sigma_{X_k}}{1000 + \delta_{e.p.}} - \frac{1000 A_{kj} \sigma_{X_k}}{1000 A_{e.p.-j}} \ln \frac{1000 + \delta_{e.p.}}{1000 + \delta_j} \right]
\end{aligned} \tag{2.16}$$

Monte Carlo simulations of uncertainty for equation 2.15 show here, as they did for equation (2.10), that the uncertainty envelope is asymmetric. Equation (2.16) slightly underestimates temperature uncertainties on the high temperature side and slightly overestimates uncertainties on the low temperature side. Values for the correlation coefficients ( $\rho$ ) of the covariance terms ( $X_i X_k$ ) are generally negative (Chayes, 1971). Consequently, they reduce the uncertainty by a small amount (approx. 5-15%). Calculations that ignore these terms will, therefore, overestimate uncertainties. Calculations made in this dissertation use equation (2.16) and ignore the covariance terms.

### Optimization of Mineral Closure Temperature Data

Uncertainties calculated with equation (2.16) for many natural samples are generally reasonable ( $\pm 50$  to  $\pm 100$  °C). Consideration of the primary source of uncertainty, however, highlights the importance of sample selection. Samples should be selected for large  $A_{e.p.-j}$  and at least one high-closing phase in low modal abundance. To be high-closing, minerals must have (a) low oxygen diffusivity, (b) high resistance to chemical recrystallization (exsolution and retrogression) and (c) high resistance to deformational recrystallization (subgrain formation and migration). Inert, slow diffusers with large  $A_{e.p.-j}$  that undergo granulation rather than recrystallization, are our best candidates for this type of isotopic thermometry. Because this method uses isotopic and modal data for all minerals, careful

petrographic examination of thin sections should be done to refine sample selection. It is also advised that the calculated closure temperatures for the same mineral in different samples be compared. Checks of this sort provide a very sensitive monitor of open-system and other types of complications. The validity and uses for comparisons of mineral closure temperatures from different samples will be discussed in more detail in the next chapter.

The importance of this methodology for isotopic thermometry studies is difficult to appreciate without considering the importance of retrograde exchange effects in mineral-pair isotopic thermometry. Figure 2.3 illustrates the mineral closure temperatures that we obtain for hornblende by using equation (2.15) and the same data as contoured by Giletti (1986), Chacko, (1990) and Eiler et al. (1992). The closure surfaces defined by equation (2.15) are significantly less sensitive to changes in modal abundance than are those for mineral-pair temperatures. Moreover, the closure surfaces defined by this equation delimit significantly larger fields of usable samples for high-temperature isotopic thermometry (Figure 2.3). The same equilibrium and closed system assumptions apply to both types of temperature data and the uncertainties are not significantly larger for the closure surface. The significance of this methodology, therefore, is that it requires less stringent sampling strategies while providing more accurate results than mineral-pair thermometry. This is because equation (2.15) quantitatively accounts for retrograde exchange between low closing phases that occurs after closure of the high closing phase.

### **System Closure Temperatures**

We can extend these methods to examine equilibrium between different samples from the same outcrop and, possibly, different samples from different outcrops. Application to multiple samples relies on the premise that, at high-temperatures, isotopic equilibrium can occur over a large area, typically on the scale of meters or larger. We define the closure temperature of this larger system ( $T_{c,ys}$ ) as the temperature given by the fractionation between two hand samples. This temperature will fall within the range over which exchange through diffusive and/or advective processes cease to maintain isotopic equilibrium within

the system. The important feature of such a system for our purposes, is that at temperatures above  $T_{c_{sys}}$ , the isotopic composition of each phase is the same everywhere within the system. Once the system cools below  $T_{c_{sys}}$ , isotopic equilibration takes place within smaller scale subsystems. The minerals in each of these subsystems evolve along their own isotopic exchange trajectories. The mode, mineral pair fractionations and closure sequence determine these IETs. The numerical method described below reads through isotopic exchange within the subsystems to calculate  $T_{c_{sys}}$ . The advantage of this technique over mineral-pair and mineral-closure thermometry is that it provides a way of recovering temperatures above the closure temperature of the highest closing phase. The disadvantage is that it requires more stringent preconditions.

The prerequisites for a valid calculation of  $T_{c_{sys}}$  are most likely realized in isothermal portions of magma bodies. Large-scale isotopic equilibrium can come about because isotopic exchange through the magma is rapid. Minerals crystallized from two coexisting melts are likely to be in equilibrium with each other, when there exists an effective means of communication. The establishment of a closure temperature for the system requires a significant decrease in the scale of equilibrium. For melt-bearing systems the decrease in scale might correspond to the crystallization of a grain boundary melt. For melt-absent systems, this might correspond to the disappearance of a grain boundary fluid. A detailed discussion of the possible scenarios that might fulfill the preconditions for application of the multiple sample method is beyond the scope of the present discussion.

$T_{c_{sys}}$  is given by the intersection between the IET's of one mineral from two or more samples (Figure 2.6). We calculate the IETs of a particular mineral by using equation (2.12). The intersection of the two trajectories gives  $T_{c_{sys}}$ . IETs from additional samples should, in principle, give the same intersection. The tightness of intersections obtained from three or more samples, provides a check on the validity of the assumptions made in formulating the model. An explicit equation for this intersection temperature is

$$T [^{\circ}C] = \left[ \frac{10^6 \left( \sum_i^{phases} X_{1i} A_{ij} - \sum_i^{phases} X_{2i} A_{ij} \right)}{1000 \ln \frac{1000 + \sum_i^{phases} X_{1i} \delta_{1i}}{1000 + \sum_i^{phases} X_{2i} \delta_{2i}}} \right]^{1/2} - 273 \quad (2.17)$$

where  $X_{1i}$  and  $X_{2i}$  represent the molar fraction of oxygen contained by mineral  $i$  in samples 1 and 2, respectively.

### Uncertainties for multiple sample thermometry

Uncertainties for multiple sample model temperatures ( $T_{c,yy}$ ) arise from the same sources as those for the single sample model temperatures (i.e., uncertainties associated with the position of the IETs and compounded uncertainties arising from the angle of intersection of the IETs). To derive an explicit equation for evaluating uncertainties on the multiple sample method, it is convenient to define the terms

$$\delta_{w.r.} = \sum_i^{phases} X_i \delta_i \quad (2.18)$$

and

$$A_{w.r.-j} = \sum_i^{phases} X_i A_{ij} \quad (2.19)$$

where  $\delta_{w.r.}$  and  $A_{w.r.-j}$  are the isotopic composition of and the temperature coefficient of the fractionation factor for the whole rock sample ( $w.r.$ ). Using these terms, the explicit equation for uncertainties on the multiple sample method is

$$\begin{aligned}
\sigma_T^2 = & \left[ \frac{1000 (A_{w,r,1} - A_{w,r,2})}{4 \cdot \left( \ln \frac{1000 \cdot \delta_{w,r,1}}{1000 \cdot \delta_{w,r,2}} \right)^3} \right] \left[ \frac{\sum_i^{p_{w,r,2}} X_{2i}^2 \sigma_{X_{2i}}^2}{(1000 \cdot \delta_{w,r,2})^2} \cdot \frac{\sum_i^{p_{w,r,1}} X_{1i}^2 \sigma_{X_{1i}}^2}{(1000 \cdot \delta_{w,r,1})^2} \cdot \frac{\sum_i^{phases} (X_{1i} - X_{2i})^2 \sigma_{A_i}^2 \left( \ln \frac{1000 \cdot \delta_{w,r,1}}{1000 \cdot \delta_{w,r,2}} \right)^2}{(A_{w,r,1} - A_{w,r,2})^2} \right] \quad (2.20) \\
& \cdot \sum_i^{phases} \left[ \frac{\delta_{1i} \sigma_{X_{1i}}}{1000 \cdot \delta_{w,r,1}} - \frac{1000 A_{1i} \sigma_{X_{1i}}}{1000 (A_{w,r,1} - A_{w,r,2})} \ln \frac{1000 \cdot \delta_{w,r,1}}{1000 \cdot \delta_{w,r,2}} \right]^2 \cdot \sum_i^{phases} \left[ \frac{\delta_{2i} \sigma_{X_{2i}}}{1000 \cdot \delta_{w,r,2}} - \frac{1000 A_{2i} \sigma_{X_{2i}}}{1000 (A_{w,r,1} - A_{w,r,2})} \ln \frac{1000 \cdot \delta_{w,r,1}}{1000 \cdot \delta_{w,r,2}} \right]^2 \\
& \cdot \sum_{i=1}^{phases} \left[ \sum_i^{phases} \frac{\delta_{1i} \rho_{1ib} \sigma_{X_{1i}}}{1000 \cdot \delta_{w,r,1}} - \frac{1000 \rho_{1ib} A_{1i} \sigma_{X_{1i}}}{1000 (A_{w,r,1} - A_{w,r,2})} \ln \frac{1000 \cdot \delta_{w,r,1}}{1000 \cdot \delta_{w,r,2}} \right] \left[ \frac{\delta_{1i} \sigma_{X_{1i}}}{1000 \cdot \delta_{w,r,1}} - \frac{1000 A_{1i} \sigma_{X_{1i}}}{1000 (A_{w,r,1} - A_{w,r,2})} \ln \frac{1000 \cdot \delta_{w,r,1}}{1000 \cdot \delta_{w,r,2}} \right] \\
& \cdot \sum_{i=1}^{phases} \left[ \sum_i^{phases} \frac{\delta_{2i} \rho_{2ib} \sigma_{X_{2i}}}{1000 \cdot \delta_{w,r,2}} - \frac{1000 \rho_{2ib} A_{2i} \sigma_{X_{2i}}}{1000 (A_{w,r,1} - A_{w,r,2})} \ln \frac{1000 \cdot \delta_{w,r,1}}{1000 \cdot \delta_{w,r,2}} \right] \left[ \frac{\delta_{2i} \sigma_{X_{2i}}}{1000 \cdot \delta_{w,r,2}} - \frac{1000 A_{2i} \sigma_{X_{2i}}}{1000 (A_{w,r,1} - A_{w,r,2})} \ln \frac{1000 \cdot \delta_{w,r,1}}{1000 \cdot \delta_{w,r,2}} \right]
\end{aligned}$$

Monte Carlo simulations of uncertainty for equation (2.20) show the same trends as are observed for mineral-pair and mineral-closure temperature determinations (i.e., asymmetry). Calculations of uncertainties for multiple sample methods in this dissertation use equation 2.20 and ignore the covariance terms. As discussed previously, the resulting determinations of uncertainty will slightly overestimate the actual uncertainty and will not portray the asymmetry that exists. Nevertheless, these modifications are minor for applicable multiple sample thermometers at most geologic temperature conditions.

### Optimization of multiple sample thermometry

Because they provide the highest-angle intersections, the best samples for multiple sample thermometry are those that have widely different modes and  $A_{w,r,j}$ . These samples are likely to be found where silicate-oxide, silicate-carbonate or silicate-silicate liquid immiscibility has occurred, where primary igneous layering is preserved, where xenoliths or restite are included in plutonic rocks, and where primary compositional layering is preserved in metamorphic rocks. Commonly, however, the assumption of large-scale high-temperature equilibrium is unjustified. Because the different rock types may each have their own specific origin, regular and systematic isotopic fractionations also pose a particularly vexing contingency. To test the robustness of multiple sample temperatures, more than one pair of samples should be examined. Moreover, the mineral closure temperatures of the

same minerals from these samples should be compared and evaluated in terms of mechanistically-constrained models of isotopic exchange and mineral closure. When isotopic and modal data violate the criteria for closed system, hand-sample-scale equilibrium, large-scale equilibrium is not an option. Krylov and Mineev. (1994) violate these criteria in their study of multiple-sample model temperatures. The requirement of large-scale equilibria, will likely only be met in rocks produced by silicate-oxide and other types of liquid immiscibility. The multiple sample methods is important, however, because it can be used to gain insight into the highest-temperature parts of the thermal history of some igneous systems.

## Summary

The use of oxygen isotope data for the purposes of geologic thermometry of slowly cooled rocks, can take many forms. Mineral-pair isotopic thermometry, except in the case of bi-mineralic rocks, is always complicated by retrograde exchange involving at least one phase in the thermometer. These apparent isotopic temperatures do not correspond to the equilibrium temperature, or the closure temperature for all but the two lowest closing phases in the rock. They represent the temperatures given by the fractionation between two minerals in the same rock. They are complicated because each mineral has its own retrograde exchange history. Insight into temperature conditions can, however, be obtained by careful selection of mineral pairs and samples. Mineral pairs should be selected to give small temperature-uncertainties (large  $A_{ij}$ ). Samples should be selected with a high proportion of the fast diffusing mineral and a low modal proportion of the slow diffusing mineral (Chacko, 1990; Eiler et al., 1992, 1993). The best samples will be bi-mineralic with a low modal proportion of the slow diffuser. The maximum recoverable temperatures from bi-mineralic samples are limited only by the closure temperature of the slow diffuser. For samples with more than two minerals, mineral-pair temperatures will always be complicated by the effects

of retrograde exchange among minerals with low closure temperatures.

Determination of mineral closure temperature data can be made by combining modal data with isotopic and equilibrium fractionation data. The numerical methods used to calculate mineral closure temperatures are premised on the calculation of isotope exchange trajectories of minerals in rocks that have behaved as closed systems on the hand-sample scale during cooling. The sample requirements for use of these techniques are similar to those for conventional isotopic thermometry, a large proportion of fast diffusing minerals and the presence of one or more slow diffusing minerals, but the sample requirements are more relaxed, because more than one fast diffuser can be present in the rock. Precision is maximized if there is a large isotopic fractionation between the fast and slow diffusing minerals. This method gives the closure temperature of the slow diffusing mineral, and possibly an estimate of peak temperature attained by the rock. The distinct advantage of this method over conventional thermometry is that it gives consistent results for a wider range of samples.

The multiple sample method provides a means of obtaining temperatures higher than the closure temperatures of constituent minerals. The multiple sample method provides an estimate of the temperature at which two samples were in equilibrium with each other, the system closure temperatures ( $T_{c,sys}$ ). This method gives best results in samples of widely different modal compositions containing minerals that partition  $^{18}O$  to very different degrees. Unlike the mineral-pair or mineral-closure temperature isotopic thermometers, the multiple sample method does not require the presence of a slow diffusing mineral.

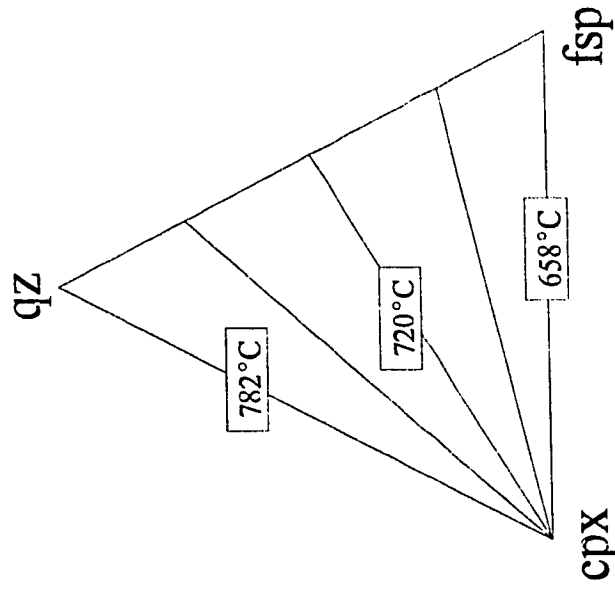
A remaining question is the applicability of these methods to rocks from different geologic environments. One potential limitation is the availability of samples with the characteristics necessary for this type of work. My experience in a number of metamorphic and igneous environments suggests that these samples are widespread. They have largely been ignored because their high variance mineral assemblages have a limited value in conventional cation thermobarometry. A second concern is the general applicability of the assumptions made in formulating the numerical models. The assumptions associated with the single-sample method are no different than those implicit in mineral-pair thermometry,

namely the establishment of isotopic equilibrium between minerals on the hand-sample scale at high temperatures and closed-system behavior during cooling. Therefore, this method is as applicable as mineral-pair thermometry to igneous and metamorphic rocks. However, the assumption of large-scale isotopic equilibration between minerals that is inherent to the multiple sample method may only be appropriate in melt-bearing systems. If this is the case, the maximum temperatures retrievable with isotopic thermometry will be those given by the mineral-pair and mineral-closure temperature methods, and limited only by the closure temperature of the highest-closing phase.

The temperatures obtained with the methods that employ mass balance, are different from the apparent mineral-pair temperatures reported in the literature. Although slightly less precise, the mineral-closure and system-closure temperatures are considerably more accurate because they quantitatively account for retrograde exchange. Because these methods require reconciliation of isotopic data from all minerals in one or more samples, however, they turn out to be much more sensitive measures of the anchoring assumptions and the validity of the temperature data than conventional mineral-pair thermometry. In the next chapter, I will describe the ways that this sensitivity can be used to assess these assumptions for all types of thermometry.



Qtz-cpx apparent temperatures  
after Chacko (1990)



Qtz-hbl apparent temperatures  
after Gilletti (1986)

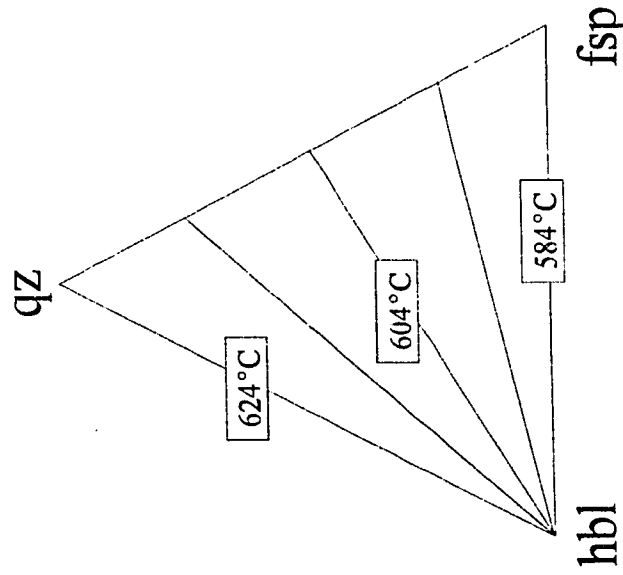


Figure 2.1 surfaces of apparent quartz hornblende and quartz-clinopyroxene temperatures after Gilletti (1986). Same parameters as Gilletti (1986).

Mineral-pair temperature data after Eiler, Baumgartner, and Valley (1992)

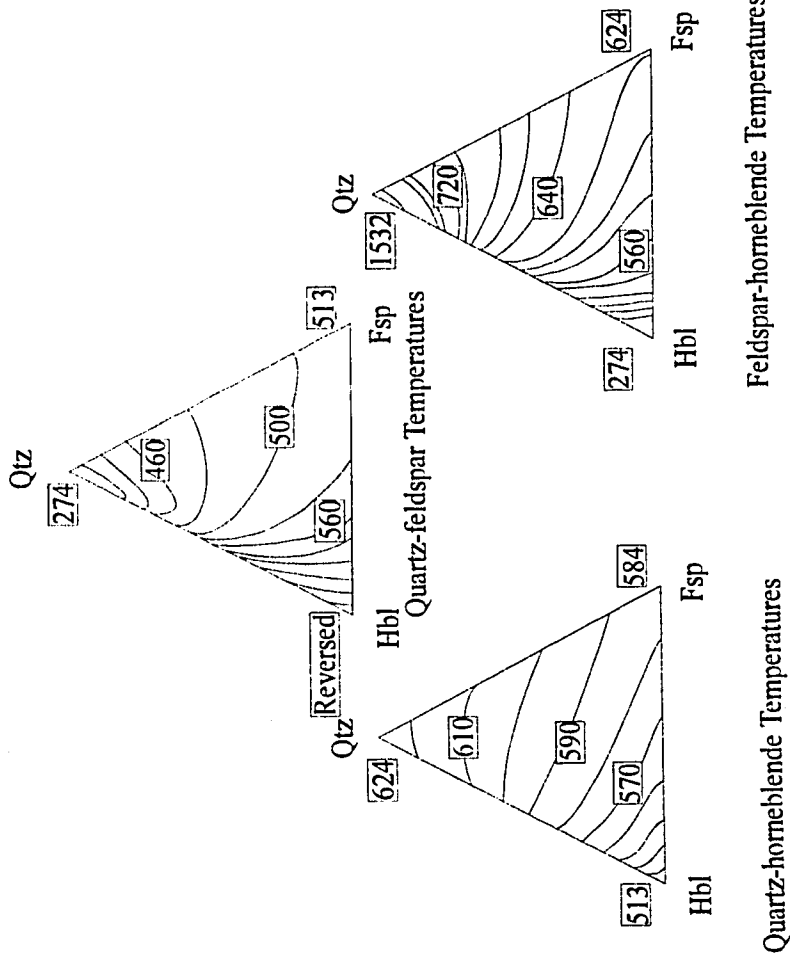


Figure 2.2 Apparent mineral pair closure temperatures after Eiler et al. (1992) See Text for Discussion.

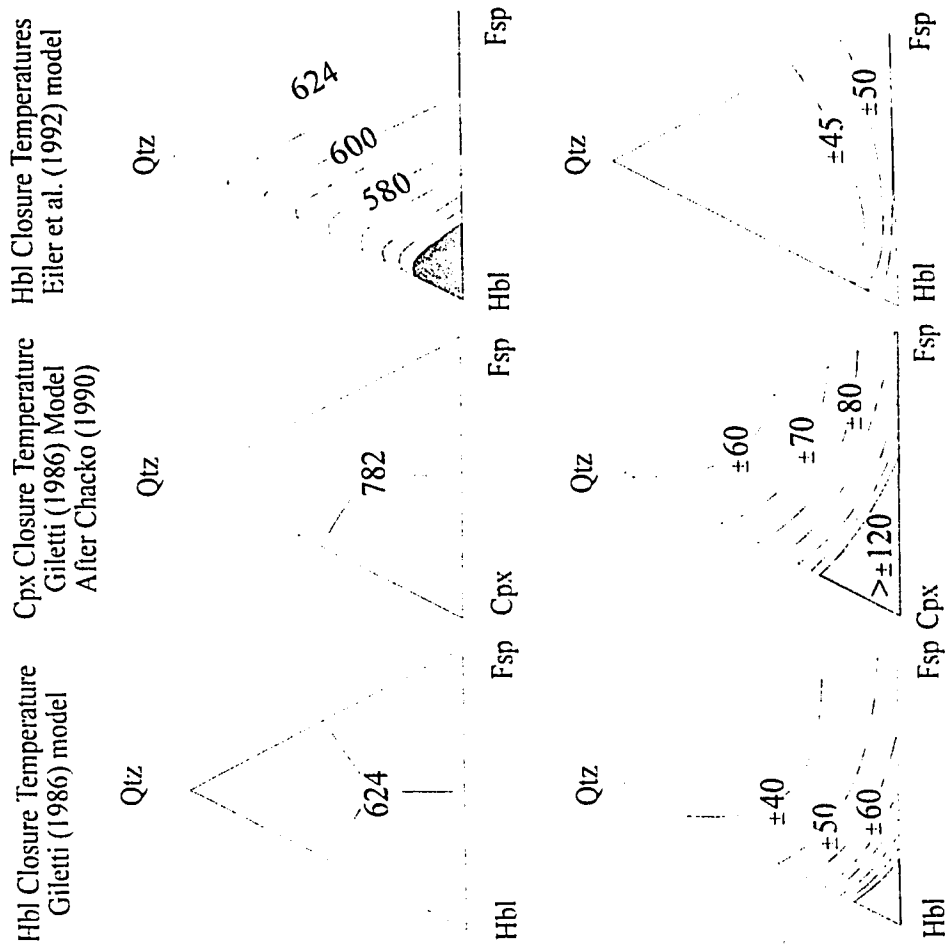


Figure 2.3 Closure temperatures (and uncertainties) for the high closing phases hornblende and clinopyroxene (contoured in °C).

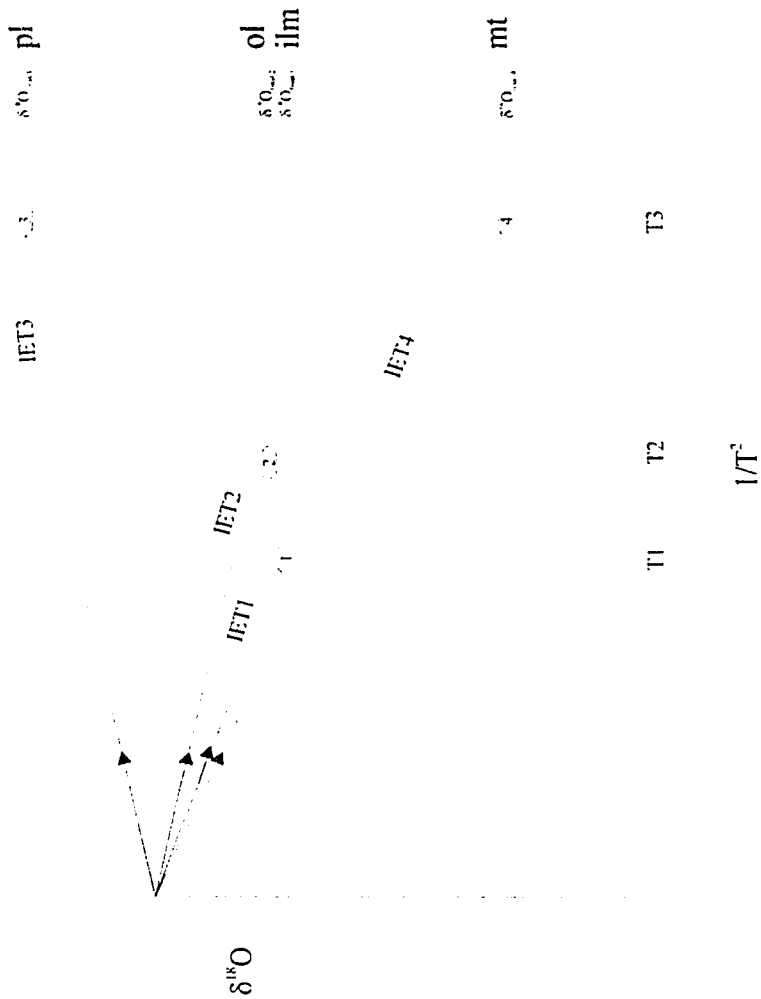


Figure 2.4 Evolution diagram for a 4 mineral rock. Minerals follow trajectories that evolve from left to right. See text for discussion.

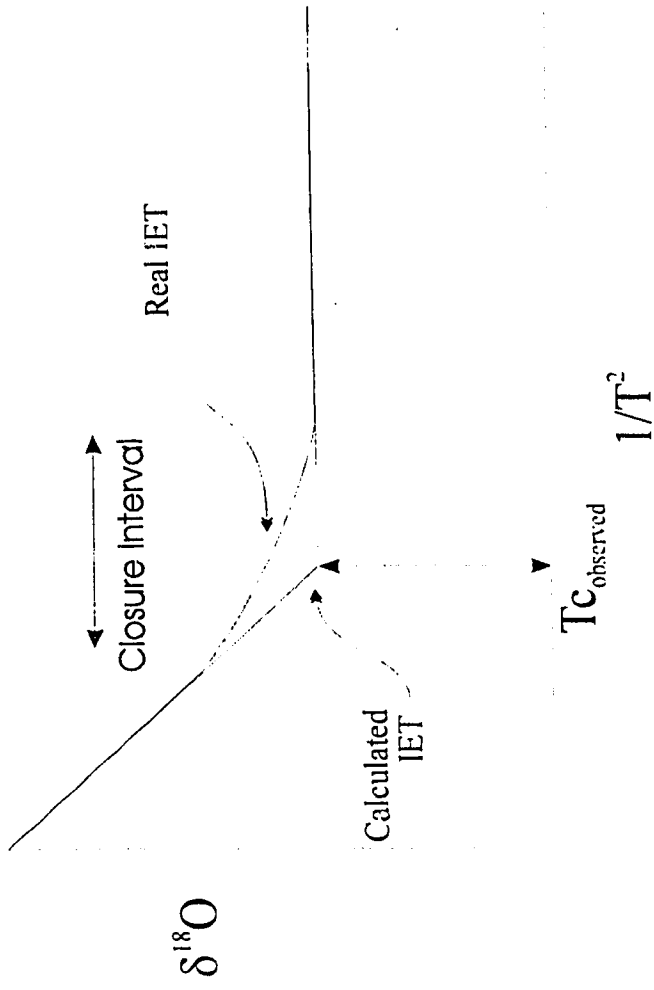


Figure 2.5 Schematic diagram of real IET versus calculated closure temperature.

High-Temperature equilibrium  
 $(\delta^{18}O_{\text{minl,rock 1}} = \delta^{18}O_{\text{minl,rock 2}})$   
 $T_{c,\text{sys}}$

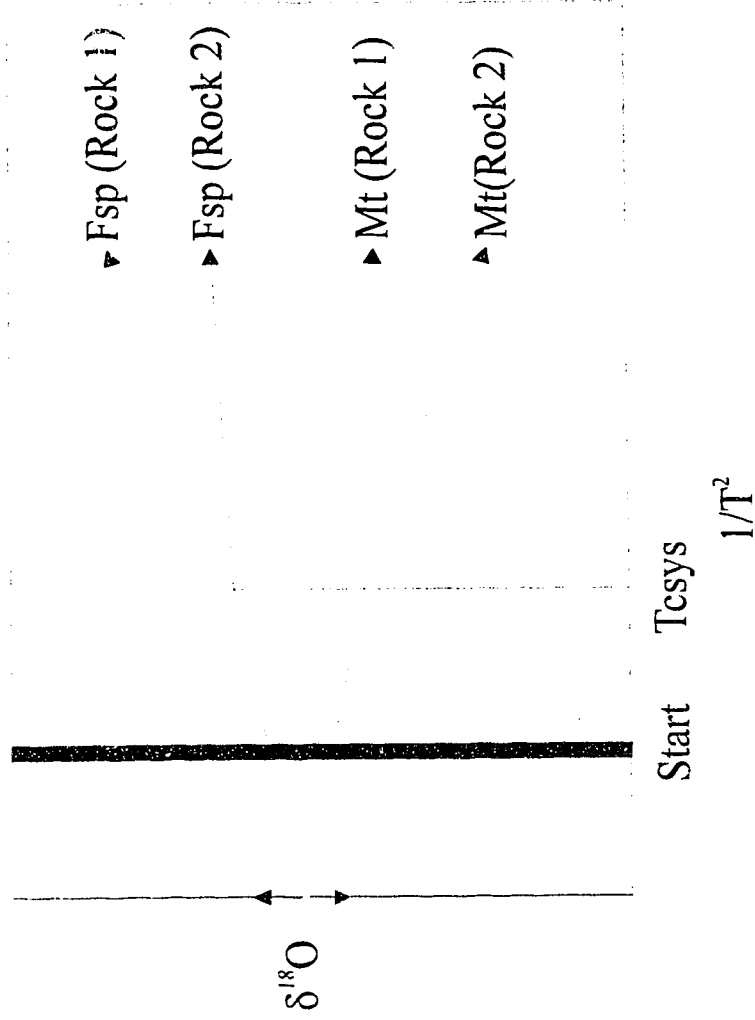


Figure 2.6 Schematic representation of the establishment of  $T_{c,\text{sys}}$ . Large scale equilibrium breaks into two equilibration volumes (See text).

Table 2.1

Table 2.1 Sample Calculation of Closure Temperatures

Mineral	Plagioclase	Olivine	Ilmenite	Magnetite
$A_{\text{mineral-ilmenite}}$	4.60 ‰	2.34 ‰	0.00 ‰	-0.28 ‰
$X_i$	70.0 %	20.0 %	5.0 %	5.0 %
Infinite Temperature to Closure of Ilmenite (1023 °C) $\delta^{18}\text{O}_{\text{c.p.}} = 7.2 \text{ ‰}$				
Calculated values when Ilmenite Closes (1023 °C)				
$\delta^{18}\text{O}$	7.38 ‰	6.39 ‰	5.00 ‰	4.83 ‰
$X_i$	73.7 %	21.1 %	0.0 %	5.3 %
Closure of Ilmenite (1023 °C) to Closure of Olivine (810 °C) $\delta^{18}\text{O}_{\text{c.p.}} = 7.31 \text{ ‰}$				
Calculated values when Olivine Closes (810 °C)				
$\delta^{18}\text{O}$	7.93 ‰	6.00 ‰	5.00 ‰	3.76 ‰
$X_i$	93.3 %	0.0 %	0.0 %	6.7 %
Closure of Olivine (810 °C) to Closure of Plagioclase & Magnetite (718 °C)				
$\delta^{18}\text{O}_{\text{c.p.}} = 7.66 \text{ ‰}$				
Calculated values when Plagioclase-Magnetite Exchange-Couple Closes (718 °C)				
$\delta^{18}\text{O}$	8.00 ‰	6.00 ‰	5.00 ‰	3.00 ‰
$X_i$	0.0 %	0.0 %	0.0 %	0.0 %
Closure of Plagioclase-Magnetite Exchange-Couple (718 °C) to 298 °C $\delta^{18}\text{O}_{\text{c.p.}} =$				
0.00 ‰				

## Chapter 3:

### Assumptions and Checks for Model Temperature Equations

#### Introduction

The data handling techniques described in the previous chapter implicitly assume that equilibrium and mass balance are the governing parameters for isotope distribution in nature. Many arguments exist to support the idea that equilibrium is established in high-temperature igneous and metamorphic environments. Experimentally determined fractionation factors are in excellent agreement with theoretical treatments of isotopic equilibria, suggesting that a reasonable approach to equilibrium can be attained for many mineral systems on laboratory time scales. Experimental data indicates oxygen diffusion rates at metamorphic and igneous temperatures, are sufficiently high to allow attainment of isotopic equilibrium for most minerals on metamorphic time-scales by volume diffusion processes alone. For example, the characteristic length-scale for diffusion of oxygen in quartz ( $\sqrt{DT}$ ) is about 2 mm 745 °C for 10 Ma (calculated by using "dry" diffusion data of Sharp et al., 1991), and studies that combine microanalytical techniques with detailed reaction progress calculations (e.g., Kohn et al. 1993; Young and Rumble, 1993) suggest that the isotopic composition systematics of slow diffusers that grow during prograde metamorphism is consistent with equilibrium fractionation processes. Agreement between model temperature data (mineral and system closure temperatures) and petrogenetic constraints is also consistent with equilibrium fractionation processes. Because these are consistency arguments, we cannot unambiguously dismiss either kinetic, surface controlled, or other non-equilibrium fractionation processes. We can argue from the above observations, however, that their contribution to isotopic fractionations in moderate to high temperature metamorphic and igneous environments is generally minor.

The governing assumption for my data handling techniques, therefore, is mass balance. The formulation of temperature equations in chapter 2 includes assumptions about measurement of mass balance, lack of interaction with external reservoirs, and attainment



of equilibrium. If we violate these assumptions, the conclusions about temperature conditions are invalid. In this chapter, I examine these assumptions in detail and provide a means of assessing their validity. This chapter contains two parts. In the first part, I focus on the concept of an equilibration volume. The equilibration volume is the volume over which retrograde exchange occurs. By obtaining mass balance constraints from mineral mode, we implicitly assume that the measured mode characterizes the volume over which equilibrium applies. In heterogeneous rocks (e.g., layered igneous and metamorphic rocks), uncertainties associated with the scale of the equilibration volume complicate measurements of mass balance. For instance, to what extent do the different parts of the rock interact? Do the leucosomes and melanosomes in a migmatite, impart some, or all of their mass balance to the mesosome? How constant was this length-scale during the metamorphic history of the sample under study? In this section, I show how my methods can be optimized to provide insight into the equilibration volume problem. The second part examines the closed-system assumption. Open system complications are a special case of the equilibration volume problem. In open systems, we lack the composition and mass balance constraints for at least one phase, often a late fluid phase. In this part of the chapter, I focus on means and methodologies for detecting and characterizing the effects of late metamorphic and igneous fluid phases. While the open system complications are in principle similar to the equilibration volume problems, the treatment of the data is different because late open system interactions can be discrete events that affect only the low closing phases. The mode of the solid fraction of the rock is assumed to be constant, and the variables are the isotopic compositions of the fast diffusers (and bulk rock). By determining the isotopic shifts of the fast diffusers, we can gain significant insight into the parameters that define the open system. Because each mineral in the rock closes to exchange with the rest of the system over a particular temperature interval, these techniques can also provide insight into the temperature conditions of fluid rock interactions. In the final part of the chapter, I present a methodology for sample collection and data interpretation that maximizes one's chances of obtaining geologically meaningful temperature data and can be used to reduce the complications introduced by assumptions made in their calculation.

## The Equilibration Volume

The idea of an equilibration volume was first elaborated by Anderson (1967) in his paper, "The dimensions of oxygen equilibrium attainment during prograde metamorphism." He notes that the oxygen isotopic compositions of any mineral must be uniform within an equilibrium system. He outlines a method where measuring "the dimension over which the oxygen isotopic composition of some convenient, common mineral remains constant, within analytical error," is used as an upper limit on the equilibration volume. He notes that

correlation[s] between the modal abundance of quartz and its oxygen isotopic composition . . . indicates that oxygen has been at least locally exchanged on a grain size (millimeter) scale, . . . [but that]. . . oxygen isotopic equilibrium attainment during prograde metamorphism is commonly limited to dimensions less than meters and may generally be limited to dimensions less than centimeters.

Shieh and Taylor (1969) examine the equilibration volume by making isotopic traverses in contact metamorphic rocks. They compare the distance between samples that have undergone 100% exchange (i.e.,) attained internal equilibrium. In their study, they note equilibration volumes ranging from 0.5 feet to 0.05 feet. The differences are attributed to different amounts of intergranular water (the inferred exchange medium) and different thermal histories for the different rocks.

My techniques mirror those employed by previous workers in the respect that I compare isotopic data from different domains in the same outcrop. My methods differ from those presented by these workers in the respect that I account for mineral closure temperatures. Below, I describe two manifestations of the equilibration volume problem and outline the methods that can be used to define them.

Figure 3.1 diagrams possible equilibration volumes for a hypothetical, heterogeneous outcrop, for example a migmatite outcrop consisting of leucosome and mesosome. The equilibration volume may be larger or smaller than the scale of heterogeneity. If larger, this volume can be thought of as a composite of several parts of the rock (e.g., volume A in figure

3.1). If smaller, multiple, distinct equilibration volumes compose the outcrop, each volume corresponding to a distinct domain (e.g., volumes B. and C. in figure 3.1.). There is no reason to assume that the equilibration volumes should be constant during the cooling history of the outcrop (e.g., volume D. shrinking during cooling to volume E. in figure 3.1), or that they should be of regular shape. The three-dimensional transport properties of the rock control the scale and shape of the equilibration volume. If these properties change during the metamorphic history, the equilibration volume changes accordingly. Factors such as the presence or absence of grain boundary media, the compositions of the minerals, and the types of grain boundary contacts govern the scale and variability of the equilibration volume. Arguments made on the basis of diffusion constraints through the mineral matrix, along grain boundaries or through an intergranular medium (e.g., Brady 1983; Eiler et al., 1992; Joesten, 1983, 1991; Wang, 1993) and the empirical observations of Taylor et al. (1963) Anderson (1967) and Shieh and Taylor (1969) suggest that the scale of the equilibration volume varies from slightly larger than average hand sample to approximately the size of a thin section. Because many outcrops have compositional heterogeneity that is of this scale, assumptions about the equilibration volume need to be examined critically for all temperature calculations obtained by using the methods outlined in chapter 2.

In the following discussion I describe the implications of the equilibration volume assumptions. I have framed most of my arguments in a geometrical context because it is easier to explain the general constraints. I stress that the conclusions are general and that the results can be proven by mathematical examples. In the following diagrams and discussion, I use the subscript  $e$  to refer to each individual exchanging phase, and I use  $e.p.$  to refer to all exchanging phases, together. Figure 3.2 outlines the possible configurations for the IETs of high-closing phases. High closing phases with all values of  $A_{e-j}$  of the same sign (e.g., the mineral has the greatest or least affinity for  $^{18}\text{O}$  in the rock), either positive or negative, will have IETs that plot externally to the bundle of IETs defined by the low-closing phases. I refer to these phases as external high-closing phases. Conversely, I call high-closing phases that plot in a position that is internal to the bundle of IETs defined by the exchanging phases, internal high-closing phases. Here, some values of  $A_{e-j}$  for the high closing phase are positive

and some are negative. The distinction between internal and external high-closing phases simplifies the discussion of the way that their IETs and model temperatures are affected by incorrect assumptions about the equilibration volume.

Figures 3.3 and 3.4 schematically illustrate the relationship between the calculated IETs, the model temperatures and the chosen mode for data reduction. For simplicity, I only represent this problem in terms of a three-mineral system. The same conclusions apply in systems with more than three minerals. For internal high-closing phases (e.g., fig. 3.3), the value of  $A_{e,p,j}$  can be both positive and negative in sign. As the proportions of exchanging phases for which  $A_{e-j}$  is positive approach one, the likelihood for  $A_{e,p,j}$  to be positive increases. The converse holds true for the proportion of minerals with negative  $A_{e-j}$ .

Figure 3.3a illustrates the IETs and model temperatures for the correct mode and mineral isotopic compositions. Here, mineral 1 is the high closing phase with an IET that plots at a position internal to the IETs of low closing phases 2 and 3. The model temperature for phase 1 is given by  $T_1$ , and the model temperatures for phases 2 and 3 are given by  $T_2$ . The isotopic composition of the exchanging phases, the system, is given by  $\delta^{18}O_{e,p}$ . Because of equilibrium constraints, the isotopic compositions of all phases converge to  $\delta^{18}O_{e,p}$  at infinite temperature. Figure 3.3b, illustrates the different IETs, model temperatures and  $\delta^{18}O_{e,p}$  that would be obtained by using a different mode in the calculations (different  $\delta^{18}O_{e,p}$ ). Important features of this diagram are the convergence of IETs 1,2 and 3 on  $\delta^{18}O_{e,p}$  and the points about which the IETs rotate, respectively, to do this. I refer to these as pivot points. Whereas the pivot points for phases 2 and 3 correspond to the points delimited by their isotopic compositions at  $T_2$ , the pivot point for phase 1 corresponds to the projection of its high-temperature IET to  $T_2$ . The reason for these pivot points is simply that they force the graphical representations to obey the equilibrium fractionation relations for constant  $\delta^{18}O_{e,p}$ . The advantage of this representation is its very concrete portrayal of the relation between mass balance,  $\delta^{18}O_{e,p}$ , the IETs, and the model temperature data. The intersection temperatures diagramed in figure 3.3b remain constant for phases 2 and 3 because the isotopic fractionation between phases 2 and 3 remains constant, but the intersection temperature for phase 1 is different (e.g., compare  $T_1$  with  $T_1'$ ) because the effect of a

changing mineral mode on  $A_{e.p.-j}$  and  $\Delta_{e.p.-j}$  forces  $T_1'$  to change. In fact, the initial direction of the temperature effect for an infinitesimal change in mineral mode is always the opposite of its effect on the absolute value of  $A_{e.p.-j}$ . For large changes in mineral mode, the situation can be more complex. Figure 3.3c illustrates the effect of changing mineral mode from ~100% phase 2 to ~100% phase 3. In evaluating this figure, it is convenient to consider the composition of the exchanging phases ( $\delta^{18}O_{e.p.}$ ) in terms of the compositions of the phases in the rock ( $\delta_{phase1}$ ,  $\delta_{phase2}$ , and  $\delta_{phase3}$ ) and the compositions given by the pivot point for the high closing phase ( $\delta_{pointA}$ ). Using these criteria, we can divide figure 3.3c into four fields.

1. The fields of inaccessible composition space.
2. The field of reversed order of temperature data.
3. The field of reversed fractionations and impossible temperature data.
4. The field of normal order of temperature data.

The system occupies a field when  $\delta^{18}O_{e.p.}$  falls within its compositional limits. The limits of accessible composition spaces are defined by the isotopic compositions of the most  $^{18}O$  enriched of the exchanging phases, in this case phase 2, and by the isotopic composition of the most  $^{18}O$  depleted of the exchanging phases, in this case phase 3.

The field where normal closure temperature order is preserved occurs for  $\delta^{18}O_{e.p.}$  intermediate between  $\delta_{phase1}$  and the inaccessible composition closer to  $\delta_{phase1}$  than to  $\delta_{pointA}$ . Temperature intercepts delimited by this field ( $T_1'$ ) are always greater than  $T_2$ , and approach infinity as  $\delta^{18}O_{e.p.}$  approaches  $\delta_{phase1}$ . Values for  $T_1'$  approach the mineral-pair apparent temperature given by the fractionation between the phases that define its limits as  $\delta^{18}O_{e.p.}$  approaches the bounding inaccessible space. In this example, this field is defined by the isotopic compositions of  $\delta_{phase1}$  and  $\delta_{phase3}$ . As a rule, the intersection temperatures in this field increase as the absolute value of  $A_{e.p.-j}$  decreases.

The field of reversed fractionations is defined by isotopic compositions of the exchanging system ( $\delta^{18}O_{e.p.}$ ) between  $\delta_{phase1}$  and its pivot point ( $\delta_{pointA}$ ). The reversed fractionations occur when the values given by  $A_{e.p.-j}$  and  $\Delta_{e.p.-j}$  are of opposite sign. The reason that this condition applies to this field is that  $\delta^{18}O_{e.p.} = \delta_{pointA}$  represents the crossover

in sign for  $A_{e.p.-j}$  and  $\delta^{18}O_{e.p.}' = \delta_{phase1}$  represents the crossover in sign of  $\Delta_{e.p.-j}$ . Thus, this field delimits reversed fractionations, and impossible isotopic temperatures.

The field of reversed intercept temperatures is defined by  $\delta^{18}O_{e.p.}'$  intermediate between the isotopic composition of pivot point of phase 1 ( $\delta_{pointA}$ ) and the inaccessible space on the side opposite the field of reversed fractionations. Intersection temperatures ( $T_1'$ ) in this field are lower than  $T_2$ , and increase as the absolute value of  $A_{e.p.-j}$  increases. The minimum value for  $T_1'$  is zero and given when  $\delta^{18}O_{e.p.}' = \delta_{pointA}$ . The maximum temperature occurs when  $\delta^{18}O_{e.p.}'$  is the same as the boundary with the inaccessible composition space, and is given by the fractionation between phase 1 and the phase that defines the bounding inaccessible composition space.

External high-closing phases have a simpler temperature dependence than internal high-closing phases because the pivot point for phase 1 (Point A) always plots in the inaccessible composition space. As a result, the last field (reversed intercept temperatures) does not exist for external high-closing phases. Figure 3.4a illustrates the fields that occur when the isotopic composition of the high closing phase is external to the range of compositions defined by the exchanging phases. This is the simplest case because the intersection temperatures increase as the absolute value of  $A_{e.p.-j}$  decreases, and the highest value for  $T_1'$  is given by the fractionation between phase 1 and the exchanging phase with which it fractionates oxygen the least (smallest  $A_{e-j}$ ), in this case phase 2. The lowest value for  $T_1'$  is given by the fractionation between phase 1 and the exchanging phase with which it fractionates oxygen the most (largest  $A_{e-j}$ ), here phase 3. Figure 3.4b illustrates the fields that occur when the isotopic composition of phase 1 is bracketed by the isotopic compositions of the exchanging phases. Here, the field of reversed fractionations exists for  $\delta^{18}O_{e.p.}'$  intermediate between the isotopic composition of phase 1 ( $\delta_{phase1}$ ) and the isotopic composition of the exchanging phase that is closest to the pivot point for phase 1, here  $\delta_{phase2}$ . When this is the case, the highest value for  $T_1'$  is infinite temperature, but the lowest value for  $T_1'$  is still give by the fractionation between phase 1 and the exchanging phase with which it most strongly fractionates oxygen (largest  $A_{e-j}$ ). The general rule for external high-closing phases is that the model temperature data will increase when the absolute value of  $A_{e.p.-j}$

decreases and decrease when the absolute value of  $A_{e,p-j}$  increases. Below I provide a worked example to illustrate the power of these geometrical arguments.

Figure 3.5 diagrams the relationship between the equilibration volume, calculated IETs and model temperature data. The model data that I used to construct these three diagrams are presented in Table 3.1. Figure 3.5 shows the effect that the equilibration-volume scale holds for calculations of IETs and model-temperature data. These diagrams were calculated from model data. The model data used to calculate the IETs in Figure 3.5 assume a composite equilibration volume (e.g., volume A in figure 3.1), consisting of 40% leucosome and 60% mesosome. In all calculations, the final isotopic compositions of the phases are the same. Figure 3.5a shows the true IETs calculated with the valid, composite volume. Figure 3.5b illustrates the effect of calculating the IETs and model temperature data with the mode of only the mesosome, and Figure 3.5c. illustrates the effect of calculating these IETs and model temperature data with the mode of only the leucosome. In each of these cases, the resulting IETs and model temperature data are different. An understanding of the underlying reasons for these differences is needed to deconvolute data like these, and to determine the correct equilibration volume. Once this is done, the correct equilibration volume can be chosen and isotopic thermometry can be undertaken.

The changes in the IETs and model temperature data represented in figures 3.5a,b and c, are best explained in terms of the equilibrium fractionation factors between the closing phase and the exchanging phases. In our derivation of the temperature equations, the quantity ( $A_{e,p-j}$ ) controls the slope of the IETs in  $\delta^{18}\text{O}-T^{-2}$  space, and the IET-mineral composition intercepts that define the model temperature data. We can use this line of reasoning to interpret the shifts represented by figure 3.5. When only the mesosome is used in calculation of model temperatures (e.g., figure 3.5b) the model temperatures of garnet and kyanite (g and k) are too high because the absolute value of the fractionation factor between each of them, respectively, and the rest of the rock, are too low because we have underestimated the amounts of quartz and feldspar in the mode that we used for calculations. The model temperatures of quartz and muscovite are lower because the absolute values of their fractionation factors with the exchanging phases are too high (less Fsp). The model

temperatures for biotite and feldspar do not change, because the fractionation of oxygen between them does not change. If the same data are analyzed with the mode of the leucosome, garnet and kyanite model temperatures are anomalously low (larger absolute fractionation factors with the exchanging phases) and the model temperatures for quartz are anomalously high (smaller absolute fractionation factors with the exchanging phases). The model temperatures for feldspar, biotite, and muscovite all change because the muscovite is driven into the field of reversed temperatures by the high modal proportion of feldspar. In Table 3.1 I have listed the values used in each set of calculations, the mineral-closure temperatures obtained by each calculation, and the apparent temperatures given by quartz-mineral isotopic thermometers. Examination of the mineral-pair temperatures in this table highlights an important feature of this problem, the only variable is the mass balance. The fractionations, mineral pair temperatures and isotopic compositions of all phases remain constant. This would not be the case if it were an open system.

Identification of equilibration volume problems requires supporting evidence from the outcrop in the form of missing parts of the mass balance - local banding, leucosomes, crosscutting features and etc...- that should have been noted during sample collection. In theory, all that is needed for determination of the equilibration volume is heterogeneous modal and isotopic data that can be contoured with respect to position in a closed-system, heterogeneous rock. By gaining an understanding of the parameters that affect the model temperature data, we can begin to devise a methodology for determining the validity of our assumptions about the equilibration volume. We can also devise a means of obtaining the equilibration volume directly. The scale of the equilibration volume can be determined by taking serial samples adjacent to features that introduce inhomogeneity. This was the technique used by Anderson, (1967), Shieh and Taylor (1969) and Eiler et al. (1995). The equilibration volume can be obtained from this data for a series of samples by relating the functional dependence of mineral mode on position to the functional dependence of mineral-closure temperature on position. In fact, this methodology should yield determinations of the equilibration volume for the temperature intervals that correspond to closure of each mineral in the rock. This latter exercise, in principle, could be used to detect changes in the



scale of the equilibration volume as a function of temperature for a specific set of samples.

In this section, I have shown the problems with incorrect assumption about the equilibration volume, the ways to detect them, and a way to make a direct measurement of the equilibration volume. Once the equilibration volume is obtained, the temperature history of the outcrop can be reevaluated by using it to guide further sampling. Whereas minerals with large  $A_{e,p,j}$  are best for thermometry because the temperature data obtained from their isotopic compositions are relatively insensitive to external factors, minerals with small  $A_{e,p,j}$  are best for assessing problems with assumptions about the equilibration volumes. Consequently, it is important that samples are chosen with at least two high closing minerals, one with large  $A_{e,p,j}$  and the other with small  $A_{e,p,j}$ . An estimate of the absolute amount of the temperature uncertainty introduced by uncertainty in the equilibration volume can be obtained by comparing the results for these two high-closing minerals. Checks for internal consistency of mineral-closure temperature data like these provide robust checks of its validity and sample collection can be optimized by collecting samples with more than one high closing phase, and by collecting samples that contain the same high closing phase, but very different  $A_{e,p,j}$ , preferably of opposite sign.

### **Open System Interactions**

Open system interactions are in one sense an extension of the equilibration volume problem because we have not included a significant portion of the mass balance in our calculation. In another sense they are very different. The isotopic composition of the unaccounted phase is unknown, and the isotopic shifts introduced by open system interactions commonly shift some minerals in the sample significantly while leaving others undisturbed. In figure 3.6, I schematically diagram open system interactions that might occur when low  $^{18}\text{O}$  meteoric water circulates through and reequilibrates with its host rocks. This type of interaction is better described by considering the effect of variable isotopic composition for certain fast diffusers, namely feldspars, but constant mode for all minerals in the rock. Open system interactions affect temperature data because in its calculation, the

mode is representative of the equilibration volume during cooling, but the isotopic compositions of the minerals are not.

Previous methods for describing open system interactions have been presented by Taylor, Gregory, Criss and their coworkers (e.g., Gregory and Criss, 1986; Criss and Taylor, 1986; Criss et al., 1987). Solution of an equation similar to the equation that defines the IETs in  $T^{-2}$  space yields a set of feasible spaces for both open and closed system evolution of the isotopic systematics of a given set of samples. Data arrays that plot outside the domain dictated by closed system constraints are taken to show open system behavior. A weakness of the method is that open system data arrays can be generated in closed systems by differential mineral closure (Giletti, 1986; Jenkin et al., 1991). Most of their studies focussed on systems that were grossly open and did not require assumptions about mineral closure. Where finer scale resolution was needed, the emphasis was shifted to include the hydrogen isotope system. Because the amount of hydrogen in rocks is much smaller than the amount of oxygen, the hydrogen isotopic systematics is a much more sensitive indicator of interactions with externally-derived meteoric waters.

The methods that I have developed do not require the addition of hydrogen isotope data to solve for small degrees of open system behavior. They require, however, modal constraints, and considerable calculations, but in return, they give a direct assessment of the effect of open system interactions on the oxygen isotope systematics. Because the hydrogen and oxygen systematics might be decoupled during the final parts of the cooling history, this direct measure is an important constraint. Moreover, because my methods rely on interpreting closure temperature data for all minerals in the rock, they can be used, in principle, to gain insight into the temperature conditions at which the open system interactions occurred. This latter insight cannot be gained by examining the hydrogen isotope systematics. When samples are correctly chosen, the sensitivity of my methods converges on the sensitivity of the hydrogen isotope methods employed by Taylor, Gregory, and their coworkers.

Here, I use two strategies to evaluate open versus closed system behavior. To test for late open system interactions, I examine the bundles of IETs and model temperatures

produced by a set of samples. If the IETs are systematically offset in a way that can be fit by arbitrarily perturbing the isotopic composition(s) of low closing phase(s), I determine the magnitude of the shifts required to bring the IETs into agreement with a geologically reasonable closure sequence. The geologically reasonable closure sequence is usually decided by using experimentally or theoretically calibrated diffusion data and models. This is clearly an arbitrary operation. Nevertheless, it is often the simplest way to explain the data, and can be a very sensitive indicator of open system shifts because in multimineralic rocks, small shifts in isotopic composition are readily resolved in the closure sequence. The most useful minerals for monitoring these shifts are high-closing phases with small  $A_{c,p-t}$  because the intersection temperatures of these minerals are very sensitive to changes in isotopic composition of the system (exchanging phases). A more rigorous test for open system interactions can be obtained by comparing the closure temperature of a particular phase in different samples. I use an approach that compares the model temperatures of a low modal abundance, slow diffusing mineral in two or more samples from the same outcrop. The samples are chosen such that they have different values of  $A_{c,p-t}$ . The model temperatures of this mineral will be similar in the two samples provided the samples have comparable grain sizes and have behaved as closed systems. In an open system, however, the model temperatures will generally differ between samples. This occurs because the IETs of all minerals vary as a complex function of mode and fractionation behavior. Shifts in the isotopic compositions of one or more minerals caused by retrograde fluid influx will perturb the IETs of the other minerals to different degrees depending on the mode of the rock. Therefore, isotopic shifts in fast diffusing phases caused in an open system will generally disturb the concordance of the model temperatures of slow diffusing phases in samples with different modal compositions.

In figure 3.7a I diagram the open system evolution of a hypothetical three phase rock. In this figure, I represent the open system interactions by an arbitrary event that lowers the  $\delta^{18}O$  of phase 3 after the isotopic compositions of phases 1 and 2 have become fixed. The isotopic compositions of phases 1, 2, and 3, produced by this hypothetical exchange history, when combined with its mode, cannot be modeled to reproduce the actual exchange history

of the minerals in the rock. Here, there are no pivot points about which the IETs rotate. Instead, the whole bundle of IETs shifts to fit the new  $\delta^{18}O_{e,p}$  and the model temperatures shift to accommodate the isotopic composition data. Note that the IETs for each mineral maintain the same slope in both representations. The IETs are parallel because the mode and fractionation factors do not change. The shift arises because the isotopic compositions of the exchanging phases are different. The effect of open system behavior on the IETs of the closed phases is much easier to explain than the effects discussed in the previous section that arise from equilibration volume uncertainties. Intercept temperatures increase when the IET has a positive slope and open-system interactions raise  $\delta^{18}O_{e,p}$ . The intercept temperatures decrease for the same shift if the slope of the IET is negative, or if the slope is positive and the  $\delta^{18}O_{e,p}$  is lowered (E.g., phases 1 and 2 in figure 3.7b).

In any given sample, the magnitude of these temperature shifts depends strongly on the values of  $A_{e,p,j}$ ; large values of  $A_{e,p,j}$  result in small shifts in model temperature, whereas small values of  $A_{e,p,j}$  result in large shifts. Therefore, the samples that provide the most sensitive test of open system behavior are those that have widely different values of  $A_{e,p,j}$ . Ideally,  $A_{e,p,j}$  would have opposite sign in the two samples as this would cause opposite directions of temperature shift. A schematic illustration of these effects is shown in figure 3.8.

Figure 3.8 illustrates schematically the effect that small degrees of open system behavior will have on two rocks with widely different  $A_{e,p,j}$ . Table 3.2 contains sample data used to construct figure 3.8. Two important features of these techniques are illustrated. First, the intersection temperatures change in different ways as a result of open system interactions and equilibration volume problems. Second, methods that involve comparing coexisting samples are significantly more sensitive than methods that rely on diffusion constraints alone to image open system effects. In figures 3.8a and b, I have plotted hypothetical isotope exchange trajectories for a plagioclase + magnetite + olivine rocks with widely different modes. Evidence for open system evidence by diffusion-constrained closure, therefore is obtained when the uncertainty brackets on the intersection temperatures no longer overlapped the feasible range of closure temperatures defined by the diffusion

constraints. Figure 3.8c and d illustrates the sensitivity of the method for detection of open system interactions. I have calculated the isotopic shift that would accompany fluid-rock interactions between the magnetite +feldspar part of the rock and a meteoric fluid with a low  $\delta^{18}\text{O}$  content. I have arbitrarily chosen to calculate the shift with the water-rock equation of Taylor (Criss and Taylor, 1986)

$$\left(\frac{W}{R}\right) = \left(\frac{O_{\text{rock}}}{O_{\text{water}}}\right)_{\text{molar}} + \ln \left( \frac{\delta^{18}\text{O}_{\text{final-rock}} - \delta^{18}\text{O}_{\text{initial-rock}}}{\delta^{18}\text{O}_{\text{initial-water}} - \delta^{18}\text{O}_{\text{final-rock}} + \Delta_{\text{water-rock}} - 1} \right) \quad (3.1)$$

where the water-rock ratio ( $w/r$ ), the isotopic composition of the fluid ( $\delta^{18}\text{O}_{\text{initial-water}}$ ), and the isotopic fractionation between the fluid and the rock ( $\Delta_{\text{water-rock}}$ ) are arbitrarily set at 0.03, 0‰ and 0‰, respectively. I assume that plagioclase and magnetite are open to exchange whereas olivine is not. I also assume that each mineral closes at the same temperature in both samples. In figure 3.8c and d I show that, unlike the case for closed system behavior, open system behavior results in a substantial difference in olivine model temperatures. This small amount of open system interactions is undetectable with other measurement techniques (e.g., Gregory and Criss, 1986). The example provided in Figure 3.8 is an unusual case, and will probably only be realized in cases where oxide- and silicate-rich rocks coexist. A case like this, however, is described later in this dissertation. In cases where application of this technique is not possible, very sensitive measures of open system interactions can be made by considering the closure temperatures of high closing phases with small  $A_{\text{e,p,j}}$ . The advantage of this method over earlier methods is that, in many cases, it can provide a more sensitive test for open system behavior. Ultimately, however, open system effects can be best evaluated through the use of micro-sampling techniques (e.g., Valley and Graham, 1991, 1993; Elsenheimer and Valley, 1993; Young and Rumble, 1993).

### **Retrograde Isotopic Zoning and Isotopic Thermometry**

The effect of retrograde isotopic zoning is also a concern for isotopic thermometry. To assess the effect of retrograde isotopic zoning I have constructed Figure 3.9. In this

figure I use Dodson's closure model (1986) to illustrate the types of isotopic profiles that might be observed in minerals that have undergone retrograde isotopic exchange. Although the infinite reservoir assumption of the Dodson model invalidates its application in a strict sense, it can still be useful because it provides an endmember case for the isotopic profiles in slowly cooled rocks. The profiles generated by this model will be more pronounced than the profiles generated by the finite reservoir model of Eiler et al. (1992) because the isotopic compositions of finite exchange reservoirs change as a result of isotopic exchange and take up some of the shift themselves. The isotopic compositions of infinite exchange reservoirs do not change as a result of isotopic exchange and all of the shifting must be accommodated by the profile in the slow diffuser. In the finite reservoir model, as the proportion of the exchanging reservoirs increase, its isotopic composition changes less, and resulting isotopic profiles for the slow diffusers become more like those predicted by the infinite reservoir model. Fortunately, because they have the lowest associated uncertainties, the best samples for the methods of isotopic thermometry described in chapter 2 are those that contain a small amount of the slow diffuser and a large amount of the fast diffusers. Because the proportion of the exchanging reservoirs are high in these samples, these are the same samples that will produce isotopic profiles in the fast diffuser that approach the profiles calculated by the Dodson infinite reservoir model. They can never match the predicted profiles because there will always be a finite reservoir around the slow diffuser, determined by the finite diffusivity of the fast diffuser. This means that the profiles produced by retrograde exchange will always be more subdued than those predicted by the Dodson model, but the Dodson model can be used to describe the maximum compositional zoning effect that closed system retrograde isotopic exchange can produce.

Diagram 3-10, illustrates the general shape of the profile generated by Dodson's retrograde exchange model. This isotopic profile consists of a broad central plateau and steeper composition gradients at the grain margins. I have also included a curve to illustrate the temperature data that would be obtained for progressive abrasion of the rim. An important feature of this curve is the relatively higher temperatures that can be obtained from an abraided grain relative to a whole grain analysis. For such grains, higher temperature data

could be obtained by analyzing core domains rather than whole grains. The relative improvements, however, are still small.

## **Summary and Conclusions**

In this chapter I have described the problems that arise with isotopic thermometry because of incorrect assumptions. The assumptions boil down to two types. The first type of incorrect assumption concerns isotopic composition. We implicitly assume that the measured isotopic compositions of minerals in a given sample are representative of those produced by the closed system cooling process. This assumption is violated when open system interactions have occurred. Open system interactions shift the isotopic compositions of some minerals and the bulk rock away from those produced by closed system cooling. The second type of incorrect assumption concerns mass balance. We implicitly assume that our measured mass balance constraints represent the mass balance that operated during the closed system reequilibration and cooling. This assumption is violated when we incorrectly choose the volume over which equilibrium occurs. The present goal is isotopic thermometry, so all assumptions have to be met to get valid temperature data. Because the methods described in chapter 2 make implicit assumptions about mass balance and equilibrium, it may be possible to extend them to describe environments where they are partially met by including position data to obtain a direct measure of the equilibration volume and the exchange history of the minerals at a given locality.

For isotopic thermometry studies, it is important to test the validity of our assumptions about mass balance and isotopic composition. These tests are of two types. The first test involves comparing calculated temperature data and observed isotopic composition data with model temperature data and model isotopic composition data produced by a reaction or exchange history calculations. These calculations are similar to those done by Gilletti (1986), Eiler et al. (1992), Jenkin et al. (1991), and make specific assumptions about cooling history, exchange pathways, exchange mechanisms, mass balance and isotopic composition. A second test involves comparing the calculated exchange histories of

minerals from samples with widely different modes. These comparisons do not require specific assumptions about the exchange mechanisms and pathways or the cooling history of the rocks, but they do assume that the exchange mechanisms and pathways and the cooling histories of minerals in samples from one outcrop are similar. There is no guarantee that these assumptions are correct, but they are less restrictive than those made in the first type of test. Both methods work well, and both can provide very good tests of the validity of the assumptions.

Through an understanding of the assumptions made in formulating the data handling techniques outlined in chapter 2, we can devise a strategy for selecting samples that will allow both retrieval of the 'best' isotopic temperature data and application of the 'best' tests for the validity of this data. The samples that will be best for isotopic thermometry will be those that have at least one high closing phase. To be high closing and to reduce uncertainties, this phase should have

1. low oxygen diffusivity,
2. resist retrogression and recrystallization,
3. be in low abundance for precise determination of the modal proportions of the fast diffusers, and
4. have a sufficiently large equilibrium isotopic fractionation with

the

rest of the rock to give temperature determinations with low analytical uncertainties.

To test the equilibration volume and closed system assumptions, we should either have samples with at least one high closing phase where the fractionations between it and its respective exchanging phases are of opposite sign in two or more samples, or samples with many minerals that fractionate and exchange oxygen in very different ways. The ideal samples for thermometry and for testing the validity of the thermometry will have two high closing phases. One phase that strongly fractionates oxygen relative to the rest of the rock and another that does not. Such samples might be

1. garnet and kyanite bearing pelitic rocks,



2. ilmenite, olivine and corundum? bearing anorthositic rocks, and
- 3 garnet, spinel and sillimanite bearing high temperature granulites.

In these rocks, the mineral that most strongly fractionates  $^{18}\text{O}$  can be used as a thermometer because of its low temperature uncertainties, and the mineral that least strongly fractionates  $^{18}\text{O}$  can be used as a test of the assumptions made in applying the model.

This brings me to the end of my discussion of the techniques, methods, and assumptions of isotopic thermometry. In the remainder of this dissertation I will present three case studies for isotopic thermometry to highlight the type information can be gained by its application, the pitfalls encountered when application to natural rocks is undertaken, and the insights that can be gained into exchange mechanisms and pathways. I will focus on three different types of igneous and metamorphic environments, the high-temperature shallow crustal plutonic igneous rocks of the Laramie Anorthosite Complex, Wyoming, the mid to deep crustal, very high temperature very dry granulites and igneous rocks of the Napier Complex, Antarctica and the Taltson Magmatic Zone, Northeast Alberta Canada, and the mid to deep crustal, amphibolite to granulite facies rocks of the Mica Creek Barrovian Sequence and adjacent Monashee Complex, British Columbia Canada. These different crustal environments were chosen because they span a wide range of crustal conditions and can be used as a test for the types of isotopic thermometry outlined by this study.

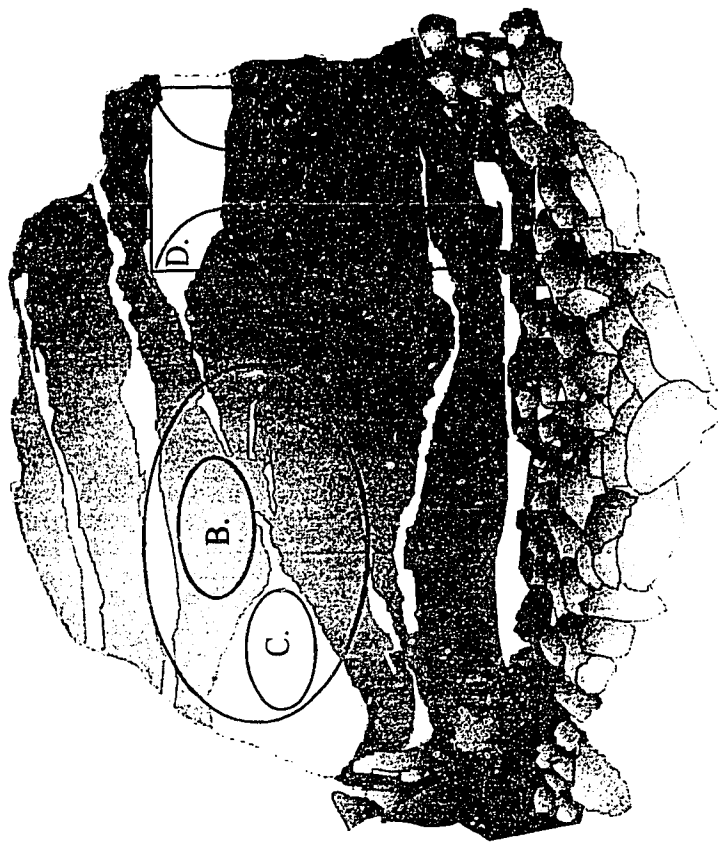


Figure 3.1 Sketch of possible equilibration volumes for a hypothetical outcrop. White = leucosome. gray = mesosome. See text for discussion.

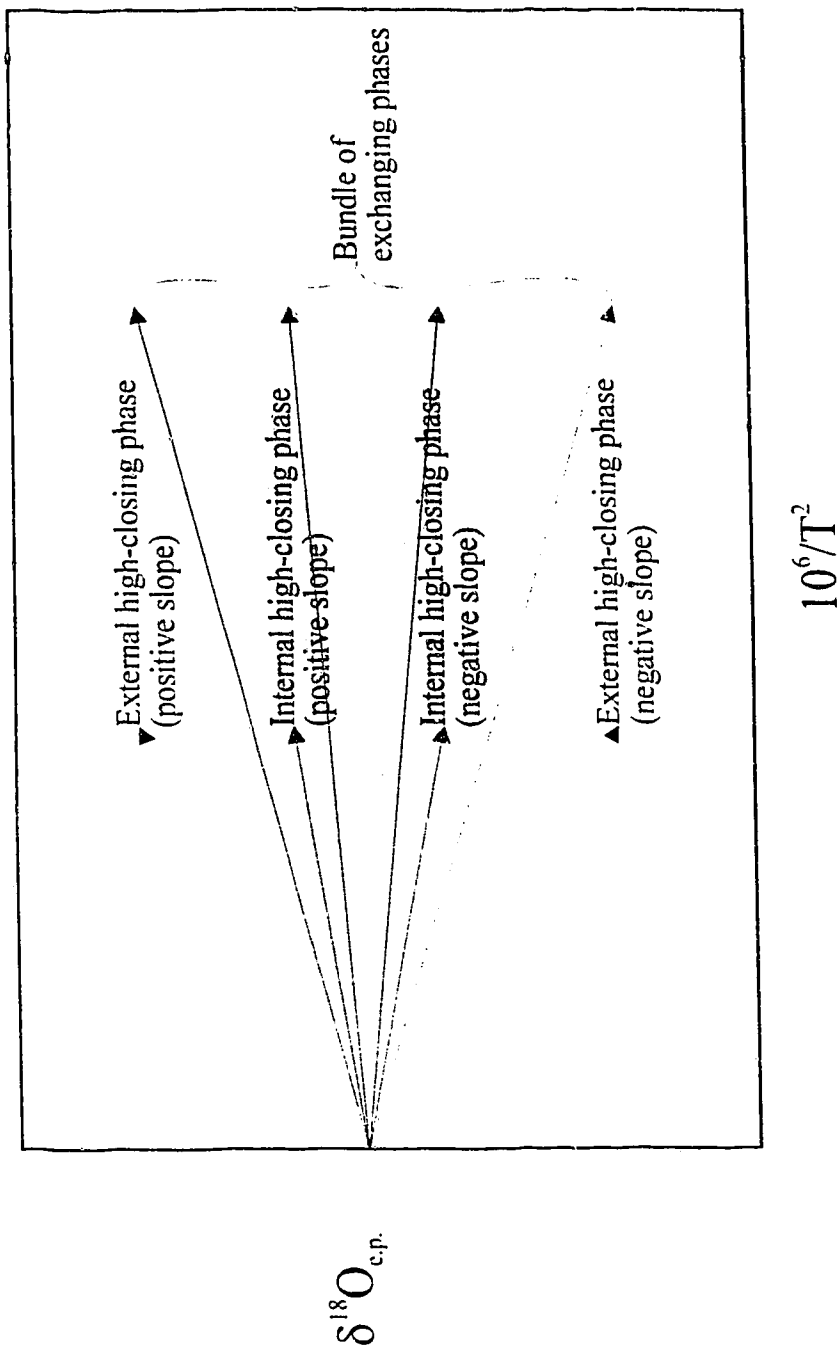


Figure 3.2 Schematic representation of internal and external high closing phases in isotopic evolution diagram. See text for more discussion.

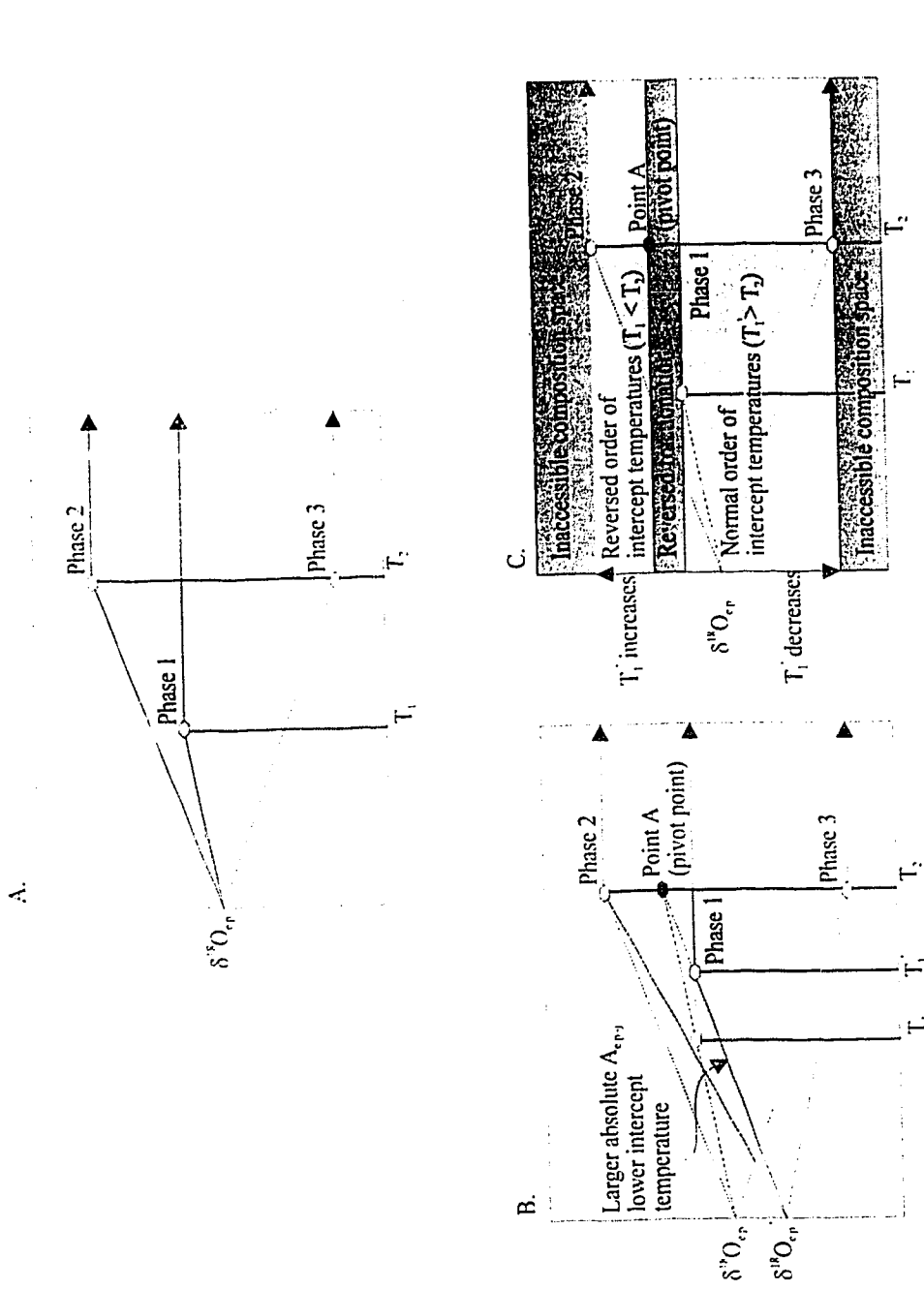


Figure 3.3 Schematic diagrams illustrating feasible spaces and pivot points for internal high closing phases. Equilibration volume problems. See text

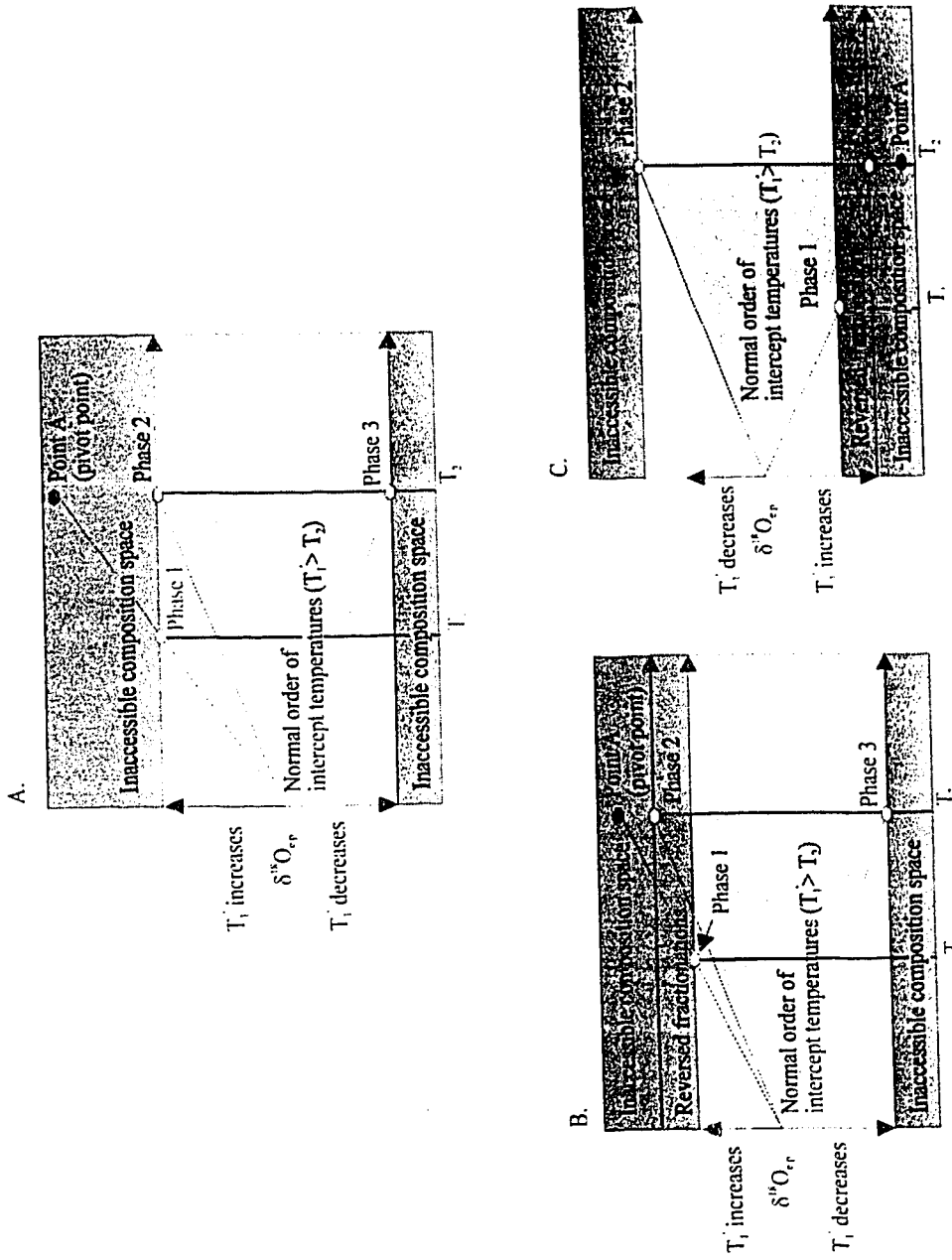


Figure 3.4 Schematic diagram illustrating feasible spaces and pivot points for external high closing phases. Equilibration volume problems. See text.

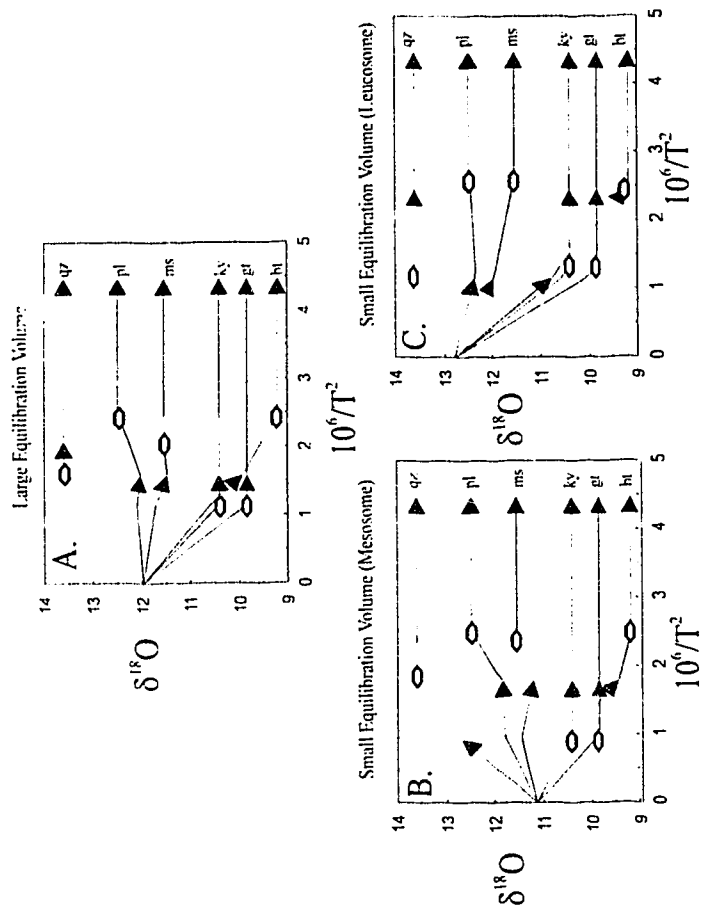


Figure 3.5 Schematic representation of equilibration volume problems for a qz-pl-ms-ky-gt-bt rock. (See text for discussion.)

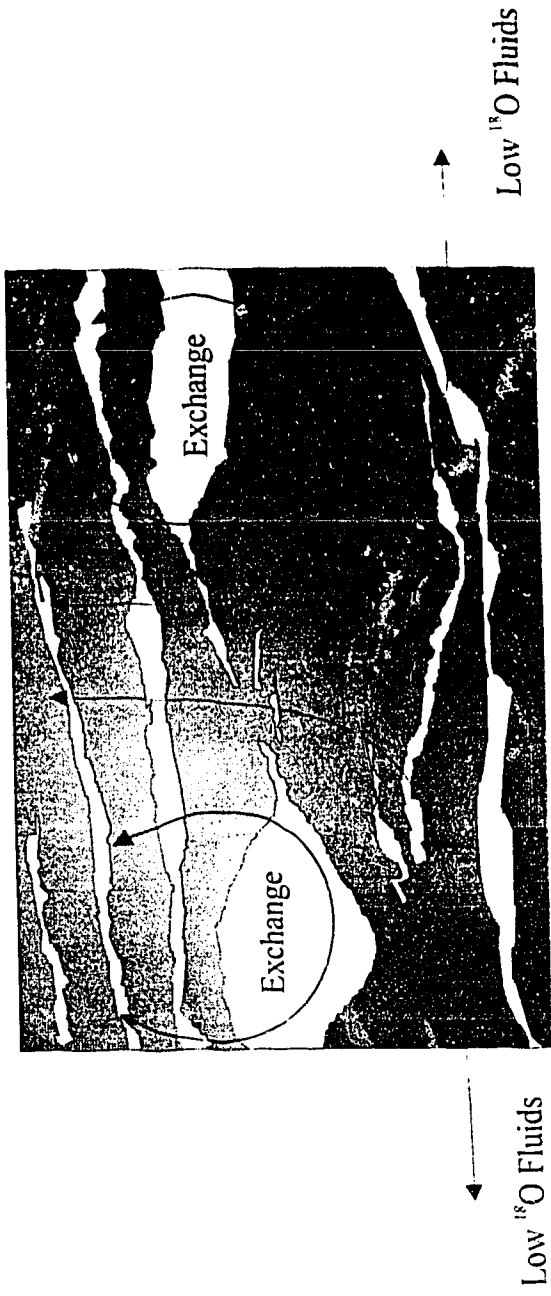


Figure 3.6 Open system cartoon.

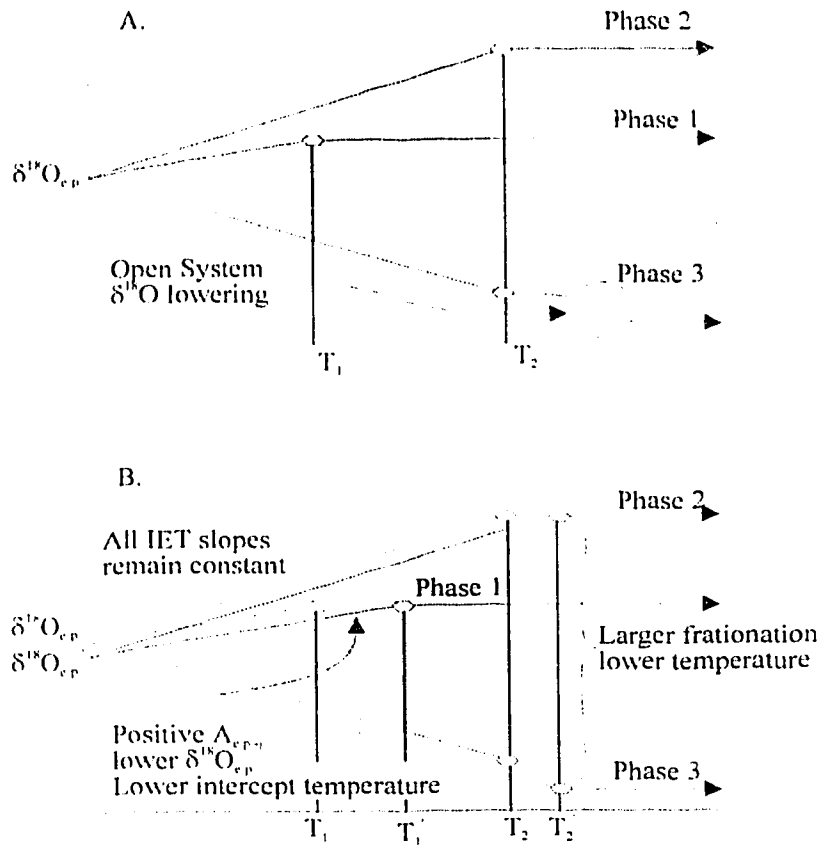


Figure 3.7 Schematic diagram illustrating effect of open system shifts on temperatures. See text for details.



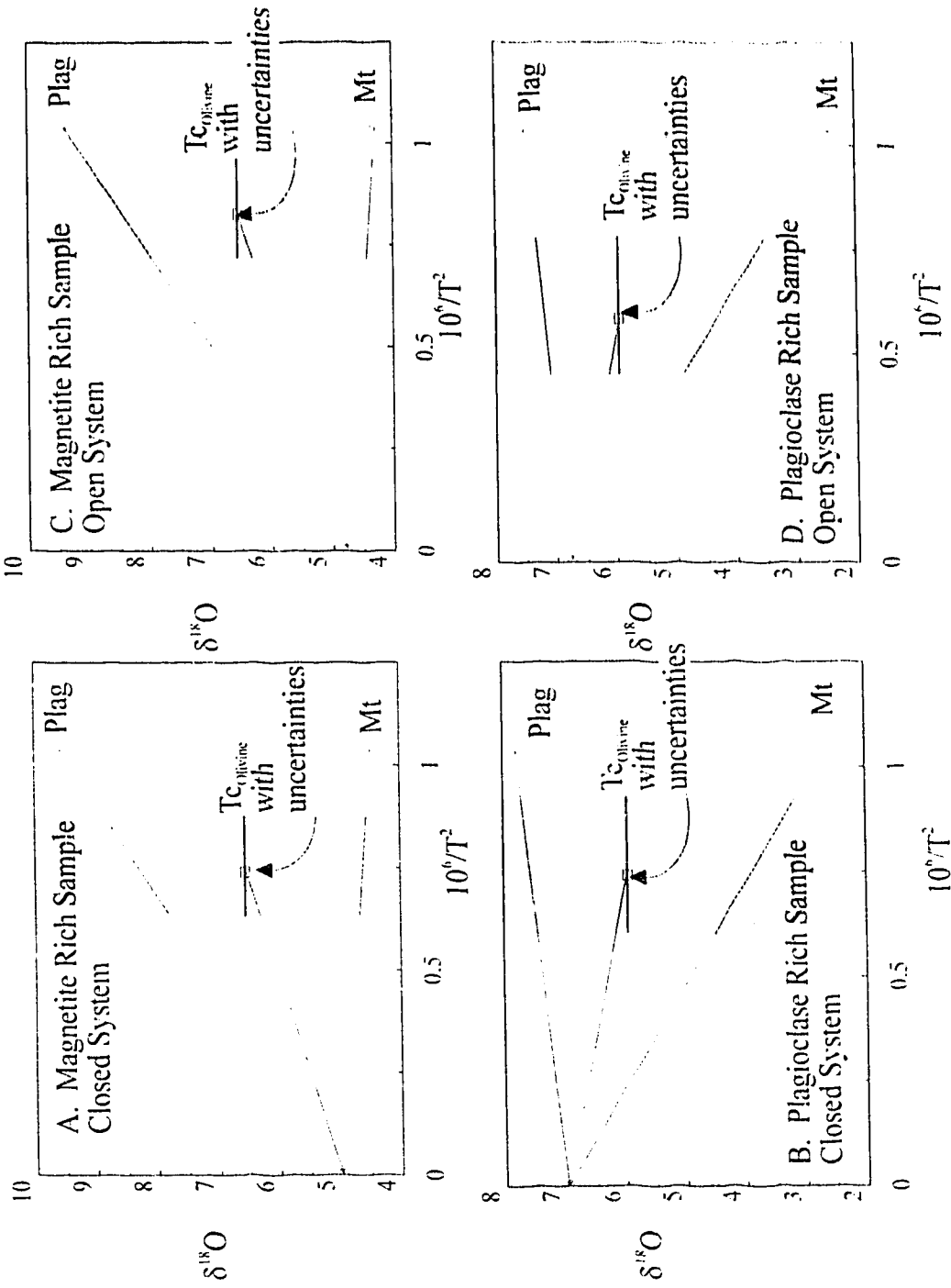


Figure 3.8 Tests for assumptions. A and B - assumptions met. C and D - assumptions violated. See Text for discussion.

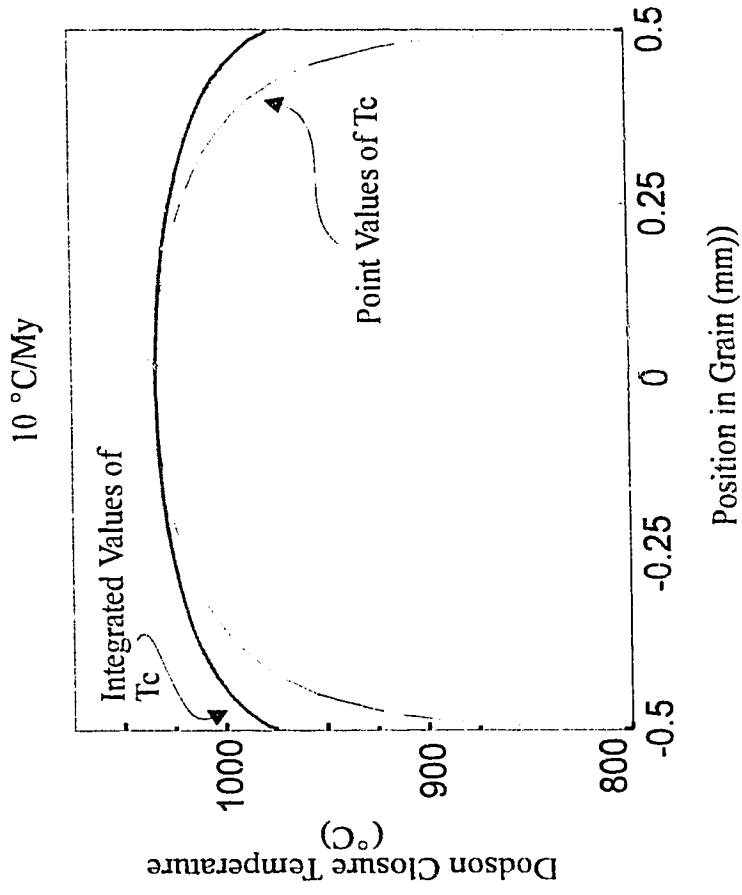


Figure 3.9 Closure profiles: 1 mm diameter hercynite grains for a cooling rate of 10 °C/My (Calculated with Dodson (1986) and Gautason and Muehlenbachs, 1993)

Table 3.1

Model data used to construct Figure 3.5

Mineral	Applicable mode (%)	Mesosome mode (%)	Leucosome mode (%)	Final isotopic compositions (‰)
Quartz	41	35	50	13.60
Albite	23	5	50	12.50
Biotite	18	30	0	9.20
Muscovite	3	5	0	11.55
Garnet	9	15	0	9.84
Kyanite	6	10	0	10.40

Table 3.2

Model Data used to construct Figure 3.8

Modal Abundances (%)	Plagioclase	Magnetite	Olivine
Sample A	74.8	8.5	16.7
Sample B	8.9	86.6	4.5
Closed System			
Sample A	7.81	2.66	5.95
Sample B	9.63	4.48	6.57
Open system w/r=0.03			
Sample A	7.54	2.39	5.95
Sample B	9.44	4.29	6.57

## Chapter 4:

### Case Study I: The Sybille Fe-Ti Oxide Pit of the Laramie Anorthosite Complex, Wyoming, U.S.A.

#### Introduction

The Laramie Anorthosite Complex (LAC) is a shallow level, high temperature plutonic igneous complex. It outcrops over an 800 km<sup>2</sup> area of southeastern Wyoming along a crustal suture, marked by the Cheyenne belt, between the Archaean rocks of the Wyoming province and the Proterozoic rocks of the Colorado province (Figure 4.1) (Duebendorfer and Houston, 1987; Fuhrman et al., 1988). The LAC is a well studied massif-type anorthosite (Goldberg, 1984; Epler et al., 1986; Fuhrman et al., 1988; Kolker and Lindsley, 1989; Kolker et al., 1990; Anderson et al., 1987, 1988; Geist et al., 1990; Frost et al., 1989; Frost et al., 1990; Frost and Touret, 1989; Grant and Frost, 1990; Scoates and Chamberlain, 1994) that consists of anorthosite, gabbroic anorthosite, ferrogabbro, monzonite, troctolite, norite, nelsonite, Fe-Ti oxide ore, syenite, and granite (Fowler, 1930; Newhouse and Hagner, 1957; Fuhrman et al., 1988, Grant and Frost, 1990). U/Pb zircon and baddeleyite ages indicate that most of the complex was emplaced between 1430 and 1440 Ma (Frost et al., 1990; Scoates and Chamberlain, 1993; Scoates et al., 1993a). The older 1758 Ma Horse Creek anorthosite outcrops south of the LAC and is separated from the complex by a septum of Early Proterozoic gneisses and granites (Scoates et al., 1993b).

The anorthosite-syenite-granite suite that constitutes the LAC is emplaced into Archean age granitic gneisses of the Laramie River complex and metasedimentary and metavolcanic rocks of the Bluegrass Creek Suite (Snyder, 1984; Grant and Frost, 1990). The granitic rocks into which the LAC intruded preserve 2500 to 2600 Ma Rb-Sr ages (Hills and Armstrong, 1974, recalculated by Grant and Frost, 1990; Peterman, 1982). The Bluegrass Creek Suite preserve evidence for amphibolite facies regional metamorphism where it is exposed away from its contact with the LAC (Grant and Frost, 1990). Where the suite contacts the LAC, the earlier amphibolite facies (kyanite + garnet + biotite + muscovite +

quartz and kyanite + garnet + biotite + staurolite + quartz + plagioclase) metamorphism is overprinted by the contact metamorphism associated with emplacement of the LAC (Grant and Frost, 1990). Grant and Frost (1990) constrain the contact metamorphic event to 650° to 800°C and  $3 \pm 0.5$  Kb. There is no petrographic evidence for metamorphism or high temperature uplift of the complex post emplacement of the LAC.

The Sybille Fe-Ti oxide quarry is located in the center of the northern part of the anorthosite (Figure 4.1). The quarry is a prospect pit that has been dug into an oxide-rich troctolite of the Laramie Anorthosite Complex (LAC). The major rock types exposed in this quarry are troctolite (olivine-bearing plagioclase-rich rocks), norite (orthopyroxene-bearing plagioclase-rich rocks), transitional rocks or nelsonite (apatite rich, magnetite-ilmenite rocks), Fe-Ti oxide ores (magnetite-ilmenite rocks), anorthosite and gabbro. Figure 4.2 is a map of the north wall of the quarry that was constructed by Bolsover (1986). This figure illustrates the meter-scale bodies of troctolite, norite, nelsonite and Fe-Ti oxide ores. These rock types are considered to be a late-stage portion of the LAC, because bodies composed of these rocks truncate the obvious magmatic layering of the anorthosite and locally contain xenoliths of anorthosite (Bolsover, 1986; Bolsover and Lindsley, 1983; Epler et al., 1986; Epler, 1987). The distinct increase in oxide content from the top to the bottom of the pit suggests that the nelsonite and Fe-Ti oxide rocks underwent gravity separation from the troctolite and norite during cooling (most likely as an immiscible melt)(Bolsover, 1986; Bolsover and Lindsley, 1987; Epler et al., 1986; Epler, 1987). At the base of the pit, the country-rock anorthosite hosts numerous tabular, dike-like bodies of Fe-Ti oxides. Bolsover (1986) interprets these bodies as having been intruded downward into the anorthosite. Plagioclase ( $An_{44}$ ) and Fe-Ti oxides are the most abundant minerals in the quarry, each constituting from 10 to >60% of various samples. Olivine is the major ferromagnesian silicate, ranging in composition from  $Fay_{52-62}$  in the silicate-rich rocks to  $Fay_{43}$  in the oxide bodies (Bolsover, 1986; Bolsover and Lindsley, 1983; Epler, 1987). The spinel phase is titanomagnetite with numerous fine-scale exsolution lamellae of ilmenite and granular exsolution blebs of hercynite. The re-integrated magnetite composition has been calculated to be  $Usp_{71}$  to  $Usp_{77}$  (Epler, 1987). There is also a coarse ilmenite present that is interpreted

to be either a primary igneous phase or one that formed by sub-solidus oxidation of magnetite very early in the cooling history of the body (Bolsover, 1986). The ilmenite is mostly single phase, but very rare hematite exsolution is also present. The composition of ilmenite is  $\text{Ilm}_{96.98}$  in the silicate-rich rock and  $\text{Ilm}_{97}$  in the ores. Minor minerals include apatite, inverted pigeonite, and high-Ti biotite. The samples are generally unaltered except for minor blue green amphibole and chlorite along veinlets in some samples (Bolsover, 1986; Bolsover and Lindsley, 1983).

Several lines of evidence indicate that crystallization and cooling of the Sybille quarry rocks occurred slowly from high temperature. Experimental melting studies indicate that the solidus for the Sybille oxide bodies is between 1050-1100°C in the presence of a carbon flux (Epler et al., 1986; Epler, 1987). This is consistent with the presence of inverted pigeonite which indicates minimum crystallization temperatures of 980°C for the olivine leuconorite (Bolsover, 1986; Bolsover and Lindsley, 1983).

Approximate cooling rates for these rocks have been determined by modelling the emplacement of a 1100°C body the size of the Laramie Anorthosite into 300°C country rocks. These calculations yield values of ~60°C/my during cooling to 900°C and ~10°C/my during cooling from 900 to 650°C (calculated by using Peacock, S.M. in F.S. Spear and S.M. Peacock, short course, 1990, unpublished manual). Furthermore, the occurrence of unaltered olivine, and the preservation of inverted pigeonite and exsolved lamellar ilmenite within titanomagnetite grains suggest a cooling history with little deformation or aqueous fluid influx. In addition, radioisotope studies indicate that rocks associated with the Laramie Anorthosite have undergone no subsequent metamorphism (Fuhrman et al., 1988; Grant and Frost, 1990). The combination of a high temperature locality, a relatively simple slow cooling history and a highly variable modal mineralogy makes this an ideal place for testing the sampling strategies and numerical methods described in the previous chapters.

### **Analytical procedures and results**

Samples showing a wide range of modal abundances and mineralogy were selected

in the field. These samples were cut into slabs which were then polished and etched with HF for modal abundance estimates. Thin sections were also used to obtain modal abundance estimates for minerals of small grain sizes. All modal abundance determinations were done using standard point counting techniques. At least 2000 points were counted for each sample yielding uncertainties better than  $\pm 2\%$  absolute for all phases and better than  $\pm 1\%$  absolute for phases that make up more than 20% of the rock. Mineral separates obtained using conventional techniques (magnetic and density separation) were further purified by hand picking. Purity was checked both optically and by XRD and is better than 95%. Oxygen was extracted from the mineral separates and converted to CO<sub>2</sub> using standard techniques (Clayton and Mayeda, 1963). The isotopic composition of CO<sub>2</sub> gas analyzed on a VG micromass 602D and is reported in conventional delta notation (‰ units deviation from *V-SMOW*). Most analyses were repeated at least twice. Nineteen analyses of the isotopic reference material NBS-28 made over the course of the study yielded a mean of  $9.69 \pm 0.15\%$  ( $1\sigma$ ). Temperature data and uncertainties for all calculations were made by using the equations presented in chapter 2.

Microprobe (EPMA) data were obtained by using ARL SEMQ at the Geology Department, University of Alberta. The accelerating potential was 15kV, the probe current was approximately 8 nanoamps measured on brass. Counting times were 20 seconds on the peak and 10 seconds on each of the high and low background positions. The data were reduced using the phi-rho(Z) program of Tracor-Northern. Standards used were a mixture of natural silicates and oxides. Most analyses were made by using a focused beam with a spot size of 2 microns. SEM photomicrographs used in this study were taken by G. Braybrook using an Cambridge Stereoscan S250 SEM housed in the Geology Department at the University of Alberta. Operating conditions were, 20KV accelerating voltage at 10 mm working distance. The samples for both EPMA and the SEM analyses were prepared as polished thin sections that were then carbon coated.

The results of this isotopic study are presented in Table 4.1. Variations in the isotopic compositions of minerals from the Sybille quarry fall into three categories: inter-sample, intra-sample and intra-grain variability. Inter-sample variability is the greatest



of the three. Intra-sample and intra-grain variability were not generally observed within our sampling and detection limits, but may occur in some cases.

The  $\delta^{18}O$  of plagioclase from different samples range from 7.73‰ in plagioclase-rich samples to 9.75‰ in plagioclase-poor samples. Intra-sample and intra-grain isotopic variability is not observed. Samples SP-7 and SP-2 exhibit little or no detectable variation between different parts of two large plagioclase grains (Fig. 4.3). Moreover, the large plagioclase from sample SP-2 exhibits no detectable differences in isotopic composition relative to two smaller grains within the same hand sample (Fig 4.3). The lack of isotopic variability occurs regardless of the contacting minerals, as one of the grains is in direct contact with several ilmenite and magnetite grains while two other grains are not.

Magnetite also exhibits large inter-sample isotopic variations. The isotopic compositions of magnetite are most  $^{18}O$ -rich for magnetite from magnetite-rich samples (4.36 to 4.53 ‰) and least  $^{18}O$ -rich for magnetite from magnetite-poor samples (2.45 to 2.81 ‰). Magnetite associated with a retrograde chlorite and amphibole veinlet in sample SP-7 (Fig. 4.3) exhibits a  $\sim 1$  ‰  $^{18}O$  depletion relative to adjacent magnetite, which may reflect the timing of the vein formation. Ilmenite from the same sample exhibits constant  $\delta^{18}O$  values regardless of proximity to the veinlet. Isotopic compositions of ilmenite grains from different samples exhibit a considerably smaller range of values, but are still more  $^{18}O$ -rich for oxide-rich samples (5.02 to 5.27 ‰), relative to oxide-poor samples (4.37 to 4.83 ‰). No attempts were made to assess intra-grain isotopic variability for either magnetite or ilmenite.

Isotopic variations for apatite, olivine, biotite and pyroxene in different rock types are smaller than those for magnetite. This narrow range may be somewhat misleading because analyses of these minerals was not possible for all samples. In all cases, however, the most  $^{18}O$ -rich grains were associated with magnetite-rich samples (7.28 ‰ apatite, 6.71 ‰ olivine, 7.85 ‰ biotite and 7.23 ‰ pyroxene) and the most  $^{18}O$ -poor grains were associated with plagioclase-rich samples (6.79 ‰ apatite, 6.18 olivine, 6.04 ‰ biotite and 7.06 ‰ pyroxene). Seven size fractions of apatite from sample SP-3 were separated, measured and analyzed for their oxygen isotopic composition (Table 4.2). The isotopic

compositions of all apatite size fractions are the same within analytical uncertainty ( $\pm 0.15\%$ ).

Oxide mineral chemistry is reported in Table 4.3. In general, the Fe/Ti of ilmenite are the same in ilmenite lamellae that are contained in magnetite grains as it was in granular ilmenite in the samples. The style of exsolution varies between the troctolites and the ores. The lamellae in the ore samples are narrower and more closely spaced than those in the troctolite (Figure 4.4).

### **Conventional isotopic thermometry of rocks from the Sybille quarry**

Experimentally and empirically calibrated oxygen isotope thermometers (Bottinga and Javoy, 1975; Smyth and Clayton, 1988; Clayton et al., 1989; Chiba et al., 1989) were applied to all samples (Table 4.4). The most sensitive of these is the plagioclase-magnetite thermometer which gives temperatures of 687-771 °C for the Sybille rocks. These relatively low temperatures suggest that plagioclase and magnetite are among the lower closing phases in quarry. This conclusion is consistent with the large variation in the isotopic composition of both minerals with variations in modal abundance.

The plagioclase-ilmenite thermometer yields temperatures ranging from 992 °C in plagioclase-rich samples to 741 °C in plagioclase-poor samples. The preservation of very high temperatures in plagioclase-rich samples suggests that ilmenite has a high closure temperature. To a small extent, this may be a spurious result, reflecting an increase in  $\delta_{ilm}$  through exchange with the isotopically lighter phase magnetite. Such a result, however, could only occur if ilmenite were to close at a temperature that was below the closure temperatures for either plagioclase or magnetite. This is unlikely for two reasons. First, ilmenite has a smaller ionic porosity than both plagioclase and magnetite and hence is predicted to have lower oxygen diffusivity (Dowty, 1980; Fortier and Giletti, 1989; Muehlenbachs and Connolly, 1991; Gautason and Muehlenbachs, 1993). Second, ilmenite isotopic compositions do not show a correlation with magnetite/ilmenite or

magnetite/plagioclase as would be expected if retrograde exchange with either magnetite or plagioclase was significant. Such correlations do occur for both the isotopic compositions of plagioclase and magnetite relative to the observed plagioclase/magnetite ratios. We suggest therefore that ilmenite in the Sybille rocks preserves a high temperature isotopic composition. If this is the case in other areas as well, then ilmenite is a much better choice for high-temperature isotopic thermometry than the more commonly used low  $^{18}O$  mineral, magnetite.

One possible reason for the large difference between the apparent plagioclase-ilmenite and plagioclase-magnetite temperatures is that magnetite and ilmenite have markedly different diffusional closure temperatures. We do not favor this hypothesis as the ionic and anionic porosities of magnetite and ilmenite are roughly comparable and the oxygen diffusivities are predicted to be similar as well (Dowty, 1980; Fortier and Giletti, 1989; Muehlenbachs and Connolly, 1991; Gautason and Muehlenbachs, 1993). An alternative explanation is that magnetite in these samples does not record a diffusional closure temperature. Rather, it records the temperature at which oxyexsolution ceased to be an effective mechanism for maintaining isotopic equilibrium between magnetite and other phases open to isotopic exchange. Such exsolution processes represent a form of dynamic recrystallization that permit isotopic exchange to temperatures well below  $T_c(\text{diffusion})$ . It is interesting to note that the apparent closure temperature for magnetite is similar to the inferred temperature for the cessation of oxyexsolution (Fuhrmann et al., 1988; Frost, 1991). Thus according to this interpretation, on cooling from  $T > 1000^\circ\text{C}$ , one oxide phase (ilmenite) underwent little exsolution and closed to exchange largely by diffusional processes, whereas the second oxide phase (magnetite) underwent significant oxyexsolution and continued exchanging to temperatures well below its  $T_c(\text{diffusion})$ . I examine this possibility in much greater detail later in this chapter.

In accordance with the predictions made with the Giletti (1986) and Eiler et al. (1992) models for isotopic re-equilibration, the best samples for high-temperature thermometry are those that contain one or more slow diffusing minerals and a high modal percentage of the fast diffusing mineral. At Sybille, the best samples are ilmenite-bearing and plagioclase-rich.

Two such samples (SP-1 and SP-2) yield plagioclase-ilmenite temperatures of  $954 \pm 45$  and  $992 \pm 48^\circ\text{C}$ , respectively. These samples provide an approximation of the closure temperature of ilmenite and a minimum estimate of peak temperature.

A variation on this sampling method was employed by Anderson (1966, 1968) who calculated crystallization temperatures for anorthosites based on plagioclase analyses from plagioclase-rich rocks and oxide analyses from oxide-rich rocks. The validity of the method hinges on the assumption that the two rocks were co-magmatic and in isotopic equilibrium. This may not strictly be true if samples are collected over a very large area. For example, temperatures obtained by combining feldspar data from the main body of the anorthosite and oxide data from rocks of the oxide quarry may be spurious. Over the limited scale of the Sybille quarry, however, this assumption is more likely to be valid. Application of the method to the Sybille rocks yields plagioclase-magnetite and plagioclase-ilmenite temperatures ranging from  $912$  to  $966^\circ\text{C}$  and from  $1004$  to  $1100^\circ\text{C}$  for these two thermometers, respectively.

### **Application of single sample model**

Additional insight can be obtained through application of the single and multiple sample numerical methods described in chapter 2. Figure 4.5 illustrates the results of single sample modelling of sample SP-1. In this calculation, all minerals evolve down temperature from one isotopic composition ( $\delta_{ur}^* = 7.12\text{‰}$ ) at infinite temperature along calculated trajectories that are determined only by the modal abundances of the minerals. In this model, these trajectories evolve until the highest closing phase reaches its closure temperature, as determined by the intersection of the calculated IET with the observed isotopic composition of that phase. For sample SP-1, the highest temperature intersection occurs for apatite at  $1444 \pm 1148^\circ\text{C}$ . As this intersection occurs at an exceedingly high temperature, we suggest that it is unlikely to represent the closure temperature for apatite in these rocks. Moreover, further modelling yields a second intersection for apatite at  $545 \pm 152^\circ\text{C}$ . This lower temperature intersection is in better agreement with experimental and theoretical

determinations of oxygen diffusivities in apatite (Farver and Giletti, 1989; Fortier and Giletti, 1989; Muehlenbachs and Connolly, 1991; Gautason and Muehlenbachs, 1993); thus we have chosen to model apatite to temperatures lower than 1444°C. We note that no subsequent anomalous intersections are obtained for the other phases in SP-1 and that, because of its low modal abundance, our choice for the modelling of apatite has negligible effect on the calculated intersection temperatures of other phases.

Given the above interpretation, the highest temperature intersection is obtained for ilmenite ( $993\pm 54^\circ\text{C}$ ) which we interpret as its closure temperature ( $T_{c_{\text{ilmenite}}}$ ) in this sample. Once ilmenite is closed to exchange, the effective mass balance of open minerals changes, altering the IETs of the remaining phases. In our modelling, these IETs evolve from  $T_{c_{\text{ilmenite}}}$  to  $T_{c_{\text{olivine}}}$  ( $952\pm 120^\circ\text{C}$ ), the next phase to reach its closure temperature. Similarly, the slopes of the IETs change again at  $T_{c_{\text{olivine}}}$  and  $T_{c_{\text{magnetite}}}$  ( $704\pm 23^\circ\text{C}$ ). The closure of magnetite causes a marked change in the effective mass balance and, in turn, pronounced changes in the slopes of IETs for both apatite and biotite. In fact, the slope of the apatite IET goes from positive to negative after the closure of magnetite. Further evolution occurs until  $T_{c_{\text{apatite}}}$  ( $548\pm 152^\circ\text{C}$ ). Below this temperature, the only remaining open phases are biotite and plagioclase. The IETs of these two phases evolve to the temperature at which one of them closes to exchange. The closure temperature of this phase corresponds to the temperature recorded by the plagioclase-biotite thermometer ( $430\pm 61^\circ\text{C}$ ).

Table 4.5 lists the model temperatures of ilmenite, olivine and magnetite for all samples in which these phases have been analyzed. Ilmenite model temperatures are consistent ( $993\text{-}1042^\circ\text{C}$ ) for the three samples with the requisite modal characteristics for this type of analysis. Olivine model temperatures are similar in samples SP-4,5,8 ( $858\text{-}882^\circ\text{C}$ ) but higher in SP-1 ( $952^\circ\text{C}$ ). We attribute the higher temperature to the larger grain size of olivine in this sample (Table 4.1). Magnetite model temperatures span a wide range of values  $698\text{-}807^\circ\text{C}$ . The reason for the wide range of  $T_{c_{\text{magnetite}}}$  is discussed in more detail later in this chapter.

It is important to note that the model temperatures for ilmenite from samples SP-1, SP-2 and SP-3 vary over a much narrower interval ( $993\pm 54^\circ\text{C}$ ,  $997\pm 47^\circ\text{C}$  and  $1042\pm 55^\circ\text{C}$ ,

respectively) than the conventional plagioclase-ilmenite temperatures for the same three samples ( $954 \pm 45^\circ\text{C}$ ,  $992 \pm 48^\circ\text{C}$  and  $795 \pm 31^\circ\text{C}$ ). This example illustrates the difference between the apparent temperatures obtained with conventional isotopic thermometry and the model temperatures calculated with the single sample method. Apparent plagioclase-ilmenite temperatures are strongly dependent on the abundance of plagioclase, and, to a lesser extent, on the abundance of the other low closing minerals. Model ilmenite temperatures, on the other hand, are effectively independent of these parameters, provided that ilmenite modal abundances are low. Thus, a distinct advantage of the single sample method is that it gives consistent temperatures for a wider range of samples than does conventional isotopic thermometry.

An additional advantage of the method is illustrated by considering isotopic thermometers that involve two of the highest closing phases in a given sample (e.g., olivine-ilmenite). For samples SP-4, SP-5 and SP-8, examination of the IETs for olivine indicate that apparent olivine-ilmenite temperatures underestimate  $T_{c_{\text{ilmenite}}}$  as a result of continued exchange of olivine with magnetite after closure of ilmenite. In contrast, a similar analysis for sample SP-1 indicates that the apparent olivine-ilmenite temperature is spuriously high as a result of continued exchange between olivine and plagioclase. Because of the high temperatures at Sybille, these shifts in recorded temperatures are all within the stated uncertainties; however, for other cases, such retrograde exchange may significantly shift apparent temperatures either up or down. Thus, the single sample method is more accurate than conventional thermometry because it accounts quantitatively for systematic shifts in the isotopic composition of low closing minerals caused by retrograde exchange.

### **Application of multiple sample model**

Application of the multiple sample methods described in chapter 2 provides a way of retrieving still higher temperature information from the rocks of the Sybille quarry. The most precise estimates of  $T_{c_{\text{syn}}}$  are obtained from samples that show widely different modal abundances and values of  $A_{\text{wt-j}}$ . Figure 4.6 shows the calculated IETs of plagioclase from

the six samples for which isotopic and modal data are available. The nine high-angle intersections obtained from these trajectories give a very precise temperature estimate of  $1068 \pm 42^\circ\text{C}$  (Table 4.6). The actual uncertainty in this estimate of  $T_{c_{yw}}$ , resulting from uncertainties in the determinations of  $\delta_i$  and  $X_i$ , is somewhat larger ( $\pm 64$  to  $\pm 133^\circ\text{C}$ ) (Table 4.6). Nonetheless, the tightness of the intersections is consistent with the assumptions made in formulating the multiple sample model, namely that the minerals from different samples were initially in isotopic equilibrium at some high temperature and that hand-sample scale subsystems effectively behaved as closed systems during cooling.

It should be noted that the calculated values for  $T_{c_{yw}}$  are above the closure temperature for all minerals in the quarry. Such a result is possible because hand-sample scale closure temperatures can be high even for samples containing minerals with high oxygen diffusivities. Thus an advantage of the multiple sample method is that its use does not require the presence of any phases with a high closure temperature, only a large diversity in modal compositions and  $A_{wr-j}$ .

The physical meaning of the  $T_{c_{yw}}$  calculated for the Sybille rocks is not entirely clear. Some possibilities include, but are not limited to: (1) the temperature of liquid immiscibility and the establishment of large-scale compositional heterogeneities in the magma body; (2) the temperature at which advective transport of magma in the crystal-magma mush ceased to effectively maintain isotopic equilibrium over a large area; and (3) the solidus temperature of the system. We suggest that the third possibility is the most likely because of the precipitous drop in bulk oxygen diffusivities that takes place in the transition from a melt-bearing to an entirely crystalline system.

The bulk oxygen diffusion coefficient (weighted average of volume diffusion and grain boundary diffusion) decreases from  $\sim 10^{-9}$  to  $10^{-12}$   $\text{cm}^2/\text{sec}$  across the solidus interval if an inter-connected grain boundary fluid is not present in the subsolidus assemblage (Brady, 1983; Joesten, 1983, 1991). Over a time scale of  $10^6$  years, this decrease in  $D_{\text{bulk}}$  corresponds to a decrease in the length scale of diffusion (length  $= 2\sqrt{D_{\text{bulk}}t}$ ) from  $\sim 3.5$  to  $\sim 0.1$  meters. This calculation does not take into account other factors such as mixing within the melt that may act to increase the effect scale of homogenization in a melt-bearing system and therefore

represents a minimum estimate of the change in equilibration scale across the solidus. Thus we propose that crystallization through the solidus temperature represents the most likely mechanism for establishing a singular temperature (or at least a narrow temperature window) over which a number of subsystems initially in isotopic equilibrium become closed to exchange with each other. The calculated value for  $T_{c_{\text{sys}}}$  is in excellent agreement with solidus temperatures established for the Sybille rocks (1050-1100°C) on the basis of experimental melting studies (Epler, 1987).

### **Testing for Closed system**

The mineral and system closure temperatures noted above were calculated on the assumption that the Sybille rocks behaved as a closed system during cooling. We cite several lines of evidence to substantiate this assumption. In thin section, the delicate textures of inverted pigeonite and exsolved magnetite grains are remarkably well preserved. Moreover, easily alterable minerals such as olivine and pyroxene are not observably retrogressed. Retrograde phases such as chlorite and amphibole are noted, but are rare and restricted to minor veinlets. Thus all the petrographic observations are consistent with little retrograde fluid influx.

The isotopic compositions of plagioclase grains (e.g., Figure 4.3) and apatite size fractions (Table 4.2) are consistent with no major retrograde  $^{18}\text{O}$  shifts. The application of additional isotopic tests (Giletti, 1986; Gregory and Criss, 1986; Criss et al., 1987; Jenkin et al., 1991) lead to a similar conclusion. All minerals plot within error of the fields defined by closed system assumptions, and the closure constraints on the constituent phases. Thus according to these methods, the system is closed to exchange with external reservoirs within the limits of their resolution. Our tests for open system that are based on the simultaneous solution of a number of intersections provide a third test for open system interactions (chapter 3). Given the stated uncertainties on the modal abundances, isotopic analyses and fractionation factors, the data from Sybille plot within error of the field defined for a closed system. Given these observations, we interpret the cooling history of our samples from the



Sybillie quarry to have occurred without significant interaction with an external reservoir.

### **Testing the Equilibration Volume Assumption**

Some of the same tests used to assess the closed system assumption can be used to assess assumptions about the equilibration volume. In Figure 4.7 I have plotted the olivine trajectories and closure temperatures (with one sigma error brackets) for samples SP-1, 4, 5 and 8. The trajectories have been normalized to the respective whole rock compositions so that they all originate from the origin of the plot. The test for the equilibration volume assumption is that the closure temperatures for olivine overlap within their uncertainties. This test is met by these four samples, and indicates that these systems behaved as closed systems and that the assumption that the modes of the samples is representative of the mass balance that operated during cooling have been met. There are both grain size differences and scatter in the measured temperatures, however. Because the grain size differences could result in different closure temperatures it is important to establish that the grain size effects will reduce the scatter rather than increase it. In this case, the highest temperature data correspond to those samples with the largest olivine grains and the lowest temperature data correspond to the samples with the smallest olivine grains. This observation indicates that if we take grain size into consideration, the scatter in temperature data would be reduced and further strengthens our arguments about the validity of the assumptions about closed system and mass balance.

A less sensitive test, but one with very interesting results is undertaken by examination of the ilmenite closure temperatures. Because the ilmenite closure temperatures are within 70°C of the system closure temperature, it is conceivable that the high temperature parts of the ilmenite closure temperature intervals may have overlapped with the low temperature parts of the system closure temperature intervals. Figure 4.8 illustrates how this complication arises. Since we calculate temperature data by assuming a constant volume, and therefore, mass balance, overlaps of this sort can cause errors in the temperature data that we calculate. Graphically, our temperature determinations are based on the intersection

between the projection of the isotopic composition that we measure and the trajectory that we calculate by using mass balance. When the system is closing to exchange, the mass balance of the subsystems is changing, and the trajectories follow curves that reflect this. If a mineral closes while this process operates, its calculated temperature will be too high by a very large amount when the trajectory that it is changing to has a smaller absolute slope than the one that it is changing from. Likewise, the calculated temperature will be too low, by a very small amount when the trajectory that it is changing to has a larger slope than the trajectory that it is changing from (e.g. Figure 4.8). The reason that the shallower sloped trajectories are offset by a greater amount than the steeper sloped trajectories arises from the  $1/T^2$  dependence of the equilibrium fractionation factor.

The ilmenite temperature data calculated for the Sybille rocks may in part reflect an equilibration volume problem connected with an overlap between the closure intervals and the system closure interval. The evidence for this may be include calculated ilmenite closure temperatures are geologically too high for the most magnetite rich-samples (e.g. Table 4.5). Caution must be exercised, however, because these interpretations are made on the basis of differences that fall within 2 sigma uncertainties. Strictly speaking, no hard and fast conclusion can be made on the basis of the present data. The data are, however, consistent with the possibility of an overlap, and more work could be done to establish whether this is in fact what has happened.

### **The Mechanics of Isotopic Exchange**

An important outgrowth of the temperature data is its interpretation in terms of the mechanics of isotopic exchange. In many studies to date it is assumed that isotopic exchange in many slowly cooled rocks is limited by volume diffusion. The calculation of observed closure temperatures, combined with the extremely good documentation of this deposit and the LAC gives us a chance to take a particularly good look at the mechanisms by which isotopes have been exchanged between minerals. The strategy of this exercise will be to compare the isotopic temperature data with predictions that are made on the basis of isotopic

exchange models, cooling rate data, petrographic data and reaction progress calculations. I will focus on ilmenite, olivine and magnetite because these are the minerals for which I have the best high temperature data.

The observed closure temperatures for ilmenite, magnetite and olivine are given in Table 4.5. Examination of these values reveals that closure temperatures for ilmenite (993-1042°C) and olivine (858-952°C) are significantly higher than those for magnetite (698-807°C). Below, we assess whether the lower magnetite temperatures are caused by smaller grain size, higher oxygen diffusivity, or a different oxygen exchange mechanism.

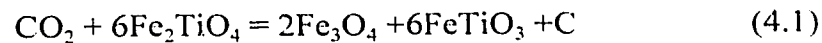
At Sybille, the radii of ilmenite, olivine and magnetite grains are similar (Table 4.1). Thus, the lower magnetite closure temperatures cannot be attributed to macroscopic grain size differences. Moreover, the style of exsolution in magnetite from the ores and magnetite from the troctolites is different. Whereas ilmenite lamellae are very closely spaced and very numerous in magnetite grains from the ores (Fig. 4.4a), they are very widely spaced and few in magnetite grains from the troctolites (Fig. 4.4B). The absence of any obvious correlation between the density of the lamellar network and the observed closure temperatures (c.f. Fig. 4, A and B and Table 4.1) suggests that intragranular domain size is also not a controlling factor.

A second possibility is that the diffusion rates for oxygen in magnetite are significantly faster than those in ilmenite and olivine. Ranges of diffusional closure temperatures for these minerals determined by using available diffusion data and the equation of Dodson (1973) are 790-1050 °C (ilmenite), 560-1000 °C (magnetite) and 650-1300 °C (olivine) (calculated from Giletti and Hess, 1988; Cole and Ohmoto, 1986; Fortier and Giletti, 1989; Jaoul et al., 1991; Sharp, 1991; Gautason and Muehlenbachs, 1993). These ranges are broad enough to satisfy the observed closure temperatures for Sybille. We suggest, however, that this does not provide a valid argument for solely diffusion controlled exchange because these diffusivities were determined for a broad range of conditions ( $fH_2O$ ,  $fCO_2$ ,  $fO_2$ , etc..[*f-fugacity*]) and it is well established that oxygen diffusivity is strongly dependent on such factors (Farver and Yund, 1991; Sharp et al., 1991; Zhang et al., 1991).

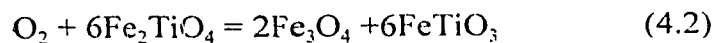
To reduce complications arising from incompatible diffusion data, the empirical

diffusion model of Gautason and Muchlenbachs (1993) was used. Although closure temperatures calculated with this model may not be correct in an absolute sense, they should provide a reasonable approximation of the relative closure temperatures of the minerals. Diffusional closure temperatures determined with this model are similar for ilmenite, magnetite and olivine grains (1000-1050 °C, 940-1000 °C, and 850-1010 °C, respectively) (Table 4.7). Notably the diffusional closure temperatures for ilmenite and olivine agree well with their observed closure temperatures whereas diffusional temperatures for magnetite are significantly higher than observed temperatures. This difference is consistent with volume diffusion moderated oxygen exchange in ilmenite and olivine. It is also consistent with oxygen exchange in magnetite that is not limited by volume diffusion but is enhanced at lower temperatures by the oxyexsolution process.

The nature of the relation between oxyexsolution and oxygen exchange is best explained in the context of the exsolution process. Epler (1987) proposed that oxyexsolution at Sybille occurred by the reaction



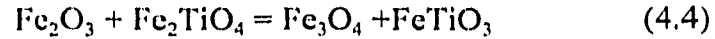
which is a linear combination of the oxyexsolution reaction (Buddington and Lindsley, 1964)



and the reaction that defines the reduction of  $\text{CO}_2$  to graphite



In addition to these reactions, an exchange reaction for Fe and Ti between the rhombohedral oxide (ilmenite-hematite solid solution) and the cubic oxide (magnetite-ulvöspinel solid solution) must also be observed. This reaction is written



The effect of this reaction on the  $f\text{O}_2$ -temperature history of the deposit is illustrated in Figure 4.9. The Sybille magmas either crystallized on, or cooled to, the graphite saturation surface (Epler, 1987). During subsequent cooling, oxyexsolution and Fe-Ti exchange resulting from reactions (4.1 and 4.4) constrained the rocks to the graphite saturation surface (path A-B-D) until the  $\text{CO}_2$ -bearing fluid was completely consumed. Whereas the troctolite remained on this surface to temperatures below 500 °C, the ore completely consumed the fluid (and stopped oxyexsolving) at higher temperatures. Subsequent evolution of the ore occurred by interoxide Fe-Ti exchange (path B-C) (Frost et al., 1988; Fuhrman et al., 1988). We can calculate isopleths of reaction progress for the oxyexsolution reaction in  $\Delta\log f\text{O}_2$ -temperature space by using compositional and modal data for the oxides in combination with equilibrium constraints from calibrations of reaction (4.2). The fields defined by magnetite ilmenite pairs for the troctolites and the ores define the temperatures given by Fe-Ti oxide thermometry. They are different for two rock types and reflect the different modal proportions of oxides and fluids present in each.

In Figure 4.10, I have calculated the isopleths of reaction progress predicted for the ores by using the compositional and modal data collected in this study, compositional data reported in Epler (1987) for the reintegrated ulvospinel, and the equilibrium constraints imposed by Andersen and Lindsley (1991). A similar diagram could be calculated by using the equilibrium constraints of Sack and Ghiorso (1991). This was not done because of the complexity of their Fe-Ti activity equations. If it were done, the isopleths of reaction progress would be shifted to lower temperatures by approximately 50 to 100 °C. To calculate the reaction progress on equation (4.1) we must consider the trajectories followed by the rock in  $\Delta\log f\text{O}_2$ -Temperature space. Since this trajectory is defined by the graphite saturation surface, the amount of exsolution can be calculated by locating the intersection of the isopleths of reaction progress for reaction (4.2) and the graphite saturation surface (reaction 4.3). Because reaction (4.3) involves  $\text{CO}_2$  as a reactant, it is important to determine the activity of  $\text{CO}_2$  ( $a_{\text{CO}_2}$ ) in the fluid phase.  $\text{CO}_2$  activities cannot be calculated rigorously

for the Sybille fluids, but reasonable inferences can be made from the available data. On the basis of a fluid inclusion study, Frost and Touret (1989) concluded that magmatic fluids associated with the Laramic anorthosite complex were both CO<sub>2</sub>-rich and highly saline and likely formed at the magmatic stage as immiscible fluid and chloride melt. On cooling, these fluid phases crystallized salt, yielding a salt saturated system and possibly a three phase, salt + brine + CO<sub>2</sub> fluid system. No direct determinations of  $a_{\text{CO}_2}$  for such salt bearing C-O-H systems exist for the temperature range estimated for Sybille (600-900 °C). However, Bowers and Helgeson's (1983) calculations at lower temperatures indicate that activity coefficients of CO<sub>2</sub> in these systems are strongly positive. Thus I infer that  $a_{\text{CO}_2}$  in the fluid was high during cooling of the Sybille rocks, and choose to bracket the calculations with  $a_{\text{CO}_2}$  values of 0.8 and 1.0. We note that the projected temperature estimates are not strongly affected by variations in  $a_{\text{CO}_2}$  for values of >0.5.

Calculations made on the basis of modal and compositional data for coexisting oxides at Sybille indicate that magnetite oxyexsolution stopped over the temperature interval 630-720 °C in the ores but continued to below 500°C in the troctolites (Fig 4.11). This disparity in oxyexsolution temperatures is not reflected in the oxygen isotope closure temperatures. Moreover in both rock types, a significant fraction (30-40%) of the total oxyexsolution took place at temperatures below the observed closure temperatures (Figure 4.11A). These observations suggest that although observed closure temperatures of magnetite are related to oxyexsolution, they do not correspond directly to the cessation or total amount of oxyexsolution.

A final possibility is that oxygen exchange is related to the rate of oxyexsolution. In Figure 4.11B, we have calculated this rate in the ore and the troctolite as a function of temperature. The oxyexsolution rate is controlled by the spacing of the magnetite isopleths (Fig. 4.9) and the cooling rate. We estimated the cooling rate by using the one dimensional conductive cooling model of S.M. Peacock (F.S. Spear and S.M. Peacock, short Course, 1991, unpublished manual). Exsolution rates are high at temperatures of >900 °C because of rapid initial cooling rates; the rates drop somewhat over the 675-900 °C range because of decreases cooling rates, but are still maintained at relatively high levels because of closely

spaced isopleths of reaction progress in this temperature interval. Below ~675 °C, exsolution rates in both the ores and the troctolites drop sharply to low levels because of the combined effects of more widely spaced isopleths of reaction progress and slower cooling rates. Although numerical values for the oxyexsolution rate depend on the input cooling rates, we note that the basic shape of the oxyexsolution rate curve will be the same for any rock that experiences rapid initial cooling followed by slower cooling as the temperature approaches the steady state geotherm. These conditions are likely to be met at Sybille because emplacement of the entire anorthosite complex occurred over a short time interval (Scoates and Chamberlain, 1993) and because there is no petrologic evidence for a complex cooling history (Grant and Frost, 1990).

The relationship between oxygen exchange and oxyexsolution may reflect a critical oxyexsolution rate is required to facilitate oxygen exchange. In atomistic terms, this critical rate may be related to the relative rates of defect production in the mineral lattice by nucleation of ilmenite molecules within the intralamellar magnetite domains during oxyexsolution and defect removal from the mineral lattice by formation and coarsening of the lamellae. If this process controlled exchange rates in magnetite, when oxyexsolution rates diminished, the steady state defect density decreased, and the process by which exchange was being enhanced ceased to operate. This is my preferred explanation for the data. An alternate interpretation is that the observed closure temperatures reflect a modified Arrhenius equation for oxygen diffusion in a defect-laden magnetite lattice (i.e., lower activation energy and preexponential terms). I cannot discount this possibility, but do not favor it because of the very different scales of domain sizes and similar closure temperatures in the two rock types. In fact, oxygen closure in magnetite in three of the four ore samples is 40-80 °C higher than that in the troctolite.

The proposal that enhanced oxygen exchange is tied to the rates of the exsolution reaction is speculative but makes an interesting and potentially testable prediction. For rocks undergoing oxyexsolution, rapid cooling results in high rates of oxyexsolution. In turn, because the model predicts a positive correlation between oxyexsolution rates and rates of oxygen exchange, closure temperatures for exsolved magnetites may decrease with

increasing cooling rate. This hypothesis is the opposite to that predicted by volume diffusional constraints alone and can be tested by comparing magnetite closure temperatures from rocks that have undergone similar amounts of exsolution at different cooling rates.

## **Conclusions**

The methods described in chapters 2 and 3 give excellent results when applied to the rocks of the Sybille quarry. The single sample numerical method yields model temperatures for ilmenite of ~1000°C, higher than any other conventional oxygen isotope temperature yet reported for slowly cooled rocks. In addition, the multiple sample method yields model temperatures of ~1070°C, nearly identical to an experimentally determined solidus temperature for these rocks (Epler, 1987). Mineral closure temperature data was obtained for other minerals from Sybille and indicates the order of mineral closure to be ilmenite > olivine > pyroxene > magnetite > apatite > biotite = plagioclase.

The temperature data obtained with these methods is better than temperature data obtained with conventional isotope thermometry because in closed systems, they provide the mineral closure temperatures rather than apparent mineral-pair temperatures. Because these temperature data can be directly linked to oxygen closure, they can be used to gain insight into the processes that control oxygen exchange. At Sybille, the data indicate that oxygen exchange in ilmenite and olivine has occurred primarily by volume diffusion processes, whereas oxygen exchange in magnetite has been enhanced by oxyexsolution. The mechanism by which this effect occurs is not straightforward in that closure cannot be correlated directly with the cessation or total amount of oxyexsolution, or to the present day domain size imposed by the network of exsolution lamellae. The preferred interpretation is that oxygen exchange is enhanced by defects produced by the oxyexsolution reaction. If this is the case, oxygen exchange is enhanced by high defect densities in the host magnetite that are made by the oxyexsolution reaction and removed by the process of lamellae formation and coarsening. Because both processes occur during cooling, the steady state defect density will be related to the relative rates of these two processes, and most directly related to the



rate of the oxyexsolution reaction. Oxyexsolution reaction rate calculations can be made by combining reaction progress and cooling rate calculations and are consistent with the interpretation that a critical oxyexsolution rate controlled enhanced oxygen exchange at Sybille.

These results indicate that isotopic thermometry can be used to obtain meaningful temperature data for at least some plutonic igneous rocks. For Sybille, the isotopic temperature data provide more consistent and higher temperature results than do cation exchange data, and are less time consuming and difficult to obtain than experimental investigations. At present, the isotopic temperature data obtained for the minerals and rocks of the Sybille quarry are among the highest quality temperature data that exist for the rocks of the Laramie Anorthosite Complex.

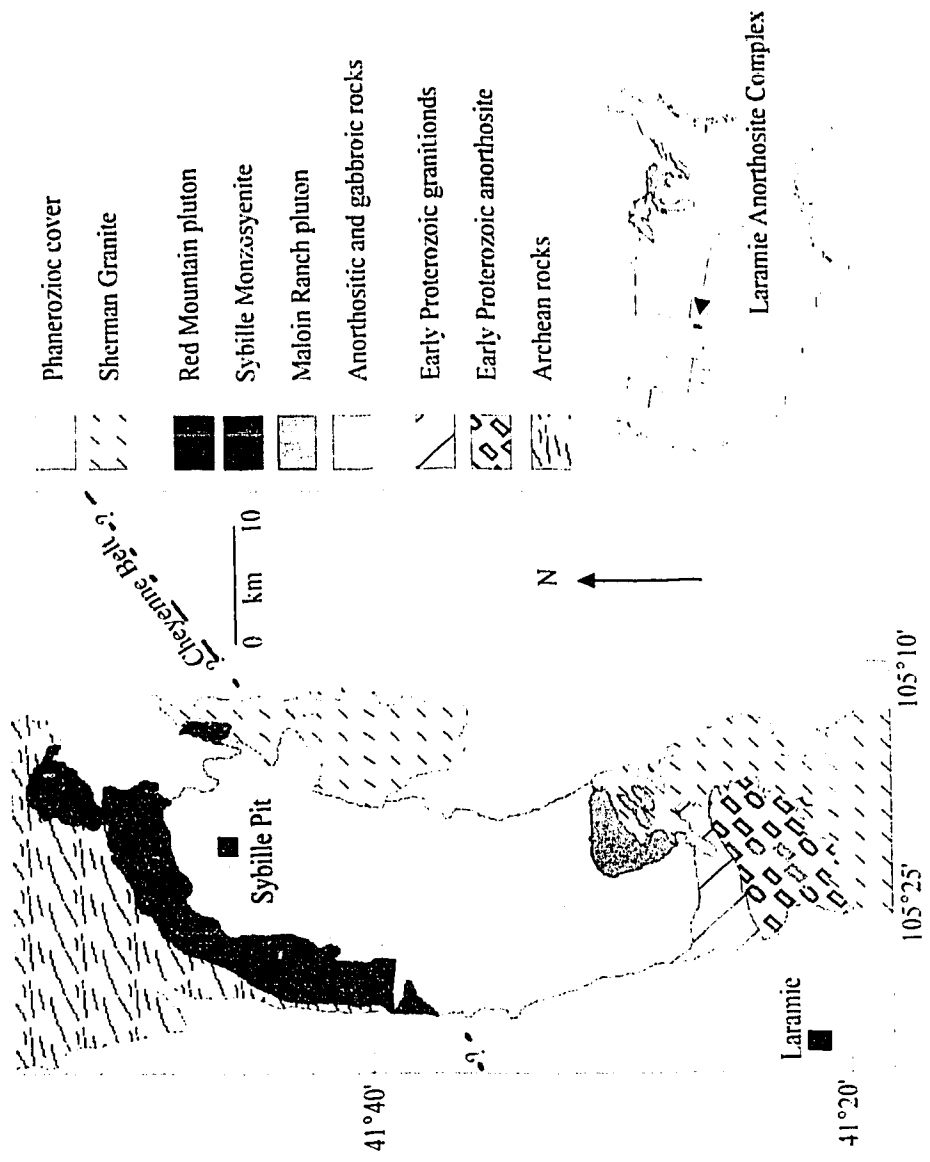


Figure 4.1 Map of the Laramie Anorthosite Complex. Modified after Newhouse and Hagner (1957), Duebendorfer and Houston (1987), and Grant and Frost (1990).

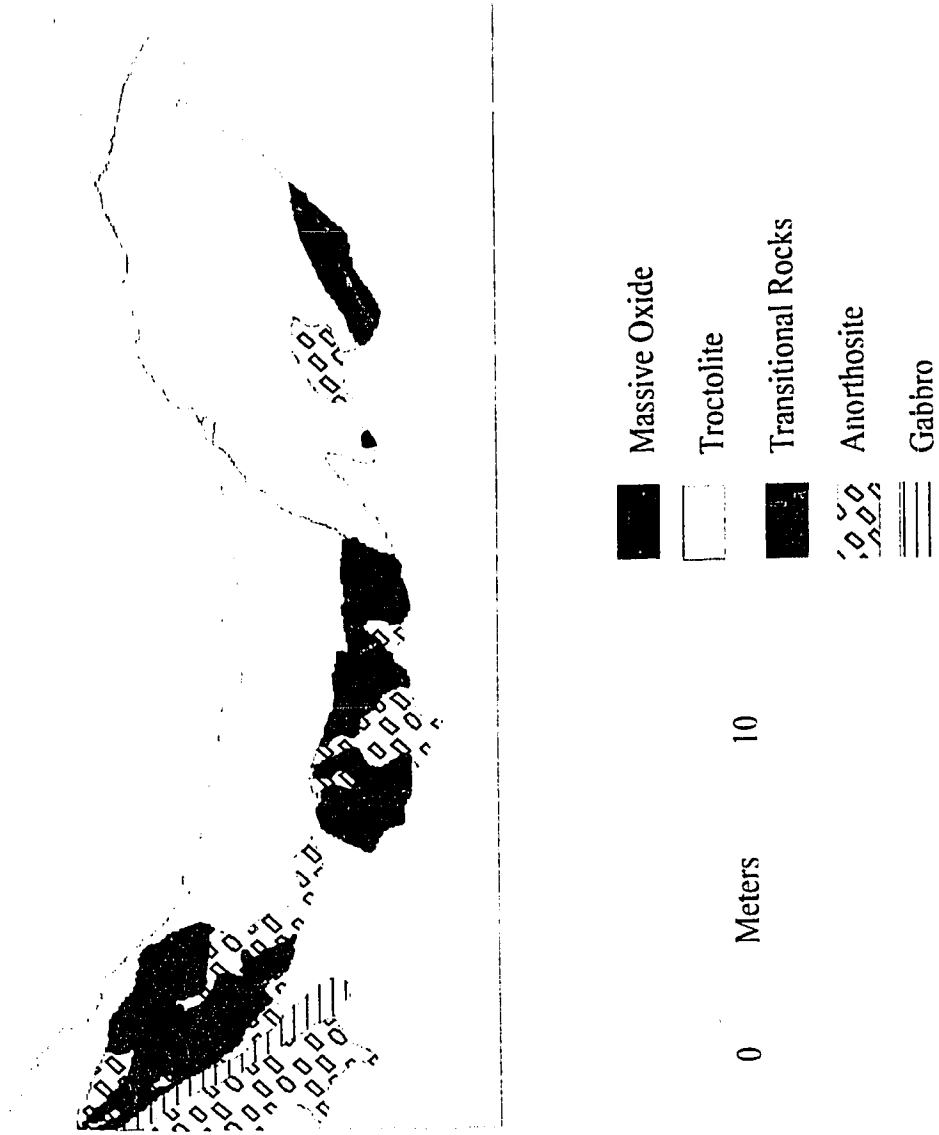
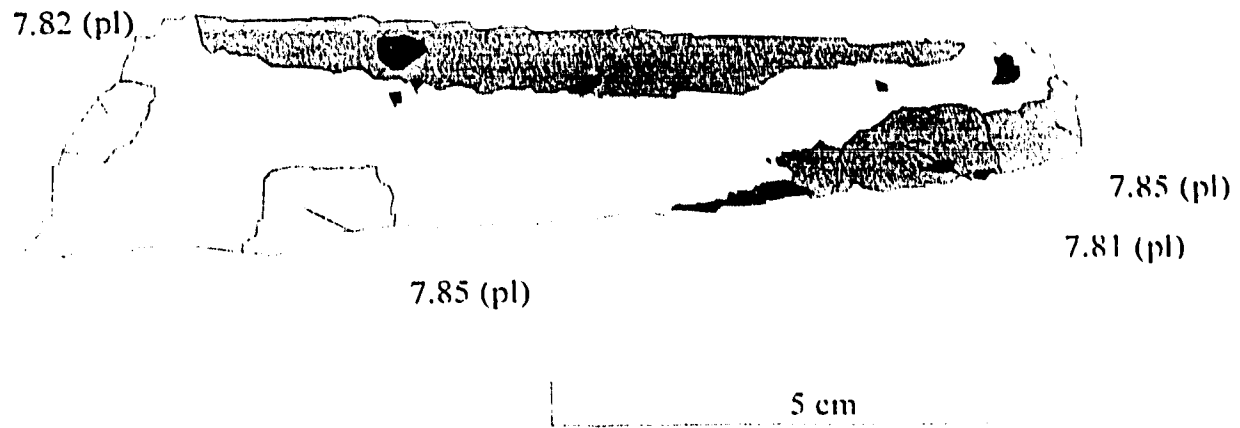


Figure 4.2 Outcrop map of the north wall of the Sybille quarry after Bolsover (1986).

SP-2



SP-7

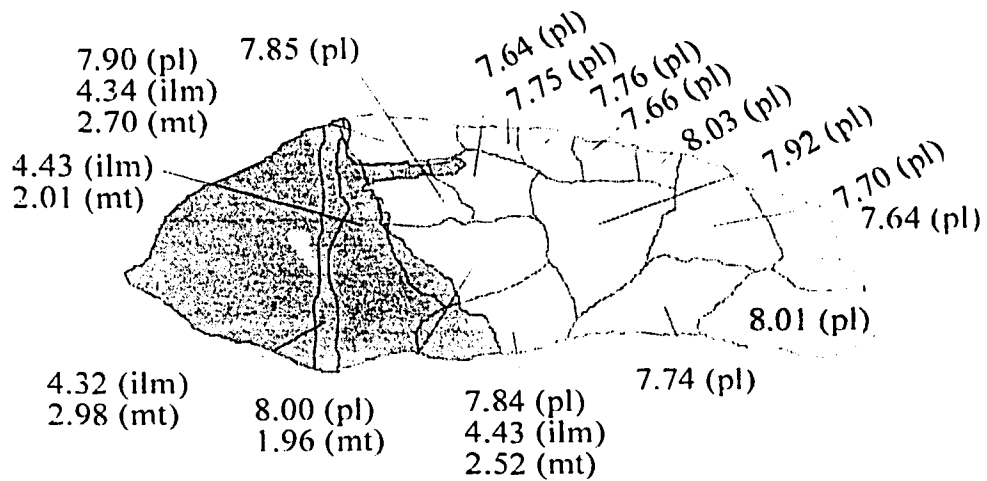


Figure 4.3 Isotopic analyses of plagioclase, ilmenite and magnetite from two large grains - SP-2 and SP-7.

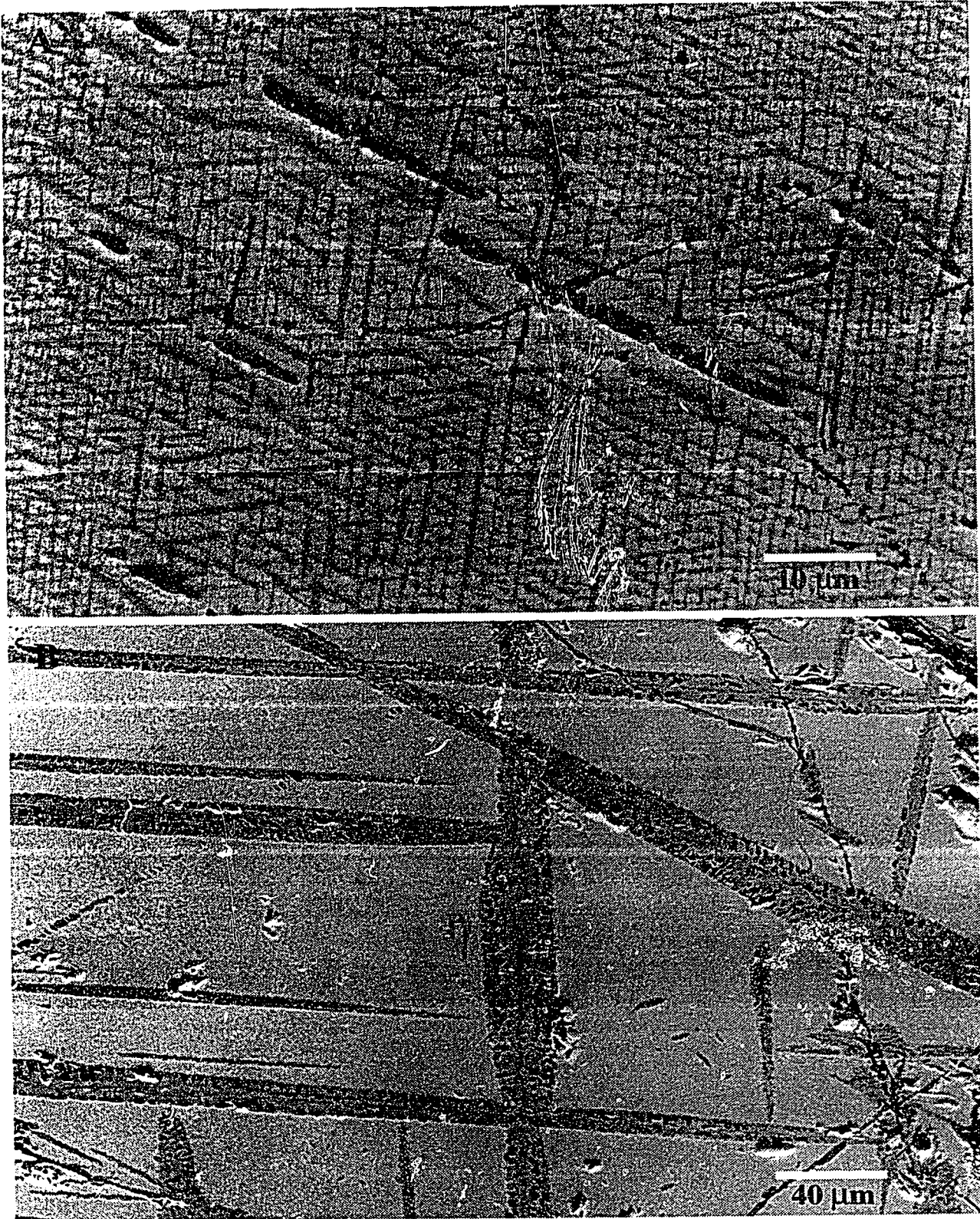


Figure 4.4 Backscattered-electron images of exsolved ilmenite (dark gray) and hercynite (black) lamellae within titanomagnetite (light gray) from ore (A) and troctolite (B). (Modified after Farquhar and Chacko, 1994.)

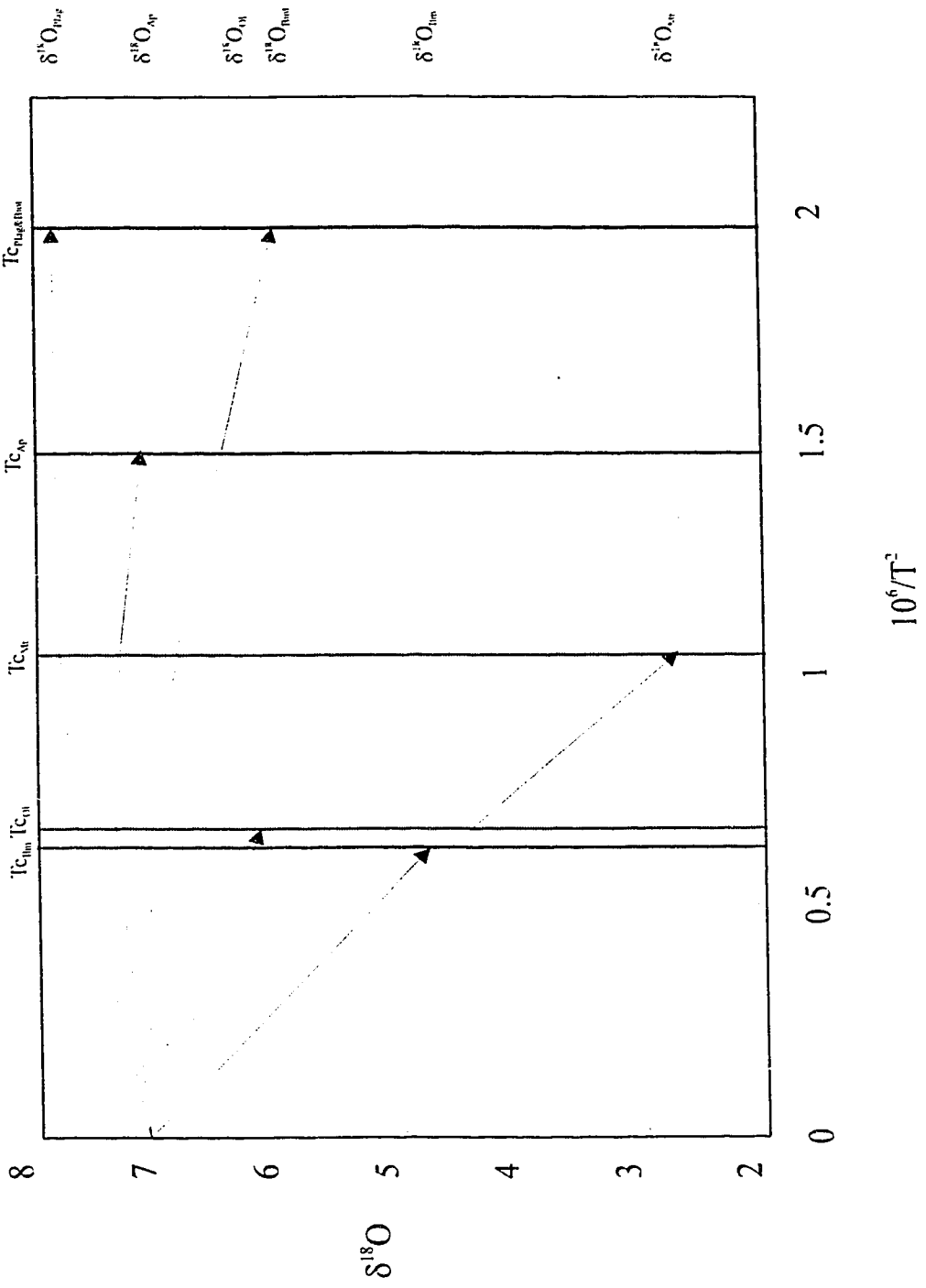


Figure 4.5 Isotope Exchange Trajectories and Closure temperatures for sample SP-1.

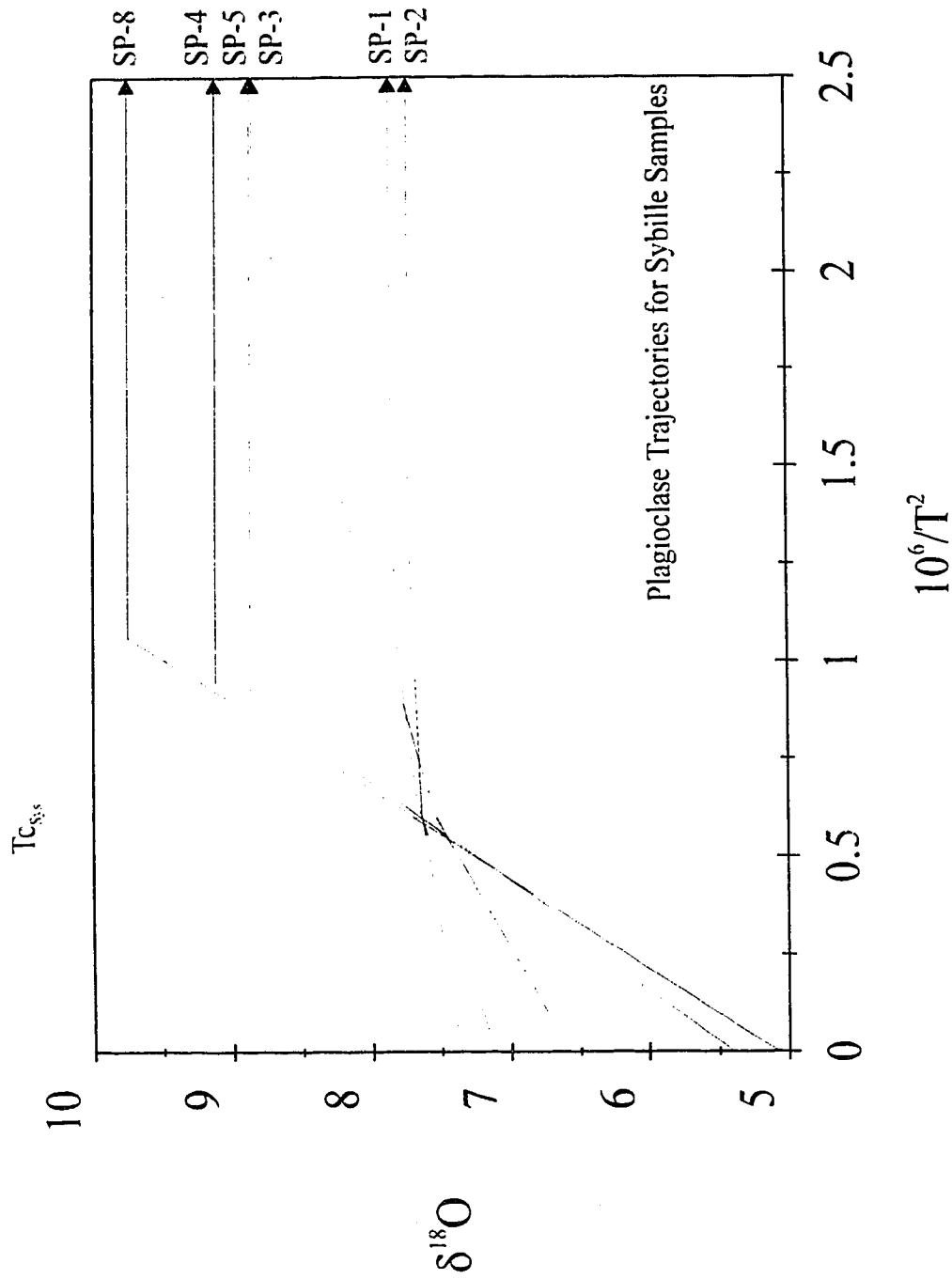


Figure 4.6 Calculation of system closure temperatures for sybille samples. (Recalculated from Farquhar et al., 1993)

Check for equilibrium LAC Olivines  
 ( $1\sigma$  envelopes only overlap for  $\pm 0.16$  ‰)

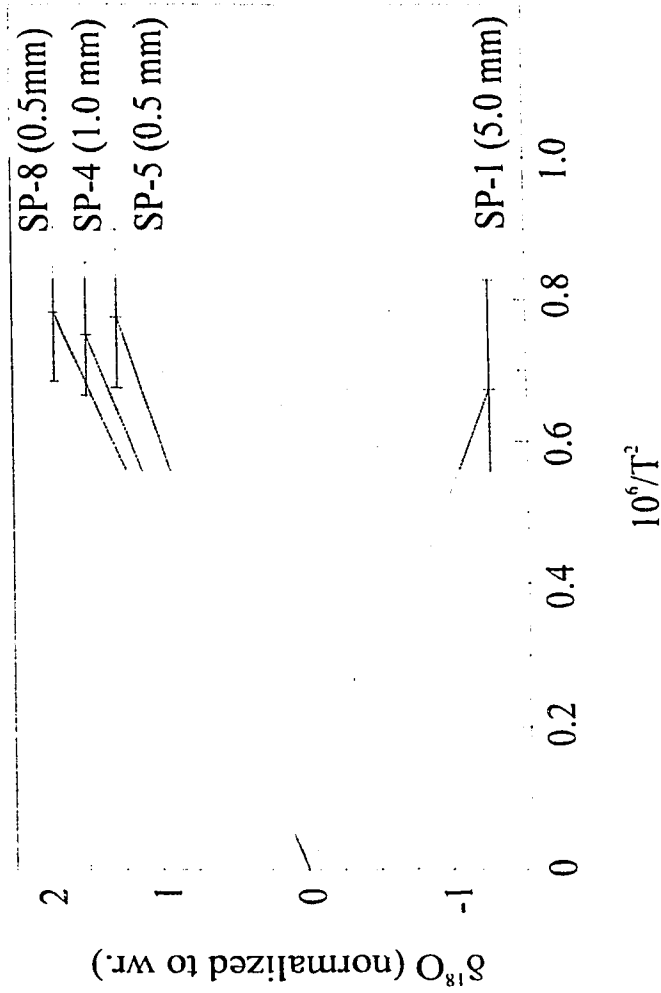


Figure 4.7 Olivine trajectories and closure temperatures for Sybille Samples. Test for assumptions (closed system-equilibration volume). See text.



Equilibration Volume Problem  
Effect of System Closure on Ilmenite Closure

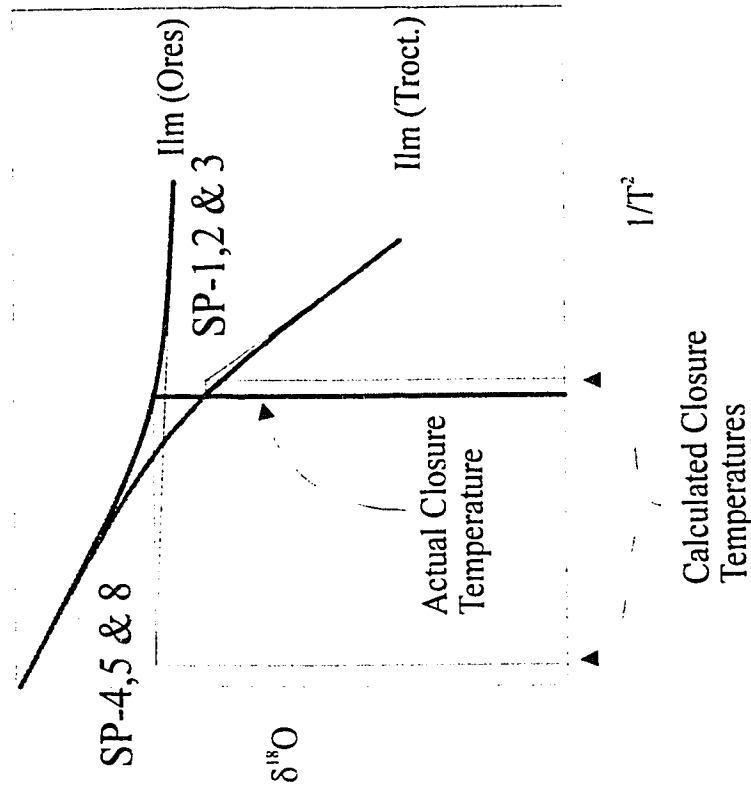


Figure 4.8 Schematic diagram to illustrate possible equilibration volume problem for ilmenite temperatures in ores. See text for details.

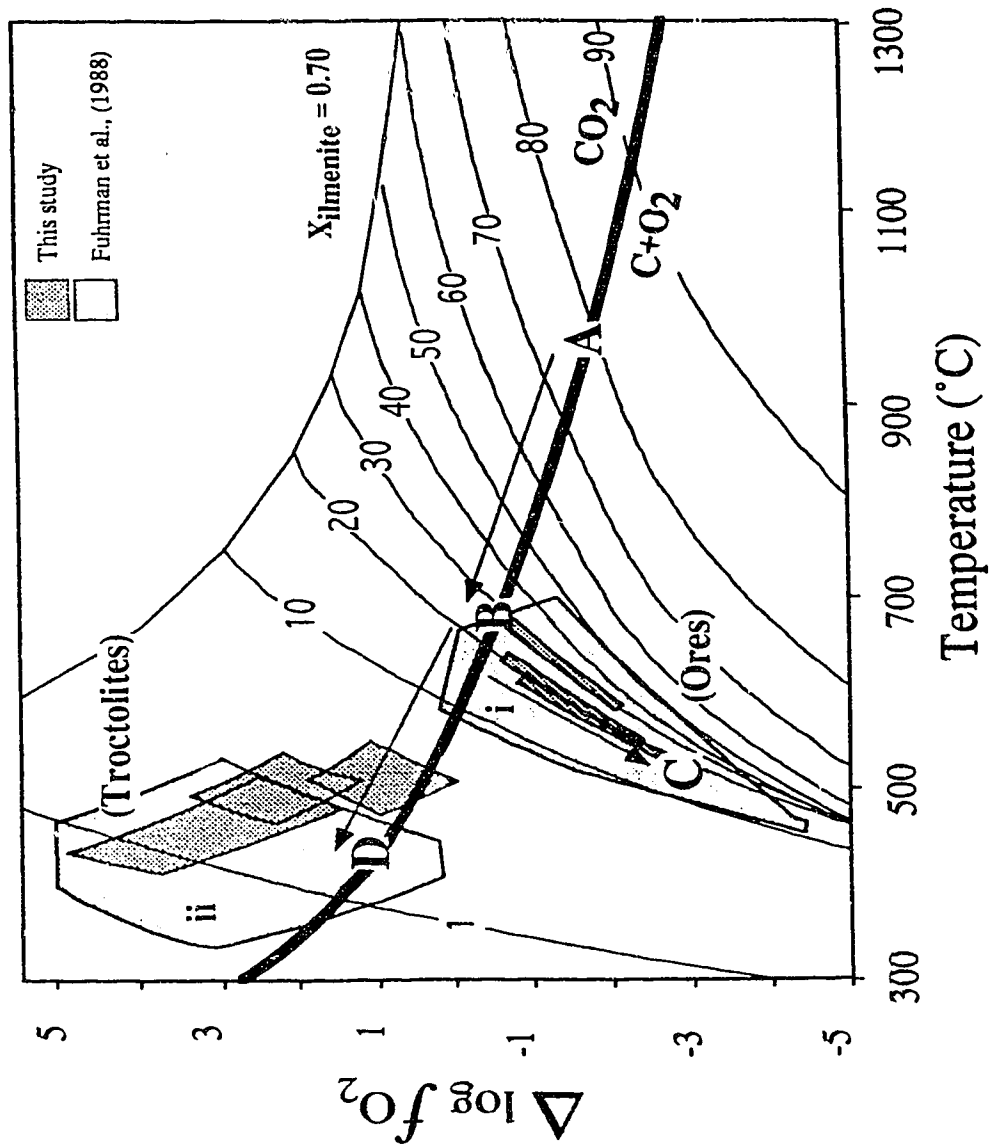


Figure 4.9 Delta log fO<sub>2</sub> temperature diagram calculated using Andersen and Lindsley (1988). Contoured with isopleths of X<sub>usp</sub> in magnetite. Shaded fields defined by present oxide compositions. See text for discussion.

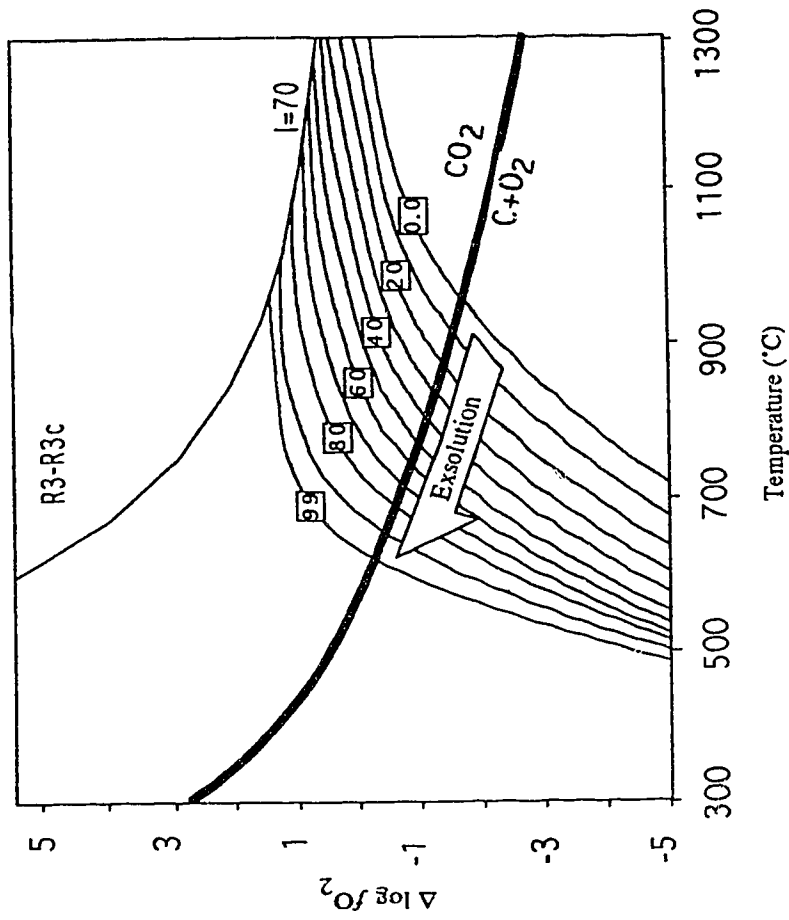


Figure 4.10 Calculated contours of percent spinel exsolved for ores.  
See text for details.

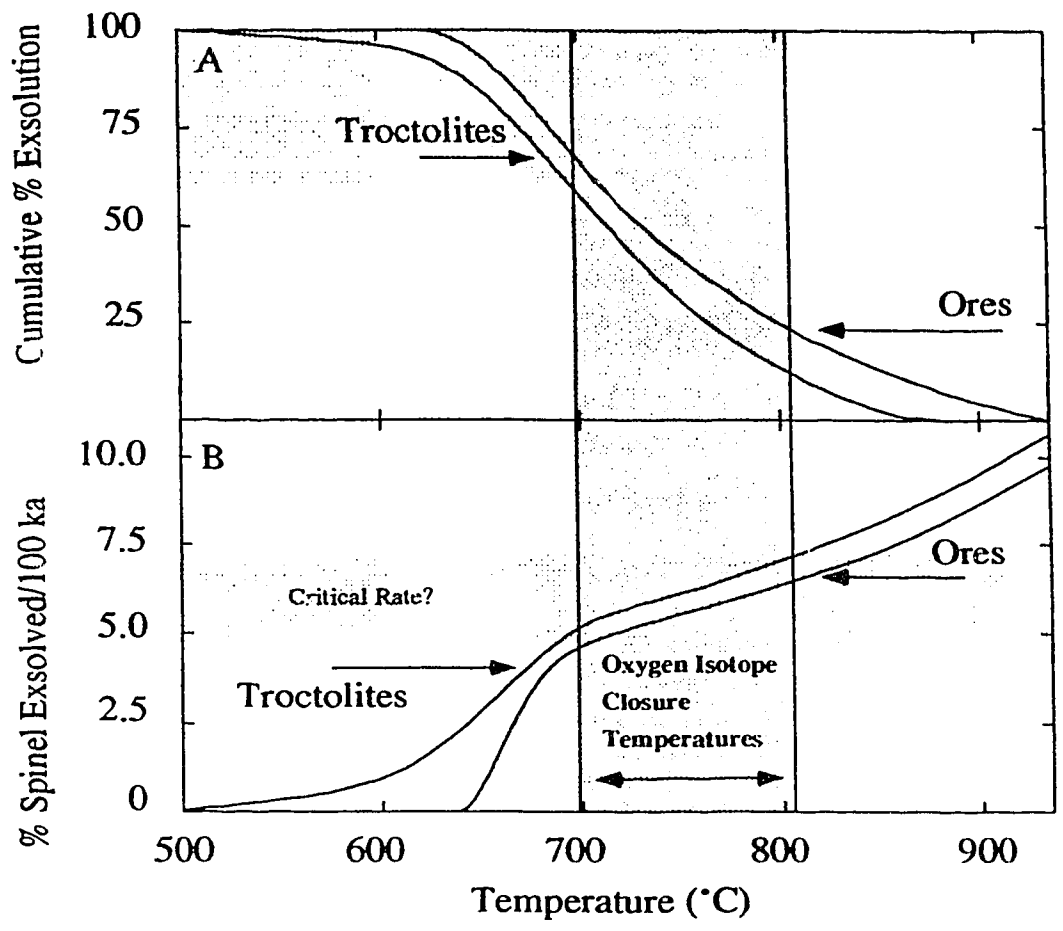


Figure 4.11A Calculated plot of cumulative exsolution for average troctolite and ore spinels. 4.11B Calculated plot of exsolution rate for troctolite and ore spinel. See text for details.

Table 4.1  
Stable isotope geochemistry and modal abundance data for rocks of the Sybille quarry

Sample	Plagioclase	Apatite	Pyroxene	Biotite	Olivine	Ilmenite	Magnetite
	‰ (%) (mm)	‰ (%) (mm)	‰ (%) (mm)	‰ (%) (mm)	‰ (%) (mm)	‰ (%) (mm)	‰ (%) (mm)
SP-1	7.86(71.4)(5.0)	6.79(4.8)(2.5)	(4.3)(5.0)	6.04(11.7)(5.0)	6.18(11.7)(5.0)	4.78(5.0)(1.5)	2.71(5.3)(1.5)
SP-2	7.73(69.9)(20)	6.79(4.8)(2.5)	7.06(21.4)(2.0)	(Tr.)(1.0)	(Tr.)	4.83(1.6)(1.0)	2.81(2.0)(1.5)
SP-3	8.85(5.2)(0.5)	7.28(68.4)(10)	7.23(5.5)(0.25)	(Tr.)	(Tr.)(0.5)	4.78(5.3)(2.0)	3.56(14.5)(3.0)
SP-4	9.12(9.0)(1.0)	---	---	(0.5)(0.5)	6.56(10.1)(1.0)	5.02(23.6)(1.5)	4.46(56.4)(2.5)
SP-5	8.87(14.0)(1.0)	---	---	7.85(1.3)(0.5)	6.54(12.1)(0.5)	5.27(20.3)(1.5)	4.36(52.0)(2.0)
SP-6	7.85(100)	---	---	---	---	---	---
SP-7	7.78 N.D.	---	---	N.D.	---	4.37 N.D.	2.45 N.D.
SP-8	9.75(7.2)(1.0)	---	---	(1.2)(0.5)	6.71 (3.6)(0.5)	5.24(18.1)(2.0)	4.53(69.6)(3.5)

Isotopic values are in delta (d) notation (permil deviation from SMOW). Numbers in Parentheses are modal abundance estimates and grain half widths, respectively. Abundances of chlorite and sulfides are not reported. N.D. = not determined; Tr.=Trace.

Table 4.2  
Isotopic analyses of apatite size fractions from sample SP-3

Sample	$\delta^{18}\text{O}$ (‰)	radius (mm)	length (mm) (minimum/broken)
SP-3a	7.27	0.5-0.6	0.5-1.2
SP-3b	7.30	0.5-0.7	1.0-1.5
SP-3c	7.33	0.8-0.9	1.0-2.0
SP-3d	7.34	0.8-0.9	1.0-1.2
SP-3e	7.30	0.9-1.1	1.0-2.5
SP-3f	7.23	1.6-1.8	2.0-3.0
SP-3g	7.13	>1.6	>1.0-3.0

Grain sizes were estimated by examining apatite crystals on graph paper with a binocular microscope. Mean isotopic composition of seven sieve fractions  $7.27 \pm 0.07$ ‰.

Table 4.3a  
Composition data for Sybille Ilmenite

Sample	SP-1	SP-2	SP-3	SP-4	SP-5	SP-8
SiO <sub>2</sub>	0.11	0.04	0.03	0.01	0.01	0.01
TiO <sub>2</sub>	50.08	50.26	50.28	50.94	51.24	50.87
Al <sub>2</sub> O <sub>3</sub>	0.11	0.09	0.09	0.11	0.08	0.07
FeO	46.94	46.82	47.59	44.62	45.35	43.82
MnO	0.52	0.69	0.64	0.53	0.52	0.50
MgO	1.09	0.81	0.26	1.81	1.60	2.49
Total	98.84	98.71	98.89	98.18	98.81	97.75
X <sub>Ilm</sub>	0.955	0.960	0.963	0.973	0.972	0.9681
X <sub>Item</sub>	0.045	0.040	0.037	0.027	0.028	3.18

Major element oxide data obtained by using ARL SEMQ at the Geology Department, University of Alberta. Values represent averages of at least five determinations on ilmenite grains in each sample. X<sub>Item</sub> and X<sub>Ilm</sub> calculated on an oxygen basis of 3 oxygens and assuming X<sub>Item</sub>=X<sub>Ilm</sub>-1.

Table 4.3b  
Composition data for Sybille Magnetite

Sample	SP-1	SP-2	SP-3	SP-4	SP-5	SP-8
SiO <sub>2</sub>	0.06	0.13	0.12	0.07	0.06	0.08
TiO <sub>2</sub>	1.02	0.48	1.55	7.89	9.05	12.03
Al <sub>2</sub> O <sub>3</sub>	0.58	0.31	0.68	2.30	2.41	2.04
FeO	90.63	92.75	91.16	83.09	83.76	80.37
MnO	0.02	0.00	0.03	0.16	0.19	0.28
MgO	0.18	0.72	0.07	0.37	0.27	0.71
Total	92.47	93.59	93.80	93.87	95.74	95.50
X <sub>Usp</sub>	0.030	0.014	0.046	0.239	0.269	0.356
X <sub>Mt</sub>	0.970	0.986	0.954	0.761	0.731	0.644

Major element oxide data obtained by using ARL SEMQ at the Geology Department, University of Alberta. Values represent averages of at least five determinations on magnetite grains in each sample. X<sub>Usp</sub> and X<sub>Mt</sub> calculated on an oxygen basis of 3 oxygens and assuming X<sub>Usp</sub> = X<sub>Mt</sub> - 1.



Table 4.4

Mineral-pair apparent temperature data for rocks of the Sybille quarry.

Sample	Plag-Mt	Plag-Ilm	Plag-Ol	Px-Mt	Ol-Mt	Ol-Ilm	Ap-Mt	Px-Ilm
SP-1	704	954	893		598	1023	727	
SP-2	726	992		642			782	940
SP-3	691	795		712			819	884
SP-4	755	791	672		847	963		
SP-5	771	862	717		826	1088		
SP-6								
SP-7	687	893						
SP-8	698	741	594		826	992		

All temperature data are based on the experimental calibrations of Clayton et al. (1989) and Chiba et al. (1989) except for fractionations involving ilmenite which are boot strapped on the empirical ilmenite-magnetite calibration of Bottinga and Javoy (1975) and fractionations involving apatite and biotite which are based on the semi-empirical calibrations of Smyth and Clayton (1988) and Smyth (1989). Temperature uncertainties are  $\pm 30^\circ\text{C}$  for Plag-Mt,  $\pm 30$  and  $\pm 50^\circ\text{C}$  for Plag-Ilm at 750 and  $1000^\circ\text{C}$ , respectively,  $\pm 50$  to  $\pm 80^\circ\text{C}$  for Plag-Ol at 700 and  $900^\circ\text{C}$ , respectively,  $\pm 33^\circ\text{C}$  for Px-Mt,  $\pm 32$  to  $\pm 60^\circ\text{C}$  for Ol-Mt at 600 and  $850^\circ\text{C}$ , respectively,  $\pm 90$  to  $\pm 115^\circ\text{C}$  for Ol-Ilm at 950 and  $1050^\circ\text{C}$ , respectively,  $\pm 35^\circ\text{C}$  for Ap-Mt and  $\pm 60^\circ\text{C}$  for Px-Ilm. Temperature uncertainties include uncertainties in both the analysis and the fractionation factor and are calculated by using the equations presented in Chapter 2.

Table 4.5  
Mineral closure temperatures for rocks of the Sybille quarry

Sample	Ilmenite Temperature	Olivine Temperature	Magnetite Temperature
SP-1	990±54°C	945±120°C	704±30°C
SP-2	997±47°C	---	726±30°C
SP-3	1042±55°C	---	807±35°C
SP-4	1333±547°C	882±72°C	755±30°C
SP-5	1989±1058°C	863±81°C	771±30°C
SP-8	(reversal)	858±78°C	698±30°C

Temperature data and uncertainties calculated by using data in Table IV-1 and equations from Chapter 2. Uncertainties include uncertainties in mode, composition and the fractionation factors used.

Table 4.6  
 Calculated values of  $T_{c,sys}$  for Sybille samples

Samples chosen	Temperature
SP-1 and SP-4	1030±67°C
SP-1 and SP-5	1048±76°C
SP-1 and SP-8	1047±67°C
SP-2 and SP-4	1027±53°C
SP-2 and SP-5	1043±59°C
SP-2 and SP-8	1043±54°C
SP-3 and SP-4	1110±90°C
SP-3 and SP-5	1150±109°C
SP-3 and SP-8	1125±89°C
Mean of 9	1068±25°C

Note that all uncertainties in this table are  $1 \sigma$  uncertainties that are calculated by using the equations presented in chapter 2. Temperatures in this table are calculated by using equations presented in chapter 2.

Table 4.7  
Observed and predicted closure temperatures for minerals from the Sybille quarry

Mineral	Closure temperatures		Grain Radii (mm)
	observed	predicted diffusional	
Ilmenite	993-1042	1000-1050	1.0-2.0
Olivine	858-952	890-1010	0.5-5.0
Magnetite (in troctolite)	704-728	940	1.5
Magnetite (in Fe-Ti ore)	698-807	960-1000	2.0-3.5

Observed closure temperatures calculated by using methods outlined in chapter 2. predicted diffusional closure temperatures calculated by using the equations of Dodson (1973) with cooling rates given in the text and the diffusion constraints of Gautason and Muehlenbachs (1993).

## Chapter 5:

### Case Study 2: High Temperature Granulites of Northwestern Canada and Enderby Land Antarctica

#### INTRODUCTION

The purpose of this chapter is to evaluate the applicability of isotope thermometry in high-temperature (>900 °C) metamorphic environments. Two localities, The Taltson Magmatic Zone of Northwestern Canada and the Napier Complex of Enderby Land Antarctica, were chosen for this study. Both are very well documented, geologically, and each represents a different end-member environment. The Taltson Magmatic Zone comprises the southern part of the (ca. 1.9-2.0 Ga) Taltson-Thelon Orogen, a northeast-southwest trending belt that extends ≈2500 Km from southern Ellesmere island to central Alberta (Figure 5.1a)(Hoffman 1988; Frith et al., 1988; Ross et al., 1991). The TMZ is a ≈200 km wide terrain that extends southward from the Great Slave Shear Zone for ≈400 km to where it is truncated by the Snowbird Tectonic Zone (Hoffman, 1988). It is sandwiched between the Archaean Rae Province to its east and the Paleoproterozoic Buffalo Head terrane to its west (Ross et al., 1991). The Taltson Magmatic Zone consists mostly of peraluminous granitoids and associated metapelitic supracrustal rocks (Bostock et al., 1987; Goff et al., 1986). The assemblage spinel-quartz-cordierite-garnet-sillimanite occurs in some of the granites and metasediments. This assemblage indicates minimum P-T constraints of 5-7 kb and 830-940 °C for parts of this terrain (Chacko et al., 1994). U/Pb zircon and monazite data indicate that peak magmatic/metamorphic activity occurred at ≈1950-1930 Ma (Bostock et al., 1987; McDonough et al., 1994; Plint and McDonough, 1995). Widespread K/Ar and Ar/Ar ages for hornblende and muscovite of ≈1900 Ma and ≈1800 Ma, respectively, suggest simple cooling and no subsequent large-scale metamorphic events (Plint and McDonough, 1995; Baadsgard and Godfrey, 1987). The combination of high regional metamorphic temperatures and a simple cooling history makes this terrain ideally suited to study of high-

temperature isotopic thermometry.

The Napier Complex (NC) is a  $\approx 200$  km wide by  $\approx 400$  km long granulite terrain that comprises the northern part of the East Antarctic shield in Enderby Land (Figure 5.1b). The Napier Complex is bound by the largely Late-Proterozoic Rayner complex to the south and by the Indian Ocean to the north (Sheraton et al., 1980). The Napier Complex comprises predominantly felsic orthogneiss with subordinate mafic/ultramafic granulite, and siliceous, ferruginous and pelitic paragneiss (Sheraton et al., 1980). Sapphirine + quartz  $\pm$  orthopyroxene  $\pm$  osumilite, orthopyroxene + sillimanite + quartz, spinel + quartz, and osumilite + garnet + orthopyroxene + quartz assemblages all occur on a regional scale in pelitic lithologies (e.g., Sheraton et al., 1980, 1987; Ellis, 1980, 1983; Grew, 1980; Harley, 1983, 1985a, 1986; Sandiford, 1985a). Inverted pigeonite and mesoperthite also occur as metamorphic minerals in the Napier Complex (Ellis, 1980; Harley, 1983, 1986, 1987; Sandiford, 1985a; Sandiford and Powell, 1986). Phase assemblage data and cation exchange data constrain peak metamorphic temperatures and pressures to 950-1020°C and 6-10 kbar (Ellis, 1980; Ellis et al., 1980; Harley, 1983, 1985a, 1986, 1987, Sandiford, 1985a; Sandiford and Powell, 1986; Sheraton et al., 1980). Isotopic studies point to a long and protracted history of metamorphic heating, cooling and deformation. Zircon populations in orthogneiss from Fyfe Hills and Mount Sones record ages of  $\approx 3800$  and  $\approx 3930$  Ma, respectively, and indicate that a component of the protolith is very old (Compston and Williams, 1982; Black et al., 1986). The age of the high-temperature metamorphism is constrained by the timing of two deformational events (D1 and D2). Rb/Sr and Sm/Nd whole-rock data indicate an age of  $\approx 3070$  Ma for D1 (Sheraton and Black, 1983; McCulloch and Black, 1984). D2 is constrained to  $\approx 2900$  Ma by a variety of techniques (Black and James, 1983; Black et al., 1986). Current interpretations suggest that very high-temperature ( $>900$  °C) conditions accompanied both D1 and D2 (e.g., Harley and Black, 1987). It remains equivocal, however, whether these conditions persisted throughout the interval between D1 and D2 (e.g., Harley and Black, 1987; Harley and Hensen, 1990). A third stage of deformation (D3) occurred a  $\approx 2460$  Ma, U/Pb Zircon, monazite and Rb/Sr data (Black et al., 1983ab, 1984, 1986). The thermal conditions for D3 have been constrained to 650-720 °C and 5-8 kbar (Black et al.,

1983ab). Metamorphism in the adjacent Rayner Complex at  $\approx 1100$  Ma locally overprints the Archaean age mineral assemblages but the overprinting is restricted to late shear zones that cross-cut the Napier Complex rocks (Ellis, 1983, Black et al., 1983b, 1984; Harley, 1985b; Sandiford and Wilson, 1984; Sandiford, 1985b; Harley et al., 1990). Preservation of delicate symplectitic intergrowths of easily retrograded minerals attests to the very dry nature of both the high-temperature metamorphic event and the subsequent events.

The protracted metamorphic history of the Napier Complex contrasts strongly with the simple cooling history for the Taltson Magmatic Zone. The juxtaposition of these terrains in this study is intentional. I chose the Taltson Magmatic zone because its simple cooling history makes it a best case end-member for high-temperature isotopic thermometry. I chose the Napier Complex because its complicated history makes it a worst case end-member. Both terrains contain rocks with a variety of mineral assemblages and modal compositions, which make them well suited to the methods described in chapters 2 and 3.

## **METHODS**

Samples from both terrains were selected according to criteria designated in chapters 2 and 3. They were selected on the basis of a simple mineralogy (2-4 modally abundant minerals), with a low modal abundance of at least one high closing phase, and with fractionation factors that yield low temperature uncertainties. Samples include metapelites and metaironstones. Temperature data were calculated by using the methods outlined in chapters 2 and 3 and the equilibrium constants presented in Table 5.1.

Mineral separates obtained using conventional techniques (magnetic and density separation) were further purified by hand picking. Purity was checked optically and by XRD and is better than 95% for most phases. Separates of mesoperthite are the only exception. Purity of mesoperthite separates is better than 85%.

Oxygen was extracted from 2-10 mg aliquots of the mineral separates and converted to  $\text{CO}_2$  by using conventional techniques (Clayton and Mayeda, 1963). I obtain high oxygen yields (90-100%) and precise analyses ( $\pm 0.15\%$   $1\sigma$ ) for samples of nominally unreactive

minerals by grinding them to grain sizes of  $\approx 10\text{-}20\ \mu\text{m}$ . I react the samples in preconditioned Ni-rod bombs for  $\approx 12$  hrs. Garnet and magnetite react easily at  $\approx 640^\circ\text{C}$ . I have found that it is important to monitor the amount of reagent consumed by the Ni-rod bomb during high-temperature fluorination to insure precise analyses. The isotopic composition of  $\text{CO}_2$  was analyzed by using a Finnigan MAT 252 and is reported in conventional delta notation ( $\text{‰}$  units deviation from V-SMOW). Most analyses were repeated at least twice. Analyses of NBS-28 give  $9.69 \pm 0.15\text{‰}$  ( $1\sigma$ ).

## ISOTOPIC SYSTEMATICS

The results of the isotopic analyses are presented in Table 5.2. Mineral isotopic compositions for samples from both granite and metasedimentary restite from the Taltson Magmatic Zone define narrow ranges of values ( $9.87\text{-}11.19\text{‰}$ ,  $9.86\text{-}10.25\text{‰}$ , and  $7.73\text{-}9.30\text{‰}$  for quartz, feldspar, and garnet, respectively). Feldspar from Pelican Rapids samples is reddish color and is in isotopic disequilibrium with coexisting quartz (e.g.,  $\delta^{18}\text{O}_{\text{feldspar}} \geq \delta^{18}\text{O}_{\text{quartz}}$ ). The quartz-garnet fractionations from the Taltson Magmatic Zone define a consistently small range ( $1000 \ln \alpha_{\text{qtz-grt}} = 2.03 \pm 0.17\text{‰}$ ). The isotopic compositions of all minerals are consistent with derivation from a source with metasedimentary-like  $\delta^{18}\text{O}$  compositions.

Mineral isotopic compositions are highly variable for the Napier Complex samples (Table 5.2). The isotopic compositions of magnetite ( $-0.46$  to  $6.06\text{‰}$ ), garnet ( $5.55\text{-}10.01\text{‰}$ ), orthopyroxene ( $1.51\text{-}10.46\text{‰}$ ), feldspar grains ( $3.26\text{-}8.27\text{‰}$ ) and quartz ( $4.10\text{-}13.38\text{‰}$ ) from the Napier Complex all span a wide range of isotopic compositions. The order of  $^{18}\text{O}$  enrichments for minerals is, generally,  $\delta^{18}\text{O}_{\text{quartz}} > \delta^{18}\text{O}_{\text{feldspar}} > \delta^{18}\text{O}_{\text{garnet}} \geq \delta^{18}\text{O}_{\text{pyroxene}} > \delta^{18}\text{O}_{\text{ilmenite}} \geq \delta^{18}\text{O}_{\text{magnetite}}$ . A striking feature of data for samples 3531, 3533, and 7728-4548 is the combination of low  $\delta^{18}\text{O}$  for quartz ( $\leq 5\text{‰}$ ), feldspar ( $\leq 5\text{‰}$ ), orthopyroxene ( $\leq 3\text{‰}$ ), and garnet ( $\leq 3\text{‰}$ ) with the small isotopic fractionations between them ( $1000 \ln \alpha_{\text{qtz-px}} \leq 3\text{‰}$ ,  $1000 \ln \alpha_{\text{fsp-grt}} \leq 3\text{‰}$ ). These isotopic compositions are consistent with derivation from a low



$^{18}\text{O}$  protolith. This protolith could only have formed as a result of high temperature interaction with low  $\delta^{18}\text{O}$  water. The existence of low  $\delta^{18}\text{O}$  water implies both the existence of large bodies of standing water (oceans) and the buffering of these bodies by plate tectonic (or plate tectonic-like) processes. Since these samples are  $>3100$  Ma, some possibly  $>3900$  Ma, this observation is worthy of further investigation.

## ISOTOPIC THERMOMETRY

Experimentally and empirically calibrated isotopic thermometers were applied to all samples (Table 5.3). Quartz-garnet fractionations from the Taltson samples define a narrow range of temperatures (917 - 998 °C) with associated uncertainties  $\leq \pm 85$  °C ( $x_s = 962 \pm 30$  °C). Quartz-feldspar fractionations, combined with the reddish color of the feldspar, strongly suggest that feldspar has been enriched in  $^{18}\text{O}$  by interaction with an external reservoir (e.g., Taylor, 1968). If quartz is also enriched in  $^{18}\text{O}$ , then the quartz-garnet temperatures reported here are invalid. These temperature data would be spuriously low. I do not think that this is the case, for the following reasons. Quartz isotopic compositions do not vary significantly ( $\delta^{18}\text{O}_{\text{quartz}} = 10.40 \pm 0.42$  ‰), and the variation that occurs is strongly correlated with the isotopic compositions of coexisting garnet ( $1000 \ln \alpha_{\text{qtz-grt}} = 2.03 \pm 0.17$  ‰). We propose that variable  $\delta^{18}\text{O}_{\text{feldspar}}$  resulted from interaction with an externally derived fluid phase at temperatures below the oxygen closure temperatures of quartz and garnet. These open system interactions, preclude calculation of garnet observed closure temperatures with the single sample method described in Chapter 2.

I report mineral-pair temperature data for quartz-garnet, quartz-pyroxene and quartz-magnetite from the Napier Complex Samples in Table 5.3. Because sample 7728-3286 has a texture that suggests late recrystallization and garnet growth, I will discuss the temperature data from this sample separately from the other Napier Complex samples. Quartz-garnet mineral-pair temperatures for all samples except 7728-3286 range from 798 to 971 °C. Samples that define the highest temperatures have high quartz/magnetite. This relationship

might be expected if magnetite-quartz exchange continued to temperatures significantly lower than quartz-garnet exchange. Quartz-pyroxene mineral-pair temperature data define a lower range (702-846 °C) than quartz-garnet mineral-pair temperature data. High quartz-pyroxene temperatures also correspond to high quartz/magnetite. This suggests that although quartz-pyroxene exchange continued at temperatures lower than quartz-garnet exchange, it stopped at temperatures above the limits of quartz-magnetite exchange. Quartz-magnetite temperature data define the lowest range (617-694 °C). This range is consistent with observed relationships between quartz/magnetite and the quartz-garnet and quartz-pyroxene temperature data, respectively. I infer that the Napier Complex minerals closed to isotopic exchange in the order garnet $\geq$ pyroxene $\geq$ magnetite $\approx$ quartz. This is consistent with the relative oxygen diffusion rates for these minerals. In contrast to samples from the Taltson magmatic Zone, the isotopic compositions of minerals from these Napier Complex samples do not suggest open system interactions.

Sample 7728-3286 gives an altogether different picture (Figure 5.2). This sample exhibits evidence for significant amounts of late recrystallization and garnet growth (garnet forms rims around previously deformed magnetite and orthopyroxene). The highest mineral-pair temperatures are the quartz-magnetite mineral-pair temperatures (602 $\pm$ 30 °C). The quartz-garnet fractionation yields 552 $\pm$ 31 °C and the quartz-pyroxene fractionation yields 506 $\pm$ 31 °C. The low quartz-garnet temperature may reflect late-stage garnet growth at low temperature, but this interpretation is problematic because it cannot account for quartz-pyroxene temperature data that clearly conflict with orthopyroxene stability. The best explanation is that this sample records evidence for interaction with an external reservoir.

Table 5.4 lists the observed closure temperatures  $T_{c-observed}$  for garnet and pyroxene for the all Napier Complex samples except 7728-3286. The garnet  $T_{c-observed}$  for these samples define a slightly higher temperatures than do the quartz-garnet mineral-pair temperatures because the calculation quantitatively accounts for the retrograde exchange between quartz, magnetite and other low closing phases. It is also for this reason that this type of temperature data, although less precise than the mineral-pair temperatures, is more accurate. All garnet  $T_{c-observed}$  overlap within uncertainty. For samples 7728-4599 and 7728-3604, the

uncertainties are excessive ( $\geq \pm 120^\circ\text{C}$ ) because the coefficient of the garnet-whole rock fractionation factor ( $A_{gr-wr} = \sum_i X_i A_{gr-i}$ ) is small. The average of garnet  $T_{c-observed}$  for the samples best suited to this type of isotopic thermometry (7628-3081 and 7628-3139) provide the best temperature estimate ( $\approx 1000^\circ\text{C}$ ) and suggest that high temperature isotopic compositions are preserved by garnets from the Napier Complex. Pyroxene  $T_{c-observed}$  also overlap within their uncertainties, but define lower temperatures ( $836 \pm 58^\circ\text{C}$ ) than the garnet  $T_{c-observed}$ . This is consistent with the quartz-pyroxene mineral-pair data.

### **PRESERVATION OF HIGH-TEMPERATURE ISOTOPIC COMPOSITIONS**

Two important conclusions can be made from the temperature data. First, high-temperature information is preserved by the isotopic compositions of garnet in both the Taltson Magmatic Zone and the Napier Complex. Second, retrograde exchange involving garnet in these environments is minor, even when the subsequent history is protracted and involves reheating and deformation. This is significant because it shows that isotopic thermometry is a robust tool that can be used to study very high-temperature metamorphic rocks. It also presents us with several interesting questions. Is the ability of garnet to preserve its isotopic composition in these environments only a function of their extremely dry nature, or does garnet preserve its isotopic composition despite  $f\text{H}_2\text{O}$ ? (i.e., Does the well established dependence of oxygen diffusion rates on factors such as  $f\text{H}_2\text{O}$  (e.g., Farver and Yund, 1990; Sharp et al., 1991; Zhang et al., 1991) comprise a significant explanation for the observations?) Does isotopic zoning in garnet preserve information about both the prograde and retrograde exchange history, or does isotopic exchange in garnet homogenize zoning in the high-temperature parts of the prograde path and effectively stop on the retrograde because of changes in  $f\text{H}_2\text{O}$ ? Presently, the data do not allow us to answer these questions, but they strongly suggest that garnet be a very important mineral for isotopic study of these high-temperature environments. Further study with microsampling techniques (e.g., Valley and Graham, 1991) is warranted.

Model mineral closure temperature data that are constrained by volume diffusion data

comprises an important type of information for addressing the temperature data. Eiler *et al.* (1992) has shown that Dodson closure temperatures are not a faithful model of mineral closure in natural systems. Because these closure temperatures do not consider the diffusivities of phases other than the closing mineral, they necessarily provide estimates for mineral closure that are too high. To calculate closure temperatures properly, one must have information on grain sizes, mineral diffusivities and cooling rates, grain boundary diffusion rates and the modal proportions of all phases. This type of information does not exist in sufficient detail for us to calculate these temperatures for samples from the Napier Complex. Instead, I have calculated Dodson closure temperatures, noted their inherent problems, and noted that they present a first-order, upper bound for mineral closure. I compare these values with the  $T_{c-observed}$  data to gain insight into the diffusion rates, and mechanisms that apply to the Napier Complex samples. Dodson closure temperatures calculated for both "wet" and "dry" diffusion data are presented in Table 5.5. For grain sizes of  $2 \pm 1$  mm and cooling rates of  $1 \pm 0.5$  °C/my, I calculate Dodson closure temperatures for garnet of  $810 \pm 50$  and  $1005 \pm 40$  for the "wet" and the "dry" data respectively. The isotopic data are in much better agreement with the "dry" diffusion model of Gautason and Muehlenbachs (1993) than the "wet" diffusion data of Coghlan (1990). This would suggest that at least part of the reason for the preservation of high garnet temperatures may be the "dry" conditions for cooling.

Another reasons why garnet preserves its high-temperature isotopic composition is its resistance to deformation-induced recrystallization. The Napier Complex samples commonly exhibit evidence for deformation and recrystallization. In some cases, these same samples also preserve relatively undeformed high-temperature reaction and exsolution textures. To explain the preservation of delicately exsolved high-temperature pigeonites from Tonagh island, Harley (1987) invokes a mechanism where strain is partitioned mostly between quartz and magnetite present in the samples. Here, I favor a similar explanation for the preservation of garnet isotopic compositions. Dynamic recrystallization involving subgrain formation and migration in quartz and magnetite grains accommodated strain, allowing garnet grains to preserve their isotopic integrity. Where deformed, garnet was predominantly granulated rather than recrystallized and did not exchange significant oxygen.

Hoffbauer et al (1994) have documented a different case for garnet from a strongly deformed rock from Sri Lanka. The garnet examined in their study is present as elongate lenses, aligned parallel to deformational fabric of the rock. They proposed that the garnet has been recrystallized during the development of this fabric. The Napier Complex garnets that were analyzed for this study were not deformed in this way. Therefore, I argue that garnet grains will preserve their high temperature isotopic compositions for cases where strain has been accommodated by mechanisms that do not involve garnet recrystallization.

## RETROGRADE INFORMATION

In contrast to garnet, pyroxene and magnetite from the Napier Complex are poor minerals for high-temperature isotopic thermometry. There is good evidence to suggest that oxygen diffusion in these minerals be significantly faster than garnet (Giletti and Yund, 1984; Giletti and Hess, 1988; Sharp et al., 1991; Coghlan, 1990; Fortier and Giletti, 1989; Gautason and Muehlenbachs, 1993). Dodson closure temperatures for  $1\pm 0.5$  mm pyroxene and magnetite grains and a cooling rate of  $1\pm 0.5$  °C/my are reported in Table 5.5. Dodson closure temperatures range from  $805\pm 35$ °C ("dry") to  $630\pm 45$ °C ("wet") for clinopyroxene, from  $875\pm 45$  ("dry") to  $720\pm 50$  ("wet") for orthopyroxene, and from  $770\pm 40$ °C ("dry") to  $465\pm 35$ °C ("wet") for magnetite. The temperature data for pyroxene match most closely with the "dry" estimates, and the temperature data for magnetite fall between the "dry" and the "wet" estimates, but are more closely matched with the "dry" estimates. In addition to faster rates for O-diffusivities in pyroxene and magnetite compared with garnet, both minerals show exsolution and/or oxyexsolution features. Magnetite is also very easily deformed (e.g., Ramdohr, 1969). The faster O-diffusivities in unrecrystallized pyroxene and magnetite, combined with the possibility that enhanced exchange may accompany exsolution and deformation, makes them less suited for high-temperature isotopic thermometry.

The large equilibrium fractionation between magnetite and most silicate minerals, however, gives small uncertainties for isotopic temperature data involving magnetite, and therefore makes it a good candidate for gaining insight into cooling histories. Quartz-

magnetite mineral-pair temperature data (617-694 °C) correspond closely with temperatures inferred for the 2460 Ma (D3) event (650-720 °C) (Harley, 1983; Black et al., 1983). This may be entirely coincidental (i.e., the low magnetite temperature data may reflect faster diffusion of oxygen in quartz and magnetite compared with that in garnet), or it may reflect exchange that has accompanied deformation of quartz and magnetite during D3.

## SUMMARY AND CONCLUSIONS

The results of the present study show that high-temperature ( $\approx 1000$  °C) isotopic compositions can be preserved in dry, slowly-cooled metamorphic rocks. These compositions can be used to gain insight into the high-temperature thermal history (e.g., for isotopic thermometry), and the cooling history of these high-grade rocks. The most important parameters for retrieving this information include careful sample selection and numerical techniques that quantitatively account for retrograde exchange among low closing phases. Samples should include a simple mineralogy, at least one slow diffusing phase that has not undergone recrystallization on the retrograde path, and a modal mineralogy that favors a large equilibrium fractionation between this phase and the rest of the rock

$$(A_{\text{min. wt}} = \sum_i X_i A_{\text{min. } i}).$$

Garnet is an ideal mineral for these purposes. It exchanges oxygen very slowly, does not exsolve on cooling, is not usually subject to dynamic recrystallization, and has a large equilibrium fractionation with many low closing silicate phases. The results of this study suggest that pyroxene and magnetite are not as well suited for high-temperature isotopic thermometry; they exchange oxygen more rapidly than garnet, may be involved in exsolution reactions that may, in turn, lead to enhanced diffusion of oxygen and, at least for magnetite, are easily recrystallized during subsequent deformation events. Because magnetite has a very large equilibrium fractionation with most silicate minerals, it is, however, good for gaining insight into the cooling history of a given sample, or set of samples.

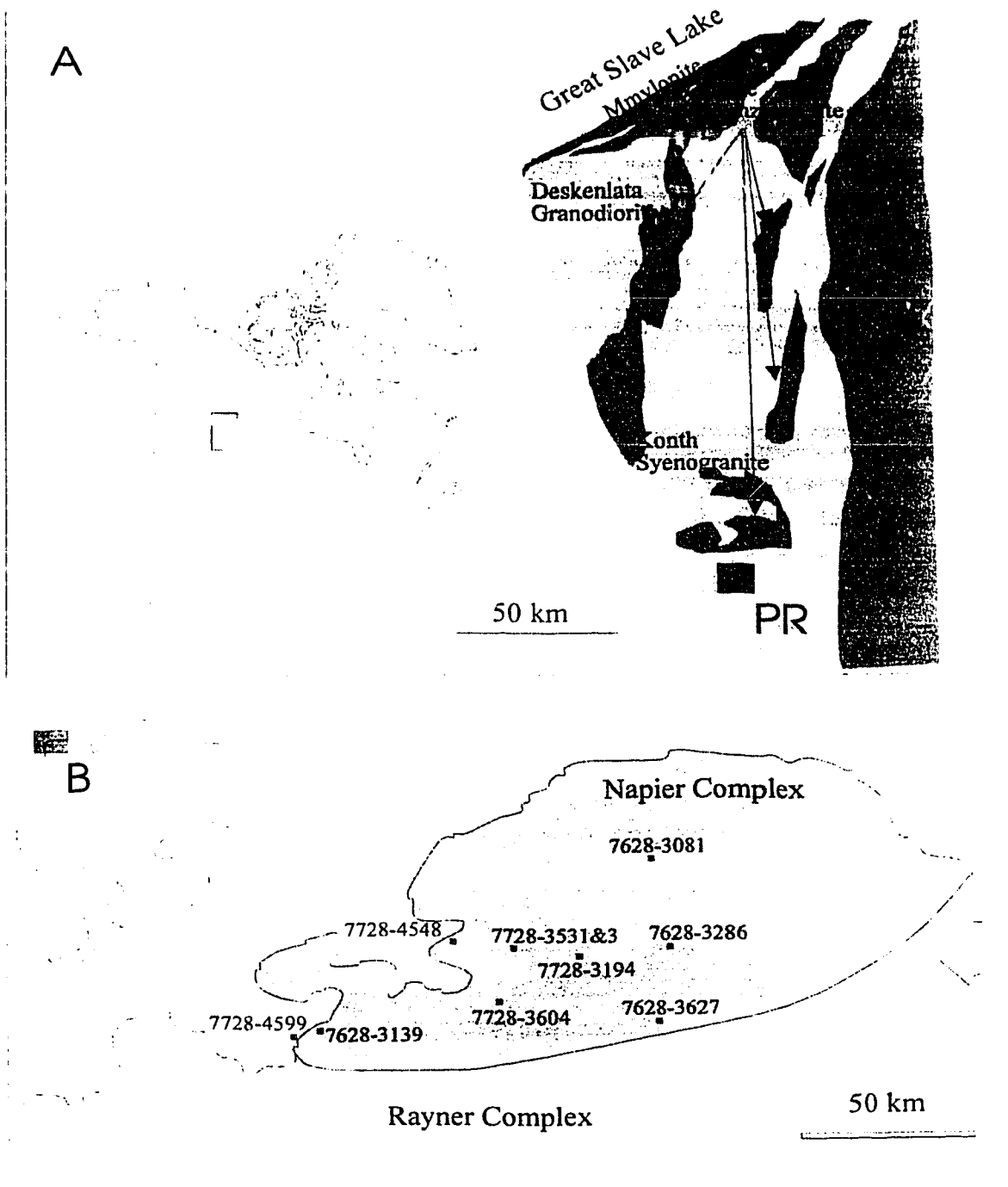


Figure 5.1A Sketch map showing location and general geology of the Taltson Magmatic Zone. PR = Pelican rapids. (After Bostock et al., 1987)  
 Figure 5.1B Sketch map showing location and metamorphic isograds of the Napier Complex, Antarctica (After Harley and Hensen, 1990)

Table 5.1

## Calculation Parameters

Mineral	$A_{Qtz-Min}$ (‰)	Molar O/Mass (mmol/g)	MolarO/Vol (mmol/cc)
Quartz	----	33.28	88.20
Orthoclase	0.94	28.74	73.58
Albite	0.94	30.51	79.93
Anorthite	1.99	28.76	79.37
Enstatite	2.75	29.88	95.91
Ferrosilite	2.75	22.74	90.04
Grossular	3.17	26.64	95.74
Pyrope	3.00	29.76	106.62
Almandine	3.00	24.11	104.10
Ilmenite	6.01	19.77	92.92
Magnetite	6.29	17.27	89.83

Molar O/Mass = (#O/formula)/(molecular wt)

Uncertainties used for error propagation:  $\pm 0.11$  ‰  $\pm 2\%$  relative for modes  $>10\%$   $\pm 1\%$  relative for modes  $<10\%$ . Sources for  $A_{qtz-min}$ : Rosenbaum et al, 1994; Chiba et al., 1989; Clayton et al., 1989, Kieffer, 1982, Smyth and Clayton, 1989. Enstatite and ferrosilite are assumed to fractionate oxygen like diopside. Ilmenite bootstrapped to magnetite with ilm-mt of Bottinga and Javoy, 1975.



Table 5.2: Isotopic and modal data

Sample	Quartz	Plag/Anti	alkali/Meso	garnet	Orthopyroxene	Magnetite	Sapphirine/Ilmenite
<u>Napier Complex Samples</u>							
7628-3081	7.50 (88.0)		5.55(8.0)		(8.0)	-0.46(2.0)	
7628-3139	9.88 (46.7)	(14.4)	8.27(0.5)/6.21(0.5)	7.82(30.5)	7.39(6.2)	2.90(1.2)	
7728-4599	12.65 (60.0)				10.01(20.0)	5.87(20.0)	
7728-3604	8.51 (15.0)			6.45(45.0)	6.30(40.0)		
7728-3194	12.36 (50.0)				9.75(30.0)	5.49(20.0)	
7728-3627	13.38 (60.0)				10.46(20.0)	6.06(15.0)	
7728-3531	4.10 (35.0)	3.75(trace)	3.26(52.0)		1.86(15.0)		2.74(10.0)-Sapph.
7728-4548	4.32 (68.0)				1.51(20.0)		-0.54(4.0)-Ilm
7728-3533		5.61(5.0)	4.59(78.0)	3.06(12.0)			
7728-3286	11.61 (50.0)			7.12(15.0)	7.04(20.0)	3.48(15.0)	
<u>Taltson Magmatic Zone Samples</u>							
<u>Pelican Rapids</u>							
FS-93-7	11.2			9.3			
FS-93-5	10.4		9.8	8.5			
FS-93-6	9.9		9.9	7.7			
FS-93-6A	10.0		10.3	8.0			
TC-SEP-2-10	10.6		9.9	8.6			

Mineral isotopic compositions in ‰ relative to SMOW. Modal abundances listed in parentheses in ‰. Modal Abundance Data from Sheraton et al. (1987) except for sample 7628-3139 which was recounted.

Table 5.3

## Mineral-pair isotopic temperature data

Sample	Qtz-Grt	Qtz-Opx	Qtz-Mt
-----Temperature (°C) -----			
<u>Napier Complex</u>			
7628-3081	971±64		617 ±31
7628-3139	937±60	782±51	679 ±33
7728-4599	798 ±47		694 ±34
7728-3604	938 ±61	846 ±57	
7628-3194		758 ±48	688 ±34
7728-3627		702 ±44	658 ±33
3531		836 ±56	
7728-4548			
3533			
7728-3286	548 ±31	506 ±31	609 ±31
<u>Taltson Magmatic Zone</u>			
	Qtz-Grt	Kfs-Grt	Qtz-Kfs
<u>Pelican Rapids</u>			
FS-93-7	993± 83		
FS-93-5	998 ±84	1008	978
FS-93-6	917 ±71	710	disequilibrium
FS-93-6A	949 ±76	690	disequilibrium
TC-SEP-2-10	953 ±76	996	873
Average	962 ±30		

Table 5.4

T<sub>c-observed</sub> for Napier Complex Samples

Sample	T <sub>c-observed</sub> (°C)
Garnet	
7628-3081	1002±78
7628-3139	991 ±82
7728-3604	1240±369
7738-3533	897±63
Pyroxene	
7628-3139	790±61
7728-4599	852±76
7728-3604	846±61
7628-3194	950±253
7728-3627	745±107
7728-3531	849±56

Calculated using modes presented in Table 5.2, fractionation factors presented in Table 5.1, and text equation (2). Uncertainties calculated by using Farquhar et al., 1993

Table 5.5

Dodson Closure Temperatures and  $T_{c-observed}$  for Napier Complex samples

Mineral	Dodson Closure Temperatures		$T_{c-observed}$
	"Wet" Diffusion Data	"Dry" Diffusion Data	
Garnet	810±50°C	1005±40°C	996±57°C
Orthopyroxene	720±50°C	875±45°C	
Clinopyroxene	630±42°C	790±40 & 805±35°C	836±58°C
Magnetite	465±35°C	770±40°C	667±30°C
Quartz	425±30°C	470±40, 645±40 & 660±50°C	667±30°C

Uncertainties on Dodson closure temperatures calculated by Monte Carlo Methods with cooling rates of  $1\pm 0.5$  °C/my and grain sizes of  $2\pm 1$  mm. and by using Coghlan (1990), Gautason and Muehlenbachs (1993), Fortier and Giletti (1989), Farver (1989), Connolly and Muehlenbachs (1988), Giletti and Hess (1988), Farver and Yund (1990), Sharp, Giletti and Yoder (1991), Elphick et al (1988).

## **Chapter 6:**

### **Case Study III: The Mica Creek Barrovian Sequence and Adjacent Monashee Complex, British Columbia, Canada**

#### **Introduction**

In this chapter, I examine the oxygen isotopic systematics of minerals from amphibolite- to granulite-facies pelites from a classic Barrovian sequence in southeastern British Columbia, Canada. Many of the samples examined in the present study were the same as those used by Bowman and Ghent (1986) in their earlier oxygen and hydrogen isotope study of the area. The present work also includes data on additional samples as well as analyses of minerals such as garnet, sillimanite, and kyanite which were not analyzed in the earlier study. These refractory minerals are critical to successful isotopic thermometry. I have used these data to obtain mineral-pair temperature data and then to take a critical look at the assumptions that go into isotopic thermometry. In turn, I have tried to use an understanding of these assumptions to examine possible matches between observed temperature data and a 'physically real' part of the metamorphic event such as mineral closure temperatures, a recrystallization event, or a specific part of the thermal history experienced by the rocks. I use the techniques outlined in chapters 2 and 3 to study two samples in greater detail and to gain insight into the volume over which isotopic equilibrium and retrograde exchange occurs (the 'equilibration volume') and also to gain insight into the types of open system processes that may complicate interpretations of the data. This aspect of the study provides information about open system processes in the general metamorphic rocks of the area and is a complement to studies that have focused on open system processes in plutonic rocks of British Columbia (e.g., Magaritz and Taylor, 1986).

#### **Regional Geology**

The Omineca Crystalline Belt extends the length of the Canadian Cordillera and

consists of high-grade metamorphic and plutonic rocks. It separates the allochthonous Intermontane and Insular Superterrane from the western edge of the north American craton (Monger et al., 1982). The Mica Creek Barrovian sequence and adjacent Monashee Complex form part of the Omineca Crystalline Belt in south-central British Columbia (Figure 6.1). The protolith for the Mica Creek sequence is the Hadrynian Horsethief Creek sediments of the Windermere Supergroup (Simony and Wind, 1970; Brown et al., 1978; Craw, 1978; Simony et al., 1980; Poulton and Simony, 1980; Pell and Simony, 1987). The Horsethief Creek Group includes pelites, semi-pelites, marbles, calcsilicates, and amphibolites which unconformably overlie basement rocks of the North American craton (Ghent et al., 1990). The adjacent Monashee Complex represents the lower plate of a metamorphic core complex uplifted during Eocene time (Parrish et al., 1990; Brown and Carr, 1990; Greenwood et al., 1991). The complex includes both basement rocks and overlying metasediments that are not inferred to be part of the Horsethief Creek Group (Brown et al., 1993). The rocks of the Monashee Complex examined in this study include pelitic paragneiss and amphibolite that overlie this basement.

These rocks have a complicated metamorphic history which includes several phases of deformation and at least two high temperature metamorphic peaks that spanned more than 50 My (Archibald et al., 1983, 1984; Parrish et al., 1988; Sevigny et al., 1990). Jurassic metamorphism of the Omineca Crystalline Belt accompanied the accretion of the Intermontane Superterrane, and Cretaceous metamorphism accompanied the accretion of the Insular Superterrane (Sevigny et al., 1989; Brown and Carr, 1990). Eocene extension also contributed to their metamorphic history (Parrish et al., 1988). Uplift and cooling of these rocks began approximately 100 Ma (Archibald et al., 1984; Parrish et al., 1988; Sevigny et al., 1990), and in some places may have generated cooling rates approaching 30°C/My (e.g., Sevigny et al., 1990).

A map of metamorphic isograds in the Mica Creek Barrovian sequence and adjacent Monashee Complex is presented in Figure 6.2. The general trend is a north to south increase in metamorphic grade. The lowest grades (garnet+biotite) occur within a synform centered just west of Kinbasket Lake. The grade increases to migmatite-in both to the northeast and

to the southwest. To the southwest, the metamorphic grade increases from staurolite zone to K-feldspar + sillimanite zone. More detailed examination reveals complex folding of metamorphic isograds to outline several synforms and antiforms in the Mica Creek area (Figure 6.2b). Between Nagle Creek and Soard's Creek, the kyanite-sillimanite isograd becomes "hot-side-up" (Ghent et al., 1990). Erosion of the folded isograd has created "inliers" of sillimanite + muscovite grade that are found north of Mica Creek and at Potlatch Creek. These "inliers" form at the axes of late, phase 3 folds that post-date the second metamorphic peak (Simony et al., 1980; Ghent et al., 1980, 1982). On the west side of the Columbia River Fault, the metamorphic grade remains at least as high as sillimanite grade for the entire Monashee Complex. Locally, conditions reach granulite facies (cordierite + garnet + K-feldspar) (Ghent et al., 1990; Nyman et al., in press). On the East side of the Columbia River Fault, the metamorphic grade decreases to garnet grade south of Birch Creek (Wheeler, 1964).

I chose these two areas because they are proximal to one another and spans a wide range of temperature conditions. The Mica Creek Sequence is a classic Barrovian sequence that extends from the middle- to upper-amphibolite facies. The adjacent Monashee Complex extends to granulite facies. The metamorphic conditions represented by these assemblages range from  $\approx 600$  °C and  $7 \pm 1$  Kbar for staurolite-bearing assemblages to  $\approx 700$  °C and  $7 \pm 1$  Kbar for sillimanite + K-feldspar-bearing assemblages as determined by mineral thermobarometry (Ghent et al., 1979, 1980, 1982 & 1983; Simony et al., 1980). Metamorphic conditions for the granulite-facies Monashee Complex rocks studied are  $\sim 720$ - $820$  °C and  $\approx 8 \pm 1$  Kbar (Nyman et al., in press).

## **Methods**

Samples analyzed in the earlier study of Bowman and Ghent (1986) for oxygen and hydrogen isotopes were reexamined in the present study. Additional samples were selected to provide more thorough coverage, and two samples were chosen for detailed study. Modal estimates on these two samples were made by counting at least 1500 points from serial thin

sections cut perpendicular to the predominant planar fabric. Mineral separates of these samples were made by standard techniques (magnetic separations and density separations followed by hand picking). Purity was assessed both optically by using a microscope and refractive index oils and by XRD. All separates are more than 95% pure.

Oxygen isotope analyses were obtained for quartz and garnet from all samples. Plagioclase, K-feldspar, muscovite and biotite were analyzed in two samples. The isotopic compositions of aluminosilicate minerals (kyanite or sillimanite) were measured for four samples. Isotopic analyses were made by using conventional externally heated Ni-rod bombs with  $\text{BrF}_3$  as the fluorinating agent (Clayton and Mayeda, 1963). Analyses of  $\text{CO}_2$  gas were made with VG 602D and Finnigan MAT 252 gas source mass spectrometers. All analyses were repeated at least twice. Oxygen yields on all extractions were better than 90% with most extractions better than 95%. Analyses of NBS-28 give  $9.69 \pm 0.15$  ‰.

It is widely held that refractory minerals such as garnet, kyanite and sillimanite are difficult or impossible to analyze properly with conventional fluorination techniques (e.g., Valley et al., 1994) Below I describe methods developed during the course of this study that allow high precision ( $\pm 0.15$ ‰) analyses of these refractory phases using conventional techniques. Three steps are critical to successful analysis of these phases:

1. grinding the samples to a small grain size ( $<20\text{-}30 \mu\text{m}$ ).
2. preconditioning the reaction vessels so that they do not consume the reagent during fluorinations, and
3. monitoring the solid reaction products, unconsumed reagent and oxygen yields.

Al-rich minerals do not react easily with  $\text{BrF}_3$ . This may reflect either the proportion of volatile fluorides (e.g.,  $\text{SiF}_4$ ,  $\text{FeF}_2$ ), to nonvolatile fluorides (e.g.,  $\text{AlF}_3$ ,  $\text{CaF}_2$  &  $\text{MgF}_2$ ) produced during the fluorination reaction or controls imposed by the structural positioning of elements (e.g., Si, Ti, Fe) that react to produce volatile fluorides within the crystalline lattice (e.g., Taylor and Epstein, 1962). To overcome this problem it is important to grind the minerals to a grain size of  $\approx 10\text{-}20 \mu\text{m}$  and to fluorinate them at higher temperatures than for more reactive minerals (e.g., quartz and feldspar). To get 90-100 % reaction yields for



garnet and aluminosilicate minerals, I react them at 640°C and 710°C, respectively. Before these high temperature reactions, I precondition the reaction vessels by heating them with excess BrF<sub>5</sub> at temperature 10-20°C higher than reaction temperature until they no longer consume reagent. I monitor the amount of reagent after the reaction to ensure that excess reagent remains. Gas produced by fluorinations where reagent is consumed are isotopically shifted, possibly because of incomplete reaction or the formation of intermediate oxygen+fluorine compounds, for example Si<sub>2</sub>OF<sub>6</sub>.

For analysis of small samples, the reaction procedures were modified to reduce the total non condensible gas and to enhance production of CO<sub>2</sub>. The waste trap was emptied and pretreated with room temperature BrF<sub>5</sub> before extractions to facilitate efficient removal of waste reagent during the extractions. Either tank oxygen gas, or oxygen gas from a single large sample was admitted to both the metal and the glass part of the line and converted to CO<sub>2</sub> before converting any small samples. This reduces problems with contamination that can be associated the first extracted small sample. The Ni-rod bombs were cooled to less than 300 °C before all extractions. During extractions the metal part of the line and Ni rod bombs were opened in stages, five minutes (timed with a timer) to a metal waste trap kept at liquid nitrogen temperatures, then two minutes to a glass spiral trap, at liquid nitrogen temperatures, and finally to the conversion chamber. Conversion of small samples was monitored on two thermocouple gauges, one at the glass spiral trap and one at the conversion chamber, and conversions were continued until the pressure was below five mtorr (zero on the conversion chamber gauge was less than one mtorr). For samples of less than 0.5 mg, the total deflection on this gauge is less than 75 mtorr. Generally the conversions went to zero on the conversion chamber gauge. If the noncondensable gas was high, all traps would be thawed, and the metal traps would be emptied. If necessary, the metal traps would be cleaned with a small amount (approximately 50 torr) of BrF<sub>5</sub>. These precautions were necessary for consistent results when analyzing small (2-5 mg) samples of garnet. Because it was found that analytical uncertainties were larger for very small (0.2-1.5 mg) samples, the smallest samples used for this study were 2.0 mg.

## Results

The oxygen isotopic compositions of mineral separates from Mica Creek and the Monashee Complex are reported in Table 6.1. Quartz from the Mica Creek area defines a very narrow range of isotopic compositions ( $\bar{X}_{15} = 14.18 \pm 1.36$  ‰), indistinguishable from values reported by O'Neil and Ghent (1975) for the adjacent, lower grade Esplanade Range ( $\bar{X}_7 = 14.35 \pm 1.12$  ‰). Quartz from pelites, not including quartz from inliers of the sillimanite isograd give  $\bar{X}_{13} = 14.39 \pm 1.33$  ‰. My measurements of quartz are approximately 1.3 ‰ greater in  $\delta^{18}\text{O}$  compared with analyses of quartz from the same samples analyzed by Bowman and Ghent (1986). I attribute this to different standardization procedures in the respective laboratories. Isotopic analyses of garnet from the Mica Creek area also define a narrow range ( $10.55 \pm 1.17$  ‰). In rocks from the Mica Creek area the order of isotopic enrichments is quartz > feldspar > kyanite ~ muscovite > garnet > biotite. The isotopic compositions of minerals from the two samples of the Monashee Complex were less  $^{18}\text{O}$  rich than those from the adjacent Mica Creek area described above. Moreover, the order of isotopic enrichments for sample 1-9 from the Monashee Complex is different quartz > sillimanite > garnet > feldspar > biotite. In both localities, the fractionation of oxygen isotopes between coexisting quartz and garnet in the same sample decreases with increasing metamorphic grade. The isotopic fractionations between quartz and biotite and quartz and muscovite obtained in this study are indistinguishable from those given by Bowman and Ghent (1986).

### Isotopic temperature data

Table 6.2 and Figure 6.3 present the quartz-garnet, quartz-kyanite and quartz-sillimanite mineral-pair isotopic temperature data for Mica Creek and the Monashee Complex. These isotopic temperature data are internally consistent and in excellent agreement with temperatures given by cation thermometry and petrogenetic grid constraints (e.g., Ghent et al., 1982). These data do not show the same evidence for resetting that is

present in the quartz-biotite, quartz-muscovite and quartz-ilmenite isotopic data of Bowman and Ghent (1986). Five quartz-garnet temperatures for garnet grade rocks from Mica Creek give an average of  $618 \pm 5^\circ\text{C}$ . Five quartz-garnet and quartz-kyanite temperature data for samples from the kyanite + biotite zone give an average of  $625 \pm 27^\circ\text{C}$ . The average of four quartz-garnet and quartz-kyanite temperature data for the kyanite-sillimanite transition give  $647 \pm 5^\circ\text{C}$ . The average temperature data for three quartz-garnet pairs from the sillimanite + K-feldspar zone give  $696 \pm 23^\circ\text{C}$ , and the average of three quartz-garnet and quartz-sillimanite temperature data gives  $767 \pm 38^\circ\text{C}$  for the granulite grade rocks of the Monashee Complex south west of Mica Creek. Taken by themselves, these data suggest that mineral-pair isotopic thermometry *can be used* to gain insight into the temperature conditions of Barrovian-type metamorphic environments.

However, closer inspection of the isotopic data yields several troubling inconsistencies. Quartz-muscovite and quartz-biotite temperatures in these rocks are  $470 \pm 26^\circ\text{C}$  and  $380 \pm 37^\circ\text{C}$ , respectively (recalculated from the data of Bowman and Ghent using the calibration of Chacko et al., in prep. and Clayton et al., 1989). In feldspar-poor rocks such as these pelites, these low quartz-mica temperatures can only be attributed to retrograde exchange between quartz and mica. Such a process will raise the  $\delta^{18}\text{O}$  of quartz. Given the approximate modal compositions of these rocks,  $\delta^{18}\text{O}_{\text{quartz}}$  will increase by 0.4 to 0.6 ‰. In turn, apparent quartz-garnet and quartz-aluminosilicate temperatures will be spuriously low by 50 to 80 °C. If we raise the quartz-garnet and quartz-aluminosilicate mineral pair temperatures by this amount, they become inconsistent with two well calibrated equilibria, the kyanite-sillimanite transition (e.g., Bohlen et al., 1991) and muscovite + quartz + plagioclase melting (e.g., Större, 1972; Peto, 1976). This observation suggests that the  $\delta^{18}\text{O}$  values of quartz grains have been lowered, possibly by open system interactions. To examine further the possibility of open system interactions, I undertook mass balance constrained calculations like those outlined in chapter 1 and 3 of this study.

## Sample 1-9

Sample 1-9 was collected from part of the Monashee Complex that crops out along the Trans-Canada Highway approximately 10 km west of Revelstoke B.C. The outcrop is 100 m below the projected surface of the Monashee Decollement and thus lies in the lower plate of a metamorphic core complex (Brown and Carr, 1990). The outcrop, which was the subject of a detailed study by Nyman et al., (in press), comprises strongly migmatized pelites with the assemblage garnet + biotite + sillimanite + K-feldspar + quartz ± cordierite. Nyman et al. (in press) postulated that the protolith for this outcrop was similar to that of the adjacent Mica Creek pelites. This can be corroborated by comparing whole-rock, major-element compositions from this outcrop with those from Mica Creek (sample MC118A) (Figure 6.4). These compositional data were calculated by combining EPMA data of major minerals collected by Nyman et al. (in press) with modal data. With the exception of Si, there is excellent agreement between the calculated mesosome compositions of samples 1-9, MC118A and with the mesosome compositions calculated from the data of Nyman et al. (in press). These results are consistent with the conclusions drawn by Nyman et al. (in press) that the leucosome in these rocks is internally-derived melt and that the protolith for the rocks was similar to those found at Mica Creek. Interestingly, the calculated whole rock  $\delta^{18}\text{O}$  value of sample 1-9 (9.3 ‰) is significantly lower than that of sample MC118A (11.7 ‰). Given the analytical and modal uncertainties, propagated uncertainties for these whole rock isotopic compositions are less than  $\pm 0.2\text{‰}$ . The different whole rock isotopic compositions and the similar inferred protoliths suggest that some processes have operated to lower the  $\delta^{18}\text{O}$  of sample 1-9 by approximately 2.4 ‰. What was this process? When in the geological history of these rocks did it operate? If it reflects open system interactions, at what temperature did it occur? Some of these questions can be answered by examination of the isotopic data. Others cannot be answered directly, but significant insight into their answers can be gained by considering the isotopic compositions of the minerals in light of constraints imposed by mass balance and equilibrium.

The timing of the  $\delta^{18}\text{O}$  lowering event can be addressed by examining the mineral

isotopic composition data. The  $\delta^{18}\text{O}$  values of garnet and sillimanite in sample 1-9 are low and the quartz-garnet and quartz-sillimanite oxygen isotope fractionations are not obviously out of equilibrium. This indicates that much of the isotopic lowering event occurred before or during crystallization of garnet and sillimanite. I infer that the whole rock  $\delta^{18}\text{O}$  value of sample 1-9 was reduced by open system interactions on the prograde path. Reversed K-feldspar-garnet and anomalous K-feldspar-biotite fractionations indicate that K-feldspar from sample 1-9 is not in equilibrium with the other minerals. The low  $\delta^{18}\text{O}$  for K-feldspar suggests either that a second phase of open system interactions affected these samples, or that the event that caused the lowering of  $\delta^{18}\text{O}$  for garnet and sillimanite was long lived and extended from the high temperature throughout much of the cooling history of the sample. I have used the techniques outlined in chapters 2 and 3 to investigate this possibility. In these calculations I have adjusted the K-feldspar isotopic composition by  $2.6\pm 0.5\text{‰}$  to a reasonable equilibrium value of  $9.8\text{‰}$ . Modes and isotopic compositions for sample 1-9 are presented in table 6.3. The results of the calculations are presented in table 6.4. Because K-feldspar constitutes only a small part of the rock, the assigned K-feldspar value and associated uncertainties have relatively little effect on the calculations. The garnet and sillimanite model temperatures shift from  $909\pm 66^\circ\text{C}$  and  $1115\pm 190^\circ\text{C}$  to  $870\pm 60^\circ\text{C}$  and  $1024\pm 130^\circ\text{C}$ , respectively, upon adjustment of the K-feldspar. These temperatures are still too high to be in accordance with independent temperature estimates of Nyman et al. (in press). In turn, this suggests that the  $\delta^{18}\text{O}$  values of quartz and biotite are too low to be in equilibrium with garnet and sillimanite. Part of the reason for the discrepant garnet and sillimanite temperatures could arise from the input equilibrium data. I do not favor this interpretation because it requires, equilibrium fractionations for quartz-garnet and quartz-sillimanite to be significantly smaller than the values reported in the literature. For garnet, I have used the theoretically based calculations of Kieffer (1982) which agree well with the high quality experimental grossular-calcite exchange data of Rosenbaum et al. (1994) and the semi-empirical calibrations of Smyth and Clayton (1988). For sillimanite, I have used the Smyth and Clayton (1988) calibration. Calibrations of Sharp and Ulmer (1993) and Hoffbauer et al. (1994) give larger values for this fractionation and exacerbate the discrepant

sillimanite temperatures; the calibration of Zheng (1993) give smaller values for this fractionation and cause temperature data that are too low. Because of its importance for assessing the validity of isotopic thermometry, future experimental studies should focus on better determining fractionation factors involving the aluminosilicate minerals.

A second possible reason for the discrepant temperatures could be a problem with determining the true equilibration volume of the sample. For example, a larger amount of leucosome may have equilibrated with this sample than was incorporated in the hand sample scale modal determination. Figure 6.5 plots the observed closure temperatures for garnet and sillimanite calculated as a function of the amount of leucosome incorporated into the mode of the mesosome. I used the mode of the mesosome that I measured for sample 1-9 and the mode of the leucosome measured by Nyman et al. (in press) for these calculations. The data are satisfied within for an equilibration volume that contains 40-100% leucosome. This large amount of leucosome is not supported by the quantitative estimates of the amount of leucosome in the outcrop made by Nyman et al. (in press) (20-30%). Consequently, I will investigate the possibility of open system effects to account for the discrepant temperatures.

Figure 6.6 shows the observed closure temperatures that would be produced for a range of open system shifts in the low closing phases quartz and biotite. In this diagram we see that the magnitude of the shifts required to bring garnet and sillimanite temperatures to 820°C is approximately 0.2 and 0.4 ‰, respectively. Shifts of approximately 0.6 and 0.7 ‰ are needed for the exchanging phases to bring the garnet and sillimanite into agreement at 720 °C. The shaded box illustrates the overlap of 1 $\sigma$  uncertainties for garnet and sillimanite intercept temperatures for the interval 720 to 820 °C. The median isotopic shift given by this box is 0.3±0.1‰ at 820°C and 0.6 ±0.2‰ at 720 °C. Another possibility is that the biotite has been shifted and that the quartz has not. This would require quartz closure temperatures significantly in excess of 500 °C which is in conflict with diffusion data (e.g., Gigetti and Yund, 1984) and suggests that biotite and quartz have been shifted to lower  $\delta^{18}\text{O}$  values. In turn this suggests that part of the  $\delta^{18}\text{O}$  lowering event occurred at temperatures above quartz closure (400-450°C).

In summary, whole rock data for 1-9 indicate a high-temperature lowering of  $\delta^{18}\text{O}$

near peak temperature conditions, and the systematics of individual minerals in this sample indicate additional lowering of  $\delta^{18}\text{O}$  during cooling but above quartz closure. This could either be two parts of one long lived event or two separate open system events.

### **Sample MC118A**

Sample MC118A is from a highly migmatized outcrop in the kyanite zone of the Mica Creek sequence. This sample contains kyanite + garnet + biotite + muscovite + quartz + plagioclase. Table 6.3 shows the modal and isotopic data for this sample. Three important observations can be made on the basis of the isotopic compositions of quartz, plagioclase, muscovite and biotite. First, the isotopic composition of plagioclase (12.65 ‰) is not anomalously low relative to the other minerals. Second, the fractionations between quartz and feldspar give reasonable isotopic temperatures. Third, the quartz-muscovite and the quartz-biotite fractionations in sample MC118A (2.9 and 4.7 ‰, respectively) are indistinguishable from the quartz-muscovite and quartz-biotite fractionations reported by Bowman and Ghent (1986) ( $2.6 \pm 0.2$  ‰ and  $5.1 \pm 0.6$  ‰, respectively). From these three observations, it can be inferred that, unlike sample 1-9, sample MC118A has not experienced significant (late) interactions with low  $\delta^{18}\text{O}$  fluids below the closure temperature of quartz.

Calculations of single sample model temperatures give  $T_{\text{kyanite}} > T_{\text{garnet}} > T_{\text{quartz}} \sim T_{\text{muscovite}} > T_{\text{biotite}} \sim T_{\text{feldspar}}$ . The calculated temperature data are presented in Table 6.4. The kyanite fractionation factor is not known well enough to make any definitive statements about the significance of the kyanite model temperature. The garnet temperature (695°C) is within  $1\sigma$  of the kyanite-sillimanite transition (Bohlen et al., 1991), but the difference is consistent with inferred 50°C shift predicted on the basis of the quartz-muscovite and quartz-biotite fractionations. The observed shift can also be satisfied either by including approximately 20-45% leucosome in the mass balance or by a high-temperature open system lowering of  $\delta^{18}\text{O}$  for the quartz, feldspar, muscovite, and biotite fraction of the rock by 0.2 to 0.4 ‰.

### **Additional evidence for open system**

Another observation is the low  $\delta^{18}\text{O}$  for garnet and quartz and small quartz-garnet fractionation observed for sample GM-78-1. Bowman and Ghent (1986) noted that sample GM-78-1 contained anomalous D/H and low quartz-biotite temperatures. Bowman and Ghent (1986) suggested that this sample experienced late interaction with low  $\delta^{18}\text{O}$  fluids. The small quartz-garnet fractionation (1.98 ‰) indicates that the quartz in this sample has been affected by open system interactions after closure of garnet. The temperatures required by diffusive exchange are closer to the infinite reservoir closure temperatures of Dodson (1973) (e.g., temperatures higher than 400-450°C) than they are to the finite reservoir closure temperatures of Eiler et al. (1992). This is because it is the isotopic composition of the quartz, and not the other exchanging phases, that must change for us to image this process. The magnitude of the open system  $\delta^{18}\text{O}$  shift of quartz in GM-78-1 is at least 1.2 ‰ (required by equilibrium with garnet at 700 °C), and more likely 1.7 ‰ (also accounting for retrograde quartz + biotite exchange). The low  $\delta^{18}\text{O}$  of garnet in this sample (9.38 ‰) may provide evidence to support a high temperature open system process that accompanied garnet growth.

Another feature of the isotopic data is the variable garnet-kyanite fractionations in kyanite and sillimanite grade samples MC104, MC107 and MC118A and B. These garnet-kyanite fractionations range from ~0.6 to 1.7 ‰. All of these analyses were repeated at least twice. The only feasible way to produce this variability is if the garnet and kyanite grew during different parts of a high-temperature open system. A final observation is the lower  $\delta^{18}\text{O}$  for garnet and quartz for samples that were collected from high temperature inliers of the sillimanite isograd.

These data suggest that in addition to regional  $^{18}\text{O}$  depletion of quartz, biotite and muscovite, local, high-temperature, near peak isotopic lowering of  $\delta^{18}\text{O}$  occurred in the Mica Creek area. Like sample 1-9, the isotopic systematics for the Mica Creek samples reflect one long lived or two discrete high-temperature  $^{18}\text{O}$  depletion events.



## Discussion

The results of this study suggest that the isotopic temperature data for the Mica Creek Barrovian Sequence and the adjacent Monashee Complex cannot be directly correlated with the thermal history of these rocks. Instead, the isotopic compositions of minerals record the effects of an event that lowered  $\delta^{18}\text{O}$  of exchanging phases. Some of the lowering may result from a larger equilibration volume and exchange between leucosome and mesosome during cooling. However, some of this lowering likely reflects interaction with high-temperature fluids (>400-450°C). If the problem is only an equilibration volume problem, quartz-garnet and quartz-aluminosilicate temperatures data will still be valid minimum estimates of peak temperature conditions for these rocks, and further study on an outcrop scale could be used to determine the appropriate equilibration volume and to determine the mineral closure temperatures that do reflect the metamorphic history. If open system effects have occurred the temperature data are invalid but these methods can still be used to constrain the temperature and amounts of open system fluid-rock interactions.

The regional lowering of  $\delta^{18}\text{O}$  values for quartz in the Mica Creek area may reflect a significant part of many metamorphic histories. Pervasive fluid influx early in the cooling history of this sequence is required to shift the isotopic compositions of quartz, feldspar and mica but not garnet or aluminosilicate. The lack of obvious hydrogen isotopic evidence for meteoric fluids suggests that isotopic lowering accompanying this fluid influx event resulted from up temperature flow and not from interaction with meteoric waters. A possible driving force for up temperature flow is the relaxation of a previously perturbed geothermal gradient. During thermal relaxation, high-temperature rocks cool as low temperature rock are heated. Fluid released from the low temperature rocks flows in an up-temperature direction and interacts with the high temperature rocks. The lack of obvious retrogression of garnet and kyanite, coupled with the observed isotopic shifts for quartz, suggests that these fluids interact with the rocks while they are still hot (>500 °C). Because I am describing a regional metamorphic feature that does not involve meteoric waters, this type of open system interaction is categorically different from the open system interactions that accompany

emplacement and cooling of the granitoid rocks in southern British Columbia (e.g., Magaritz and Taylor, 1986). The late lowering of  $\delta^{18}O$  for K-feldspar and possibly biotite in sample 1-9, however, may be due to a process similar to that invoked by Magaritz and Taylor (1986). Hydrogen isotopic analyses should be undertaken to confirm this latter possibility. The possibility that high temperature, retrograde,  $\delta^{18}O$ -lowering processes have operated in other metamorphic sequences warrants further investigation.

The results of this study highlight the importance of considering both mass balance and equilibrium constraints when interpreting isotopic data. The conclusions are hinged on the holistic approach developed in chapters 2 and 3. Further study in the Mica Creek area should focus on distinguishing between equilibration volume and open system effects. If open system interactions have occurred, their spatial relationship to large scale syn- and post-metamorphic features such as folded isograd surfaces and high-grade inliers should be investigated. Further study in the Monashee Complex should investigate the relationship between the distribution of open system rocks and crustal scale features such as the Monashee Decollement and Columbia River Fault. An important focus for both studies will be to image the temperature conditions at which open system interactions occurred.

# Map of southern Omineca Belt

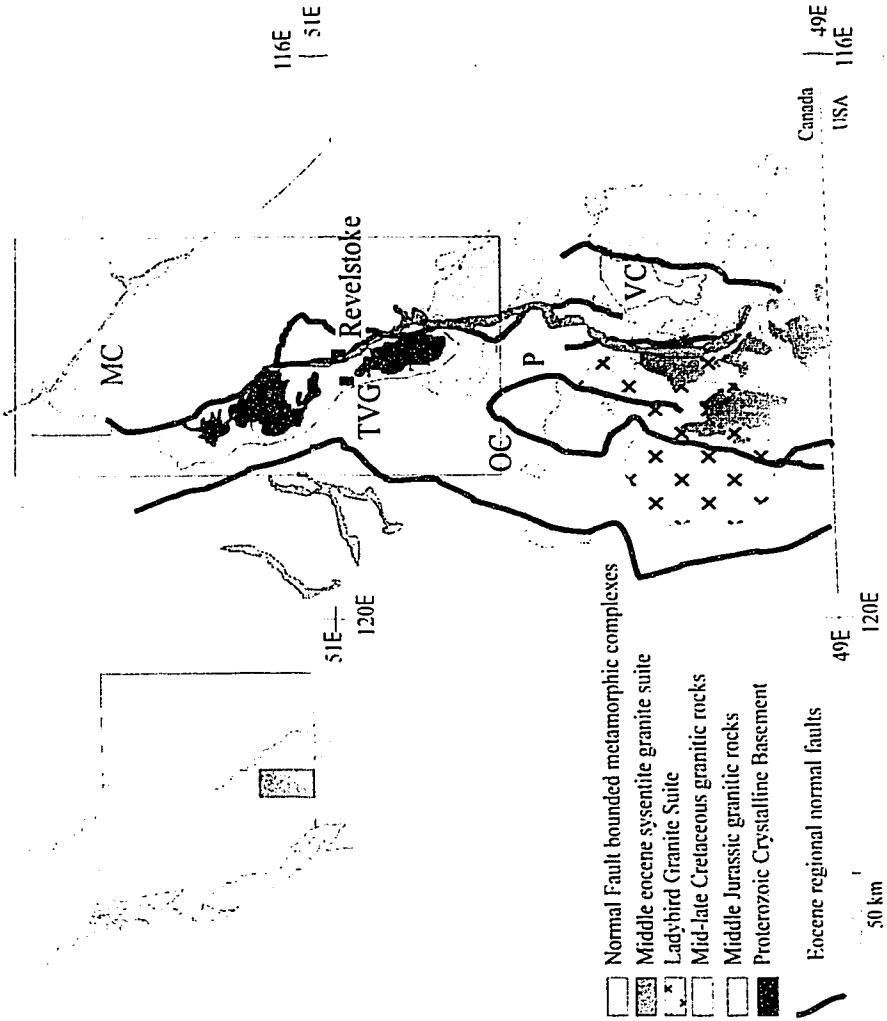


Figure 6.1 Map of study area. (After Parrish et al., 1988)

# Metamorphic Map of Study Area

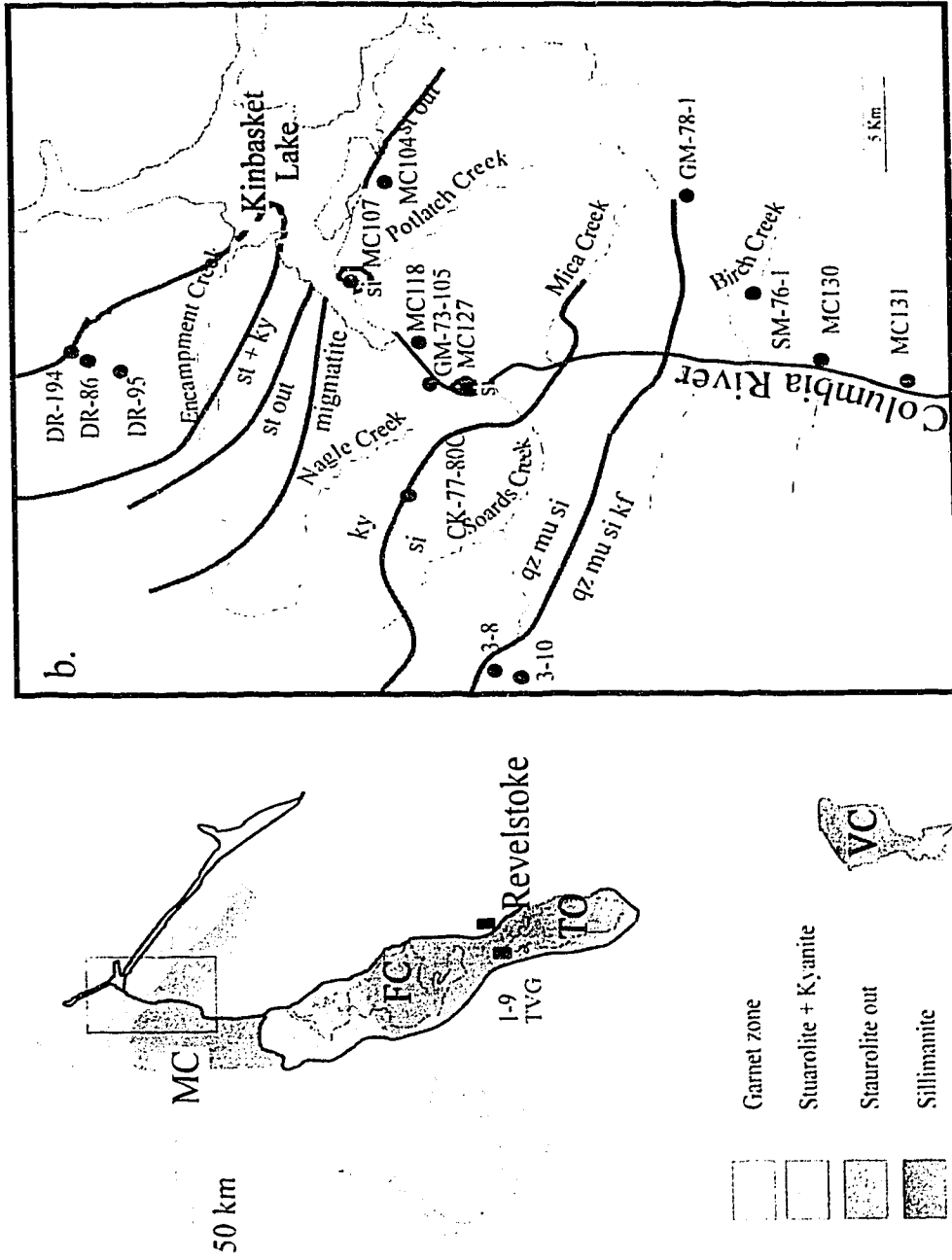
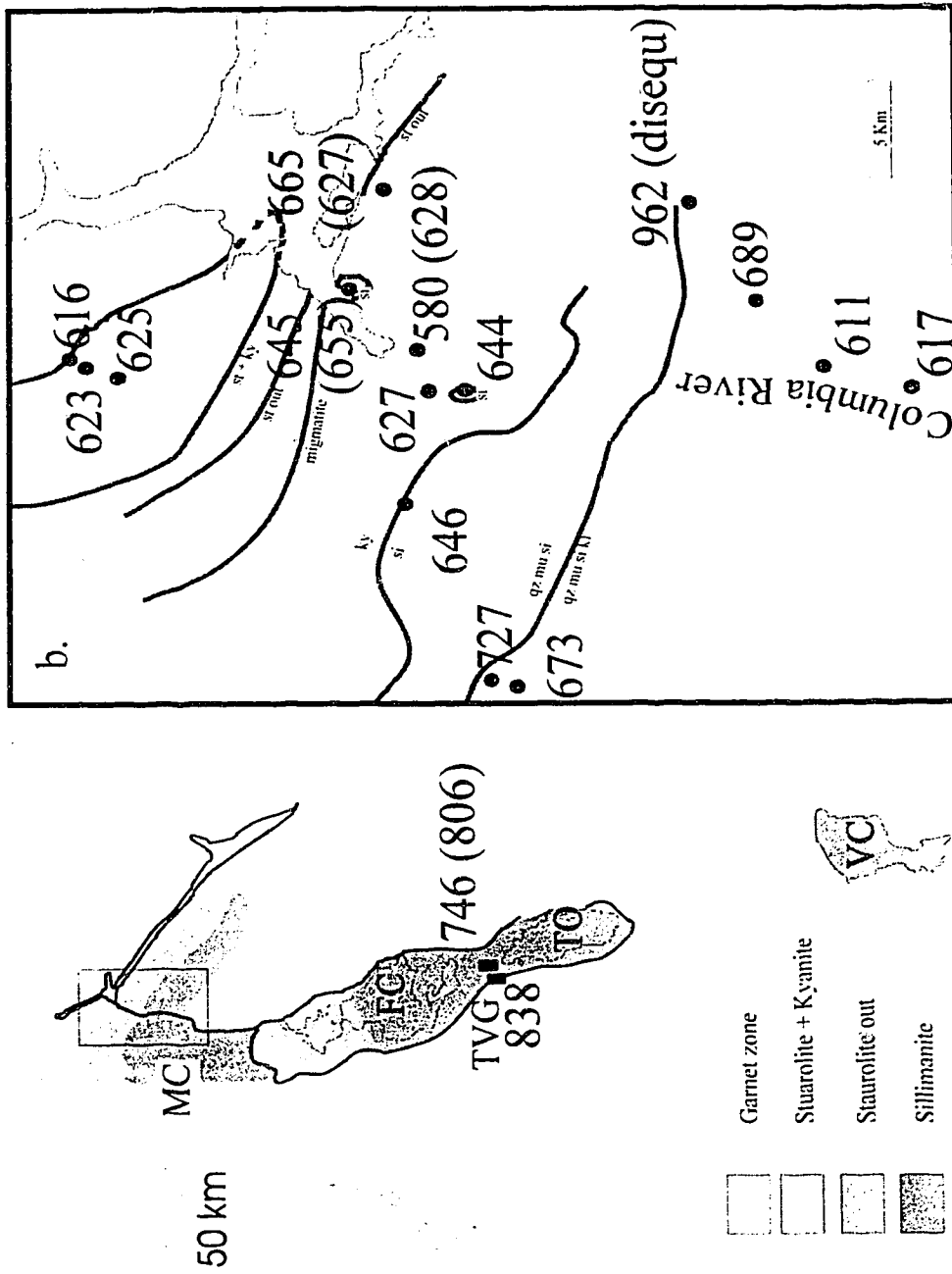


Figure 6.2. Metamorphic map of study area. (After Ghent et al., 1982, 1990)

Figure 6.3 Quartz-garnet (quartz-kyanite or sillimanite) mineral-pair temperature data.



Calculated cation abundances (percent by weight)  
 (from mineral composition and modal data)

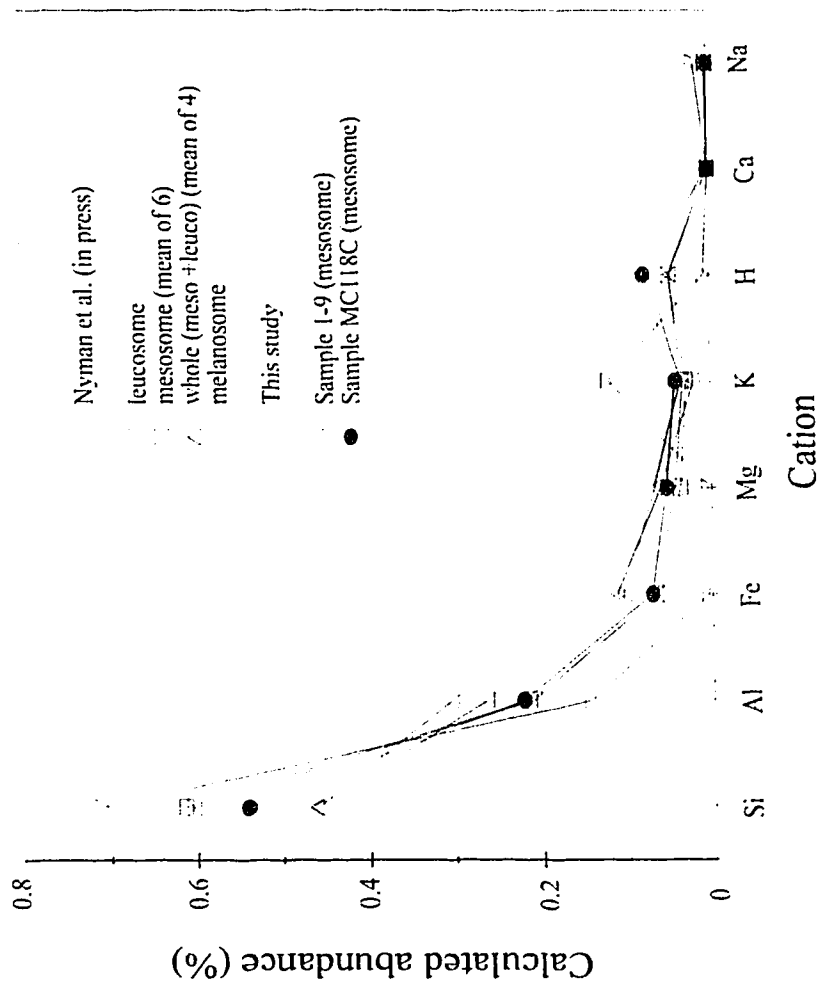


Figure 6.4 Calculated whole rock composition data for samples from outcrop 1-9 and MC118. See text for details.

Plot of intercept temperature versus fractional amount of leucosome in equilibration volume in mass balance for sample 1-9

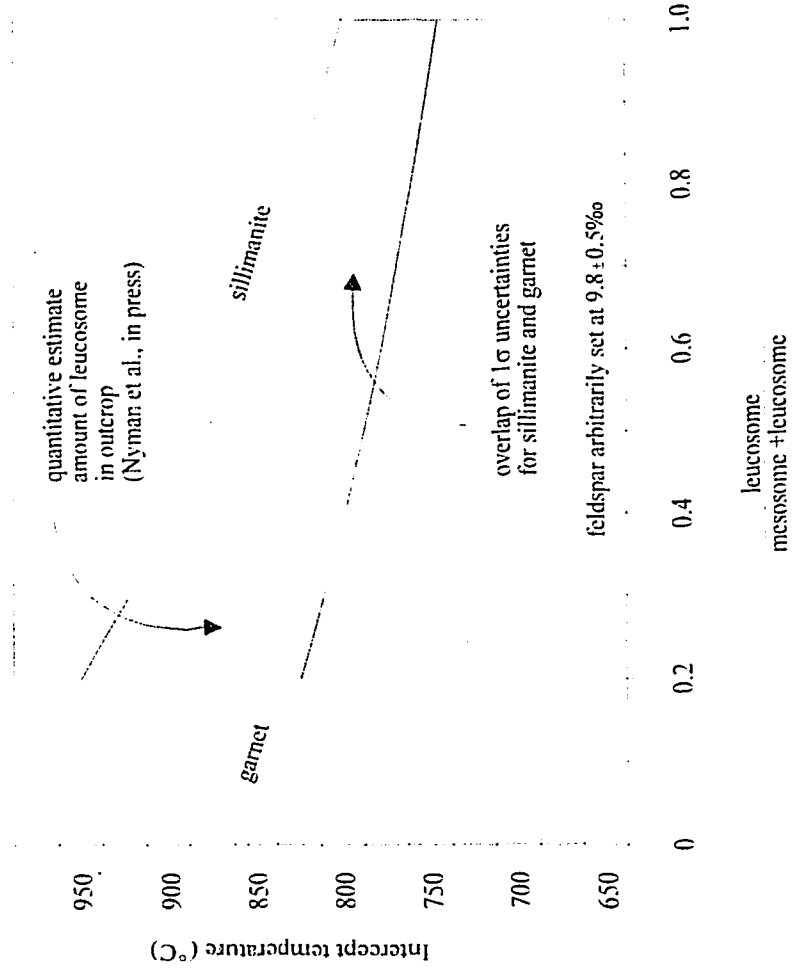


Figure 6.5 Plot to illustrate possible equilibration volume problems for sample 1-9. See text for details.

Plot of intercept temperatures versus arbitrary open system shift for sample 1-9  
quartz + feldspar + biotite fraction of rock

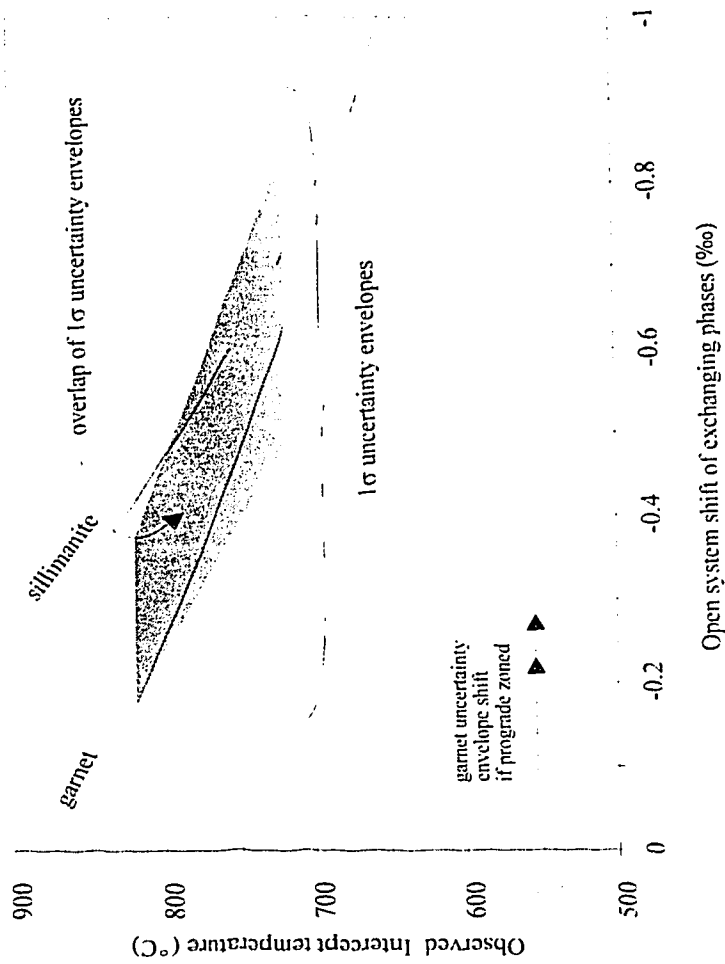


Figure 6.6 Plot to illustrate opens system shifts required to satisfy isotopic data.  
See text for details.



Table 6.1 Isotopic compositions of quartz, garnet, kyanite and Sillimanite

Sample	quartz (‰)	garnet (‰)	kyanite (‰)	Sillimanite (‰)	notes
DR-86	14.68	10.87			garnet
DR-95	14.20	10.41			garnet
DR-194	15.04	11.17			garnet
MC104	13.81	10.34	10.94		kyanite
MC107	13.05	9.43	10.35		sillimanite <sup>†</sup>
MC118A	13.95	9.73	11.06		kyanite
MC118B		9.52	11.26		kyanite
MC127	12.48	8.58			sillimanite <sup>†</sup>
GM 73-105	14.69	10.91			kyanite
CK-77-80C	16.72	13.09			kyanite/sillimanite
GM-78-1	11.38	9.38			sillimanite-Kfs
SM76-1	16.25	12.94			sillimanite-Kfs
3-8	14.68	11.62			sillimanite-Kfs
3-10	14.82	11.40			sillimanite-Kfs
MC130B	12.48	8.58			garnet <sup>††</sup>
MC131	14.42	10.57			garnet <sup>††</sup>
1-9	10.85	7.91		8.86	granulite
TVG 1	9.00	6.54			granulite <sup>†††</sup>

<sup>†</sup>inlier of sillimanite isograd <sup>††</sup>semipelite <sup>†††</sup>quartz vein in mafic lithology

Table 6.2 Mineral-pair temperature data

Sample	qz-gt (°C)	qz-ky (°C)
DR-86	623	
DR-95	625	
DR-194	616	
MC104	666	637
MC107	645	665
MC118A	578	634
MC127	644	
GM 73-105	627	
CK-77-80C	646	
GM78-1	962	
SM76-1	689	
3-8	727	
3-10	673	
MC130B	612	
MC131	618	
1-9	745	774 <sup>†</sup>
TVG 1	839	

Uncertainties on quartz garnet temperatures data are  $\pm 30$  and  $\pm 25$  °C at 700 and 600°C respectively. Uncertainties on quartz-kyanite temperatures are  $\pm 46$ °C at 650°C and uncertainties on quartz sillimanite temperatures are  $\pm 60$  °C. All uncertainties determined assuming  $\pm 0.2\%$  uncertainty on the fractionation factors. Fractionation factors used are Kieffer (1982) for quartz-garnet, Sharp (1993) for quartz-kyanite and Smyth (1989) and Smyth and Clayton (1988) for quartz-sillimanite. <sup>†</sup>quartz-sillimanite.

Table 6.3

Mineral	$\delta^{18}\text{O}$ (‰)	mode (vol%)	MolarO/Vol (mmol/cc)	$A_{\text{qz-mineral}}$ (‰)
MC118A				
quartz	13.93	38.6	88.20	0
plagioclase	12.65	3.8	76.40	1.23
muscovite	10.98	4.9	85.27	1.38
kyanite	11.06	14.4	110.78	2.35
biotite	9.21	27.7	79.58	2.15
garnet	9.73	9.9	104.25	3.02
1-9				
quartz	10.85	49.3	88.20	0
K-feldspar	7.20	3.8	74.73	.94
muscovite	N.D.	1.6	85.27	1.38
biotite	6.31	15.4	79.58	2.15
sillimanite	8.86	17.2	100.29	2.16
garnet	7.92	10.7	104.25	3.02

Isotopic composition data reported relative to V-SMOW. Modal abundance data collected as described in the text. Conversion factors determined from data presented in Deere Howie and Zussman. Temperature coefficients for the fractionation factors taken from Clayton et al. (1989), Clayton Group study (in review); Smyth (1989) and Smyth and Clayton (1988); Sharp (1993); Kieffer (1982).

Table 6.4 Intercept temperature data for samples MC118A and 1-9

Sample	mineral	temperature data (°C)
MC118A	kyanite	959±190°C
	garnet	693±62°C
	quartz	419±84°C
	muscovite	409±135°C
		425±132°C
	biotite	246±57°C
	plagioclase	246±57°C
1-9	sillimanite	1115±154°C
	garnet	909±66°C
	biotite	426±34°C
	quartz	236±55°C
	K-feldspar	236±55°C

Temperature data and uncertainties calculated by using equations presented in chapters 2 and 3 with data from table 6.4. Note that uncertainties presented in this table include the effect of modal correlations. \*Muscovite temperature data for quartz included in mode and for quartz not included in mode. The actual intercept temperature is intermediate between these two values.

## Chapter 7

### Concluding Remarks

In this thesis I have shown that isotopic thermometry is a useful tool and can be applied successfully to understand the thermal history of igneous and metamorphic rocks. In traditional isotopic thermometry, isotopic temperatures are calculated from mineral-pair isotopic fractionations. The fundamental problem with this type of isotopic thermometry is resetting (Deines, 1977; Gilletti, 1986). In this study I have shown that it is possible to account quantitatively for this resetting by adding the constraints imposed by mass balance. Two new types of temperature data can be calculated in this way. Single sample model temperatures can be calculated from a single hand sample by determining the fractionations between the high closing phases and the phases remaining open to exchange. In closed systems, when the mass balance is properly defined, these single sample model temperatures are mineral closure temperatures. The second type, multiple sample model temperatures, can be calculated in special cases. These temperatures are calculated by comparing the isotopic systematics of two or more samples with widely different modal compositions. They are whole rock isotopic temperatures. The additional requirement for meaningful multiple sample temperatures is the existence of high-temperature, large-scale equilibrium. The calculated multiple sample temperature could correspond to the disappearance of a melt phase, the disappearance of a fluid phase or any process that causes a large decrease in the equilibration length scale. Both the single sample and the multiple sample methods give more consistent temperature data than conventional thermometry because they quantitatively account for the effect of retrograde exchange among low closing phases. At the same time the uncertainties are only slightly larger, and the sampling requirements are less stringent than for mineral-pair thermometry.

Application of these methods to three types of metamorphic and plutonic igneous environments gives excellent results. The first place where these methods were applied was the Sybille Fe-Ti Oxide pit quarry of the Laramie Anorthosite Complex. Here conventional mineral-pair temperatures involving plagioclase, magnetite, ilmenite and olivine give a very

wide range of temperature data (600-1100°C). Single sample temperature data for ilmenite (~1000°C), olivine (~900°C) and magnetite (~750°C) are consistent for a range of samples and can be directly correlated with mineral closure during cooling. System closure temperature data for multiple samples from the Sybille quarry gives ~1070°C which is in excellent agreement with the experimentally determined solidus for the ores (Epler, 1987).

Application of these methods to very high temperature, slowly-cooled granulites from the Napier Complex, Enderbyland Antarctica and Taltson Magmatic Zone, Alberta, Canada give similar results. In the Napier complex, conventional mineral-pair temperatures involving quartz, garnet and orthopyroxene for samples span a wide range of values (700-970°C). Single sample temperatures from these same samples give garnet temperature data (~1000°C), orthopyroxene temperature data (820°C) and magnetite temperature data (~700°C). These single sample temperature data are in excellent agreement with best available estimates of the P-T conditions for this terrane (Ellis, 1980; Ellis et al., 1980; Harley, 1983, 1985a, 1986, 1987, Sandiford, 1985a; Sandiford and Powell, 1986; Sheraton et al., 1980). Quartz-rich samples from Pelican rapids give very consistent quartz-garnet fractionations and mineral pair temperature data of (~960°C). These data are in excellent agreement with minimum P-T estimates of Chacko et al. (1994).

Application of these methods to the Barrovian sequence rocks of the Mica Creek and Monashee Complex yielded an unexpected result. Although conventional quartz-garnet mineral pair temperature data are in excellent agreement with metamorphic P-T estimates, careful application of these methods suggests that high-temperature open system fluid rock interactions have occurred. This invalidates the temperature data and highlights a potentially important extension of these methods. Because these methods compare mineral isotopic compositions in equilibrium space (i.e., with respect to the constraints dictated by mass balance and equilibrium) they can be very sensitive indicators of open system interactions. In the Mica Creek and Monashee Complex, application of these techniques indicates the operation of a high-temperature (>400-450°C) open system. Extension of these techniques to open system problems should be done to determine the amounts and temperatures of open system interactions in metamorphic and igneous environments.

## References

- Andersen, D.J. and Lindsley, D.H. (1988) Internally consistent solution models for Fe-Mg-Mn-Ti oxides, *Am. Mineral.*, 73, 714-726.
- Anderson, I.C., Geist, D.J., Frost, B.R. and Lindsley, D.H. (1988) Rare earth depletion during late stage fractionation, Red Mountain pluton, Laramie Anorthosite Complex, Wyoming, *EOS*, 69, 524.
- Anderson, I.C., Frost, B.R. and Lindsley, D.H. (1987) Crystallization conditions of the Red Mountain Syenite, Laramie Anorthosite Complex, Wyoming, *EOS*, 68, 442.
- Anderson, A.T. Jr. (1966) Mineralogy of the Labrieville anorthosite, Quebec, *Am. Mineral.*, 51, 1671-1711.
- Anderson, A.T. Jr. (1967) The dimensions of oxygen isotopic equilibrium attainment during prograde metamorphism, *Jour. Geol.*, 75, 323-332.
- Anderson, A.T. Jr., Clayton, R.N. and Mayeda, T.K. (1971) Oxygen isotope thermometry of mafic igneous rocks, *Jour. Geol.*, 79, 715-729.
- Anderson, A.T. Jr. (1968) Oxidation of the LaBlache lake titaniferous magnetite deposit, Quebec, *Jour. Geol.*, 76, 528-547.
- Archibald, D.A., Glover, J.K., Price, R.A., Farrar, E. and Carmichael, D.M. (1983) Geochronology and tectonic implications of magmatism and metamorphism, southern Kootenay Arc and neighboring regions, southeastern British Columbia :Part I: Jurassic to mid-Cretaceous, *Can. Jour. Earth Sci.*, 20, 1891-1913.
- Archibald, D.A., Krogh, T.E., Armstrong, R.L. and Farrar, E. (1984) Geochronology and tectonic implications of magmatism and metamorphism, southern Kootenay Arc and neighboring regions, southeastern British Columbia :Part II: Mid-Cretaceous to Eocene, *Can. Jour. Earth Sci.*, 21, 567-583.
- Armstrong, J.E. (1982) Cordilleran metamorphic core complexes - from Arizona to southern Canada, *Ann. Rev. Earth Planet. Sci.* 10, 129-154.
- Baadsgaard, H. and Godfrey, J.D. (1967) Geochronology of the Canadian shield in northeastern Alberta: I Andrew Lake area, *Can. J. Earth Sci.*, 5, 541-563.
- Baertschi, P. and Silverman, S.R. (1951) The determination of relative abundances of the oxygen isotopes in silicate rocks, *Geochim. Cosmochim. Acta*, 1, 317-328.

- Becker, R.H. and Clayton, R.N. (1976) Oxygen isotope study of a Precambrian banded iron formation, hammersley Range, Western Australia. *Geochim. Cosmochim. Acta*, 40, 1153-1165.
- Bevington, P.R. (1969) *Data reduction and error analysis for the physical sciences*. McGraw Hill Inc, 336p.
- Bevington, P.R. (1969) *Data reduction and error analysis for the physical sciences*. McGraw Hill Inc, 336p.
- Bigeleisen, J. and Mayer, M.G. (1947) Calculation of equilibrium constantes for isotopic exchange reactions, *Jour. Chem. Phys.*, 15, 261-267.
- Bigeleisen, J. (1958) The significance of the Product and sum rules to isotope fractionation processes. in Kistenmaker, J., Bigeleisen, J. and Nier, A.O.C. (eds.) *Proceedings of the International symposium on isotope separation*, North Holland Publ. Co., Amsterdam, 121-157.
- Black, L.P., James, P.R. and Harley, S.L. (1983a) The geochronology, structure and metamorphism of early archaean rocks at Fyfe Hills, Enderby land, Antarctica, *Precambrian Research*, 21, 197-222.
- Black, L.P. and James, P.R. (1983) Geological history of the Archaean Napier Complex of Enderby Land; in, Oliver, R.L., James, P.R. and Jago, J.B. (eds.) *Antarctic Geoscience*, University Press. Cambridge, 11-24.
- Black, L.P., Williams, I.S. and Compston, W. (1986) Four zircon ages from one rock: the history of a 3930 ma-old granulite from Mount Sones, Enderby Land, Antarctica. *Contrib. Mineral. petrol.*, 94, 427-437.
- Black, L.P., Harley, S.L. and McCulloch, M.T. (1987) The Rayner Complex of East Antarctica: complex isotopic systematics within a Proterozoic mobile belt, *J. Metamorph. Geol.*, 5, 1-26.
- Black, L.P., James, P.R. and Harley, S.L. (1983b) Geochronology and geological evolution of metamorphic rocks in the Field Islands area, East Antarctica, *J. Matamorph. Geol.*, 1, 277-303.
- Black, L.P., Fitzgerald, J.D. and Harley, S.L. (1984) Pb isotopic composition, colour, and microstructure of maonazites from a polymetamorphic rock in Antarctica, *Contributions to Minaralogy and Petrology*, 85, 141-148.
- Bohlen, S.R., Montana, A. and Kerrick, D.M. (1991) Precise determination of the



equilibria kyanite=sillimanite and kyanite= andalusite and a revised triple point for the  $\text{Al}_2\text{SiO}_5$  polymorphs, *Am. Mineral.*, 76, 677-680.

- Bolsover, L.R., and Lindsley, D.H. (1983) Sybille oxide deposit: Massive Fe-Ti Oxides Intrusive into the Laramie Anorthosite Complex (LAC) Wyoming. EOS 64, 328.
- Bolsover, L.R. (1986) Petrogenesis of the Sybille iron-titanium oxide deposit, Laramie anorthosite complex, Laramie Mountains, Wyoming, Unpubl. M.S. thesis, SUNY at Stony Brook, 78 p.
- Born, M. and Huang, K. (1954) Dynamical theory of crystal lattices, Oxford University Press, London, 430 p.
- Bostock, H.H., van Breemen, O. and Loveridge, W.D. (1991) Further geochronology of plutonic rocks in the northern Taltson magmatic Zone, District of Mackenzie, N.W.T., in Radiogenic Age and isotopic studies: Report 4, Geological Survey of Canada, Paper 90-2, 67-78.
- Bostock, H.H., van Breemen, O. and Loveridge, W.D. (1987) Proterozoic geochronology in the Taltson magmatic Zone, N.W.T., in Radiogenic Age and Isotopic Studies: Report 1, Geological Survey of Canada, Paper 87-2, 73-80.
- Bostock, H.H. and Loveridge, W.D. (1988) Geochronology of the Taltson Magmatic Zone and its eastern cratonic margin, District of Mackenzie, in Radiogenic Age and Isotopic Studies: Report 2, Geological Survey of Canada, Paper 88-1, 59-65.
- Bottinga, Y. and Javoy, M. (1975) Oxygen isotope partitioning among the minerals in igneous and metamorphic rocks, *Rev. Geophys. and Space Phys.*, 13, 401-418.
- Bottinga, Y. (1969) Carbon isotope fractionation between graphite, diamond and carbon dioxide, *Earth and Planet. Sci. Lett.*, 5, 301-307.
- Bottinga, Y. and Javoy, M. (1973) Comments on oxygen isotope geothermometry, *Earth. Planet. Sci. Lett.* 20, 250-265.
- Bowers, T.S. and Helgeson, H.C. (1983) Calculation of the thermodynamic and geochemical consequences of nonideal mixing in the system  $\text{H}_2\text{O}-\text{CO}_2-\text{NaCl}$  on phase relations in geologic systems: Equation of state for  $\text{H}_2\text{O}-\text{CO}_2-\text{NaCl}$  fluids at high pressures and temperatures, *Geochim. Cosmochim. Acta.* 47, 1247-1275.
- Bowman, J.R. and Ghent, E.D. (1986) Oxygen and hydrogen isotope study of minerals from metapelitic rocks, staurolite to sillimanite zones, Mica Creek, British Columbia, *J. Met. Geol.*, 4 131-141.

- Brady, J.B. (1983) Intergranular diffusion in metamorphic rocks, *Am. J. Sci.* 283-A, 181-200.
- Brown, R.L. and Read, P.B. (1983) Shuswap terrane of British Columbia: A Mesozoic "core complex", *Geology*, 11, 164-168.
- Brown, R.L., Tippet, C.R. and Lane, L.S. (1978) Stratigraphy, facies changes, and correlations in the northern Selkirk Mountains, southern Canadian Cordillera, *Can. Jour. Earth Sci.*, 15, 1129-1140.
- Brown R.L. and Journey, J.M. (1987) Tectonic denudation of the Shuswap metamorphic terrane of southeastern British Columbia, *Geology*, 15, 142-146.
- Brown, R.L. and Carr, S.D. (1990) Lithospheric thickening and orogenic collapse within the Canadian Cordillera, *Jour. of Australasian Inst of Mining and Metallurgy*, 2, 1-10.
- Brown, R.L., Crowley, J.L. and Johnson, B.J. (1993) Cordilleran Transect, Rocky Mountain foreland and Omineca hinterland, Southeastern British Columbia, Part 2: A transect of the southern Omineca belt, *in* Brown, R.L., McDonough, M.R., Crowley, J.L., Johnson, B.J., Mountjoy, E.J., and Simony, P.S., *Field Trip Guidebook B-9 Cordilleran Transect, Rocky Mountain Foreland and Omineca Hinterland, southeastern British Columbia*, GAC/MAC Joint annual meeting, 1993.
- Buddington, A.F. and Lindsley, D.H. (1964) Iron-titanium oxide minerals and synthetic equivalents, *J. Petrol.* 5, 310-357.
- Chacko, T., Creaser, R.A. and Poon, D. (1994) Spinel + quartz granites and associated metasedimentary enclaves from the Taltson magmatic zone, Alberta, Canada: a view into the root zone of a high temperature, S-type granitic batholith, *Min. Mag.*, 58A, 161-162.
- Chacko, T., Hu, X., Mayeda, T.K., Clayton, R.N., Goldsmith, J.R. (1995) Oxygen isotope fractionations in muscovite, phlogopite, tremolite, and rutile, *Geochimica et Cosmochimica Acta*, submitted.
- Chacko, T. (1990) Oxygen isotope geothermometry: Application of new calibrations to metamorphic rocks; *in* Pattison, D.R.M., Ghent, E.D. and Gordon, T.M. (eds.) *Metamorphic styles in young and ancient orogenic belts*, IGCP project 235 and 304, 22.
- Chayes, F. (1971) *Ratio correlation*, University of Chicago press, 99p.

- Chiba, H., Chacko, T., Clayton, R.N. and Goldsmith, J.R. (1989) Oxygen isotope fractionations involving diopside, forsterite, magnetite, and calcite: Application to geothermometry, *Geochim. Cosmochim. Acta* 53, 2985-2995.
- Clayton, R.N., Goldsmith J.R. and Mayeda, T.K. (1989) Oxygen isotope fractionation in quartz, albite, anorthite and calcite, *Geochim. Cosmochim. Acta* 53, 725-733.
- Clayton, R.N. and Mayeda, T.K. (1963) The use of bromine pentafluoride in the extraction of oxygen from oxides and silicates for isotopic analysis, *Geochimica et Cosmochimica Acta*, 27, 43-52.
- Clayton, R.N. and Kieffer, S.W. (1991) Oxygen isotopic thermometer calibrations; in Taylor, H.P.Jr., O'Neal, J.R. and Kaplan, I.R. (eds.) *Stable isotope geochemistry: a tribute to Samuel Epstein*, The Geochemical Society: Special Publication No. 3. 3-10.
- Clayton, R.N. and Epstein, S. (1961) The use of oxygen isotopes in high-temperature geological thermometry, *Jour. Geol.*, 69, 447-452.
- Clayton, R.N. and Epstein, S. (1958) The relationship between O<sup>18</sup>/O<sup>16</sup> ratios in coexisting quartz, carbonate, and iron oxides from various geologic settings, *Jour. Geol.*, 66, 352-371.
- Clayton, R.N. (1961) Oxygen isotope fractionation between calcium carbonate and water, *Jour. Chem. Phys.* 34, 724-726.
- Clayton, R.N. (1981) Isotopic Thermometry, in Newton, R.C, Navrotsky, A. and Wood, B.J. (eds.) *Thermodynamics of minerals and melts*, Springer Verlag, Berlin, 85-109.
- Coghlan, R.A. (1990) Studies in diffusional transport: grain boundary transport of oxygen in feldspars, diffusion of oxygen, strontium and the REE's in garnet, and thermal histories of granitic intrusions in south-central Maine using oxygen isotopes. Ph.D. dissertation, Brown University.
- Cole, D.R. and Ohmoto, H. (1986) Kinetics of isotopic exchange at elevated temperatures and pressures, in Valley, J.W. Taylor H.P. and O'Neil J.R. (eds.) *Stable isotopes in High Temperature Geological Processes*, Mineral. Soc. Am., *Rev. Mineral.* 16., 41-90.
- Compston, W. and Williams, I.S. (1982) Protolith ages from inherited zircon cores measured by a high mass resolution ion microprobe. Fifth International Conference on Geochronology, Cosmochronology and Isotope Geology, Nikko,

Japan, 63-4 (Abstract).

- Connolly, C. and Muehlenbachs, K. (1988) Contrasting oxygen diffusion in nepheline, diopside and other silicates and their relevance to isotopic systematics in meteorites, *Geochimica et Cosmochimica Acta*, 52, 1585-1591.
- Craig, H. and Boato, G. (1955) Isotopes, in *Ann. Rev. Phys. Chem.*, 6, 403-432.
- Craig, H. (1953) The geochemistry of the stable carbon isotopes, *Geochim. Cosmochim. Acta*, 3, 53-92.
- Craig, H., Boato, G. and White, D.E. (1956) Isotopic geochemistry of thermal waters, in *Nuclear processes in geologic settings national academy of Sci. NRC publ.*, 400, 29-38.
- Crank, J. (1975) *The mathematics of diffusion*, Oxford University Press, New York, 414p.
- Craw, D. (1978) Metamorphism, structure, and stratigraphy in the southern park ranges, British Columbia, *Can. Jour. Earth Sci*, 15, 86-98.
- Criss, R.E., and Taylor, H.P.Jr. (1986) Meteoric hydrothermal systems, in Valley, J.W. Taylor H.P. and O'Neil J.R. (eds.) *Stable isotopes in High Temperature Geological Processes*, Mineral. Soc. Am., *Rev. Mineral.* 16, 373-424.
- Criss, R.E. (1991) temperature dependence of isotopic fractionation factors, in Taylor, H.P. Jr., O'Neil, J.R. and Kaplan, I.R. (eds.) *Stable isotope geochemistry: A tribute to Samuel Epstein*, The Geochemical Society Special Publication, 3, 11-16.
- Criss, R.E., Gregory, R.T. and Taylor, H.P.Jr. (1987) Kinetic theory of oxygen isotope exchange between minerals and water. *Geochim. Cosmochim. Acta* 51, 1099-1108.
- Deines, P. (1977) On the oxygen isotope distribution among mineral triplets in igneous and metamorphic rocks, *Geochim. Cosmochim. Acta* 41 1709-1730.
- DePaolo, D.J., Manton, W.I., Grew, E.S. and Halpern, M. (1982) Sm-Nd, Rb-Sr and Uth-Pb systematics of granulite facies rocks from Fyfe Hills, Enderby Land Antarctica, *Nature*, 298, 614-618.
- Dodson, M. (1986) Closure profiles in cooling systems, *Mat. Sci. Forum*, 7, 145-154.
- Dodson, M.H. (1973) Closure temperature in cooling geochronological and petrological

- systems, *Contrib. Mineral. Petrol.* 40, 259-274.
- Dowty, E. (1980) Crystal-chemical factors affecting the mobility of ions in minerals, *Am. Mineralogist* 65, 174-182.
- Duebendorfer, E.M. and Houston, R.S. (1987) Proterozoic accretionary tectonics at the southern margin of the Archean Wyoming craton, *Geol. Soc. Am. Bull.*, 98, 554-568.
- Dunham, J.L. (1932) *Phys. Rev.*, 41, 721-731.
- Dunn, S.R. and Valley, J.W. (1991) Calcite-graphite isotope thermometry: a test for polymetamorphism in marble, Tudor gabbro aureole, Ontario, Canada, *Jour. Metamorphic Geol.*, 10, 487-501.
- Eiler, J.M., Baumgartner, L.P. and Valley, J.W. (1992) Intercrystalline stable isotope diffusion: A fast grain boundary model. *Contributions to Mineralogy and Petrology*, 112, 543-557.
- Eiler, J.M., Valley, J.W., Baumgartner, L.P. (1993) A new look at stable isotope thermometry, *Geochim. Cosmochim. Acta* (In Press).
- Eiler, J.M., Valley, J.W., Graham, C.M. and Baumgartner, L.P. (1995) Ion microprobe evidence for the mechanism of stable isotope retrogression in high-grade metamorphic rocks, *Contrib. Mineral. Petrol.*, 118, 365-378.
- Eiler, J.M., Valley, J.W. and Baumgartner, L.P. (1993) A new look at stable isotope thermometry, *Geochim. Cosmochim. Acta*, 57, 2571-2583.
- Ellis, D.J. (1983) The Napier and Rayner Complexes of Enderby Land, Antarctica: Contrasting styles of metamorphism and tectonism; in: Oliver, R.L., James, P.R. and Jago, J.B. (eds.) *Antarctic Geoscience*, University Press, Cambridge, 25-30.
- Ellis, D.J. (1980) Osumilite-sapphirine-quartz granulites from Enderby Land Antarctica: P-T Conditions of metamorphism, implications for garnet-cordierite equilibria and the evolution of the deep crust, *Contributions to Mineralogy and Petrology*, 74, 201-210.
- Ellis, D.J., Sheraton, J.W., England, R.N. and Dallwitz, W.B. (1980) Osumilite-sapphirine-quartz-granulites from Enderby Land, Antarctica - Mineral assemblages and reactions, *Contributions to Mineralogy and Petrology*, 72, 123-143.

- Elphick, S.C., Graham, C.M. and Dennis, P.F. (1988) An ion microprobe study of anhydrous oxygen diffusion in anorthite: A comparison with hydrothermal data and some geological implications, *Contrib. Mineral. Petrol.* 100, 490-495.
- Elsenheimer, D. and Valley, J.W. (1993) Submillimeter scale zonation of  $\delta^{18}\text{O}$  in quartz and feldspar, Isle of Skye, Scotlane, *Geochim. Cosmochim. Acta*, 57, 3669-3676.
- Engel, A.E.J., Clayton, R.N. and Epstein, S. (1958) Variations in isotopic composition of oxygen and carbon in Leadville limestone (Mississippian, Colorado) and in its hydrothermal and metamorphic phases, *Jour. Geol.*, 66, 374-393.
- Epler, N.E. (1987) Experimental study of Fe-Ti oxide ores from the Sybille Pit in the Laramie Anorthosite, Wyoming, Unpubl. M.S. thesis, SUNY at Stony Brook, 67 p.
- Epler, N.E., Bolsover, L.R. and Lindsley, D.H. (1986) Nature and origin of the Sybille Fe-Ti oxide deposit, Laramie Anorthosite Complex, Wyoming, *Geol. Soc. Am. Abstr.* 18, 595.
- Epstein, S. (1956) Variations of the  $\text{O}^{18}/\text{O}^{16}$  ratios of fresh waters and ice, in *Nuclear processes in geologic settings national academy of Sci.* NRC publ., 400. 20-28.
- Epstein, A. and Mayeda, T.K. (1953) Variations in  $\text{O}^{18}$  content of waters from natural sources, *Geochim. Cosmochim. Acta*, 31, 181-214.
- Farquhar, J., Chacko, T. and Ellis, D.J. (1994) High-temperature oxygen isotope thermometry in two contrasting terranes, the Taltson Magmatic Zone, Canada and the Napier Complex, Antarctica, *Min. Mag.*, 58A, 265-266.
- Farquhar, J. and Chacko, T. (1994) Exsolution-enhanced oxygen exchange: Implications for oxygen isotope closure temperatures in minerals, *Geology*, 22, 751-754.
- Farquhar, J., Chacko, T. and Frost, B.R. (1993) Strategies for high-temperature oxygen isotope thermometry: a worked example from the Laramie Anorthosite Complex, Wyoming, USA, *Earth and Planet. Sci. Lett.*, 117, 407-422.
- Farver, J.R. (1989) Oxygen self diffusion rates in diopside with application to cooling rate determinations, *Earth and Planet. Sci. Lett.*, 92, 386-396.
- Farver, J.R. and Giletti, B.J. (1989) Oxygen and strontium diffusion kinetics in apatite and potential applicaitons to thermal history determinations, *Geochim. Cosmochim. Acta* 53, 1621-1632.

- Farver, J.R. and Yund, R.A. (1991) Oxygen diffusion in quartz: Dependence on temperature and water fugacity, *Chem. Geol.* 90, 55-70.
- Farver, J.R., and Yund, R.A. (1990) The effect of hydrogen, oxygen and water fugacity on oxygen diffusion in alkali feldspar, *Geochim. Cosmochim. Acta* 54, 2953-2964.
- Fortier, S.M. and Giletti, B.J. (1989) An empirical model for predicting diffusion coefficients in silicate minerals, *Science* 245, 1481-1484.
- Fowler, K.S. (1930) The anorthosite area of the Laramie Mountains, Wyoming, *Am. Jour. Sci.*, 19, 305-315, 373-403.
- Friedman, I. (1953) Deuterium content of natural waters and other substances, *Geochim. Cosmochim. Acta*, 4, 89-103.
- Frisch, T. (1988) Reconnaissance geology of the Precambrian shield of Ellesmere, Devon, and Coburg Islands, Canadian Arctic Archipelago, *Geol. Surv. Can. Mem.*, 409, 102p.
- Frost, B.R. (1991) Magnetic Petrology: Factors that control the occurrence of magnetite in crustal rocks, *in* Lindsley, D.H. (ed.) *Oxide minerals: Petrologic and magnetic significance*, *Rev. in Mineral.*, 25, 489-509.
- Frost, B.R., Lindsley, D.H. and Andersen, D.J. (1988) Fe-Ti-oxide silicate equilibria: Assemblages with fayalitic olivine, *Am. Mineral.*, 73, 727-740.
- Frost, B.R. (1979) Mineral equilibria involving mixed volatiles in a C-O-H fluid phase: the stabilities of graphite and siderite, *Am. Jour. Sci.*, 279, 1033-1059.
- Frost, B.R., Fyfe, W.S., Tazaki, K. and Chan, T. (1989) Grain-boundary graphite in rocks and implications for high electrical conductivity in the lower crust, *Nature*, 340, 134-136.
- Frost, C.D., Meier, M. and Oberli, F. (1990) Single-crystal, U-pb zircon age determination of the Red Mountain pluton, Laramie Anorthosite Complex, Wyoming, *Am. Mineral.*, 75, 21-26
- Frost, B.R. and Touret, J.L.R. (1989) Magmatic CO<sub>2</sub> and saline melts from the Sybille Monzosyenite, Laramie Anorthosite Complex, Wyoming, *Contrib. Mineral. Petrol.*, 103, 178-186.

- Fuhrman, M.L., Frost, B.R. and Lindsley, D.H. (1988) Crystallization conditions of the Sybille Monzosyenite, Laramie Anorthosite Complex Wyoming, *J. Petrol.* 29, 699-729.
- Garlick, G.D. and Epstein, S. (1967) Oxygen isotope ratios in coexisting minerals of regionally metamorphosed rocks, *Geochim. Cosmochim. Acta*, 31, 1325-1335.
- Gautason, B. and Muehlenbachs, K. (1993) Oxygen diffusion in perovskite: Implications for electrical conductivity in the lower mantle, *Science*, 260, 518-521.
- Geist, D.J., Frost, C.D. and Kolker, A. (1990) Sr and Nd isotopic constraints on the origin of the Laramie Anorthosite Complex, Wyoming, *Am. Mineral.*, 75, 13-20.
- Ghent, E.D., Simony, P.S. and Knitter, C.C. (1980) Geometry and pressure-temperature significance of the kyanite-sillimanite isograd in the Mica Creek area, British Columbia, *Contrib. Mineral. Petrol.*, 74, 67-73.
- Ghent, E.D., Knitter, C.C., Raeside, R.P. and Stout, M.Z. (1982) Geothermometry and geobarometry of pelitic rocks, upper kyanite and sillimanite zones, Mica Creek Area, British Columbia, *Can. Mineral.*, 20, 295-305.
- Ghent, E.D., Stout, M.Z. and Raeside, R.P. (1983) Plagioclase-clinopyroxene-garnet-quartz equilibria and geobarometry and geothermometry of garnet amphibolites from Mica Creek, British Columbia, *Can. Jour. Earth Sci.*, 20, 699-706.
- Ghent, E.D., Robbins, D.B. and Stout, M.Z. (1979) Geothermometry, geobarometry and fluid compositions of metamorphosed calc-silicates and pelites, Mica Creek British Columbia, *Am. Mineral.*, 64, 874-885.
- Ghiorso, M.S. and Sack, R.O. (1991) Thermochemistry of the oxide minerals, in Lindsley, D.H. (ed.) *Oxide minerals: Petrologic and magnetic significance*, *Rev. in Mineralogy*, v. 25, *Min. Soc Am.*, 221-264.
- Giletti, B.J. (1986) Diffusion effects on oxygen isotope temperatures of slowly cooled igneous and metamorphic rocks, *Earth. Planet. Sci. Lett.* 77, 218-228.
- Giletti, B.J. and Yund, R.A. (1984) Oxygen diffusion in quartz, *Journal of Geophysical Research*, 89B, 4039-4046.
- Giletti, B.J. and Hess, K.C. (1988) Oxygen diffusion in magnetite, *Earth and Planetary Science Letters*, 89, 115-122.



- Goff, S.P., Godfrey, J.D. and Holland, J.G. (1986) Petrology and geochemistry of the Canadian Shield of northeastern Alberta, Alberta Res. Council Bull., 51, 60 p.
- Goldberg, S.A. (1984) Geochemical relationships between anorthosite and associated iron-rich rocks, Laramie Range, Wyoming, Contrib. Mineral. Petrol, 87, 376-387.
- Grant, J.A. and Frost, B.R. (1990) Contact metamorphism and partial melting of pelitic rocks in the aureole of the Laramie Anorthosite Complex, Morton Pass, Wyoming, Am. J. Sci. 290, 425-472.
- Greenwood, H.J., Woodsworth, G.J., Read, P.B., Ghent, E.D. and Evenchick, C.A. (1991) Metamorphism, chapter 16 in Gabrielse, H. and Yorath, C.J. (eds.) Geology of the Cordilleran Orogen in Canada, Geol. Surv. Canada, Geology of Canada, 4, 533-570.
- Gregory, R.T. and Criss, R.E. (1986) Isotopic exchange in open and closed systems, in Valley, J.W., Taylor, H.P., J.R. and O'Neil, J.R. (eds.) Stable isotopes in High Temperature Geological Processes, Mineral. Soc. Am., Rev. Mineral. 16, 91-127.
- Grew, E.S. (1980) Sapphirine + quartz association from Archaean rocks in Enderby Land, Antarctica, American Mineralogist, 65, 821-836.
- Grover, T.W., McDonough, M.R. and McNicoll, V.J. (1993) Preliminary report of the metamorphic geology of Taltson magmatic zone, Canadian Shield, northeastern Alberta. in Current Research, Part C, Geological Survey of Canada, Paper 93-1C, 233-238.
- Harley, S.L. (1985b) paragenetic and mineral-chemical relationships in orthoamphibole-bearing gneisses from Enderby Land, east Antarctica: a record of Proterozoic uplift. Journal of Metamorphic geology, 3, 179-200.
- Harley, S.L. (1985a) Garnet-orthopyroxene bearing granulites from Enderby Land, Antarctica: Metamorphic Pressure-Temperature-Time Evolution of the Archaean Napier Complex, journal of petrology, 26. 819-856.
- Harley, S.L. (1983) Regional geobarometry-geothermometry and metamorphic evolution of Enderby Land, Antarctica; in, Oliver, R.L., James, P.R. and Jago, J.B. (eds.) Antarctic Geoscience, University Press, Cambridge, 25-30.
- Harley, S.L. and Black, L.P. (1987) The Archaean geological evolution of Enderby Land, Antarctica; in Park, R.G. and Tarney, J. (eds.) Evolution of the Lewisian and Comparable Precambrian High Grade Terrains, Geological Society Special Publication No. 27, 285-296.

- Harley, S.L. (1987) Pyroxene-bearing meta-ironstone and other pyroxene-granulites from Tonagh Island, Enderby Land, Antarctica: Further evidence for very high temperature (>980°C) Archaean regional metamorphism in the Napier Complex, *Journal of Metamorphic Geology*, 5, 341-356.
- Harley, S.L. (1986) A sapphirine-cordierite-garnet-sillimanite granulite from Enderby Land, Antarctica: Implications for FMAS petrogenetic grids in the granulite facies, *Contributions to Mineralogy and Petrology*, 94, 452-460.
- Harley, S.L., Hensen, B.J. and Sheraton, J.W. (1990) Two-stage decompression in orthopyroxene-sillimanite granulites from Forefinger Point, Enderby Land, Antarctica: implications for the evolution of the Archaean Napier Complex, *J. Metamorph. Geol.*, 8, 591-613.
- Harley, S.L. and Hensen, B.J. (1990) Archaean and Proterozoic high-grade terranes of East Antarctica (40-80 °E): a case study of diversity in granulite facies metamorphism; in Ashworth, J.R. and Brown, M. (eds.) *High Temperature Metamorphism and Crustal Anatexis*, Unwin-Hyman, 320-370.
- Hills, F.A. and Armstrong, R.L. (1974) Geochronology of Precambrian rocks in the Laramie Range and implications for the tectonix framework of Precambrian southern Wyoming, *PreCamb. Res.*, 1, 213-225.
- Hoefs, J. (1980) *Stable isotope geochemistry*, Springer Verlag, Berlin, 208 p.
- Hoernes, S. and Friedrichsen, H. (1974) Oxygen isotope studies on metamorphic rocks on the western Hohe Tauern area (Austria) *Schweizerische Mineralogische und Petrographische Mitteilungen*, 54, 769-788.
- Hoernes, S. and Friedrichsen, H. (1978) Oxygen and hydrogen isotope study of the polymetamorphic area of the northern Ötztal-Stubai Alps (Tyrol). *Contrib. Mineral. Petrol.*, 67, 305-315.
- Hoffbauer, R., Hoernes, S. and Fiorentini, E. (1994) Oxygen isotope thermometry based on a refined increment method and its application to granulite-grade rocks from Sri Lanka, *Precambrian Research*, 66, 199-220.
- Hoffman, P.F. (1988) United plates of America: the birth of a craton, *Annual review of Earth and Planetary Sciences*, 16, 543-603.
- Hollister, L.S. (1966) Garnet zoning: an interpretation based on Raleigh fractionation model, *Science*, 154, 1647-1651.

- James, H.L. and Clayton, R.N. (1962) Oxygen isotope fractionation in metamorphosed iron formation of the lake superior region and in other iron-rich rocks, in Petrologic Studies: A volume to honor A.F. Buddington, Geol. Soc. Am. Washington D.C., 217-239.
- Jaoul, O., Sautter, V. and Abel, F. (1991) Nuclear microanalysis: a powerful tool for measuring low atomic diffusivity with mineralogical applications, in Ganguly, J. ed. Diffusion, atomic ordering and mass transport: advances in Phys. Geochem., 8, 198-220.
- Javoy, M., Fourcade, S. and Allegre, C.J. (1970) Graphical method for examination of  $^{18}\text{O}/^{16}\text{O}$  fractionations in silicate rocks, Earth Planet. Sci. Lett., 10, 12-16.
- Javoy, M., Fourcade, S. and Allegre, C.J. (1970) Graphical method of examination of  $^{18}\text{O}/^{16}\text{O}$  fractionations in silicate rocks, Earth Planet. Sci. Lett., 10, 12-16.
- Jenkin, G.R.T., Linklater, C. Fallick, A.E. (1991) Modeling of mineral  $\delta^{18}\text{O}$  values in an igneous aureole: Closed-system model predicts apparent open-system  $\delta^{18}\text{O}$  values, Geology 19, 1185-1188.
- Jenkin, G.R.T., Farrow, C.M., Fallick, A.E. and Higgins, D. (1994) Oxygen isotope exchange and closure temperatures in cooling rocks, J. Metamorph Geol. 12, 221-236.
- Joesten, R. (1983) Grain growth and grain-boundary diffusion in quartz from the Christmas mountains (Texas) contact aureole. Am. J. Sci. 283-A, 233-254.
- Joesten, R. (1991) Kinetics of coarsening and diffusion-controlled mineral growth, in Kerrick, D.M. (ed.) Contact Metamorphism, MSA, Rev. in Mineralogy. 26, 507-582.
- Kawabe, I. (1978) Calculation of oxygen isotope fractionation in quartz-water system with special reference to the low temperature fractionation, Geochim. Cosmochim. Acta, 42, 613-621.
- Kerrick, D.M. and Jacobs, G.K. (1981) A modified Redlich-Kwong equation for  $\text{H}_2\text{O}$ ,  $\text{CO}_2$  and  $\text{H}_2\text{O}-\text{CO}_2$  mixtures at elevated pressures and temperatures, Am. Jour. Sci., 281, 735-767.
- Kieffer, S.W. (1979c) Thermodynamics and lattice vibrations of minerals. 3. Lattice dynamics and an approximation for minerals with application to simple substances and framework silicates, Rev. Geophys. and Space Phys., 17, 35-59.

- Kieffer, S.W. (1982) Thermodynamics and lattice vibrations of minerals: 5. Applications to phase equilibria, isotopic fractionation, and high-pressure thermodynamic properties, *Rev. Geophys. and Space Phys.*, 20, 827-849.
- Kieffer, S.W. (1979a) Thermodynamics and lattice vibrations of minerals. 2. Mineral heat capacities and their relationship to simple lattice vibrational models, *Rev. Geophys. and Space Phys.*, 17, 1-??
- Kieffer, S.W. and Navrotsky, A. (1985) Scientific perspective, in Kieffer, S.W. and Navrotsky, A. (eds.) *Microscopic to macroscopic atomic environments to mineral thermodynamics*, M.S.A. Rev. in Mineral., 14, 1-8.
- Kohn, M.J., Valley, J.W., Elsenheimer, D. and Spicuzza, M.J. (1993) O isotope zoning in garnet and staurolite: Evidence for closed system-mineral growth during regional metamorphism, *Am. Mineral.*, 78, 988-1001.
- Kohn, M.J. (1993) Modelling of prograde mineral  $\delta^{18}\text{O}$  changes in metamorphic systems, *Contrib. Mineral. Petrol.*, 113, 249-261.
- Kolker, A. and Lindsley, D.H. (1989) Geochemical evolution of the Maloin Ranch pluton, Laramie Anorthosite Complex, Wyoming, Petrology and mixing relations, *Am. Mineral.*, 74, 307-324.
- Kolker, a., Lindsley, D.H. and Hanson, G.N. (1990) Geochemical evolution of the Maloin Ranch pluton, Laramie Anorthosite Complex, Wyoming: Trace elements and petrogenetic models, *Am. Mineral.*, 75, 572-589.
- Krylov, D.P. and Mineev, S.D. (1994) The concept of model-temperature in oxygen isotope geochemistry: An example of a single outcrop from the Rayner Complex (Enderby Land, East Antarctica) *Geochim. Cosmochim. Acta*, 58, 4465-4473.
- Krylov, D.P. (1985) "Model temperatures" estimated on the bases of oxygen isotopic distribution, *Dokl.Acad.Nauk SSSR*, 285,1201-1204.
- Kyser, T.K., O'Neil, J.R. and Carmichael, I.S.E. (1986) Reply to possible non-equilibrium  $^{18}\text{O}/^{16}\text{O}$  effects in mantle nodules, an alternative to the Kyser-O'Neil-Carmichael  $^{18}\text{O}/^{16}\text{O}$  geothermometer, *Contrib. Mineral. Petrol.*, 93, 120-123.
- Kyser, T.K., O'Neil, J.R. and Carmichael, I.S.E. (1981) Oxygen isotope thermometry of basic lavas and mantle nodules, *Contrib. Mineral. Petrol.*, 77, 11-23.
- Magaritz, M. and Taylor, H.P.Jr. (1986) Oxygen  $^{18}$ / oxygen  $^{16}$  and D/H studies of

- plutonic granitoid and metamorphic rocks across the Cordilleran batholiths of southern British Columbia. *Journal of Geophysical Research*, 91, 2193-2217.
- McCrea, J.M. (1950) On the isotopic chemistry of carbonates and a paleotemperature scale, *Jour. Chem. Phys.*, 18, 849-857.
- McCulloch, M.T. and Black, L.P. (1984) Sm-Nd isotopic systematics of Enderby Land granulites and evidence for the redistribution of Sm and Nd during metamorphism, *Earth and Planetary Science Letters*, 71, 46-58.
- McDonough, M.R., Grover, T.W., McNicoll, V.J. and Lidsay, D.D. (1993) Preliminary Report of the geology of the southern Taltson magmatic zone, northeastern Alberta, in *Current Research, part C, Geological Survey of Canada Paper 93-1C*, p. 221-232.
- McKinney, C.R., McCrea, J.M., Epstein, S., Allen, H.A. and Urey, H.C. (1950) Improvements in mass spectrometers for the measurement of small differences in isotope abundance ratios, *Rev. Sci. Instr.*, 21, 724-730.
- Monger, J.W.H., Price, R.A. and Ternpelman-Kluit, D.J. (1982) Tectonic accretion and the origin of the two major metamorphic and plutonic belts in the Canadian Cordillera, *Geology*, 10, 70-75.
- Morse, P.M. (1929) Diatomic molecules according to the wave mechanics-II. vibrational levels. *Phys. Rev.*, 24, 57-64.
- Muehlenbachs, K., and Connolly, C. (1992) Oxygen diffusion in leucite: Structural controls, in *Stable isotope geochemistry: A tribute to Samuel Epstein, the Geochem. Soc. Spec. Pub. No. 3*, H.P. Taylor, J.R. O'Neil and I.R. Kaplan, 27-34.
- Newhouse, W.H. and Hagner, A.F. (1957) Geologic map of anorthosite areas southern part of Laramie Range, Wyoming, USGS, Mineral Investigations Fields Studies Map MF119.
- Nier, A.O. and Gulbransen, E.A. (1939) Variations in the relative abundance of the carbon isotopes, *Jour. Am. Chem. Soc.*, 61, 697-698.
- Nier, A.O., Ney, E.P. and Ingrham, M.G. (1947) A null method for the comparison of two ion currents in a mass spectrometer, *Rev. Sci. Instr.* 18, 294.
- Nier, A.O. (1947) A mass spectrometer for isotope and gas analysis, *Rev. Sci. Instr.* 18, 398-411

- Nyman, M.W., Pattison, D.R.M. and Ghent, E.D. (1995) Melt extraction during formation of K-feldspar + sillimanite migmatites, west of Revelstoke, British Columbia. *Jour. Petrology*, (in press).
- O'Neil, J.R. (1986) Theoretical and experimental aspects of isotopic fractionation, in Valley, J.W., Taylor, H.P. Jr. and O'Neil, J.R. (eds.) *Stable isotopes in high temperature geological processes*, M.S.A. *Rev. Mineral.*, 16, 1-40.
- O'Neil, J.R. and Ghent, E.D. (1975) Stable isotope study of coexisting metamorphic minerals from the Esplanade Range, British Columbia, *Geol. Soc. Am. Bull.* 86, 1708-1712.
- Parrish, R.R., Carr, S.D. and Parkinson, D.L. (1988) Extensional tectonics of the southern Omineca Belt, British Columbia, *Tectonics*, 7, 181-212.
- Pell, J. and Simony, P.S. (1987) New correlations of Hadrynian strata, south-central British Columbia, *Can. Jour. Earth Sci.*, 24, 302-313.
- Peterman, Z.E. (1982) Geochronology of the southern Wyoming age province—a summary in Goldich, S.S. ed., *Archean Geochemistry Conference*, 1-23.
- Peto, P. (1976) An experimental investigation of melting relations involving muscovite and paragonite in the silica-saturated portion of the systems  $K_2O-Na_2O-Al_2O_3-SiO_2-H_2O$  to 15 kb total pressure, *Progress in Experimental Petrology NERC London*, 3rd report, 41-45.
- Plint H.E. and McDonough, M.R. (1995)  $^{40}Ar/^{39}Ar$  and K/Ar age constraints on shear zone evolution, southern Taltson magmatic zone, northeastern Alberta, *Can. J. Earth Sci.*, 32, 281-291.
- Poulton T.P. and Simony, P.S. (1980) Stratigraphy, sedimentology, and regional correlation of the Horsethief Creek Group (Hadrynian, Late Precambrian) in the northern Purcell and Selkirk mountains, British Columbia. *Can. Jour. Earth Sci.*, 10, 292-305.
- Richet, P., Bottinga, Y. and Javoy, M. (1977) A review of hydrogen, carbon, nitrogen, oxygen, sulphur, and chlorine stable isotope fractionations among gaseous molecules, *Ann. Rev. Earth and Planet. Sci.*, 5, 65-110.
- Rosenbaum, J.M., Mathey, D.P. and Elphick, S. (1994) Equilibrium garnet-calcite oxygen isotope fractionation, *Min. Mag.*, 58A, 787-788.
- Ross, G.M., Parrish, R.R., Villeneuve, M.E. and Bowring, S.A. (1991) Geophysics and

- geochronology of the crystalline basement of the Alberta Basin, western Canada, *Canadian Journal of Earth Sciences*, 28, 512-522.
- Sandiford, M. and Powell, R. (1986) Pyroxene exsolution in granulites from Fyfe Hills, Enderby Land, Antarctica: Evidence for 1000°C metamorphic temperatures in Archaean continental crust, *American Mineralogist*, 71, 946-954.
- Sandiford, M. (1985b) The origin of retrograde shear zones in the napier Complex: implications for the tectonic evolution of Enderby Land, Antarctica, *Journal of Structural Geology*, 7, 477-488.
- Sandiford, M. (1985a) The metamorphic evolution of granulites at Fyfe Hills: implications for Archaean crustal thickness in Enderby Land, Antarctica, *J. Metamorph. Geol.*, 3, 155-178.
- Sandiford, M. and Wilson, C.J.L. (1986) The origin of Archaean Gneisses in the Fyfe Hills region, Enderby Land; Field occurrence, Petrography and geochemistry, *Precambrian Research*, 31, 37-68.
- Sandiford, M. and Wilson, C.J.L. (1984) The structural evolution of the Fyfe Hills-Khmara Bay region, Enderby Land, East Antarctica, *Australian Journal of Earth Sciences*, 31, 403-426.
- Scoates, James S., Frost, Carol D. Mitchell, Jeremy N. and Chamberlain, Kevin R. (1993a) Sybille monzosyenites revisited, Laramie anorthosite complex Wyoming. *Geol. Soc. Am. Ann. Mtg. Abstr. with Prog.*, v. 25, A446.
- Scoates, James S., Chamberlain Kevin R. (1993) The duration of anorthositic magmatism in the 1.43 Ga Laramie anorthosite complex, Wyoming, *Geol. Soc. Am. Ann. Mtg. Abstr. with Prog.*, v. 25, No. 6, A446.
- Scoates, James S., Chamberlain, Kevin R. and Mitchell, Jeremy N. (1993b) The 1758 Horse Creek anorthosite: oldest massif-type anorthosite in north america, *Geol Soc. Am. Ann Mtg. Abstr. with Prog.*, v. 25 No.6, A447.
- Sevigny, J.H., Parrish, R.R., Donelick, R.A. and Ghent, E.D. (1990) Northern Monashee Mountains, Omineca Crystalline Belt, British Columbia: Timing of metamorphism, anatexis, and tectonic denudation, *Geology*, 18, 103-106.
- Sevigny, J.H., Parrish, R.R. and Ghent, E.D. (1989) Petrogenesis of peraluminous granites, Monashee Mountains, southeastern Canadian Cordillera, *Jour. Petrol*, 30, 557-581.

- Sharp, Z.D., O'Neil, J.R. and Essene, E.J. (1988) Oxygen isotope variations in granulite-grade iron formations: Constraints on oxygen diffusion and retrograde isotopic exchange, *Contrib. Mineral. Petrol.* 98, 490-501.
- Sharp, Z.D., Giletti, B.J. and Yoder, H.S.Jr. (1991) Oxygen diffusion rates in quartz exchanged with  $\text{CO}_2$ , *Earth. Planet. Sci. Lett.* 107, 339-348.
- Sharp, Z.D. and Ulmer, P. (1993) Stable isotope geochemistry of the aluminosilicates, *Geol. Soc. Am. Abstr with Prog.*, a25.A100.
- Sharp, Z.D. (1991) Determination of oxygen diffusion rates in magnetite from natural isotopic variations, *Geology* 19, 653-656.
- Sheraton, J.W. and Black, L.P. (1983) Geochemistry of Precambrian gneisses: relevance for the evolution of the East antarctic Shield, *Lithos*, 16, 273-296.
- Sheraton, J.W., Tingey, R.J., Black, L.P., Offe, L.A. and Ellis, D.J. (1987) Geology of Enderby Land and Western Kemp Land, Antarctica, Australian Bureau of Mineral Resources Bulletin 233, 51 pp.
- Sheraton, J.W., Offe, L.A., Tingey, R.J. and Ellis, D.J. (1980) Enderby Land, Antarctica-an unusual Precambrian high-grade metamorphic terrain, *Journal of the Geological Society of Australia*, 27, 1-18.
- Shieh, Y.N. and Taylor, H.P. Jr. (1969) Oxygen and hydrogen isotope studies of contact metamorphism in the Santa Rosa range, Nevada, and other areas, *Contrib. Mineral. Petrol.*, 20-306-356.
- Silverman, S.R. (1951) The isotope geology of oxygen, *Geochim. Cosmochim. Acta*, 2, 26-42.
- Simony, P.S. and Wind G. (1970) Structure of the Dogtooth Range and adjacent portions of the Rocky Mountain Trench: in Wheeler, J.O. (ed.) *Geol. Assoc. Can. Spec. Pap.* 6, 45-51.
- Simony, P.S., Ghent, E.D., Craw, D. and Robbins, D.B. (1980) Structural and metamorphic evolution of northeast flank of Shushwap Complex, southern Canoe River area, British Columbia, *Geol. Soc. Am. Mem.*, 153, 445-461.
- Smyth, J.R. and Clayton, R.N. (1988) Correlation of oxygen isotope fractionation and electrostatic site potentials in silicates, *EOS* 69, 1514.
- Smyth, J.R. (1989) Electrostatic characterization of oxygen sites in minerals, *Geochim.*



Cosmochim. Acta 53, 1101-1110.

- Snyder, G.L. (1984) Preliminary geologic maps of the central Laramie Mountains, Albany and Platte Counties, Wyoming, U.S. Geol. Survey Open File report 84-358, Parts A through M.
- Spear, F.S. and Peacock, S.M. (1990) Metamorphic P-T-t paths: Program manual and computer exercises for the calculation of metamorphic phase equilibria, pressure-temperature-time paths and thermal evolution of orogenic belts, Geol. Soc. Am short course, 188p.
- Större, B. (1982) Dry melting of muscovite + quartz in the range  $P_s = 7$  kb to  $P_s = 20$  kb, Contrib. Mineral. Petrol., 37, 87-89.
- Taylor, H.P. Jr. and Coleman, R.G. (1968) O18/O16 ratios of coexisting minerals in glaucophane-bearing metamorphic rocks, G.S.A. Bull., 79, 1727-1756.
- Taylor, H.P. Jr., Albee, A.L. and Epstein, S. (1963) O18/O16 ratios of coexisting minerals in three assemblages of kyanite-zone pelitic schist, Jour. Geol., 71, 513-522.
- Taylor, H.P. Jr. and Epstein, S. (1962) Relationship between O18/O16 ratios in coexisting minerals of igneous and metamorphic rocks: Part I principles and experimental results, G.S.A. Bull., 73, 461-480.
- Taylor, H.P. Jr. (1968) The oxygen isotope geochemistry of igneous rocks, Contrib. Mineral. Petrol., 19, 1-71.
- Thompson, J.B. Jr. (1982) Reaction Space: An algebraic and geometric approach, in Ferry, J.M. (ed.) Characterization of metamorphism through mineral equilibria, MSA Rev. Mineral 10, 33-52
- Urey, H.C., Lowenstam, H., Epstein, S. and McKinney, S.R. (1951) Measurement of paleotemperatures and temperatures of the Upper Cretaceous of England, Denmark and the southeastern United States, Geol. Soc. Am. Bull. 62, 399-416.
- Urey, H.C. (1947) The thermodynamic properties of isotopic substances, Jour. Chem. Soc. London, 562-581
- Urey, H.C. and Grief, L.J. (1935) Isotopic exchange equilibrium, Jour. Am. Chem. Soc., 57, 321-327.
- Valley, J.W. and Graham, C.M. (1993) Cryptic grain-scale heterogeneity of oxygen isotope ratios in metamorphic magnetite, Science, 1729-1733.

- Valley, J.W., Chiarenzelli, J.R. and McLelland, J.M. (1994) Oxygen isotope geochemistry of zircon, *Eart. Planet. Sci. Lett.*, 126, 187-206.
- Valley, J.W. and Graham, C.M. (1991) Ion microprobe analysis of oxygen isotope ratios in granulite facies magnetites: diffusive exchange as a guide to cooling history, *Contrib. Mineral. Petrol.* 109, 38-52.
- Vennemann, T.W. and Smith, S.H. (1990) The rate and temperature of reaction of  $\text{ClF}_3$  with silicate minerals, and their relevance to oxygen isotope analysis, *Chem. Geol.*, 86, 83-88.
- Vogel, D.E. and Gallick, G.D. (1970) Oxygen isotope ratios in metamorphic exlogites, *Contrib. Mineral. Petrol.*, 28, 183-191.
- Wang, H.F. (1992) Double medium diffusion in rocks with a small, continuous fluid phase, *Contrib. Mineral. Petrol.*, .
- Wheeler, J.O. (1964) Big Bend (82ME) British Columbia, *Geol. Surv. Can. Map 12-1964*, scale 1 inch = 4 miles.
- Wilson, A.F., Green, D.C. and Davidson, L.R. (1970) The use of oxygen isotope geothermometry on the granulites and related intrusives, Musgrave ranges, Central Australia, *Contrib. Mineral. Petrol.*, 27, 166-178.
- Young, E.D. (1993) On the  $^{18}\text{O}/^{16}\text{O}$  record of reaction progress in open and closed metamorphic systems, *Eart. Planet. Sci. Lett.*, 117, 147-167.
- Young, E.D. and Rumble, D.III (1993) The origin of correlated variations in in-situ  $^{18}\text{O}/^{16}\text{O}$  and elemental concentrations in metamorphic garnet from southeastern Vermont, USA, *Geochim. Cosmochim. Acta*, 57, 2585-2597.
- Zhang, Y., Stolper, E.M. and Wasserburg, G.J. (1991) Diffusion of a multi-species component and its role in oxygen and water transport in silicates: *Earth and Planetary Science Letters*, 103, 228-240.
- Zheng, Y-F (1993) Oxygen isotope fractionation in  $\text{SiO}_2$  and  $\text{Al}_2\text{SiO}_5$  polymorphs: effect of crystal structure, *Eur. J. Mineral.*, 5, 651-658..